



**TESTING AND EVALUATING DEPLOYMENT PROFILES OF THE
CANISTERIZED SATELLITE DISPENSER (CSD)**

THESIS

Stephen K. Tullino, Capt, USAF

AFIT-ENY-MS-17-M-296

**DEPARTMENT OF THE AIR FORCE
AIR UNIVERSITY**

AIR FORCE INSTITUTE OF TECHNOLOGY

Wright-Patterson Air Force Base, Ohio

DISTRIBUTION STATEMENT A
APPROVED FOR PUBLIC RELEASE; DISTRIBUTION UNLIMITED

The views expressed in this thesis are those of the author and do not reflect the official policy or position of the United States Air Force, Department of Defense, or the United States Government. This material is declared a work of the United States Government and is not subject to copyright protection in the United States.

TESTING AND EVALUATING DEPLOYMENT PROFILES OF THE
CANISTERIZED SATELLITE DISPENSER (CSD)

THESIS

Presented to the Faculty

Department of Astronautical Engineering

Graduate School of Engineering and Management

Air Force Institute of Technology

Air University

Air Education and Training Command

In Partial Fulfillment of the Requirements for the
Degree of Master of Science in Astronautical Engineering

Stephen K. Tullino, BS

Captain, USAF

March 2017

DISTRIBUTION STATEMENT A
APPROVED FOR PUBLIC RELEASE; DISTRIBUTION UNLIMITED

TESTING AND EVALUATING DEPLOYMENT PROFILES OF THE
CANISTERIZED SATELLITE DISPENSER (CSD)

THESIS

Stephen K. Tullino, BS
Captain, USAF

Committee Membership:

Eric D. Swenson, PhD
Chairman

Carl R. Hartsfield, PhD
Member

Capt. Andrew J. Lingenfelter, PhD
Member

Abstract

Planetary Systems Corporation (PSC) developed the Canisterized Satellite Dispenser (CSD) to provide a more secure and predictable deployment system for CubeSats of different sizes. The CSD is designed to provide predictable and consistent payload deployment performance. Though the CSD has proven its safety and reliability, there is still not enough data required to predict accurately CSD linear and angular deployment rates. In this research, various analytical models were developed, and their predictions were compared with respect to experimental deployments. Any errors were analyzed to tune the models to better understand the deployment dynamics and the variables that affect performance.

To my wife and son, and for the forgotten souls in Purgatory

Acknowledgments

I would like to thank Dr. Eric Swenson for all his ceaseless assistance and encouragement as thesis advisor. Moreover, I would like to thank Dr. Carl Hartsfield and Capt Andrew Lingenfelter for taking an active interest in my research and providing invaluable assistance and feedback. A special thanks to Walt Holemans and Chris Flood from PSC for all their assistance getting the author started in his project. In addition, a special thanks to Randall Sharp, Phil Smith, Sean Miller, Matt Lippert, and Chris Sheffield for help with designing, building, and consultation for all apparatuses needed for this research. Another thanks to Eric Neumann and Luke Ogorzaly from NASA GRC for their assistance with the drop towers. A special thanks to Scott Spearing from NASA Marshall, who provided project concept validation and helped facilitate discussion of this project with the Space Launch System Secondary Payloads team.

I would also like to express my appreciation to the NASA team who provided project consultation and vetting: Joseph Pelfrey from NASA Marshall, Bruce Yost and Elwood Agasid from NASA Ames, and Scott Higginbotham from NASA KSC. A special thanks goes out to Dr. Jitendra Joshi, Technology Integration Lead for the Advanced Exploration Systems Division at NASA Headquarters for providing vetting, feedback, and expressing his interest in this project. I would like to thank Lt Col Christopher Allen from AFRL Space Vehicles Directorate for facilitating the funding of future work with the NASA Glenn Research Center drop towers.

Finally, I would like to thank my wife Jess, for her technical advice, love, support, and affection as I embarked on my turn in getting my M.S, and for putting up with my long and odd hours in this work. Overall, I could not have been able to accomplish all this without the grace of Almighty God: Father, Son, and Holy Spirit. Amen.

Stephen K. Tullino

Table of Contents

	Page
Abstract.....	iv
Acknowledgments.....	vi
Table of Contents.....	vii
List of Figures.....	x
List of Tables.....	xvi
I. Introduction.....	1
1.1 General Issue.....	1
1.2 Problem Statement.....	2
1.3 Scope.....	2
1.4 Research Objectives.....	2
1.5 Investigative Focus Areas.....	3
1.6 Methodology.....	4
1.7 Assumptions/Limitations.....	4
II. Literature Review.....	6
Chapter Overview.....	6
2.1 Background.....	6
2.2 Initial Tests Conducted by Planetary Systems Corp.....	13
2.2.1 Motivation.....	13
2.2.2 PSC Test Setup.....	13
2.2.3 PSC's Test Results.....	18
2.3 NASA's Use of the CSD.....	22
2.4 Characterization of Payload Motion as a Result of CSD Ejection.....	27
2.4.1 Rotational Motion.....	27
2.4.2 Linear Motion.....	29
2.4.3 Motion Data Gathering.....	30
2.4.4 Potential Sources of Perturbations.....	33
2.5 Deployment Evaluation Methodology Options.....	34
2.5.1 Lab-Based Experimental Setup Options.....	34
2.5.2 Micro-Gravity Drop Towers.....	37
2.5.3 Deployment Evaluation Methodology Analysis.....	40
Summary.....	42

III. Methodology	44
Chapter Overview	44
3.1 Push Plate Force Test	44
3.2 Initial CSD Ejection Velocity Test	46
3.3 CSD Ejection Tests with IMU	47
3.4 Rail Friction	52
3.4.1 <i>Determine Friction via Incline Method</i>	53
3.4.2 <i>Determine Friction via Suspended Mass</i>	54
3.4.3 <i>Determine Friction via Impulse-Deceleration</i>	55
3.5 Door Interference	59
3.6 Push Plate Feet Contact.....	66
3.7 MATLAB Simulation Model	68
Summary	71
IV. Results.....	72
Chapter Overview	72
4.1 Push Plate Force Test Results	72
4.2 Initial CSD Ejection Velocity Test Results.....	79
4.3 CSD Ejection Tests with IMU Results	85
4.4 Rail Friction Test Results.....	95
4.4.1 <i>Determine Friction via Inclination</i>	96
4.4.2 <i>Determine Friction via Suspended Mass</i>	99
4.4.3 <i>Determine Friction via Impulse-Deceleration</i>	103
4.4.4 <i>Friction Overall Characterization</i>	107
4.5 Door Interference Experimental Results	110
4.6 Push Plate Feet Contact Experimental Results	115
4.6.1 <i>All Feet Contact</i>	118
4.6.2 <i>Three Feet Contact</i>	120
4.6.3 <i>Two Feet Contact</i>	122
4.6.4 <i>One Foot Contact</i>	124
4.6.5 <i>Tabs Only Contact</i>	126
4.6.6 <i>Push Plate Feet Contact Overall</i>	128
4.7 MATLAB Simulation Model Tuning Results.....	128
Summary	131
V. Conclusions and Recommendations	132
Chapter Overview	132
Conclusions of Research	133
Recommendations for Action	136
Recommendations for Future Research	136
Summary	138
Appendix A.1 – Test Plan: CSD Push Plate Force Profile Testing	140

Appendix A.2 – Test Plan: Deployment Test	157
Appendix A.3 – Test Plan: Friction Tests.....	173
Appendix A.4 – Test Plan: Door Interference Test	191
Appendix A.5 – Test Plan: Push Plate Feet Contact Test.....	215
Bibliography	230

List of Figures

	Page
Figure 1. 3U, 6U, and 12U CubeSat Configurations [5]	7
Figure 2. CAD Model of P-POD (left) and an Internal View of P-POD (right) [6]	7
Figure 3. ISIS ISIPOD (4x3U QuadPack Version) [7]	8
Figure 4. Risk of Payload with Rails [2]	9
Figure 5. PSC Depiction of the CSD Deploying a CubeSat [2]	9
Figure 6. Contact Feet on the Pumpkin SUPERNOVA 6U CubeSat [10]	10
Figure 7. Wear Marks from Pumpkin SUPERNOVA Vibration Test [11]	11
Figure 8. 6U CSD-Compatible CubeSat Chassis with Tabs [12]	11
Figure 9. Payload and Predicted Dynamic Response Due to Preloaded Tabs [2]	12
Figure 10. CSD C-9 Test Setup [1]	14
Figure 11. PSC Mass Representation with IMU (6U Variant Shown) [1]	15
Figure 12. C-9 “Vomit Comet”	16
Figure 13. C-9 Flight Path to Produce Zero-G [1]	16
Figure 14. Raw Acceleration with Respect to Parabolic Flight Path [1]	17
Figure 15. Raw Rotation Rate Data with Respect to Parabolic Flight Path [1]	17
Figure 16. 6U CubeSat Payload Rotation Rates Coupled with Rotation from C-9 [1]	18
Figure 17. PSC’s Accelerometer Data Showing Bias Drift Error [1]	19
Figure 18. 3U Separation Results [2]	20
Figure 19. 6U Separation Results [2]	21
Figure 20. PSC Payload Ejection Velocity Profiles Based on C-9 Data [2]	22

Figure 21. NASA CAD Rendition of CSDs (See Arrows) on SLS Upper-Stage Adaptor [18].....	23
Figure 22. CSD Locations on SLS [19].....	24
Figure 23. Payload “Bubble” Clearance Zone [19].....	25
Figure 24. Chassis with Normal Tabs.....	26
Figure 25. NASA Experimental CSD Test Mass with Tab Bar [19].....	26
Figure 26. Piezoelectric Accelerometer Function [25]	31
Figure 27. Internal Operational View of a MEMS Gyroscope [25]	32
Figure 28. NASA GRC 5.18 s Drop Tower with Experiment Being Hoisted [32]	38
Figure 29. Preps (top left), Hoisting (top right), and Tower Rendition (bottom), [32] ...	39
Figure 30. Tower Experiment Setup [33]	40
Figure 31. CSD with Static Force Reading Apparatus	45
Figure 32. Push/Pull Gauge on Guide Rod.....	45
Figure 33. Midé Slam Stick [36].....	46
Figure 34. Slam Stick X Error Profile [37].....	46
Figure 35. Slam Stick Orientation	47
Figure 36. NGIMU in Bracket Attached to Chassis Base Plate	50
Figure 37. NGIMU Orientation	51
Figure 38. CSD Guide Rail with Features	52
Figure 39. Incline Method [25].....	54
Figure 40. Suspended Mass Method [25]	55
Figure 41. Constant Force Spring with Pinned End [46].....	57
Figure 42. NGIMU Y Axis Linear Velocity: Model Prediction vs. Measured Data	59

Figure 43. CSD Door Striking Base Plate	60
Figure 44. CSD Bolted to Flat Plate in Vertical Position	61
Figure 45. Locations of Accelerometers on CSD Door (Circled)	62
Figure 46. SignalCalc Graphic User Interface (Settings Circled).....	63
Figure 47. TTL Signal [25]	64
Figure 48. Camera Setup with Lights and Photography Linen.....	64
Figure 49. Phantom Camera Control GUI (Focus Point Circled).....	65
Figure 50. Wear Marks from Vibe Test Demonstrating Uneven Contact [11]	67
Figure 51. 3-D Printed 6U Chassis with Contact Feet.....	67
Figure 52. Model Coordinate System and Force Distribution Points [8]	69
Figure 53. Average Force Readings per Depth.....	72
Figure 54. Coefficients of t-Test as a Function of Sample Size for 95% Confidence Interval.....	75
Figure 55. Force Reading Spread.....	77
Figure 56. Force Reading Percent Deviation with Respect to Depth	78
Figure 57. 12U Chassis Prevented from Full Deployment due to Friction Caused by a Gravitational Torque.....	80
Figure 58. Slam Stick Lab Test Output (Base Plate Only)	81
Figure 59. Slam Stick Linear Translation Acceleration (Y Axis Isolated).....	82
Figure 60. Slam Stick Y Axis Linear Velocity: Model Prediction vs. Measured Data	83
Figure 61. Slam Stick Y Axis Linear Displacement: Model Prediction vs. Measured Data	83

Figure 62. PSC Payload Ejection Velocity Profiles Based on C-9 Experiments (Configuration Agreement Circled) [2]	84
Figure 63. NGIMU Accelerometer Readout for Base Plate Deployment (Y Axis Isolated)	86
Figure 64. NGIMU Y Axis Linear Velocity: Model Prediction vs. Measured Data	88
Figure 65. NGIMU Y Axis Linear Displacement: Model Prediction vs. Measured Data	88
Figure 66. NGIMU Angular Rates.....	89
Figure 67. CSD Door Striking Base Plate	91
Figure 68. NGIMU Accelerometer Readout for Base Plate Deployment (No Door).....	92
Figure 69. NGIMU Linear Velocity: Model Prediction vs. Measured Data (No Door)...	93
Figure 70. NGIMU Linear Displacement: Model Prediction vs. Measured Data (No Door).....	93
Figure 71. NGIMU Angular Rates (No Door).....	94
Figure 72. Friction Test Setup with Two Mass Stacks	95
Figure 73. CSD Attached to Tilting Apparatus with Inclinometer	96
Figure 74. Top of Rail Coefficients of Kinetic Friction Distribution (Inclination Method)	97
Figure 75. Bottom of Rail Coefficients of Kinetic Friction Distribution (Inclination Method).....	98
Figure 76. Brass Masses	100
Figure 77. Suspended Mass Apparatus (In Rail Top Testing Configuration)	101
Figure 78. Top of Rail Coefficients of Kinetic Friction Distribution (Suspended Mass Method).....	102

Figure 79. Bottom of Rail Coefficients of Kinetic Friction Distribution (Suspended Mass Method).....	103
Figure 80. Noisy Raw Accelerometer Data from Impulse-Deceleration Test.....	104
Figure 81. Friction Impulse Test: Top Rail with Base Plate Only.....	104
Figure 82. Friction Impulse Test: Bottom Rail with Base Plate Only	106
Figure 83. Kinetic Friction Distribution for Top Rail.....	109
Figure 84. Kinetic Friction Distribution for Top Rail.....	109
Figure 85. Door Accelerometer Readout Example (Top Right Quadrant Location).....	110
Figure 86. Phantom Camera Control GUI (Focus Point Circled).....	112
Figure 87. Door Orientation During Ejection	112
Figure 88. Modeling of CSD Door Orientation from 0-0.2 s	113
Figure 89. Modeling of CSD Door Orientation from 0.2-0.45 s	114
Figure 90. Full Modeling of CSD Door.....	115
Figure 91. Vertical Ejection of 3-D Printed 6U Chassis.....	116
Figure 92. 3-D Printed 6U Chassis with Contact Feet and IMU	116
Figure 93. Diagram Demonstrating Force Distribution in Model [8].....	117
Figure 94. All Feet Contact Case Simulation Prediction.....	118
Figure 95. All Feet Contact Case IMU Readout.....	119
Figure 96. Three Feet Contact Case Simulation Prediction.....	120
Figure 97. Three Feet Contact Case IMU Readout.....	121
Figure 98. Tabs Only Contact Case Simulation Prediction	122
Figure 99. Two Feet Contact Case IMU Readout.....	123
Figure 100. One Foot Contact Case Simulation Prediction.....	124

Figure 101. One Foot Contact Case IMU Readout.....	125
Figure 102. NASA Experimental CSD Test Mass with Tab Bar [19].....	126
Figure 103. Tabs Only Contact Case Simulation Prediction	127
Figure 104. Tabs Only Contact Case IMU Readout	127
Figure 105. Deployment Model (Using Sample Force Distributions).....	129
Figure 106. Spacecraft Angular Rates (left) & Inertial Frame Angular Momentum (right)	129

List of Tables

	Page
Table 1. Bosch BMI160 IMU Calculated Noise Specs From Datasheet [42]	50
Table 2. t-Statistic as a Function of Sample Size for a 95% Confidence Interval [51]	74
Table 3. Slam Stick Calibration Check Results	79
Table 4. NGIMU Accelerometer Check Results	85
Table 5. NGIMU Gyroscope Check Results.....	85
Table 6. Top of Rail Coefficients of Kinetic Friction (Inclination Method)	97
Table 7. Bottom of Rail Coefficients of Kinetic Friction (Inclination Method).....	98
Table 8. Brass Mass Calibration	100
Table 9. Top of Rail Coefficients of Kinetic Friction (Suspended Mass Method).....	101
Table 10. Bottom of Rail Coefficients of Kinetic Friction (Suspended Mass Method) .	102
Table 11. Data from Impulse-Deceleration Tests (Top of Rail).....	106
Table 12. Data from Impulse-Deceleration Tests (Bottom of Rail)	107
Table 13. PCB Accelerometer Check Results	110
Table 14. Four Feet Contact Case Statistics	119
Table 15. All Feet Contact Case Measurements	119
Table 16. Three Feet Contact Case Statistics.....	121
Table 17. Three Feet Contact Case	121
Table 18. Two Feet Contact Case Statistics.....	123
Table 19. Two Feet Contact Case	123
Table 20. One Foot Contact Case Statistics.....	125
Table 21. One-Foot Contact Case	125

Table 22. Tabs Only Contact Case Statistics	128
Table 23. Tabs Only Contact Case	128

TESTING AND EVALUATING DEPLOYMENT PROFILES OF THE CANISTERIZED SATELLITE DISPENSER (CSD)

I. Introduction

1.1 General Issue

In 2014, as part of product qualification, Planetary Systems Corporation (PSC) conducted four days of deployment tests on the NASA C-9 “Vomit Comet” in order to measure rotation rates and linear velocities of 3U and 6U payloads as they eject from a Canisterized Satellite Dispenser (CSD) in a simulated zero-g environment. Data was collected via an onboard inertial measurement unit (IMU), and was verified by a high-speed camera. Their objective was to discover performance deficiencies and failure modes, because CubeSats statistically have roughly a 50% chance of failure while on-orbit failure for many reasons [1].

Data from these tests was not as accurate as desired, as PSC noted multiple sources of error. Regardless, PSC determined that they were able to gather a sufficient amount of data for them to develop rudimentary linear ejection profiles. Unfortunately, they found that the angular rate data covered a wide range, which resulted in PSC setting on characterizing deployment angular rotation by using the worst-case angular rate seen: a maximum of 10°/s per axis [2] [3].

Researchers at AFIT determined that it was necessary to explore further the ejection properties of the CSD in order to bring a greater understanding of what is involved in a CubeSat being deployed from the CSD. Moreover, AFIT’s desire to further refine these properties was in response to NASA recently purchasing 13 CSDs to be used to deploy secondary payloads for the maiden flight of the Space Launch System, Exploration Mission 1 (EM-1) [3].

1.2 Problem Statement

Higher fidelity ejection profiles need to be measured and developed in order to assist payload planners with hardware design and configuration, as well as mission planners to execute stabilization maneuvers in order to counteract any tumbling that may be experienced upon ejection from the CSD. This thesis creates and tunes analytical models, and conducts experiments to refine these models so linear and angular ejection rates can be predicted

1.3 Scope

Both PSC 6U and 12U CSDs (both were engineering development units) have been used in the experimental component of this research. Initial deployment and push plate tests have been used on the 12U CSD due to its availability (versus the 6U). Subsequent tests have exclusively been used on the 6U CSD mainly because the 12U CSD cannot fit in the NASA GRC Zero-Gravity Facility drop towers. Moreover, aside from sizing, the 6U and 12U CSDs are mechanically identical, as they use the same spring and clamping configurations [2]. AFIT did not have access to a 3U CSD, but data collected from the 6U/12U configurations were used to characterize the 3U, as again, mechanics are very similar and use similar parts (i.e. same springs and clamps).

1.4 Research Objectives

The objective of this research is to be able to predict the linear and angular rates of payloads being ejected by the CSD through simulations and experiments. This is challenging because the CSD is a nonlinear system with many unknown characteristics, and is complex

compared to other deployers. First, an analytical simulation-model was created based on CSD specs and physical measurements. The model was subsequently tuned using data collected in experiments to characterize push plate force, friction and door interferences, push plate contact, and ejection tests. The main outcome of the thesis is a basic dynamics model to allow CubeSat mission planners to predict deployment rates on orbit, and allow mission planners to plan detumbling operations upon ejection. After more research, the model is ultimately intended to become a high fidelity means to reduce mission risk of CubeSat missions upon deployment.

1.5 Investigative Focus Areas

There are several factors that make creating a high fidelity dynamics model challenging. First, uneven ejection force is a very common issue, so experiments need to be conducted to identify potential risks and root causes that may need to be mitigated. It will need to be determined if the CSD induces any undesired moments or perturbations onto the dispensed payload. Any significant interferences encountered by the CubeSat payload imposed by the CSD itself will need to be identified. The effects of only pushing on the CubeSat chassis tabs during deployment is another major item since it is an option currently being explored by NASA (discussed later). The relationship between the center of mass location and the push plate contact feet with respect to tumble rates is another area of interest. Overall, the right balance ensuring the accuracy of payload configuration, yet keeping costs down, and simplifying processes/mechanisms would have to be considered. These variables make this problem difficult, as there are many unknowns that yet to be discovered, and exploring these focus areas

can assist in better understanding the dynamics of the CSD, and ultimately work towards a high fidelity dynamics model by collecting, analyzing, and applying empirical data.

1.6 Methodology

The study will first derive the basic equations of motion governing satellite motion while in orbit. A basic model will be developed from the direct measurement of the CSD and analysis of its specifications. This model will be subsequently adjusted and tuned based on additional deployment experiments, specifically characterization of the constant force push plate, friction encountered in the CSD rails through measuring friction forces, and any interference from the CSD door.

1.7 Assumptions/Limitations

Several assumptions have to be made and limitations considered in conducting this investigation. First is that when determining the friction profile, the row of roller bearings lining the bottom of the CSD guide rails would be modeled using the basic Coulomb friction model for the entire set of bearings, rather than determining the friction of each bearing. This is because the payload interacts with the row of bearings as distributed surface, rather than interacting with each individual bearings. Additionally, the initial iteration of the MATLAB simulator-model assumes that the moment applied to the ejecting payload is applied during the last 0.5 inches in the guide rail prior to release. Most of the tests are limited by gravity because the CSD is designed to operate in micro gravity, and cannot operate at full potential in gravity. For example, a payload will cantilever and arc while deploying horizontally in gravity. If a

payload is too heavy, it will be stuck in the rails as it cantilevers. Another aspect is that if there is a vertical upward deployment, the push plate/payload acceleration must exceed the acceleration due to gravity, so applying Newton's Second Law, a lightweight payload must be used in order for any test to work. Because of these two main issues, lightweight payloads were used in order to minimize gravitational effects, as well as to minimize wear on the CSD, and maximize deployment range of motion. Efforts were made to secure use of micro-gravity drop towers at NASA Glenn Research Center (GRC), Cleveland, OH, however timing did not permit execution of these experiments before finalization of this thesis. These tests at NASA GRC are planned to be conducted later in 2017, and the goal is to present results through other means.

II. Literature Review

Chapter Overview

Planetary Systems Corporation's (PSC) Canisterized Satellite Dispenser (CSD) was developed as the next step in advancing CubeSat technologies. As part of their tests, PSC discovered that much more was to be desired with the angular and linear rate data they collected from deployment tests in microgravity. [1] Coupled with interest in the CSD from high profile customers, such as NASA, it was determined that a greater degree of characterization and tests were needed for the US Government. This can be done through isolating each facet of CSD deployment, as well as overall system deployment. These approaches can allow a more resolute understanding of CSD ejection performance in order to predict performance, and reduce mission risk.

2.1 Background

California Polytechnic State University (Cal Poly) created the CubeSat in 1999, in order to enable academia to perform space exploration and science. A basic CubeSat (designated 1U) is a 10 cm³ cube (1L in volume), with a maximum mass of 1.33 kg. Since 1999, subsequent sizes in 2, 3, and 6U were developed by arranging 1U stacks in standard configurations (Fig. 1). In recent times, a 12U chassis was recently developed, and the concept of the 27U CubeSat is currently in development [4].

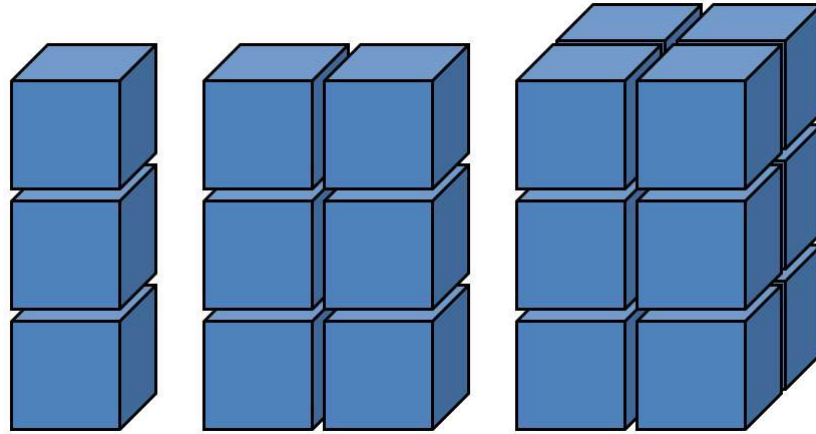


Figure 1. 3U, 6U, and 12U CubeSat Configurations [5]

CubeSats mandate a separate deployment device, as most launch vehicles are configured to only accommodate main payload(s). Initially, the primary dispensing devices available to most CubeSat developers included Cal Poly's Pico-satellite Orbital Deployer (P-POD), Innovative Solutions in Space (ISIS) Pico-satellite Orbital Deployer (ISIPOD), and other similar designs. These deployers ejected their payloads using one or multiple large coil springs connected to a push-plate, as seen in Fig. 2.

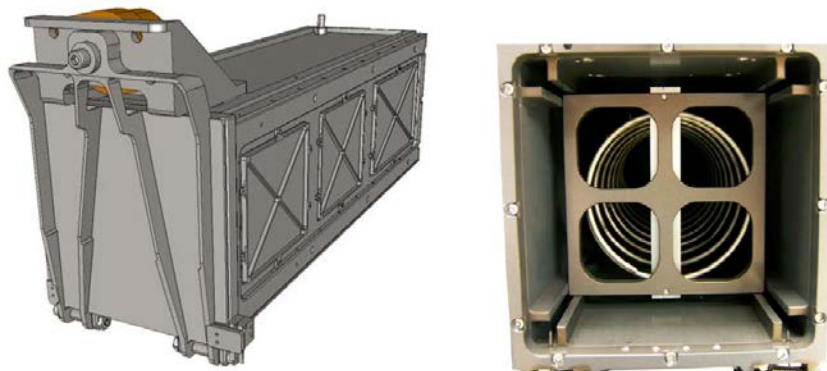


Figure 2. CAD Model of P-POD (left) and an Internal View of P-POD (right) [6]

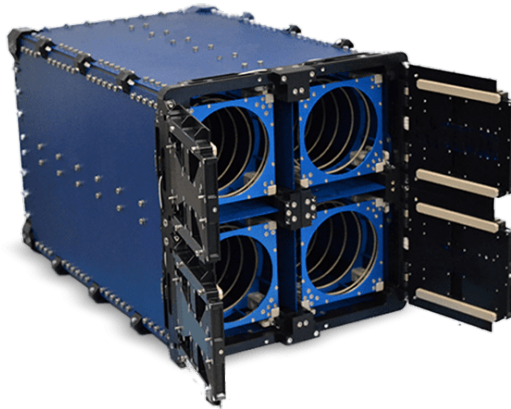


Figure 3. ISIS ISIPOD (4x3U QuadPack Version) [7]

Despite the deployer's simplicity in design and operation, a coil spring yields a non-uniform force being applied to the push-plate, and may transfer forces out of line with the CubeSat's center of mass. If the net force does not pass through the center of mass, it may yield an undesired torque on the CubeSat, which could introduce an initial spin during CubeSat deployment [4]. Moreover, these deployers use four guide rails, which required slight gaps with extremely tight tolerances in order to ensure proper rail alignment. In fact, improperly torqued screws can cause the structure to misalign and break tolerances [8]. Specifically, Cal Poly requires P-POD payloads have smooth guide rails with edges rounded to a minimum radius of 1mm. Moreover, at least 75% (85.125mm of a maximum of 113.5mm) of the rail must contact the deployer guide rails. The cross section of the P-POD payload must have a cross section of 100mm x 100mm [6]. Overall, there is a tolerance of a ± 0.1 mm gap for the payload to fit. The problem with these gaps is that it allows the CubeSat to vibrate during transportation and launch, which runs the risk of misalignment and subsequent rotating deployment or even failure

to deploy, as well as something as simple as an improperly torqued screw breaking the 0.1mm tolerance. [4]. According to PSC, Fig. 4 illustrates the risk of payloads with rails.

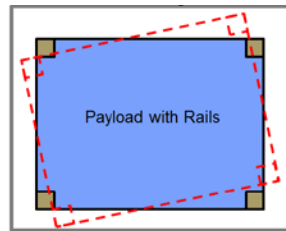


Figure 4. Risk of Payload with Rails [2]

As CubeSats continue to get more and more sophisticated, it becomes essential to provide an equally refined dispenser. PSC designed and qualified the CSD with the help of the Air Force Research Laboratory (AFRL), Kirtland AFB and the Operationally Responsive Space (ORS) office via a Small Business Innovative Research (SBIR) grant.

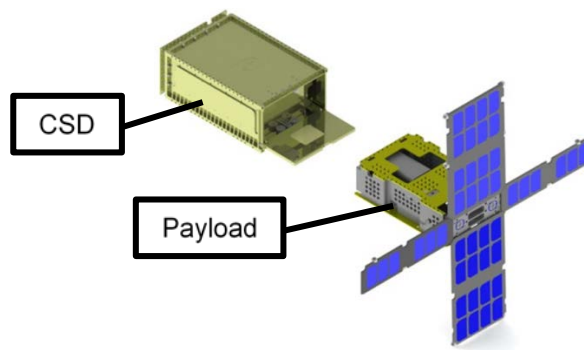


Figure 5. PSC Depiction of the CSD Deploying a CubeSat [2]

PSC created the CSD in order to combat uneven deployment forces and the four cumbersome guide rails. PSC addressed the deployment forces via the use of one (or more) constant-force springs (i.e. a wound steel band, like a tape measure). These two springs provide

an even and predictable dispensing force, as they do not obey Hooke's Law, where the force provided by a compressed spring is proportional to the compressed distance. Conversely, since the P-POD and ISIPOD have traditional coil springs, their deployment force is expected to decrease linearly [4]. The constant force springs are attached to a push plate, which subsequently thrusts the payload out of the canister. To ensure proper push plate contact, PSC specifications mandate that payloads must have at least three contact points interfacing with the push plate. Moreover, these contact points must envelope the payload's center of mass in order to avoid/reduce induced moments during ejection [9]. Fig. 6 below shows an example of contact feet installed on a CubeSat.

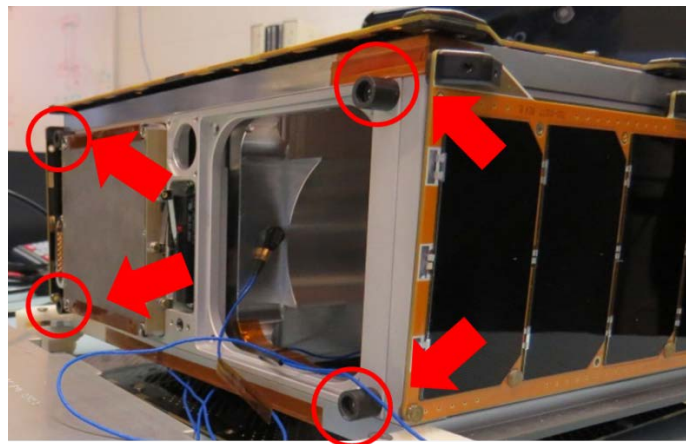


Figure 6. Contact Feet on the Pumpkin SUPERNOVA 6U CubeSat [10]

It is imperative that these contact feet or points be in full contact with the push plate, in order to avoid any moments being induced about the center of mass upon ejection. Fig. 7 provides an example of such uneven push plate contact, where the Pumpkin SUPERNOVA underwent

random vibrational analysis within the CSD, and the push plate yielded uneven wear marks. These uneven wear marks imply that the contact feet were not properly contacting the push plate, which could have a variety of root causes, originating from either the CubeSat or the CSD.

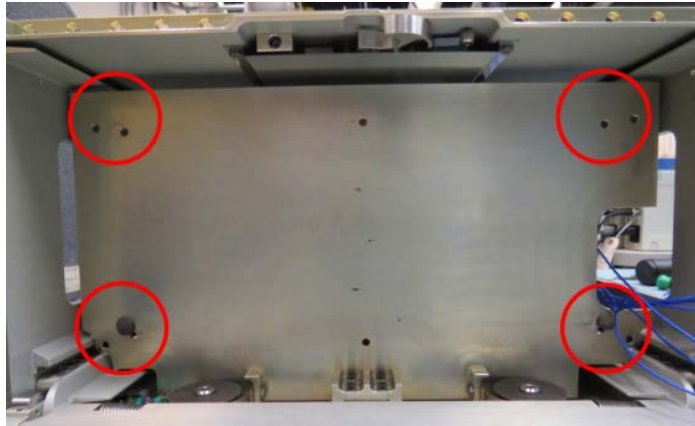


Figure 7. Wear Marks from Pumpkin SUPERNOVA Vibration Test [11]

Instead of guide rails, the CSD uses two clampdown guide rails. A CubeSat payload chassis has a base plate with two tabs running along the chassis sides.



Figure 8. 6U CSD-Compatible CubeSat Chassis with Tabs [12]

The tabs interface with two guide rails that provide a lateral channel to guide the payload as the payload is ejected [4]. The guide rails are also used to restrain the payload during launch, and this is done via clamps within the rails, where closing the CSD door automatically preloads the payload tabs. The benefit of preloading the payload to the CSD via tab clamping is that it creates a stiff invariant load, thus allowing accurate dynamic modeling to predict responses from vibratory testing and space flight [2].

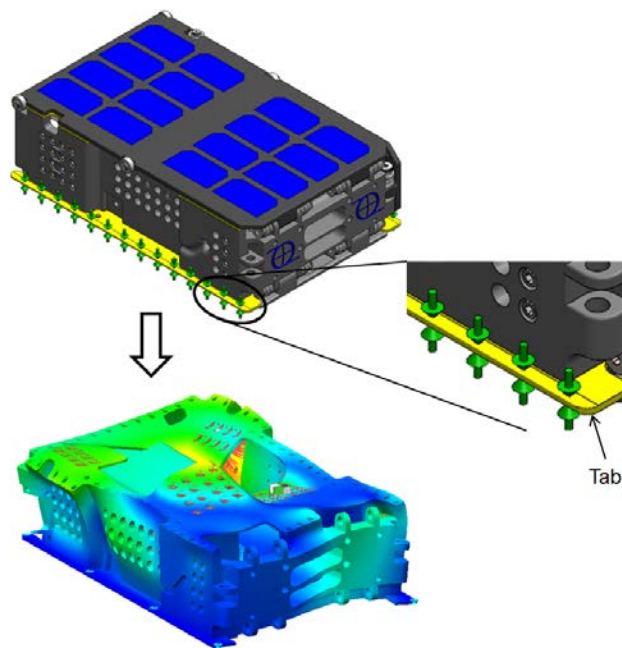


Figure 9. Payload and Predicted Dynamic Response Due to Preloaded Tabs [2]

According to PSC, the CSD (specifically the 3U variant) met Technology Readiness Level (TRL) 9 on its inaugural launch on 29 Sep 2013, when it deployed the Utah State University's Polar Orbiting Passive Atmospheric Calibration Sphere (POPACS) mission. POPACS was a secondary payload on the SpaceX Falcon 9 v1.1 CAScade, Smallsat and IOnospheric Polar Explorer (CASSIOPE) mission [13].

2.2 Initial Tests Conducted by Planetary Systems Corp

2.2.1 Motivation

A P-POD experienced a hang-fire in December 2010 where the deployer was triggered, the door opened, but no data was collected from the satellite. [1] This subsequently indicated a failure to deploy. Due to this hang fire, PSC was motivated in finding predictable rotation and velocity rates, mainly because they are crucial in determining initial conditions of a CubeSat spacecraft. Initial conditions are useful because engineers can use them to configure properly their satellites and their attitude control systems, as well as predicting how long it would take to build up satellite constellations. Moreover, it was their goal to determine failure modes and areas of deficiency in deployment operations prior to launch.

2.2.2 PSC Test Setup

In 2014, PSC conducted four days of deployment tests on a NASA C-9 “Vomit Comet” in order to measure rotation rates and velocities of payloads as they eject from a CSD (both done for 3U and 6U variants) in a simulated zero-g environment. Their setup, as shown in Fig. 10, consisted of an aluminum frame with a CSD affixed to it on one end, and a catcher net on the other end used to assist in stopping an ejected payload. A high-speed camera was also attached to the side of the test frame in order to provide visual verification of CSD ejection performance.

The CSD would deploy a payload mass representation at the maximum mass rating at that time for each configuration (6kg for 3U, 12kg for 6U) [2]. Inside this mass was an inertial

measurement unit (IMU) running at 50 Hz, which was used to gather linear and angular deployment data [3].

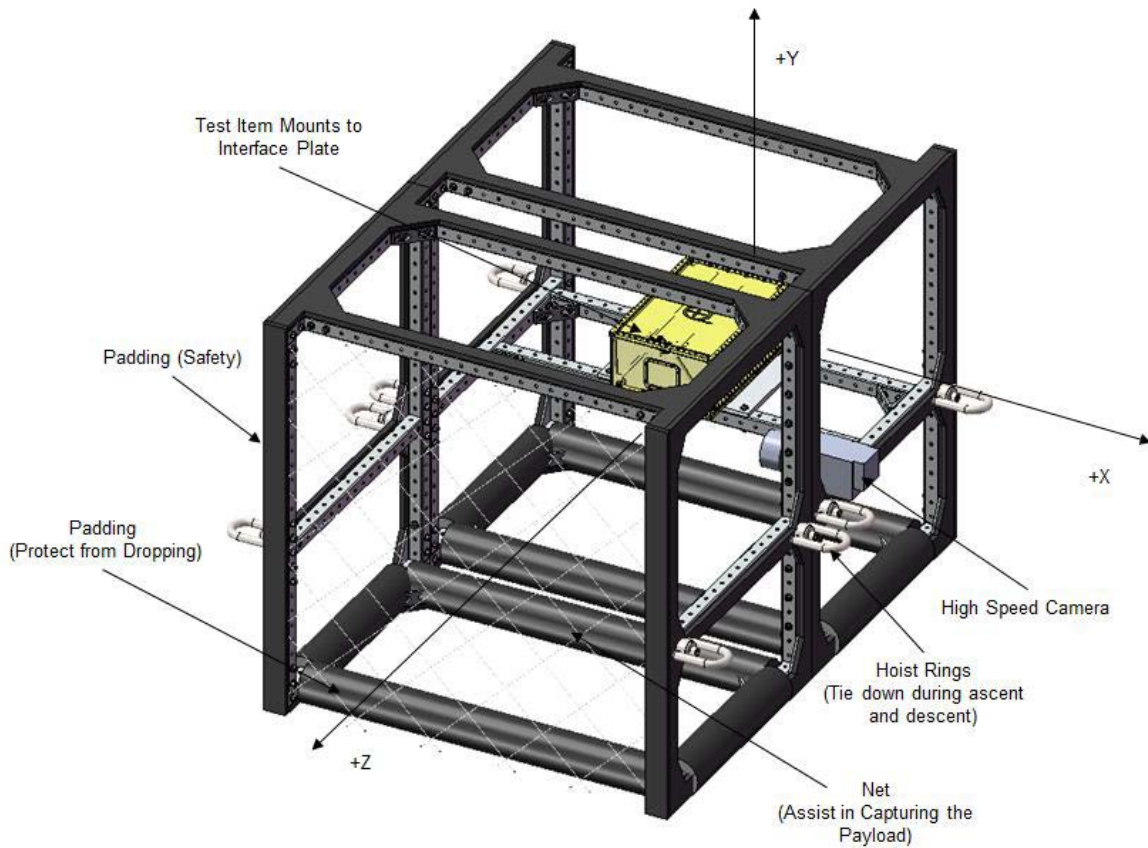


Figure 10. CSD C-9 Test Setup [1]

Per CSD spec, the mass payloads had three contact points centered on their respective centers of mass: the two tabs used with the CSD rail system, and a centered tab at the top [9]. (Shown below in Fig. 11)

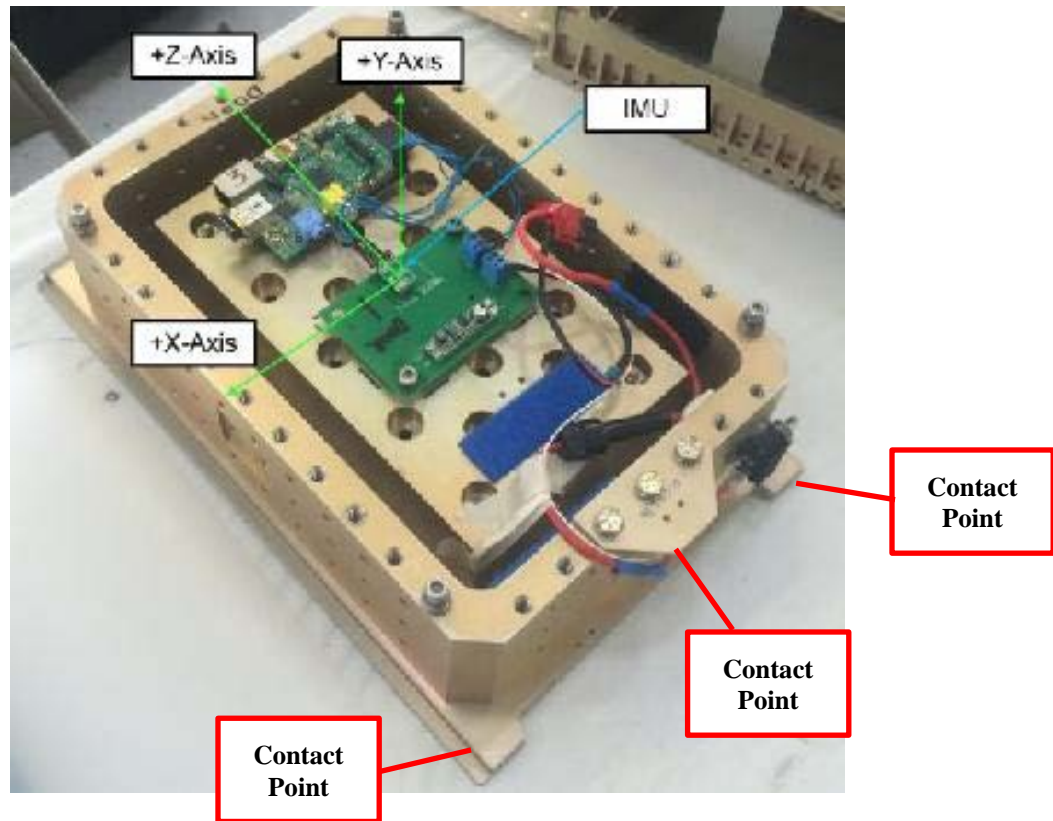


Figure 11. PSC Mass Representation with IMU (6U Variant Shown) [1]

The C-9 flies in a “parabola” flight path, where the plane first climbs with a pitch angle of 45° , and then the airplane is put into freefall by reducing thrust and lowering the nose in a neutral free-fall configuration. The plane and its occupants fall freely together, and since the plane shields the occupants, they experience no reaction forces. A lack of reaction forces yields a net “g” level of $\sim 0g$, or only experience the pull of gravity and nothing else, thus the occupants experience freefall, commonly referred to as “weightlessness”. This phenomenon thus creating a “weightless” environment until the airplane ends up pitching downward [14]. (Shown below in Fig. 12 and Fig. 13.)

It is good to note that 0g is more of a theoretical concept, as it is infinite in its reach. An object in freefall will still experience the effects of air drag, solar pressure, etc. However, it is possible to simulate microgravity, where fractions of a g can be achieved (from 10^{-2} to 10^{-6} g) [15].



Figure 12. C-9 “Vomit Comet”

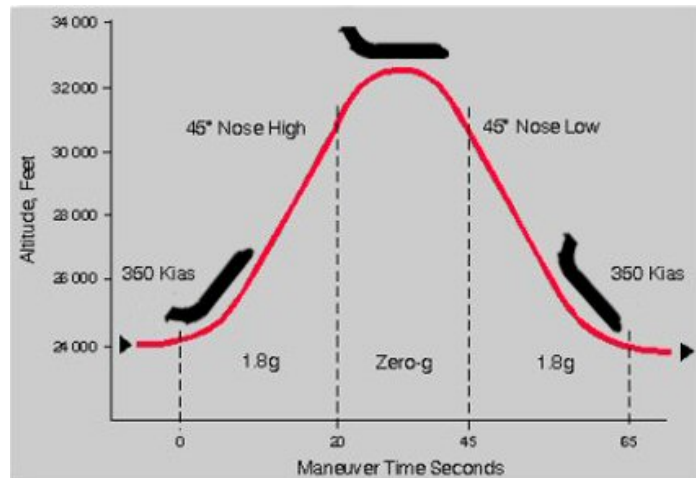


Figure 13. C-9 Flight Path to Produce Zero-G [1]

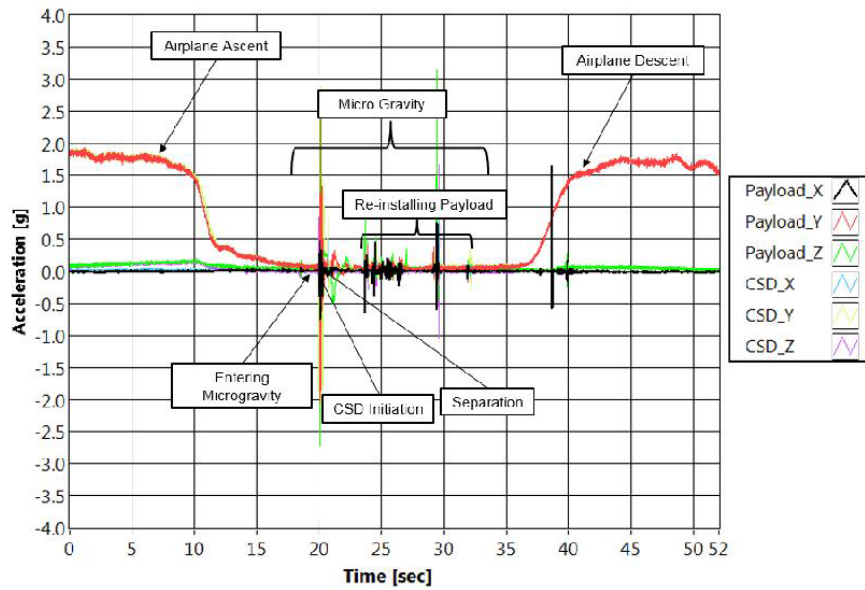


Figure 14. Raw Acceleration with Respect to Parabolic Flight Path [1]

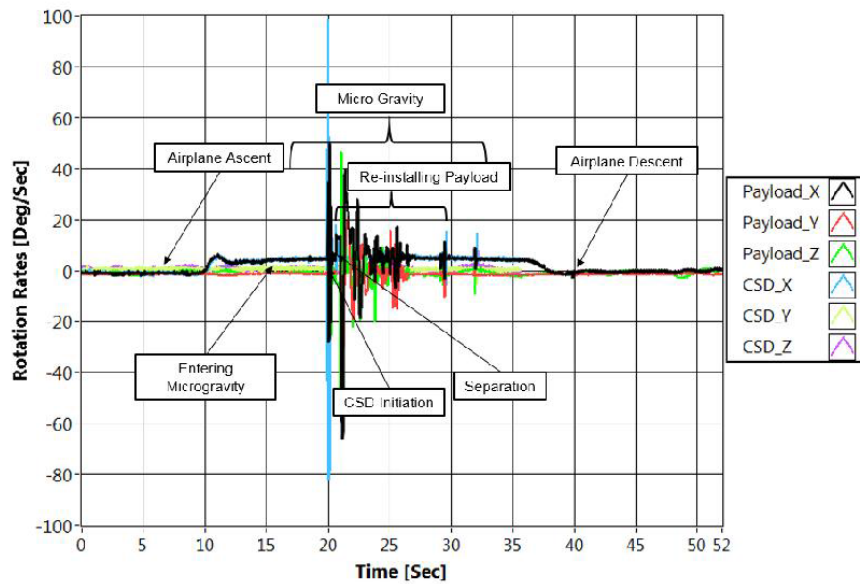


Figure 15. Raw Rotation Rate Data with Respect to Parabolic Flight Path [1]

2.2.3 PSC's Test Results

Upon analyzing raw data collected from the IMU, PSC researchers found that the CSD payload deployment rotation rates are 1-2 orders of magnitude lower than other dispensers [1]. They came to this conclusion when comparing with missions such as the SwissCube mission, which was deployed by a P-POD in 2009 [16]. According to their data, the SwissCube team from the Swiss Space Center reported an initial angular norm speed of over 600°/s, and required almost 500 days to bring norm angular rates down to 1-10 °/s due to magneto torque issues [17].

Unfortunately, PSC encountered multiple sources of error, primarily that the C-9 induces rates of rotation ($\sim 6^\circ/\text{s}$) not present in spaceflight. These initial induced rates yield higher measured angular rates after payload deployment. These couplings of pre and post rates are subsequently shown in Fig. 16.

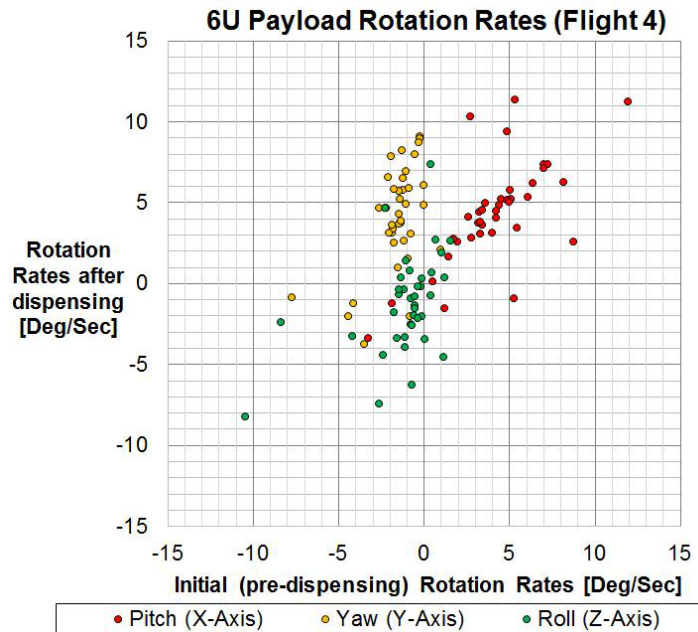


Figure 16. 6U CubeSat Payload Rotation Rates Coupled with Rotation from C-9 [1]

Another source of error noted was the IMU's bias and drift. This issue created substantial error in the measurement of ejection velocity, where the accelerometer would suddenly deviate from zero down to another "baseline" rate. This deviation subsequently skewed the collected data from the deployment tests, and required corrections. This is clearly shown below in Fig. 17.

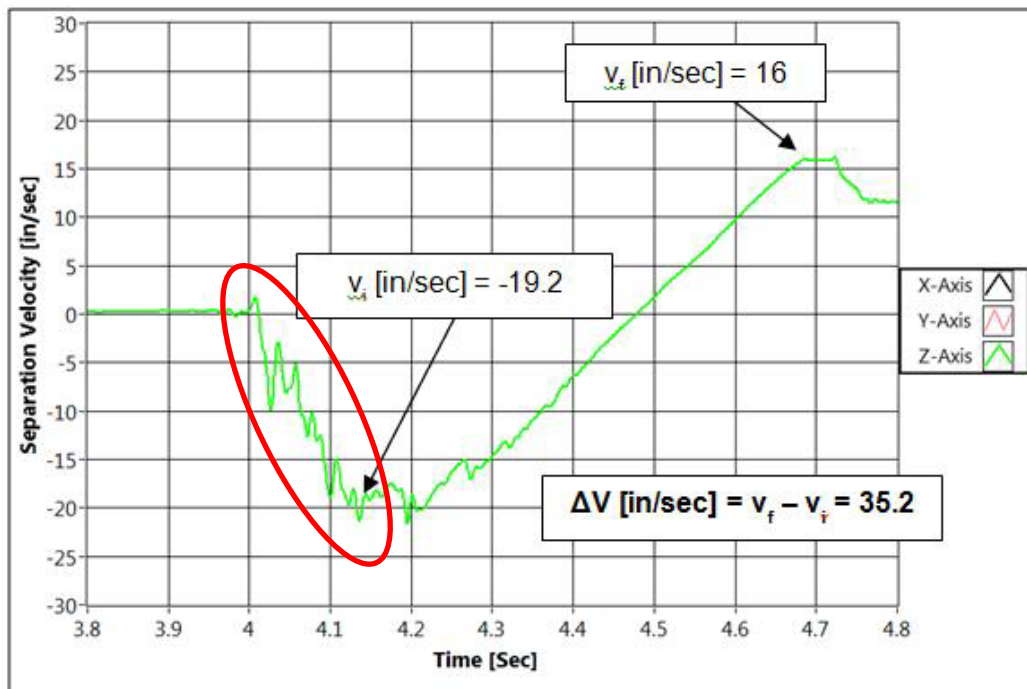


Figure 17. PSC's Accelerometer Data Showing Bias Drift Error [1]

PSC also encountered issues with their test setup. The frame used to secure the CSD was not stiff enough, as PSC noted that when the CSD door opened, oscillations/vibrations were produced. Moreover, the use of the C-9 included lots of tuning and acclimating (i.e. getting used to the flight profile of the C-9), which resulted in missing 24 out of 160 available (40 parabolas per day) dispensing opportunities. In fact, misalignment with the C-9's roll, pitch, and yaw

could explain why there were initial induced rates, as discussed earlier. Given this issue, it would probably take more than one flight campaign to attain all the desired data. Unfortunately, with a price tag of \$400K+ per flight, this would prove difficult from a budgetary perspective [1].

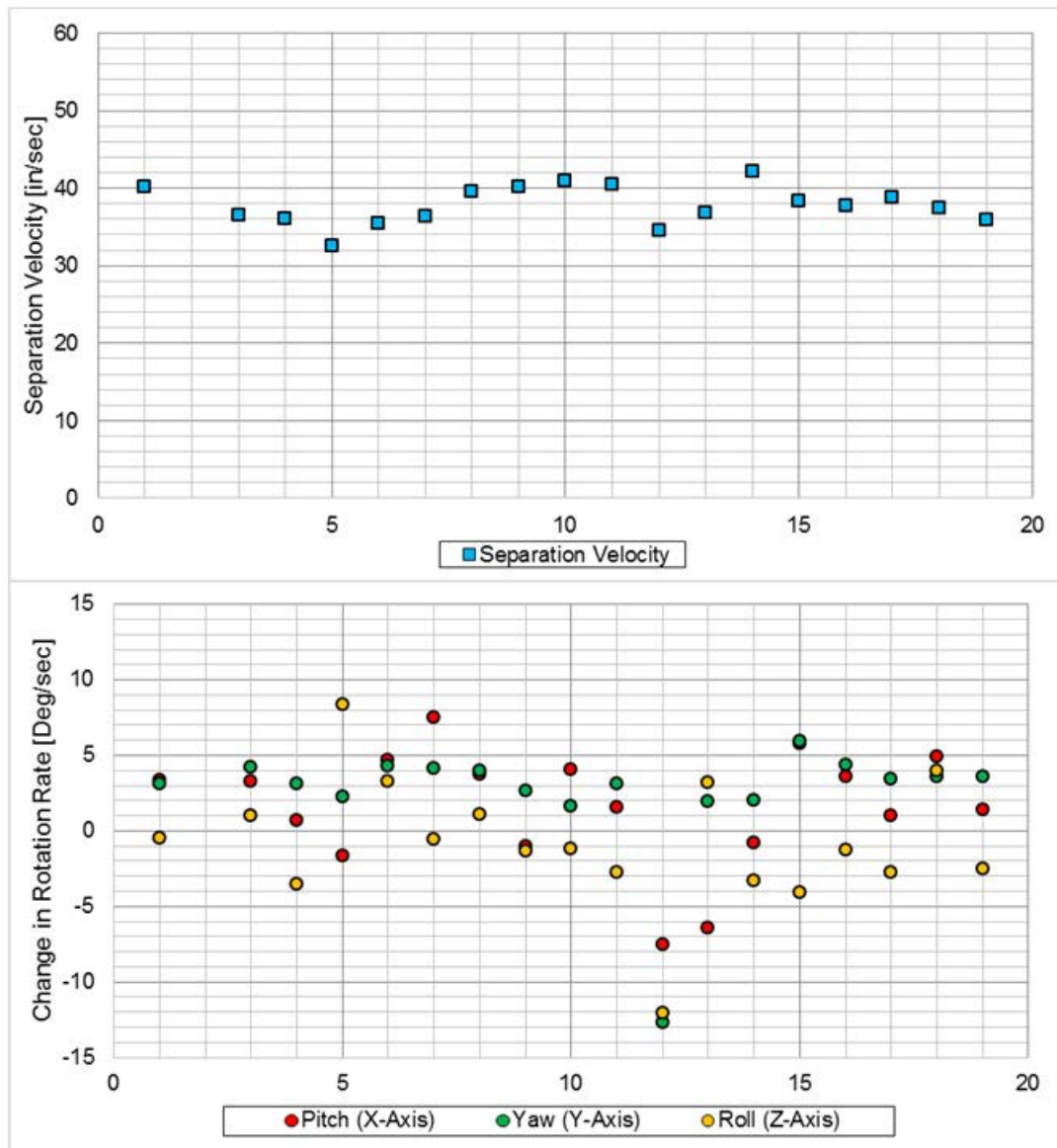


Figure 18. 3U Separation Results [2]

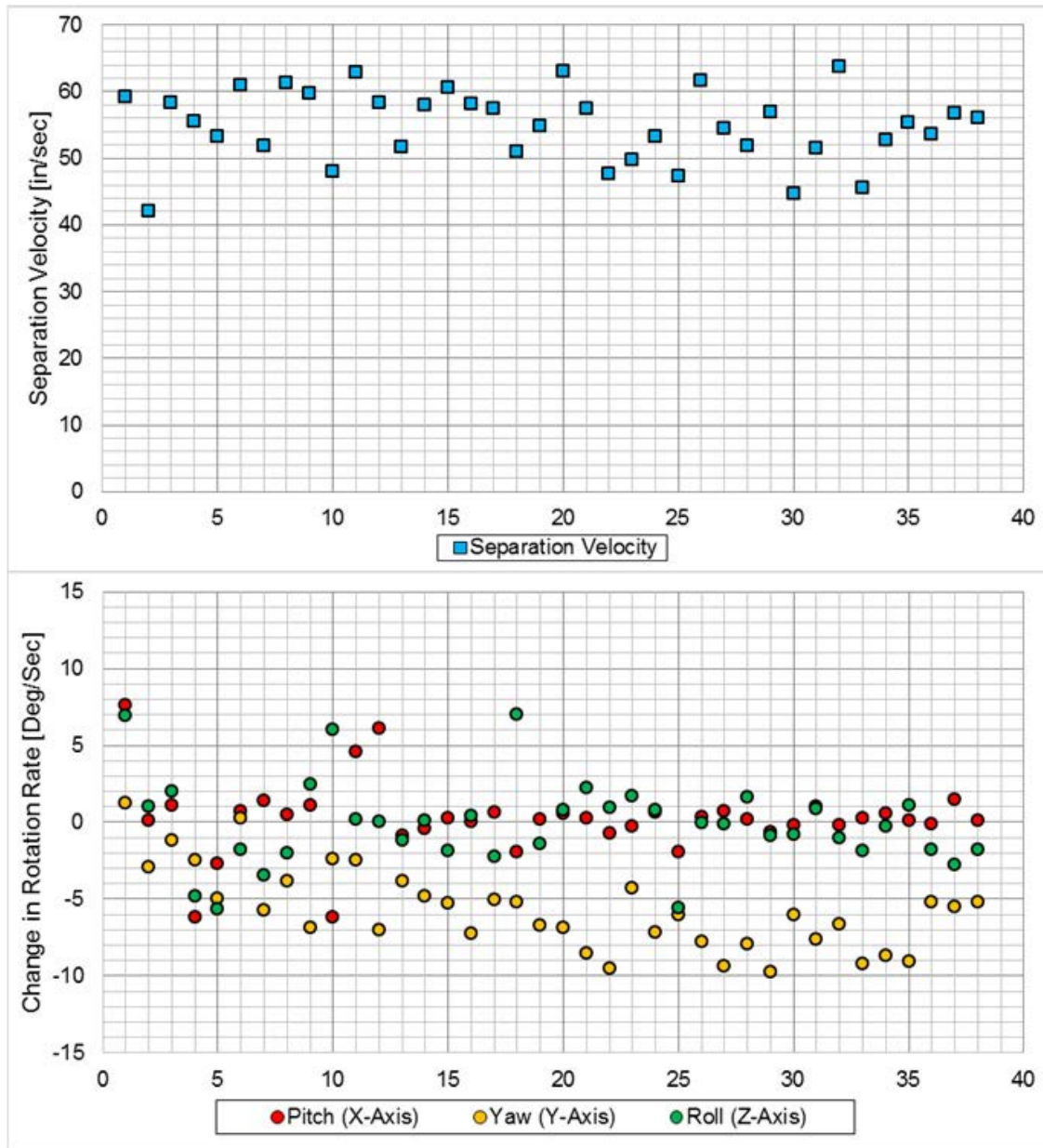


Figure 19. 6U Separation Results [2]

With the gathered data displayed above in Fig. 18 and Fig. 19, PSC was still able to use it to develop rudimentary linear ejection profiles seen in Fig. 20. Because the angular rate data

covered a wide range, the easiest way for PSC to characterize angular rotation due to ejection was to select the worst-case angular rate seen on any axis, which was around $10^\circ/\text{s}$ [2] [3].

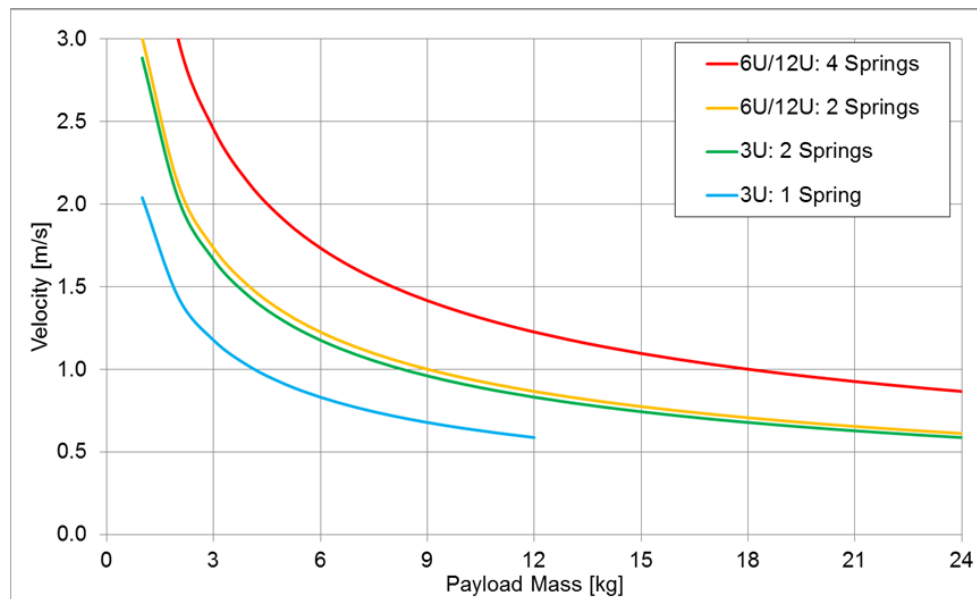


Figure 20. PSC Payload Ejection Velocity Profiles Based on C-9 Data [2]

2.3 NASA's Use of the CSD

NASA has purchased 13 CSDs from PSC to deploy secondary payloads for the maiden flight of the Space Launch System, Exploration Mission 1 (EM-1) [3]. The SLS Spacecraft and Payload Integration Office was tasked to manage the integration of 13 CubeSats from government, international mission partners, as well as independent and academic payloads that will be selected in a series of ground tournaments. These missions are expected to accomplish invaluable research [18] [19] [20]. Below are some of the current missions that have secured one of the 13 slots:

- NASA JPL/NASA Marshall/UCLA *Lunar Flashlight* – Mapping lunar ice and identify locations where resources can be extracted
- NASA Ames *BioSentinel* – Identifying effects of deep space radiation on DNA (specifically contained in yeast cells) over long durations in space
- NASA Marshall *NEA Scout* – rendezvous w/ a Near Earth Asteroid to survey asteroid characteristics/risks for future human exploration

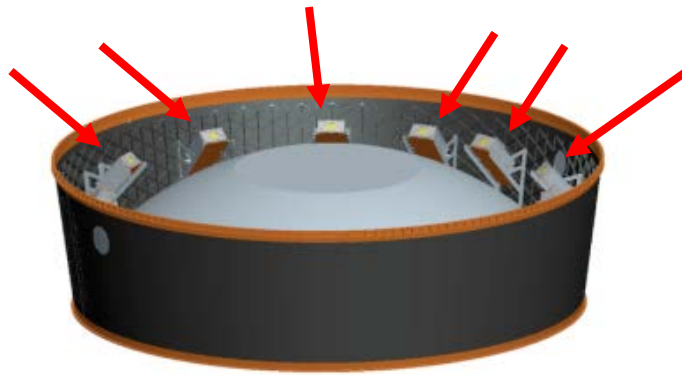


Figure 21. NASA CAD Rendition of CSDs (See Arrows) on SLS Upper-Stage Adaptor [18]

The 13 CSDs will be attached to SLS' Multi-Purpose Crew Vehicle (MPCV) Stage Adaptor (MSA) via an angled (56°) bracket, which will allow the each CSD to eject its designated payload through the Orion Stage Adaptor, as shown below in Fig. 22 [19].

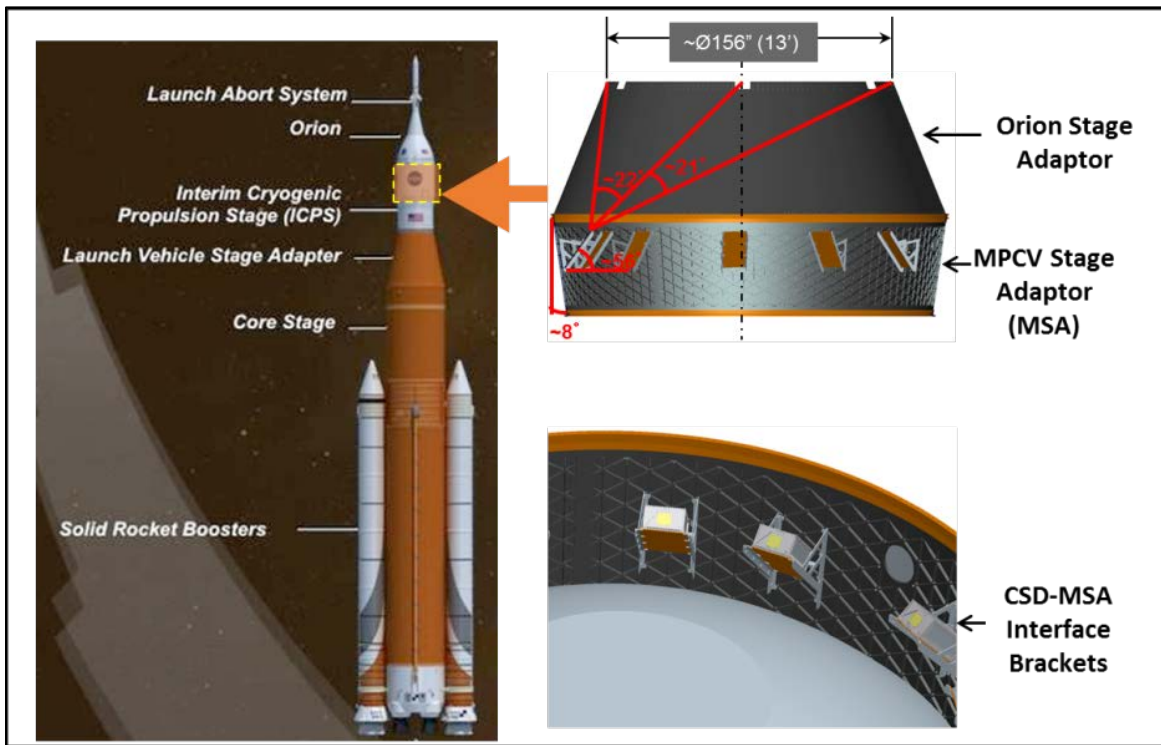


Figure 22. CSD Locations on SLS [19]

Within Fig. 22, the picture on the left shows the location of the stage adaptor with respect to the whole launch vehicle. The pictures on the right show the installation and orientation of the CSD, along with expected flight path [19].

To ensure the safety of both the SLS and secondary payloads, NASA is requiring that each CubeSat payload have a 4ft (1.219m) clearance zone upon ejection. A potential concern is that upon passing through the Orion Stage Adaptor, each payload's clearance "bubble" has only ~2.5ft (0.762m) clearance between it and the lip of the vehicle, as shown in Fig. 23 [19].

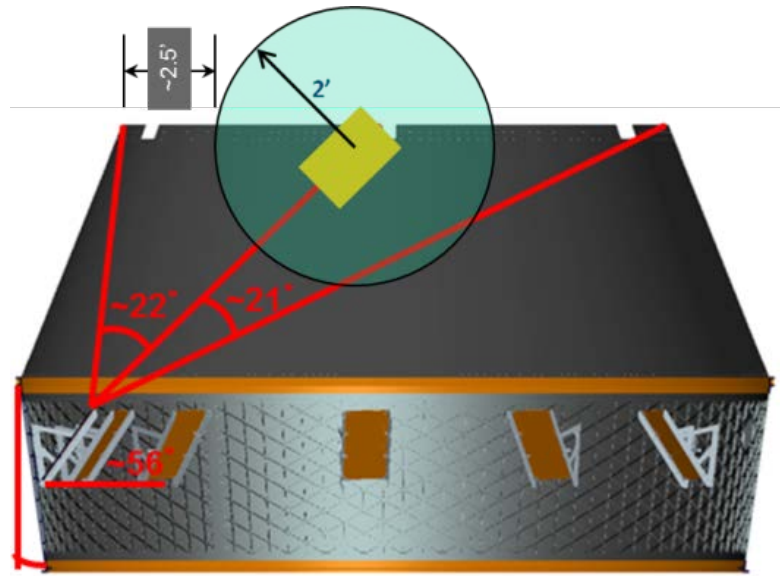


Figure 23. Payload “Bubble” Clearance Zone [19]

The configuration runs the risk that excessive CubeSat tumbling, coupled with induced transients from ejection (as suspected by PSC) could increase the risk of impact with the vehicle, which may result in collateral damage. This fact in itself is justification for the need to further refine the mapping of the CSD’s ejection profile. According to NASA’s Secondary Payload team, better understanding of how the CSD deploys, would aid payload developers in both their hardware design and attitude control system mission planning [19]. However, after coordinating with representatives from NASA Marshall and NASA Kennedy, they are content with what is currently in place, as there is no risk to the SLS vehicle itself.

Another notable item is that in order to simplify payload development, NASA is recommending CubeSat developers to not use the standard contact feet and instead only contact the push plate via the tabs on -Z face. This configuration avoids uneven feet contact, as the tabs

are at a set length, and potential push plate deflection. NASA has developed a prototype in which the tabs are extended to protrude on the $-Z$ face in order to provide a full contact bar.

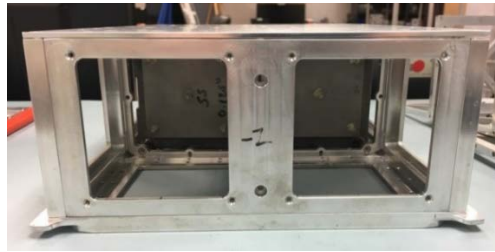


Figure 24. Chassis with Normal Tabs

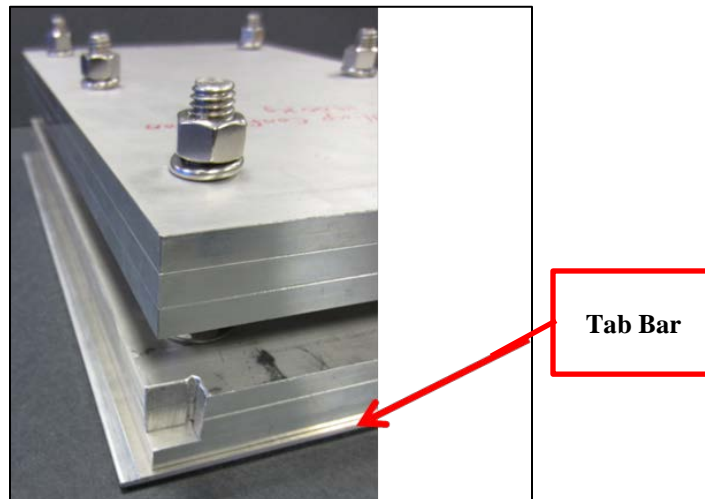


Figure 25. NASA Experimental CSD Test Mass with Tab Bar [19]

Despite being a design simplification, this will risk having an enhanced moment along the horizontal axis upon ejection. Unless the center of mass is close to the base plate of a CubeSat payload, the applied force is guaranteed to be offset from the center of mass, which will definitely induce a significant moment (assuming the center of mass is within the 80 mm x

60 mm window around the geometric center per PSC’s 6U payload spec) [9]. On the other hand, this setup does reduce moments along the vertical axis, which does allow mission planners to focus primarily on counteracting one induced moment upon deployment.

2.4 Characterization of Payload Motion as a Result of CSD Ejection

2.4.1 Rotational Motion

Because CubeSats are relatively small and compact for their typical masses, one can assume that it behaves as rigid body when deriving rotational equations of motion. In the angular realm, this is governance is described through a derivation of Newton’s Second Law which relates an applied moments \vec{M}_o about a point (denoted as subscript “o”) to the time derivative of a rigid body’s angular momentum \vec{H}_o . (Typically, this is about the body’s center of mass, which is case during this study) This relation is known as Euler’s Equation (Eq. (1)), and is the fundamental equation of rigid body dynamics. [21]

$$\vec{M}_o = \dot{\vec{H}}_o \quad (1)$$

$$\vec{H}_o = I_b \vec{\omega}^{bi} \quad (2)$$

$\vec{\omega}_{bi} \equiv$ Angular Velocities of the body frame with respect to inertial frame (bi)

$I_b \equiv$ Rigid body mass moments of inertia second order tensor

Inserting Eq. (2) into Eq. (1)., the relationship can be expanded further between the applied moment in the inertial frame (denoted with superscript “i”) and the time derivative of

angular momentum in the body frame (denoted with superscript “ b ”) via the Transport Theorem as shown below in Eq. (3), and simplified to yield it’s final form in Eq. (4). (The Transport theorem allows one to differentiate motion of a body expressed in the body frame, while expressing the final output in terms of the inertial frame).

$$\vec{M}_o = \frac{d}{dt} \vec{H} = \frac{d}{dt} \vec{H} + \vec{\omega}^{bi} \times \vec{H} \quad (3)$$

$$\vec{M}_o = I_b \dot{\vec{\omega}}^{bi} + \vec{\omega}^{bi} \times I_b \vec{\omega}^{bi} \quad (4)$$

Eq. (4) relates external torques/moments \vec{M}_o to angular velocities $\vec{\omega}^{bi}$ and accelerations $\dot{\vec{\omega}}^{bi}$. Moreover, Euler’s equations is a set of three nonlinear, coupled, a first order differential equations. Eq. (4) can be seen if it is expanded to fully show the moments in all three axes shown as.

$$M_x = I_x \dot{\omega}_x - (I_y - I_z) \omega_y \omega_z \quad (5)$$

$$M_y = I_y \dot{\omega}_y - (I_z - I_x) \omega_z \omega_x \quad (6)$$

$$M_z = I_z \dot{\omega}_z - (I_x - I_y) \omega_x \omega_y \quad (7)$$

For the case of a deploying CubeSat, the main concern would be the moment side of the equation, as many, CubeSats do not have sophisticated measures to counter external torques, with the exception of reaction wheels, magnetic torquers (common), and (unlikely) thrusters.

The other set of equations are the kinematic equations. The kinematic equations define the relation between angular velocity and orientation parameter derivatives, also known as the spacecraft’s attitude. There are two primary forms of kinematic equations: Euler’s Equations,

which uses an orientation angles form (Eq. (8) for a 3-2-1 rotation sequence in this case) and quaternion form (Eq. (9)) [22]

$$\dot{\boldsymbol{\theta}} = \begin{bmatrix} 0 & \sin\theta_3/\cos\theta_2 & \cos\theta_3/\cos\theta_2 \\ 0 & \cos\theta_3 & -\sin\theta_3 \\ 1 & \sin\theta_3\sin\theta_2/\cos\theta_2 & \cos\theta_3\sin\theta_2/\cos\theta_2 \end{bmatrix} \quad (8)$$

$$\dot{\underline{\mathbf{q}}} = \frac{1}{2} \begin{bmatrix} \mathbf{q}^\times + q_4 \mathbf{1} \\ -\underline{\mathbf{q}}^T \end{bmatrix} \quad (9)$$

To fully define the spacecraft's state, as described in Eq. (10) using Euler angles, and Eq. (11) using quaternions, the kinematic and kinetic variables are arranged together in an array. [23]

$$\bar{\mathbf{x}} = [\theta_1 \ \theta_2 \ \theta_3 \ \omega_1 \ \omega_2 \ \omega_3]^T \quad (10)$$

$$\bar{\mathbf{x}} = [q_1 \ q_2 \ q_3 \ q_4 \ \omega_1 \ \omega_2 \ \omega_3]^T \quad (11)$$

2.4.2 Linear Motion

The linear equations of motion are developed from Newton's Second Law. The push plate acceleration $a_{payload}$, can be measured with an accelerometer. The payload and push plate acceleration, (which are assumed coupled at this point by virtue of the push plate making the payload accelerate with it), would be the same during ejection. Using the determined acceleration and given a known payload mass $m_{payload}$, the dynamic push plate force $F_{push \ plate}$ can be determined. This relationship can be described.

$$F_{push \ plate} = m_{payload} a_{payload} \quad (12)$$

Using data collected from the accelerometer/IMU attached to the payload, the linear velocity of the payload can be determined through a single integration of the data with respect to time, as seen in Eq. (13).

$$v_{payload} = \int_{t_1}^{t_2} a_{payload} dt \quad (13)$$

Because accelerometer/IMU data does not have elementary functions as antiderivatives, a method like the Trapezoidal rule would be useful, as all is needed is the collected data (i.e. acceleration) and the associated time intervals (which are consistent by virtue of accelerometer/IMU settings). An added benefit of integrating this data is that noise is reduced versus directly measuring velocity or position at high rates.

To compute displacement, the acceleration data needs to be integrated twice the same way (i.e. calculated velocity data is integrated once), as seen in Eq. 14.

$$d_{payload} = \int_{t_1}^{t_2} v_{payload} dt = \iint_{t_1}^{t_2} a_{payload} dt \quad (14)$$

2.4.3 Motion Data Gathering

Now that we have discussed the dynamics Equations of Motion and the linear kinetics, we will now discuss how accelerometers and gyroscopes work. PSC used both an IMU and a high-speed camera to gather performance data on CSD payload ejection performance. An IMU is a device that measures a body's acceleration via an accelerometer, and angular rates via a one or multiple gyroscopes, or a set of accelerometers.

Accelerometers typically work by sensing stresses due to forces felt during acceleration. A common type of accelerometer used in industry is via piezoelectric effects, where an accelerometer has microscopic crystal structures that when experiencing stress from a force due to acceleration, a voltage is created (see Fig. 26 below). Through calibration, the level of voltage is associated with the level of acceleration experienced. Another common method is measuring the change in capacitance between two microscopic structures while being stressed. This change is subsequently converted into voltage change, which again is measured against calibrated acceleration levels [24].

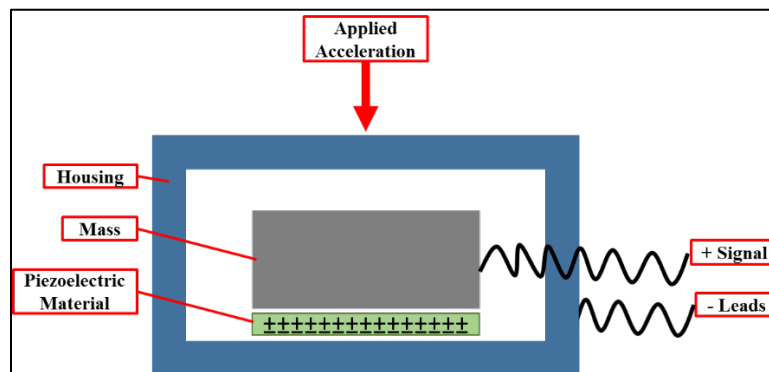


Figure 26. Piezoelectric Accelerometer Function [25]

Gyroscopes traditionally work by having a spinning wheel mass around an axis, and they sense changes in angular rates through the measuring of applied Coriolis acceleration to the sensor/wheel. A popular form of gyroscope these days is the microelectromechanical system (MEMS), as they are compact, inexpensive, and getting more accurate over the years. MEMS gyroscopes have a small resonating mass (e.g. like a tuning fork) commonly made out of silicon

crystal. When a gyroscope is rotated, the resonating mass is shifted when there are changes in angular velocity (as seen in Fig. 27 below). This movement is converted to an electrical signal, which is read as an angular rate by a microcontroller [26].

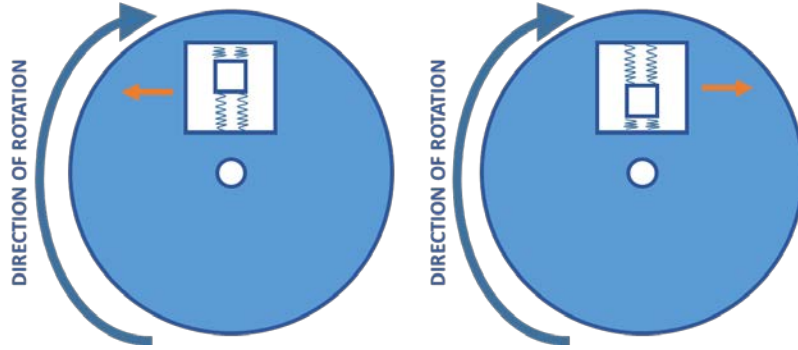


Figure 27. Internal Operational View of a MEMS Gyroscope [25]

High speed cameras are one of the most basic methods to measure an object's motion, as they provide a set frame rate, which is used as a constant time interval dt . For example, if a camera is run at 10,000 frames/s, then an analyst knows that the time difference between two sequential photographs is 0.0001 s. Because the frame rate is constant, the time difference is also constant. In this research, high-speed photography is calibrated by first taking a picture of a known reference length. Just like a scale distance in a map, this reference length is used to compare changes in motion detected in photograph analysis. Change in position is measured with respect to the reference length, and differentiated by the known time (Eq. 15). Acceleration is subsequently found by differentiating one more time (Eq. 16).

$$\vec{v}_{instantaneous} = \lim_{\Delta t \rightarrow 0} \frac{\Delta \vec{x}}{\Delta t} = \frac{d\vec{x}}{dt} \quad (15)$$

$$\vec{a}_{instantaneous} = \lim_{\Delta t \rightarrow 0} \frac{\Delta \vec{v}}{\Delta t} = \frac{d\vec{v}}{dt} = \frac{d^2\vec{x}}{dt^2} \quad (16)$$

One must take extreme caution when differentiating this data, as differentiation amplifies small errors in the displacement vs time data, and can occur with high frequency [27]. Moreover, any noise that is differentiated will be magnified, thus generating even more noise. Errors from high-speed camera data primarily come from mismeasurement of the change in displacement either through perception error, or through a phenomenon known as “pixel lock.” Pixel lock is a bias error where a signal peak location or image is biased towards the nearest pixel, primarily when an image occupies two pixel spaces and results in the image representation shifting towards the nearest subsequent pixel [28]. This is typically mitigated through having a sampling rate much faster than the velocity of the test article [29]. Also, by having high pixel resolution, it is an inherent source of uncertainty because error is at a minimum one pixel of uncertainty in the location.

2.4.4 Potential Sources of Perturbations

In order to accurately model the CSD, its errors and perturbations must also be accounted for, as it makes the data more realistic. A main source of perturbation would be from friction. However, the guide rails of the CSD are lined with roller pin bearings on the bottom, the top of the rails are of a coated metal surface. Any imbalance when the clamping force of the rails release could result in contact being made with the payload tabs. Another source of interference could be from the door upon opening, as it is spring-loaded. A final possible source

of perturbation actually deals with the payload itself. PSC requirements state that a payload must have at least three contact points centered on the center of mass touching the push plate [9]. When working nominally, no moments would be induced during deployment. However, if there is an imbalance on contact points, etc., then a moment will be imparted about the center of mass.

2.5 Deployment Evaluation Methodology Options

Various experiments are needed to verify tune dynamic model predictions through testing the characterizations described previously in Section 2.5. These experiments would ideally negate gravitational and air drag interferences. Aside from the previously described NASA C-9 “Vomit Comet,” the other main options considered include local lab-based experimental setups and the micro-gravity drop towers at NASA Glenn Research Center (GRC) in Cleveland, OH.

2.5.1 Lab-Based Experimental Setup Options

Building an apparatus locally at AFIT using commercial off-the-shelf supplies is the default option when determining an experimental setup. The following concepts were considered based on the need to gather valuable data while minimizing the effects of gravity and air drag.

1. Horizontal Deployment

- This method is the most simple where the CSD is affixed to the top of a table, and right below the CSD on the floor, a catcher is placed. Once the payload is ejected, it freefalls until it hits the catcher on the floor.
- Pros: simple design, allows payload free rotation without interference while in flight, compact footprint, and it's easy to accommodate various CubeSat sizes since all that is required is to place and secure a CSD on a table/platform.
- Cons: gravity needs to be negated (heavy bias on pitch motion of payload), wear to CSD and payload tabs as they are designed to be used in micro-gravity [2] [3]

2. Horizontal Deployment on a Low-Friction Surface

- In this method, the CSD is placed on a surface along with a low-friction track (e.g. air table, greased/lubricated surface, maglev, rollers, etc.) At the end of the track, a catcher is placed. In order to prevent interference between the CSD and track, either the CSD door has to be modified (e.g. remove the door and replace with an actuator that would allow the clamping tabs to be engage), or space needs to be made in the track to accommodate the door.
- Pros: simple design, negates gravity via low friction barrier, could potentially be used in a vacuum chamber.

- Cons: low friction track takes up floor space, may require modification of the CSD, and interferes with rotation about the pitch and roll rotation of the ejected payload. Safety would also be a concern if drops were long.

3. Downward vertical deployment with flywheel arrestor

- In this method, the CSD is suspended in a downwards configuration. A hole would have to be cut in the backside of the CSD and the pusher plate in order to accommodate a tether, which would be connected to a flywheel affixed above the CSD. The Payload is then jettisoned downward out of the CSD and freefalls while the flywheel eventually applies gradual resistance (e.g. through an electric motor) until the payload stops. Right below the CSD, a foam pit/net could be installed if desired. This configuration is limited to lighter weights in order to ensure the force of gravity does not negate the acceleration due to the push plate.
- Pros: Allows free rotation to a degree without interference during freefall. Pitch and yaw of the payload would experience some constraint when tether physical limits are met. This configuration has a compact footprint, and would not take up much floor space. It would also be able to accommodate various CSD sizes.
- Cons: Gravity would need to be negated, and gravity limits use of lighter payloads only. Tether can interfere with rotations, and the use of said tether requires a hole to be cut/drilled into the CSD and pusher plate. Finally, the

payload would need an acceptable tether point. Safety would also be a concern if drops were long.

4. Downward vertical deployment with catcher

- In this method, the CSD is suspended in a downwards configuration. The Payload is then jettisoned downward out of the CSD and freefalls until the payload is stopped by a foam pit/net. This configuration is limited to lighter weights in order to ensure the force of gravity does not negate the push plate acceleration.
- Pros: The design is simple, does not take up much space, and allows full free rotation without interference during freefall. It also can accommodate any CubeSat size.
- Cons: Gravity would need to be negated, and gravity limits use of lighter payloads only.

2.5.2 Micro-Gravity Drop Towers

Drop towers operate on the principle of literal freefall, where a test subject is isolated from external forces (i.e. air drag) either through use of a vacuum chamber, or a drag shield. NASA GRC has two drop towers: a 5.18 and a 2.2 second (s) tower.

The 5.18 s works by providing a 1.6 m long, 1 m diameter cylinder envelope for experiments to be installed in. This tower utilizes a 143 m steel vacuum chamber set to a

pressure of 0.01 torr, which evacuates most of the air. The experiment within the envelope is hoisted to the top of the tower, and when depressurization is complete, the experiment is able to fall freely for 132m at an acceleration less than $0.00001g$ [30]. Three drops can be done per day, at about \$8000 per day without permits and labor costs [31].



Figure 28. NASA GRC 5.18 s Drop Tower with Experiment Being Hoisted [32]

NASA GRC also has the 24 m (79 ft) 2.2 s drop tower, which is a more affordable option (at about \$2000 per day without labor, etc.) for smaller experiments [31].

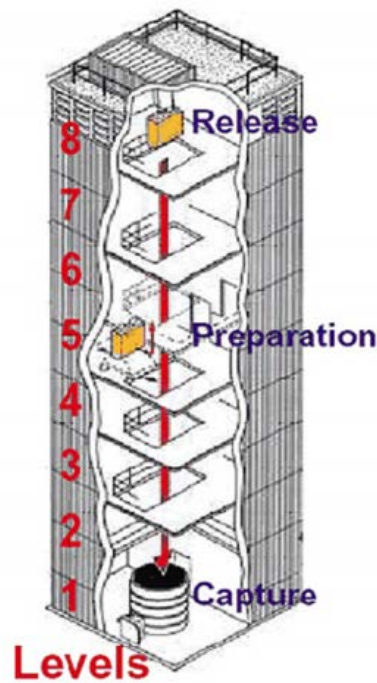


Figure 29. Preps (top left), Hoisting (top right), and Tower Rendition (bottom), [32]

The tower works by having an experiment sit within a frame, which is then placed in a drag shield. Both the drag shield and inner frame are suspended and subsequently dropped. The drag shield protects the inner experiment frame from air drag, thus allowing the experimental

frame to freefall and experience microgravity, as shown in Fig. 30. Since there is no vacuum chamber, up to 12 drops can be accomplished per day.

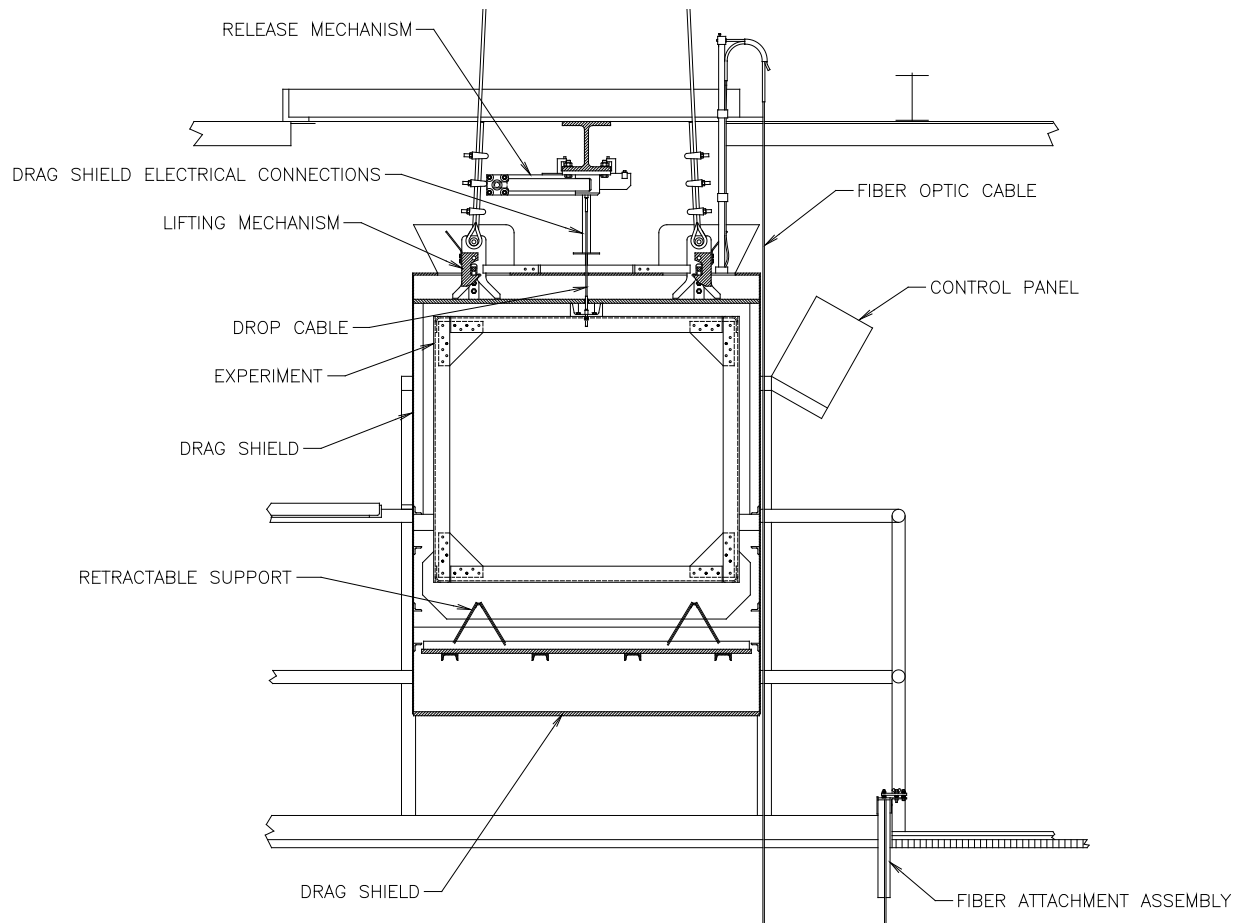


Figure 30. Tower Experiment Setup [33]

2.5.3 Deployment Evaluation Methodology Analysis

After weighing all options with the AFIT team who assisted with this project, the following items were determined for each option:

1. Lab-Based Experimental Setup

- Pros: Most affordable because of commercial “off-the-shelf” materials as well as use of AFIT personnel to build and operate apparatus.
 - Cons: These would cost time to build a new setup, and depending on the degree of deployments, safety regulations/certifications may be required. Moreover, it is difficult to counter gravity-induced errors. If the deployment tests are vertical, gravity will need to be counteracted *if* the ejection acceleration is greater than gravitational acceleration. This will definitely limit heavier test articles, as the push plate will have no chance of applying acceleration on the payload since gravity would have already pulled down on it. If the deployment tests are horizontal, wear on the CSD is a risk, as the rails are not designed for extensive wear caused by tipping payloads due to gravity-induced moments [3]. A counteracting apparatus (e.g. roller bearing leveling out an ejecting payload to provide grinding on guide rails, etc.) will have to be created, which PSC has done. However, this frustrates collecting worthwhile deployment data, as any data would be corrupted. Finally, these could take up a lot of space. AFIT is limited on available space.
2. Zero-Gravity Drop Towers (either 2.2 s or 5.18 s drops) at NASA Glenn Research Center (GRC)
- Pros: The towers are simple in concept, and have had tens of thousands of successful experiments. Experiments are in freefall because they are literally falling freely, thus they are experiencing microgravity. A bonus is that infrastructure at NASA GRC already exists, so the only thing needed to be built

is a custom frame to house the CSD, and required distance to allow a payload to be ejected (discussed later). Because the towers are in a controlled area by subject matter experts dedicated to these types of experiments, the towers are much safer.

- Cons: Experiments are limited to operate only in specific envelopes. (More about this later). Moreover, pricing can be beyond some budgets (e.g. ~2k/day without including prep and labor) [31] [30] [32].

3. NASA C-9 “Vomit Comet”

- Pros: In one day, one can achieve many (up to 160) opportunities of micro-gravity to conduct tests [1]. Moreover, the large test area in the main bay of the airplane enables a larger span to gather valuable data.
- Cons: This is most expensive option (~\$400k/day) [1]. As PSC found out, it is very difficult to configure experiment due to pre-existing rotational rates. Finally, this service is no longer available due to budget cuts [34].

Summary

Based on lessons learned from PSC, it is necessary to use isolated tests to identify friction and other perturbations experienced upon ejection. Moreover, it was decided that horizontal and vertical free deployments were to be utilized with base plates only in order to gather notional data through the use of accelerometers and IMUs directly attached to payloads, along with (when possible) to verify motion through the use of a high speed camera. The

objective was to use this data to preliminarily test a MATLAB-based simulator model, which would be used to predict deployment translational and rotational rates.

The model was initially created through the application of the kinetic and kinematic equations, along with using the physical geometry of the CSD. In the next chapter, how the model was created and how it was tuned will be discussed in further detail. Moreover, in addition to lab tests, it was also decided to try to pursue the NASA Glenn Research Center's drop tower facility in Cleveland, OH, as it is the most cost-effective solution to gather true data on ejection performance in a microgravity environment, as the CSD is specifically designed to operate in these conditions. As mentioned before, PSC highly advises against gravity deployments. Use of the drop tower will be discussed in further detail in Chapter 5.

III. Methodology

Chapter Overview

This chapter describes the experiments taken to characterize deployment dynamics of the CSD in order to create and tune an analytical model for predicting on-orbit behavior. These individual tests aim to isolate each possible variable that could have an effect on a payload's deployment performance. At the end of the chapter, the simulation model will be discussed as a whole to give a general overview of its form and function. Chapter IV will provide the data and results from every test described in this chapter.

3.1 Push Plate Force Test

The objective of the Push Plate Force Test is to create a preliminary 6/12U CSD push plate force profile by gathering static force readings at 10 evenly spaced push plate depression depths. PSC has adopted the use of a constant force spring system in order to provide a more predictable deployer to reduce uneven deployment profiles that are prevalent with other systems [4]. The test required the creation of a frame that bolted to a 12U CSD, as shown in Fig. 31, and a spring push/pull gauge that was guided by a rod [35]. The calibrated push/pull gauge used had a maximum reading of 10 lbs (44.482 N), with an accuracy of +/- 0.1 lbs (0.444 N). The gauge was centered onto the CSD push plate by the frame, and the guide rod had 10 equally spaced depth increments between the push plate being fully depressed and fully extended. At each increment, the push plate was manually pushed back to give the gauge/rod enough clearance to be set and locked at a specific depth, and then the plate was gently released to press onto the gauge, thus applying a force. Afterwards, the plate again would be depressed, the rod was taken

out, and the force was read and recorded. This was repeated for each of the 10 measurement points. Each point was measured three times, yielding 30 data points. These measurements were valid for both 6U and 12U CSDs because they use the same spring configurations (2 or 4 springs) yielding a range of 15.6 N - 46.7 N [2].

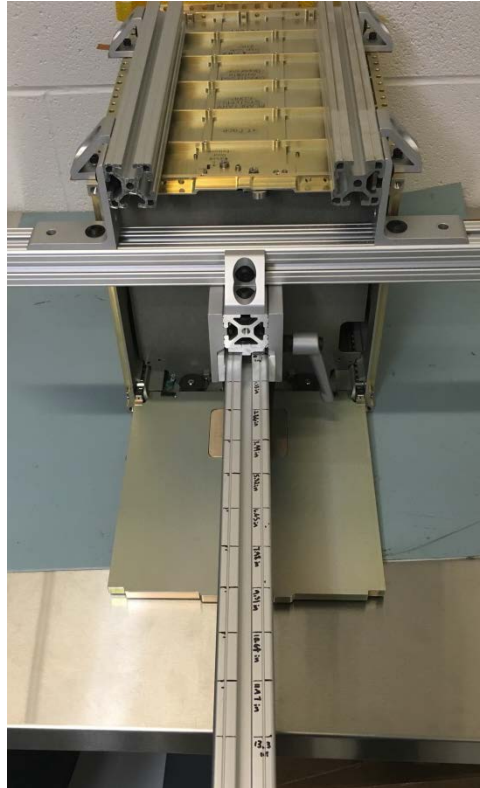


Figure 31. CSD with Static Force Reading Apparatus



Figure 32. Push/Pull Gauge on Guide Rod

3.2 Initial CSD Ejection Velocity Test

The purpose of this test is to obtain a rough measurement of the CSD deployment linear velocity using an empty chassis (or base plate), along with the Midé Slam Stick X accelerometer.



Figure 33. Midé Slam Stick [36]

The Slam Stick X is a simple pre-calibrated self-contained piezoelectric accelerometer intended to be used for qualification testing and high frequency vibrations [36]. Below in Fig. 34 is a summary of the Slam Stick X's error profile.

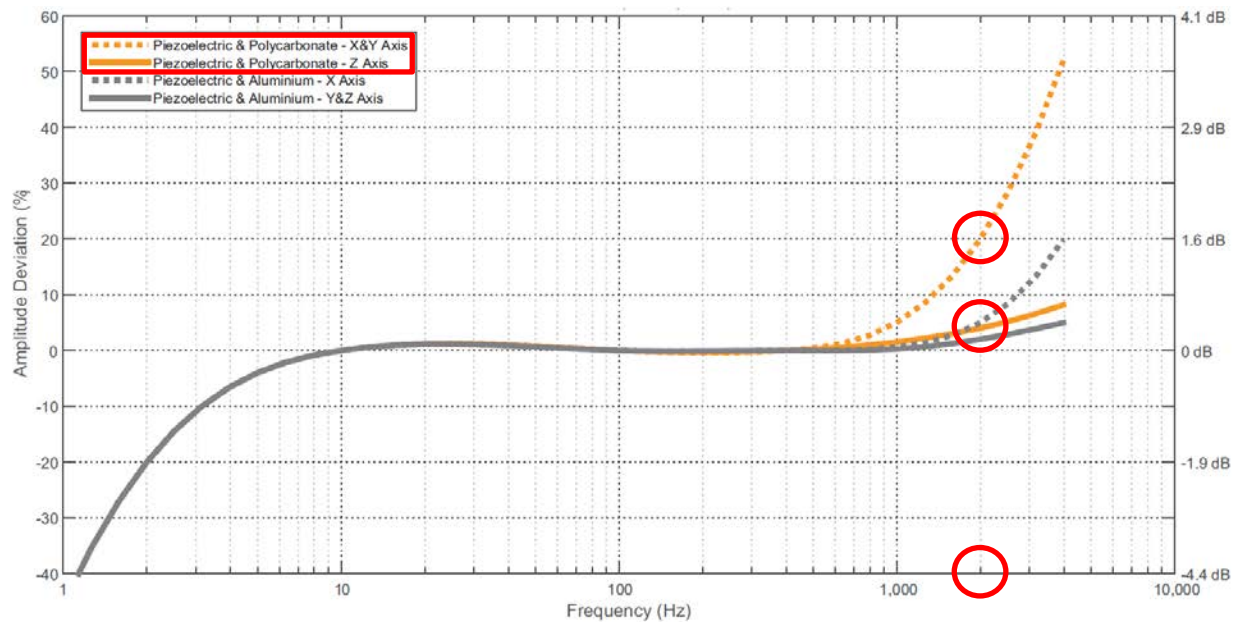


Figure 34. Slam Stick X Error Profile [37]

The Slam Stick was set to run at 2000 Hz, as it was estimated that a CSD deployment would be fast, but with a short duration according to PSC data (~ 3 m/s) [2]. With that, error on the X and Y-axes was rated with a deviation of 20% amplitude (g's), and $\sim 5\%$ (g's) on the Z-axis. Once the Slam Stick is attached (via double-sided tape), the chassis/base plate was ejected from the 12U CSD on top of a lab bench.

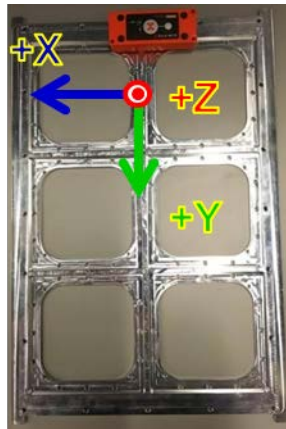


Figure 35. Slam Stick Orientation

Six deployments were conducted in order to collect sufficient data. This test was conducted on both an available empty 12U chassis, as well as the corresponding chassis base plate. As stated before, collected data is valid for both the 6U and 12U due to identical spring configurations.

3.3 CSD Ejection Tests with IMU

With the ultimate objective of conducting deployment tests with an actual CubeSat chassis, it was necessary to acquire an IMU that senses angular rates in all three axes. It was

required that the IMU have a standalone capability, where it was lightweight, and could operate on its own without require wiring, excessive integration with batteries or controller boards, etc. Moreover, it had to have a reasonable data rate where it was not as low as PSC's 50 Hz, but not too high (PSC noted that 1000 Hz is excessive). The most important part was that the IMU error had to be less than $0.25^{\circ}/s$ per axis [3]. The primary IMUs that were investigated were the SparkFun 9 Degrees of Freedom – Razor IMU, the Analog Systems ADIS16400 Triaxia Inertial Sensor with Magnetometer, and the X-Io Technologies Next Generation IMU (NGIMU).

The SparkFun 9 Degrees of Freedom – Razor IMU uses an InvenSense triple-axis digital output MEMS gyroscope (ITG-3200), and an Analog Devices ADXL345 Digital Accelerometer. The accelerometer is rated up to ± 16 g's and is rated to an output data rate of 3200 Hz. Typical noise is estimated to be around <1.0 Least Significant Bits (LSB) rms for the x and y axes, and <1.5 for the z axis [38]. The IMU is rated up to $\pm 2000^{\circ}/s$, and has a total noise of $0.38^{\circ}/s$ -rms [39]. This IMU would have to be connected to an AFIT-provided power supply, memory storage, and an attitude control system. The SparkFun IMU is primarily manufactured for video gaming and human motion sensing.

The Analog Systems ADIS16400 Triaxia Inertial Sensor with Magnetometer is a high accuracy IMU that can have a gyroscope range of $\pm 300^{\circ}/s$, and an accelerometer range of ± 18 g's. The gyroscope has a rate noise density of $0.05^{\circ}/s\sqrt{Hz}$ rms, and the accelerometer has a noise density of 0.5 m-g/ \sqrt{Hz} rms [40]. Both the accelerometer and IMU sample at 330 Hz. Just like the SparkFun IMU, this IMU would require being integrated with an AFIT-provided attitude control system and a power supply. This IMU has been used by AFIT for CubeSat

design classes, as well as actual CubeSat missions. This IMU would be attached to an AFIT attitude determination system, memory bank, and power supply.

X-Io Technologies Next Generation IMU is a standalone high-performance IMU that has internal memory, internal power, USB connectivity, and can be configured to be triggered by motion or by Wi-Fi signal. The gyroscope has a range of +/- 2000 °/s, with a resolution of 0.06 °/s, and runs at a sample rate of 400 Hz. The accelerometer has a range of +/- 16 g, with a resolution of 490 µg, and runs at 400 Hz. The heart of the system is the Bosch BMI 160 IMU, which is designed for augmented reality and immersive gaming and indoor navigation.

It was decided that among the three, the NGIMU was the best option. The Analog Systems IMU was expensive, and AFIT was running low on inventory. The SparkFun IMU did not have the desired resolution and had considerable noise from past experiences [8]. (Again, PSC specifically mentioned that the gyroscope should have a resolution less than 0.25 °/s). The NGIMU's resolution was far superior, and Bosch provided justification of this resolution with the total noise equation [41]. The gyroscope has a noise density of 0.007°/s/rt(Hz) and the accelerometer has a noise density of 180 µg/rt(Hz). Using this equation, Table 1 shows the different noise levels for various ranges of data sampling [42].

$$Noise\ Level\ (RMS) = Noise\ Density \times \sqrt{1.22 \times Bandwidth} \quad (15)$$

Table 1. Bosch BMI160 IMU Calculated Noise Specs From Datasheet [42]

Accelerometer Running Frequency (Hz)	Bandwidth Associated with Frequency (Hz)	Accelerometer Noise Level (RMS) (g's)		Gyroscope Running Frequency (Hz)	Bandwidth Associated with Frequency (Hz)	Gyroscope Noise Level (RMS) ($^{\circ}$ /s)
12.5	5.06	0.0004				
25	10.12	0.0006		25	10.7	0.0253
50	20.25	0.0009		50	20.8	0.0353
100	40.5	0.0013		100	39.9	0.0488
200	80	0.0018		200	74.6	0.0668
400	162	0.0025		400	136.6	0.0904

Moreover, the NGIMU made configuration simple as it was standalone and did not require hardware configuration. A bracket was 3-D printed to house the NGIMU, and was attached to a CubeSat chassis base plate, as seen in Fig. xx.

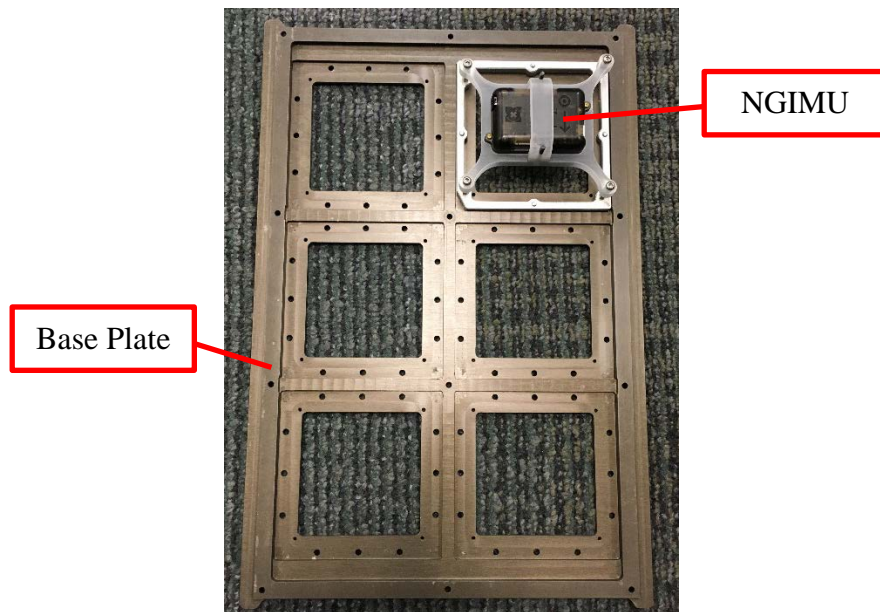


Figure 36. NGIMU in Bracket Attached to Chassis Base Plate

The process described in Section 3.2 was repeated with the NGIMU running at 400 Hz, again to ensure the maximum amount of data would be captured. As noted in Table 1, this means accelerometer resolution is expected to be 0.0025 g's, and gyroscope resolution is expected to be 0.0904 °/s.

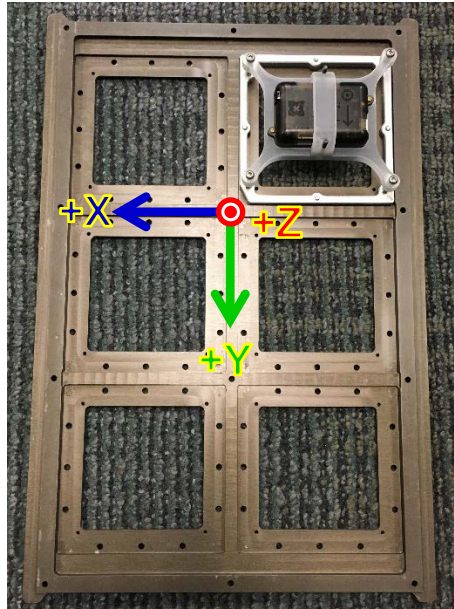


Figure 37. NGIMU Orientation

Six deployments were also conducted in order to collect sufficient data. This test was conducted on a CubeSat chassis base plate. The main difference from the Slam Stick deployment is that the base plate was hard anodized per PSC specifications. It is estimated that performance should improve, as the coating made the metal surface smoother to the touch. Again, as stated before, collected data is valid for both the 6U and 12U due to identical spring configurations.

3.4 Rail Friction

Since a payload is travelling out of the CSD while contacting the top and bottom surfaces of the guide rail (i.e. the top clamp and bearings, as seen in Fig. 38), the surface needs to be characterized, specifically for this research is measuring its kinetic friction profile. For the sake of this research, the goal is to identify kinetic friction that a deploying CubeSat experiences with respect to the distance travelled.

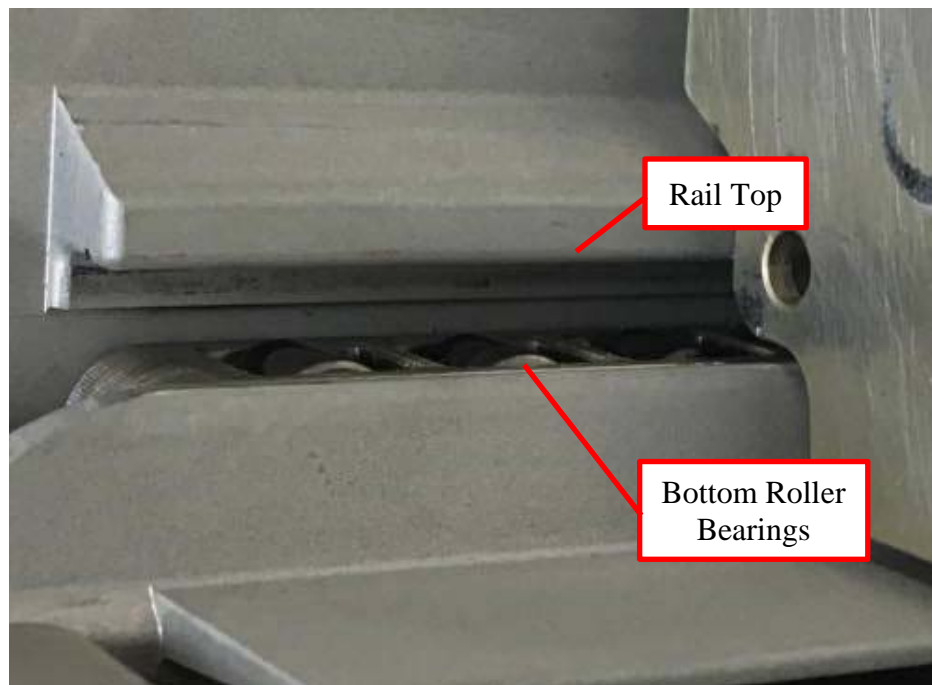


Figure 38. CSD Guide Rail with Features

Static friction was not considered, because it can be safely assumed that a deploying payload does not experience it since the push plate by default nearly-instantaneously overcomes static friction. Even though the bottom portion of the CSD rails are comprised of a multitude of roller

bearings, the rails are considered as a surface, thus it is assumed that the standard Coulomb Friction model applies. This allows focus on the *overall* friction profile that the ejecting payload experiences over distance, rather than what each roller bearing experiences. The top of the rails on the other hand, are a flat surface, and standard Coulomb Friction definitely applies. There are three common ways to determine kinetic friction on an unknown surface: impulse-deceleration, incline angle, and suspended mass. All three of these methods were conducted three times in order to avoid excessive surface wear on the CSD rails, especially since these tests are iterative and require many trials just to find the conditions required for calculation of the coefficient of kinetic friction.

3.4.1 Determine Friction via Incline Method

Measure friction via incline angle involves placing the CSD (with base plate/chassis) on incremental inclines. At each increment, the chassis/base plate is gently nudged in order to try to get it into motion (thus by overcoming static friction). If the plate/chassis slows to a stop, then kinetic friction overcomes the force of gravity [43]. This experiment is repeated until an angle is found where the chassis/plate moves down the incline at a constant speed. This angle determines the coefficient of kinetic friction due to the relationship between the force of friction and the gravity force down the incline.

$$F_{incline} = mg\sin\theta \quad (16)$$

$$F_f = \mu_k mg\cos\theta \quad (17)$$

Since the force of gravity over the incline must overcome the force of friction, the break-even coefficient of friction is found by setting the two forces together, and solving for μ_k .

$$\mu_k = \tan\theta \quad (18)$$

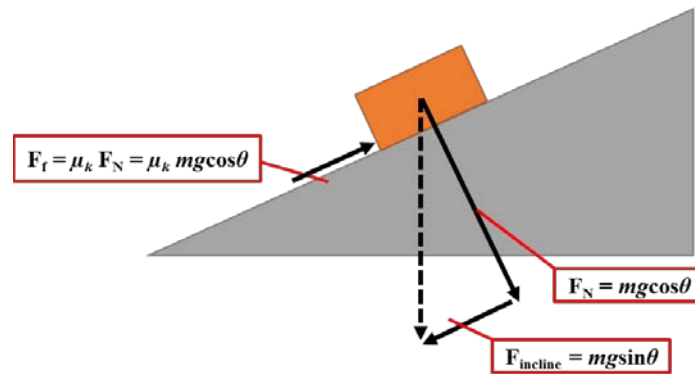


Figure 39. Incline Method [25]

3.4.2 Determine Friction via Suspended Mass

Measuring friction via suspended mass involves attaching a suspended mass to the base plate/chassis, which is in the CSD [44]. At each weight increment, the chassis/base plate is gently nudged in order to try to get it into motion (thus by overcoming static friction). If the plate/chassis slows to a stop, then kinetic friction overcomes gravitational force. This experiment is repeated until a weight is found where the chassis/plate moves horizontally at a constant speed. It is this mass that determines the coefficient of kinetic friction, due to the direct force gravity imparts on the mass, and that the pulley converts the force into a horizontal force.

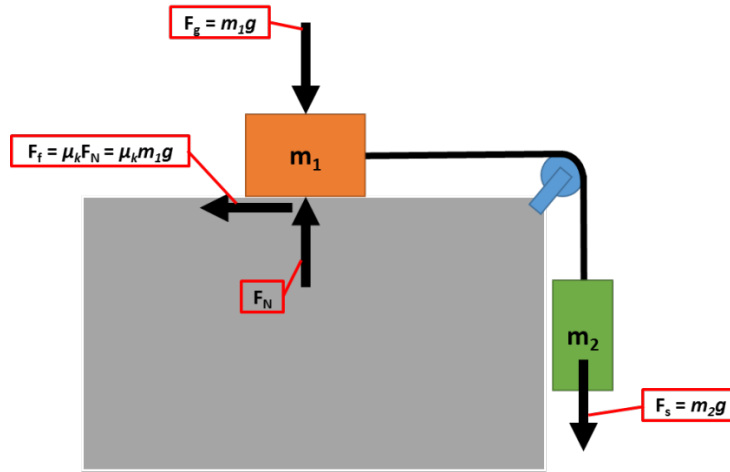


Figure 40. Suspended Mass Method [25]

$$F_f = \mu_k m_1 g \quad (19)$$

$$F_s = m_2 g \quad (20)$$

We then use the definition of Coulomb friction to find the coefficient of friction by equating it to the horizontal force.

$$\mu_k = \frac{m_2}{m_1} \quad (21)$$

3.4.3 Determine Friction via Impulse-Deceleration

The impulse-deceleration method works by an impulsive force applied to an object that is large enough to make it travel across a surface. [8] Using an accelerometer, deceleration experienced can be measured. With a known average deceleration over a period of time and object mass, the force of friction can be found via Newton's Second Law:

$$F_f = ma_{decel} \quad (22)$$

Using the Coulomb Friction equation, we can then estimate the coefficient of kinetic friction, μ_k

$$F_f = \mu_k F_N = \mu_k mg \quad (23)$$

These measurements can be verified via the Work-Energy relations and Conservation of Energy [45]:

$$KE_f + PE_f = KE_i + PE_i + W_{NC} \quad (24)$$

where the total energy (kinetic plus potential) of the body at the final time is equal to the total energy (kinetic plus potential) plus the work performed by nonconservative forces.

Starting with total energy, the potential (stored) energy of a constant force spring [46]:

$$PE_{const-force} = \int_0^l \frac{M^2 ds}{2EI} \quad (25)$$

$ds \equiv$ length energy is stored in ($l \equiv$ total spiral length)

$E \equiv$ Young's Modulus (of Elasticity)

$I \equiv$ moment of inertia of spring cross section

Where:

$$M = M_o \left(1 + \frac{y}{r}\right) - M_1 \frac{y}{r} - Rx \text{ (bending moment at any point)} \quad (26)$$

x & $y \equiv$ bending moment coordinates

$M_o \equiv$ external torque

$M_1 \equiv$ spring end clamping moment

$R \equiv$ radial force (passing through pivot point O)

Moreover:

$$M_o = Pr + M_1 \text{ (external torque)} \quad (27)$$

$P \equiv$ axial load

$r \equiv$ mean coil radius

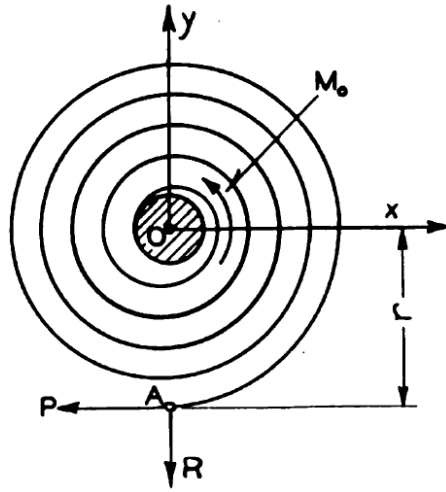


Figure 41. Constant Force Spring with Pinned End [46]

For the CSD, there is no induced bending moment upon the spring, thus x and y are negligible.

There is also no spring end clamping moment, as the CSD uses a pinned outer end. Moreover,

the CSD has one to four springs [2]. Factoring in these, Eq. (25) simplifies to:

$$PE_{CSD} = (\# \text{ springs}) \times \int_0^l \frac{(Pr)^2 ds}{2EI} \quad (25)$$

The kinetic energies of linear and angular motion are expressed as Eqs. (26) and (27), respectively.

$$KE_{linear} = \frac{1}{2} m \vec{v}^2 \quad (26)$$

$$KE_{angular} = \frac{1}{2} \vec{\omega} \times I \vec{\omega} \quad (27)$$

Nonconservative forces are those forces that perform work on a body, but do not conserve energy [45]. These forces include friction, drag, damping, etc. Since the payload travels only a short distance and has a small cross section, drag would be negligible. Friction due to any door impacts would also be negligible due to the lack of substantial time the payload could potentially have in contact with the door.

The primary nonconservative force that would perform work on the system would be that of friction, because the payload is constantly in contact with some combination of the top plate and bottom roller bearings of the CSD guide rails. Using the work equation, the energy lost due to friction on a surface is simply the force of friction multiplied over the distance travelled along that surface. Since there are two surfaces that would impart friction, the work due to friction would become:

$$W_f = F_{f1}x_1 + F_{f2}x_2 \quad (28)$$

The energy lost due to heat is small in this case, and difficult to measure without sensitive equipment. For this study, this will be considered negligible.

3.5 Door Interference

After analyzing data collected from preliminary horizontal deployments of the base plate with the NGIMU, a high-speed camera needed to be used to provide additional insight into the causes of the variable accelerations measured. Figure 42 shows velocity data from a deployment. Looking closely, one can see perturbations in the velocity profile, and that is why it was decided to utilize a high-speed camera to further analyze the deployment profile. There are drops in velocity, and it is suspected that this is caused by the oscillation of the door, which both contacts the plate, and re-engages the locking clamps.

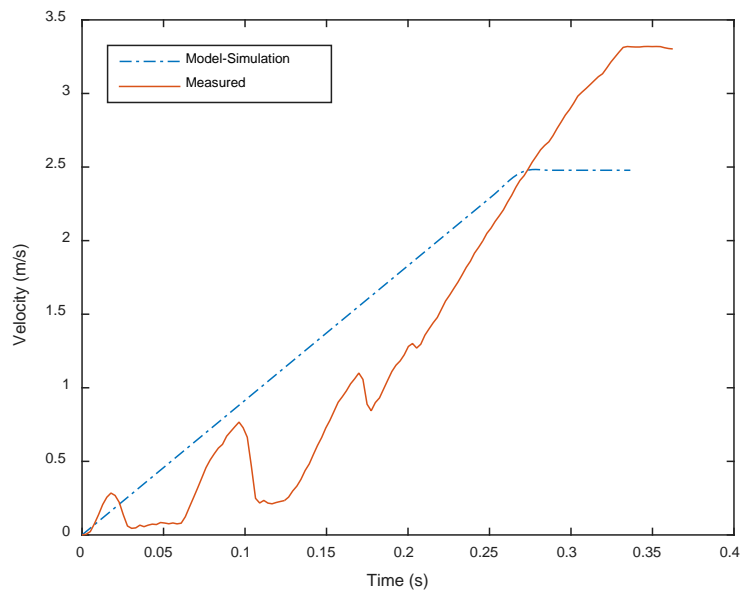


Figure 42. NGIMU Y Axis Linear Velocity: Model Prediction vs. Measured Data

During a deployment, a Phantom v1611 high-speed camera was run collecting images at a rate of 10,000 frames/s, with an exposure of 20 μ s. Upon analysis, it was noted that the door

oscillated after the CSD was triggered and actually made contact with the bottom of the deploying base plate multiple times.



Figure 43. CSD Door Striking Base Plate

Before testing, the only hint of door contact is made in a footnote in the back of PSC's payload spec guide, where it suggests, "During ejection the door of the CSD may bounce and contact the payload's -Y face. To prevent payload damage avoid placing sensitive components on the -Y face near the +Z leading edge of the payload. Ensure sensitive components do not protrude. Utilize a structural protrusion or bumper to help protect sensitive components." [2]

In response to this, it was determined that further analysis was necessary to measure the amount of force the door impacted an ejecting payload. To do this, the CSD was placed in a vertical position where it deploys upwards (see Fig. 44) in order to attempt minimize the effects

of gravity creating extra different moment on the door. The CSD was bolted to a secured flat plate that met PSC's flatness requirements of 0.005 in (0.13 mm) [2]

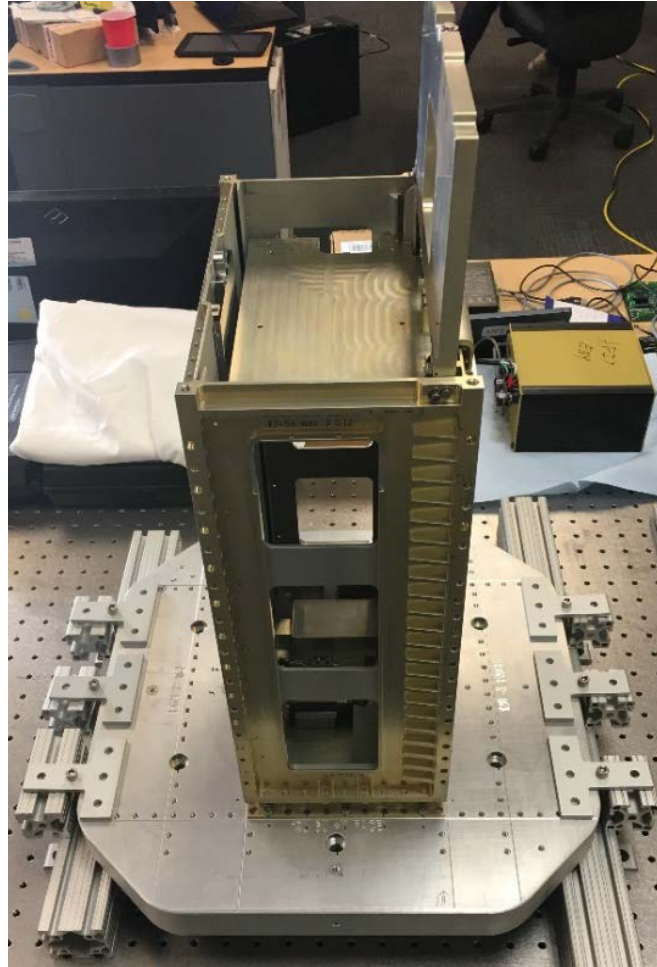


Figure 44. CSD Bolted to Flat Plate in Vertical Position

Four PCB Piezotronics 352C22 single-direction accelerometers were then placed on each corner of the door, as shown in Fig. 45. Locations of Accelerometers on CSD Door (Circled). These accelerometers have an average sensitivity (+/- 15%) of 1.0mV/ (m/s²).

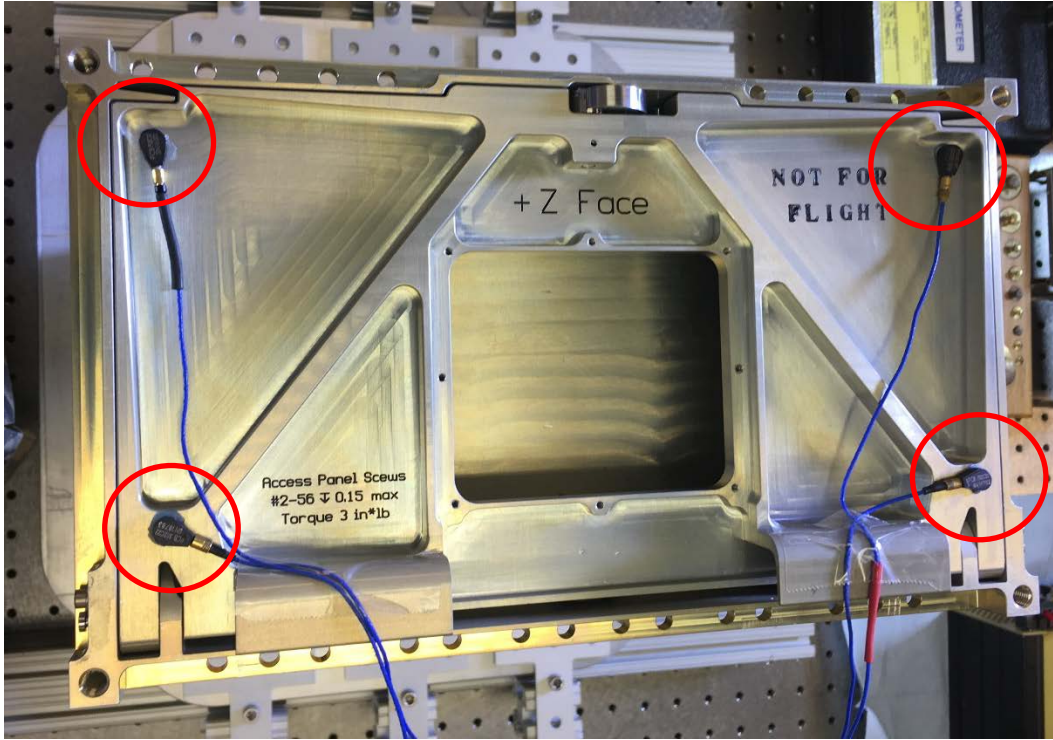


Figure 45. Locations of Accelerometers on CSD Door (Circled)

The accelerometers were connected to a signal conditioner, and then the data feed was inputted into a Data Physics Abacus dynamic signal analysis tower, which was connected to a laptop running Data Physics' SignalCalc Mobilyzer Fast Fourier Transfer (FFT) data analysis software suite. SignalCalc was set to read four *AC differential* (just in case there is not common ground) input channels from the accelerometers. The program was set at a frequency span F of 6.4 kHz with 51200 lines in order to get a 61.04 μ s sampling time interval dt . This sampling time is found by dividing the frequency span by sampling block size (Eq. (29)). The relation (as shown in Eq. (30)) between number of spectral lines, sample block size, and effective bandwidth E_b , is typically 1/2.56 for FFT data analysis instruments. [47]

$$dt = \frac{F}{\text{Block Size}} \quad (29)$$

$$\text{Block Size} = \frac{\# \text{ Lines}}{E_b} \quad (30)$$

This time interval is the smallest SignalCalc can get down to in the time domain, and this was done in order to best match the 20 μs exposure that the high-speed camera was set to in order to reduce any chance of misaligned data points. If there were any missing data points from the accelerometers, the camera data would be able to provide a verification check to ensure reasonable data sampling. The test run was also set to 8 s in duration (even though the high speed camera can only run for ~3.3 s due to memory limitations) in order to have a reasonable amount of buffer for human error. The SignalCalc settings can be seen in Fig. 46

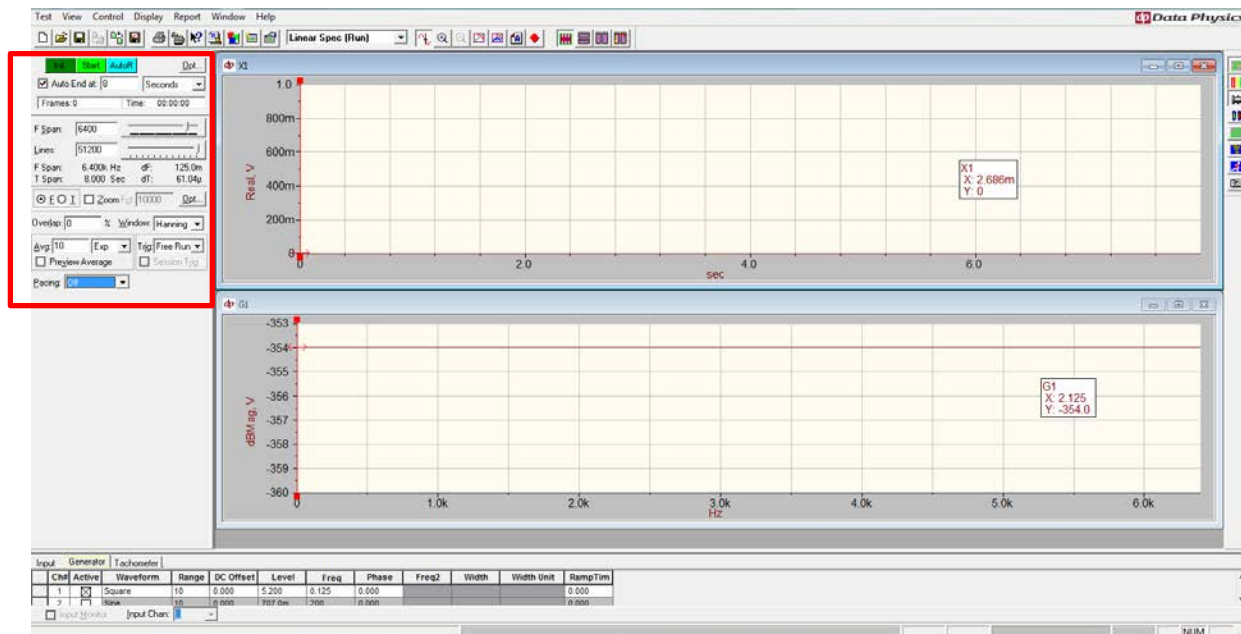


Figure 46. SignalCalc Graphic User Interface (Settings Circled)

The SignalCalc was also set to send out a simultaneously generated square wave at 5.2 V, with a frequency of 0.125 Hz (to match the 8 s data collection interval). In order to be remotely triggered, the Phantom high-speed camera requires a 5 V transistor-transistor logic (TTL) signal (see Fig. 47 [48]).

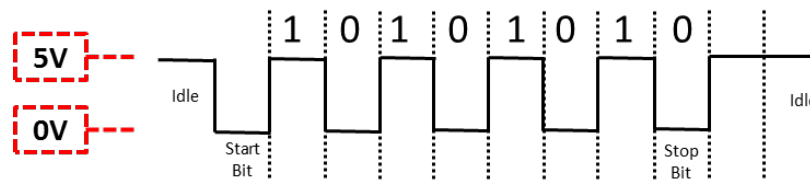


Figure 47. TTL Signal [25]

Since a TTL signal is a basic on-off square wave, that setting for the SignalCalc generator function was selected.

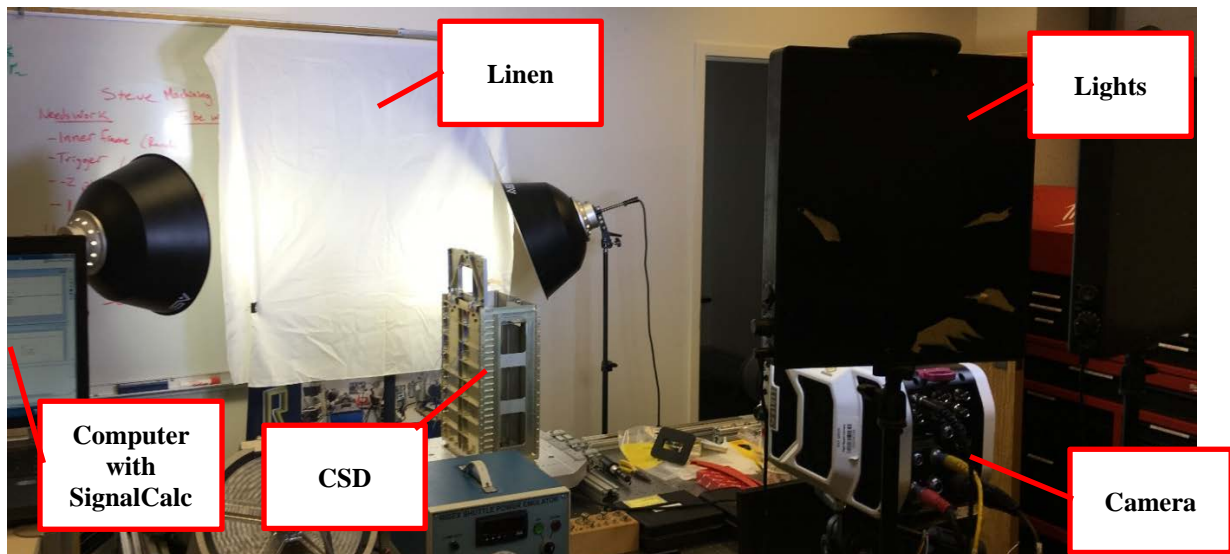


Figure 48. Camera Setup with Lights and Photography Linen

To set up the camera, it was centered on a reference point of the open door (Fig. 48). A white photography linen was placed behind the CSD and two lights were shining on it. This method (known as the infinity setup) illuminates the background of the photograph target in order to highlight its features with sharp contrasts. The bright uniform background enables the camera operator to focus less on light positioning, and more on the item being photographed [29] [49]. Two more lights were placed at each side of the camera shining onto the door of the CSD, yielding a picture shown in Fig. 49.

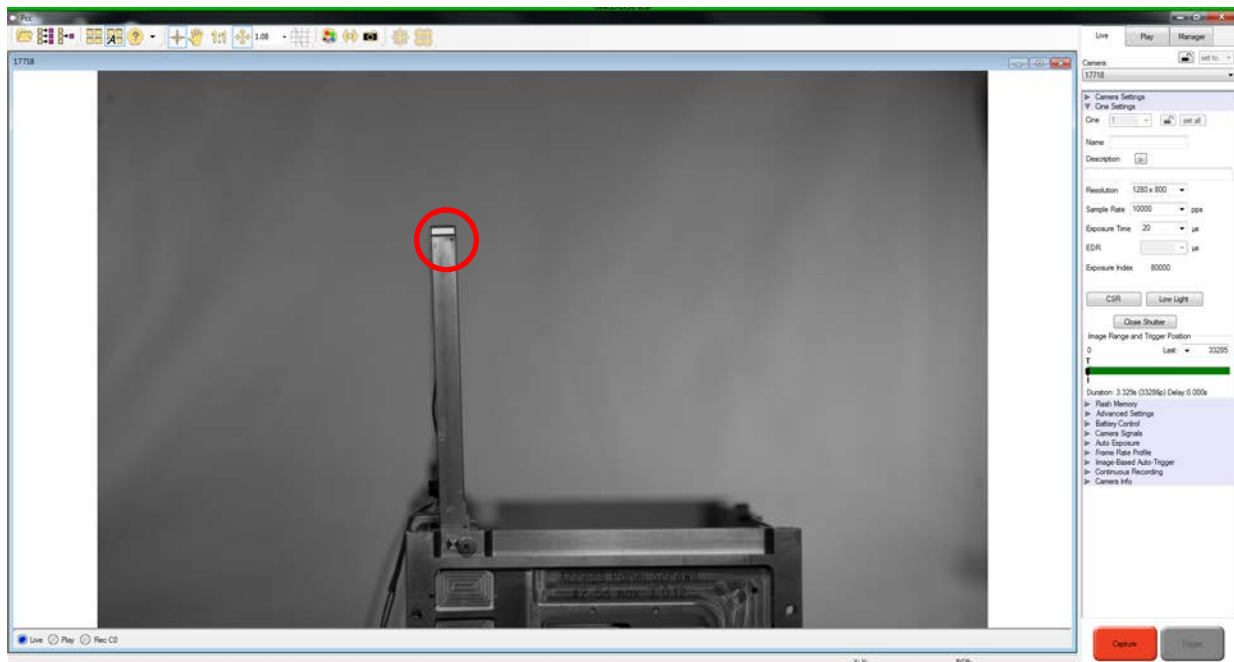


Figure 49. Phantom Camera Control GUI (Focus Point Circled)

When ready for initiation, the high-speed camera is set into capture mode (seen above in Fig. 49), where it constantly records in a loop until it is triggered, where then the camera will save the images. When the SignalCalc is initiated, the accelerometers begin recording, and the

square wave is simultaneously sent to the camera. At initiation, the person triggering the SignalCalc verifies that the camera has also been triggered, and upon verification, notifies the person triggering the CSD door to unlock the door latch, deploy the base plate, and catch the plate once it left the CSD door. The data from the accelerometers is then extracted to be analyzed in MATLAB. The videos are saved, and are used as a reference in order to verify movement of the accelerometers since they are synchronized. This experiment is to be repeated five times, and data will then be further analyzed in order to use it to model door motion in the simulation model.

3.6 Push Plate Feet Contact

CSD CubeSats are deployed via a push plate, which transfers its ejection force to the payload through contact points on the backside of the payload. PSC requires that there be at least three contact points with the push plate centered on the payload's center of mass. A recent test by AFIT of the Pumpkin SUPERNOVA CubeSat inspired the investigation of how important these feet are (see Fig. 6). The CubeSat was placed in a 6U CSD, and subsequently underwent random vibration testing. After the testing, uneven wear-marks were noticed on the CSD push plate. This implies uneven contact with the push plate. In theory, if there is an imbalance in push plate feet contact, or the feet not centered on the center of mass, a moment about the center of mass can be induced [9]. To test this concept, a 3-D 6U chassis was printed and reduced in mass in order to make it light as possible, yet maintaining a full chassis shape.

The chassis was printed and reduced in mass because this foot contact test had to be done in gravity conditions.

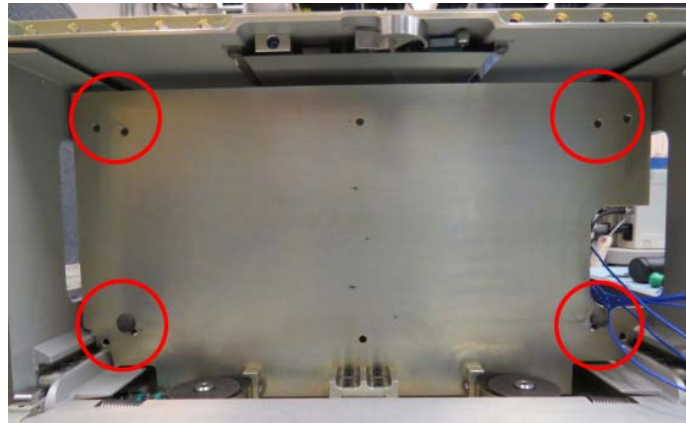


Figure 50. Wear Marks from Vibe Test Demonstrating Uneven Contact [11]

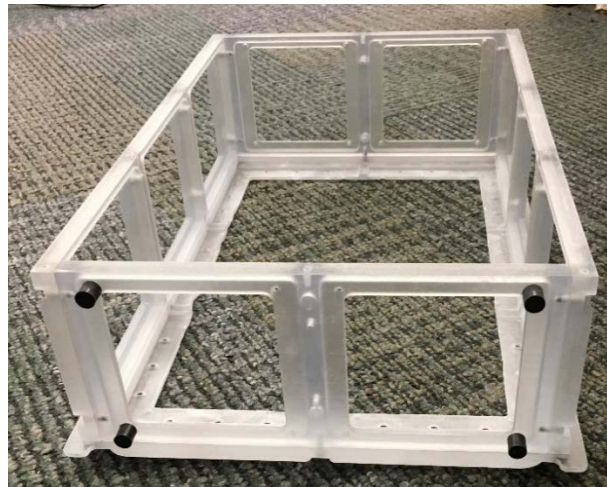


Figure 51. 3-D Printed 6U Chassis with Contact Feet

Since it was measured (discussed in Chapter IV) that the push plate exerts an average of 7.89 N of force while ejecting a payload, a payload lighter than 0.8 kg would be needed in order for the acceleration due to the CSD pusher plate to exceed the acceleration due to gravity. This

is important because the 3-D printed chassis was ejected upwards vertically in order to prevent gravity from influencing initial angular rates. The printed chassis had contact feet attached to its backside in order to test the effects the feet have on a deploying payload. These force distribution tests will test a range of scenarios in order to develop a profile characterizing the effects of uneven force distribution being applied to the payload. The following configurations are being considered, and those that are selected will be tested five times:

- a. All 4 feet contact (ideal scenario)
- b. 3 feet full contact (4 possible scenarios)
- c. 2 feet full contact (4 possible scenarios)
- d. 1 foot full contact (4 possible scenarios)
- e. Tabs contact only (similar to the NASA tab bar configuration)

3.7 MATLAB Simulation Model

An ultimate objective of this research was to develop a dynamics model to simulate the ejection of a CubeSat out of the CSD. The first set of equations of motion was Euler's Equations of Motion (expressed in the body frame) as discussed in Chapter II. These nonlinear, coupled, first order differential equations relate external torques to angular velocities and accelerations. The simulator's code defines a CubeSat's motion profile using Euler's Equations (Eq. (4)), as well as using kinematic equations in quaternion form (Eq. (9)) in order to relate angular velocity to orientation parameter derivatives, also known as the attitude of a spacecraft

[8]. The code defines the spacecraft's state with both these kinematic and kinetic equations, as described in Eq. (11).

The code also included linear equations of motion in order to predict linear velocities and distances over time. Assuming a constant force push plate, the linear acceleration was determined using Newton's Second Law, where the push plate acceleration was derived from the given push plate force divided by the CubeSat mass. Acceleration of the payload was applied throughout the entire measured internal rail length of the CSD of 13.3 in (0.338 m). This acceleration was then used to find displacement and velocity via integrating over the set time intervals (see Eq. (13) and Eq. (14)). Once the CubeSat payload traveled 0.338 m, the acceleration dropped down to zero m/s^2 , which signifies the release of the payload.

This analytical model includes a contact force distribution over four contact points in order to estimate ejection moments caused by any contact point variations. In order to model moments induced by contact point distribution, the code has the user define the contact feet positioning and level of contact with respect to the payload center of mass.

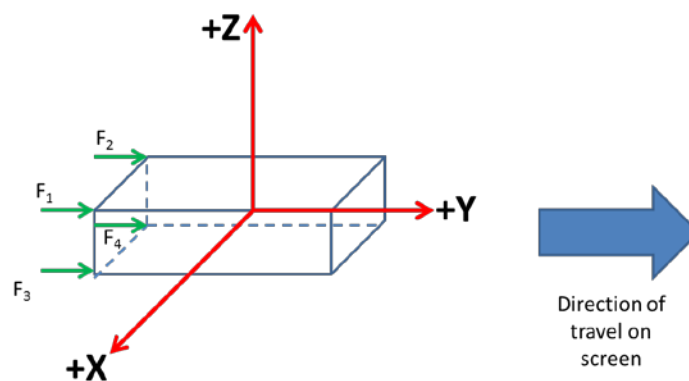


Figure 52. Model Coordinate System and Force Distribution Points [8]

The effects of these moments are applied for a small amount of time at the end of travel within the CSD (by setting the code to apply at the last 0.5 in (0.013 m) of travel through the CSD rails) because this is roughly where the tabs are likely to no longer be constrained. Specifically, once the payload tabs clear the second to last bearing, the payload can turn up to some degree. However, the continuous top rail will prevent the payload from pitching down significantly. Once the last bearing is cleared, the payload can pitch up, but pitching down would still be limited. This will be adjusted once data from the IMU is analyzed to see when and where these moments are applied. The linear rate calculation described in Eq. (13) is also included. The model applies a constant ejection force that constantly accelerates the payload until it reaches the point when the instantaneous moment is applied and is “ejected.”

The code prompts the user to provide the following information:

- Whether deploying a base plate, a 6U Chassis, or a 12U chassis
- Whether using standard geometric moment of inertia matrix or user-defined principal moment of inertia matrix
- Contact feet configuration
- Whether the simulation is to be done in gravity or in micro-gravity (assuming horizontal deployment orientation)
- If the user wants spacecraft attitude information in 3-2-1 Body Euler Angles, Quaternions, or neither.

The following values are computed for the CSD payload:

- Optional Attitude information (in the body frame with respect to the inertial frame) [50]

- Linear displacement and velocity profile (in the body frame)
- Angular rates (in the body frame) [21]
- Angular momentum in both inertial and body frames [21]
- Timing information (time to applied moment, release time, flight time within set period, time from trigger to end). This information is more for the micro-gravity drop tower estimations. (Discussed in Chapter V)

Summary

Chapter III discusses the approach for establishing a baseline. First, tests of the constant-force spring were conducted in order to verify that it is indeed consistent in its force while ejecting payloads from the CSD. Next, ejection tests in gravity were employed to better verify the linear aspects of its deployment profile, as well as to establish baselines for the angular portion. Moreover, experiments were conducted to identify major perturbations that the CSD could impart onto the ejecting payload, with the objective of modeling them in the MATLAB simulator and generate profiles with this data.

IV. Results

Chapter Overview

This chapter describes the results from the multiple experiments and tests that were conducted on the CSD. Analysis results on tuning the simulator model will also be discussed.

4.1 Push Plate Force Test Results

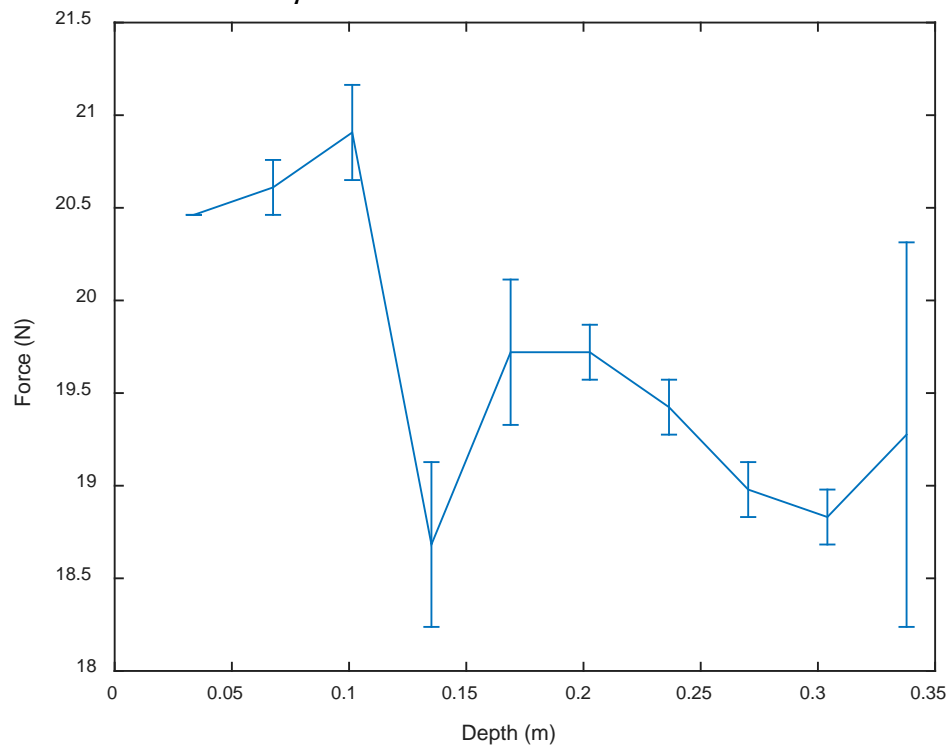


Figure 53. Average Force Readings per Depth

The methodology of this experiment is described in Section 3.1 in Chapter III. Push plate force readings with the push-pull gauge were taken three times at each depth, and the averages are plotted in Fig. 53. The error bars are 1- σ standard deviation of the three

measurements taken at each depth. Three measurements were selected in order to minimize wear on the CSD surfaces and especially the springs, as this experiment requires multiple push plate depressions. However, the result of the small number of measurements is that the confidence interval would have to be quite large if we wanted to be certain that the actual mean push plate force at each depth increment is within a certain percent interval (typically 95% is used). Since the small number of measurements at each depth cannot be definitively labeled as normal in distribution, nor can it be represented with certainty the standard deviation of a small sampling of the overall data set (typically under 30 samples), Student's t-Test can be used to describe the data [51]. Unlike standard normal distribution, the t-Test depends on the number of samples in order to adjust the curve distribution. Lesser data points yields a broader distribution curve because of a higher degree of uncertainty of the actual mean, while more data points narrows the curve because more data gives a lower degree uncertainty and a better idea of where the actual mean likely lies. This is described in Eq. (31).

$$\mu = \bar{x} \pm t_{\alpha/2} \frac{\sigma}{\sqrt{n}} \quad (31)$$

where

$\mu \equiv \text{actual population mean}$

$\bar{x} \equiv \text{sample mean}$

$t_{\alpha/2} \equiv t \text{ statistic}$

$\sigma \equiv \text{sample standard deviation}$

$n \equiv \text{sample size}$

The t-statistic is typically found through look-up tables by using the sample size and desired confidence interval. Table 2 shows a sample look-up table used to find the t-statistics for a 95% confidence interval. To better demonstrate how the t-Test relates number of samples to the bounds of the confidence interval, consider Fig. 54, which relates the number of samples to the calculated $\frac{t_{\alpha/2}}{\sqrt{n}}$ coefficient in front of the sample standard deviation for the 95% confidence interval.

Table 2. t-Statistic as a Function of Sample Size for a 95% Confidence Interval [51]

n (2-15)	t-Statistic	n (16-31)	t-Statistic
2	12.706	17	2.12
3	4.303	18	2.11
4	3.182	19	2.101
5	2.776	20	2.093
6	2.571	21	2.086
7	2.447	22	2.08
8	2.365	23	2.074
9	2.306	24	2.069
10	2.262	25	2.064
11	2.228	26	2.06
12	2.201	27	2.056
13	2.179	28	2.052
14	2.16	29	2.048
15	2.145	30	2.045
16	2.131	31	2.042

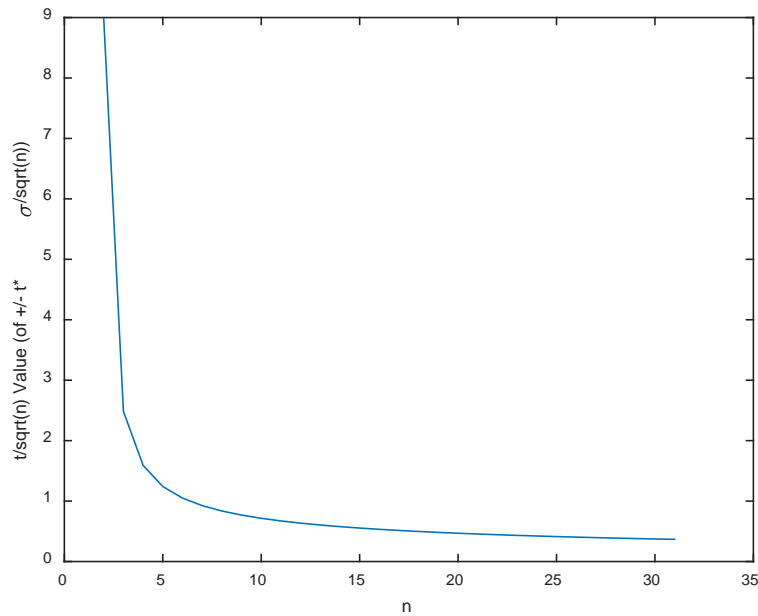


Figure 54. Coefficients of t-Test as a Function of Sample Size for 95% Confidence Interval

From Student's t-Test, the confidence interval for three measurements would be quite large (specifically $\pm 2.484\sigma$ from the sample mean), and would prove difficult to affirm the constant force nature of the push plate. What is seen from Fig. 54 is that the confidence intervals decrease exponentially in size as more data points are measured. For example, by only having six measurements, the interval is brought down to $\pm 1.050\sigma$ from the sample mean. This is a significant improvement in certainty of the location of the actual mean. To get a more confident assessment of the force profile with the t-Test in mind, all 30 measurements were assessed a whole set. The average force measured was at 4.42 lbs (19.661 N) with a 1- σ standard deviation of 0.17 lbs (0.776 N), a median force of 4.40 lbs (19.572 N), and the overall force profile has a tight spread, as seen in Fig. 55, which correlates with the low standard

deviation [52]. (N.B.: Using the precision of the gauge, both the average and median forces would read 4.4 lbs.) To verify normality of these readings, the Shapiro-Wilks Test was used. This test verifies normality by comparing the shape of the sample distribution to a normal curve. Typically, this test evaluates a distribution of sizes between three to 2000 numbers. This test first calculates a test statistic shown in Eq. (31), and evaluates the correlation between sampled data and ideal normally distributed data [53]. For example, if $W = 1$, then the sampled data is perfectly normal, and thus the null hypothesis is perfect. When $W \ll 1$, that means the distribution is non-normal.

$$W = \frac{(\sum_{i=1}^n a_i x_{(i)})^2}{\sum_{i=1}^n (x_i - \bar{x})^2} \quad (32)$$

where

$$(a_1, \dots, a_n) = \frac{m^T V^{-1}}{(m^T V^{-1} V^{-1} m)^{\frac{1}{2}}} \equiv \text{constants} \quad (33)$$

and

$$m = (m_1, \dots, m_n)^T \equiv \text{expected values of variables}$$

$$x_{(i)} \equiv \text{nth order statistic (nth smallest number in sample)}$$

$$\bar{x} \equiv \text{sample mean}$$

$$V \equiv \text{covariance matrix of order statistics}$$

The standard α (significance level) of 0.05, (or 95% confidence) is used when verifying the null hypothesis (mean = 19.661 N) via the P-value. The P-value is the smallest level of significance that would lead to rejection of the null hypothesis (i.e. when the P-Value is less

than α) [54]. Using a MATLAB code employing the Shapiro-Wilks method, the distribution analysis yields a test statistic of $W = 0.9364$, and a P-value of 0.0729 calculated from the test statistic. Since the test statistic is close to one, and the P-value satisfies the significance level criterion, it can be assumed that the data collected, as shown in Fig. 55, is normal.

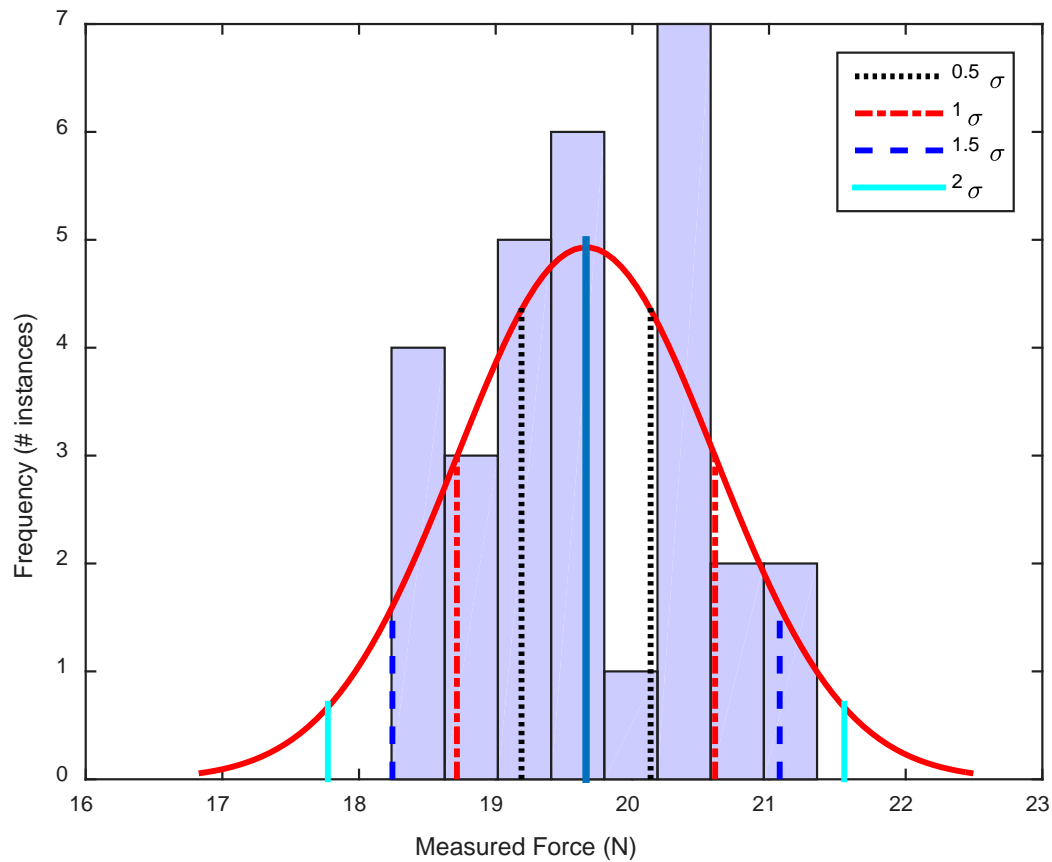


Figure 55. Force Reading Spread

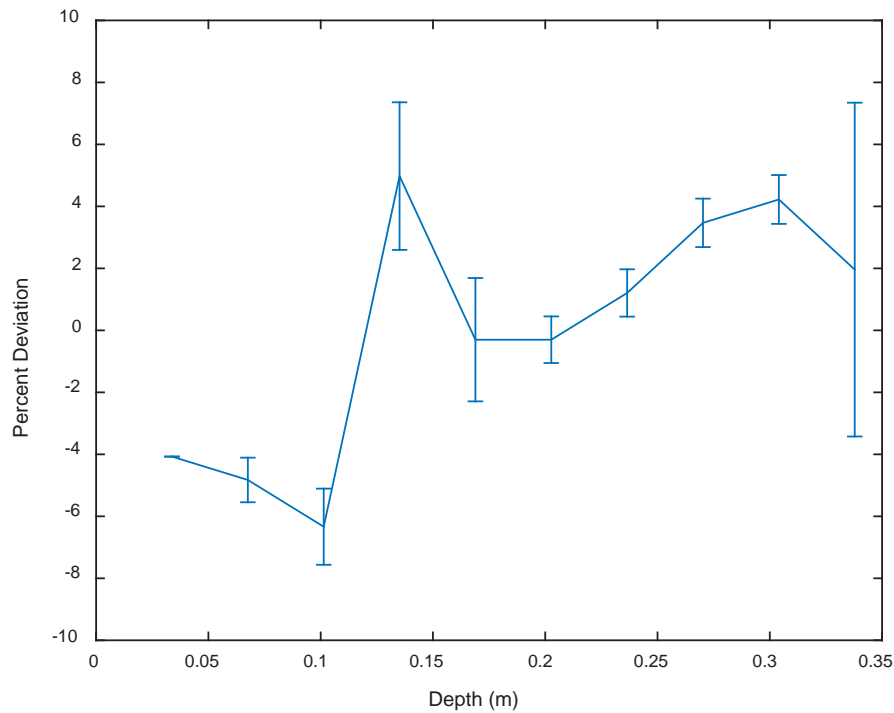


Figure 56. Force Reading Percent Deviation with Respect to Depth

In Fig. 56 above, an average percent deviation ranging between -6.335% and 4.977% is shown (top) at each increment. Error bars were calculated based on the 1- σ standard deviation of the three measurements taken at each depth. The root mean square (RMS) error of the percent deviation shown in Fig. 56. An odd phenomenon was seen at 0.1m and 0.14 m, where major deviation force spikes (20.91N) and drops (18.68N) at these two specific depths, respectively, occurred. However, these numbers were within PSC's CSD specs between 15.6–46.7 N [2]. These readings were not expected to be high in precision, given the use of a basic push-pull gauge with a tolerance of ± 0.1 lb (0.444 N). In addition, the guide rod increment markings used in this test were marked with a marker and an engineering ruler. The objective was to get a

notional idea of any variations, and if the overall static force applied by the push plate were within PSC spec. However, this leads to the question whether or not these force readings reflect the CSD's dynamic motion (discussed later).

4.2 Initial CSD Ejection Velocity Test Results

The methodology of this experiment is described in Section 3.2 in Chapter III, and its corresponding test plan in Appendix A.2. To determine the accuracy of the Slam Stick, each axis of the accelerometer underwent a calibration check using a handheld shaker stick. This stick oscillates at a set frequency (in this case 159.2 Hz peak-to-peak) with an amplitude of 0.99 g. The results of this calibration check are presented below in Table 3.

Table 3. Slam Stick Calibration Check Results

	X Axis	Y Axis	Z Axis
Mean (m/s^2)	9.0677	8.1574	8.3277
Standard Deviation (m/s^2)	0.15949	0.15984	0.76062
RMS Error (against 9.7 m/s^2)	0.6583	1.5592	1.5771

In this experiment, a 12U CSD was used, along with a 12U chassis and a non-anodized base plate. Under gravity conditions, it was discovered that an empty 12U chassis (~3kg) is too heavy to completely eject in a horizontal orientation from a CSD [5]. The gravitational force applied too much of a moment about the chassis and friction stopped the deployment midway.

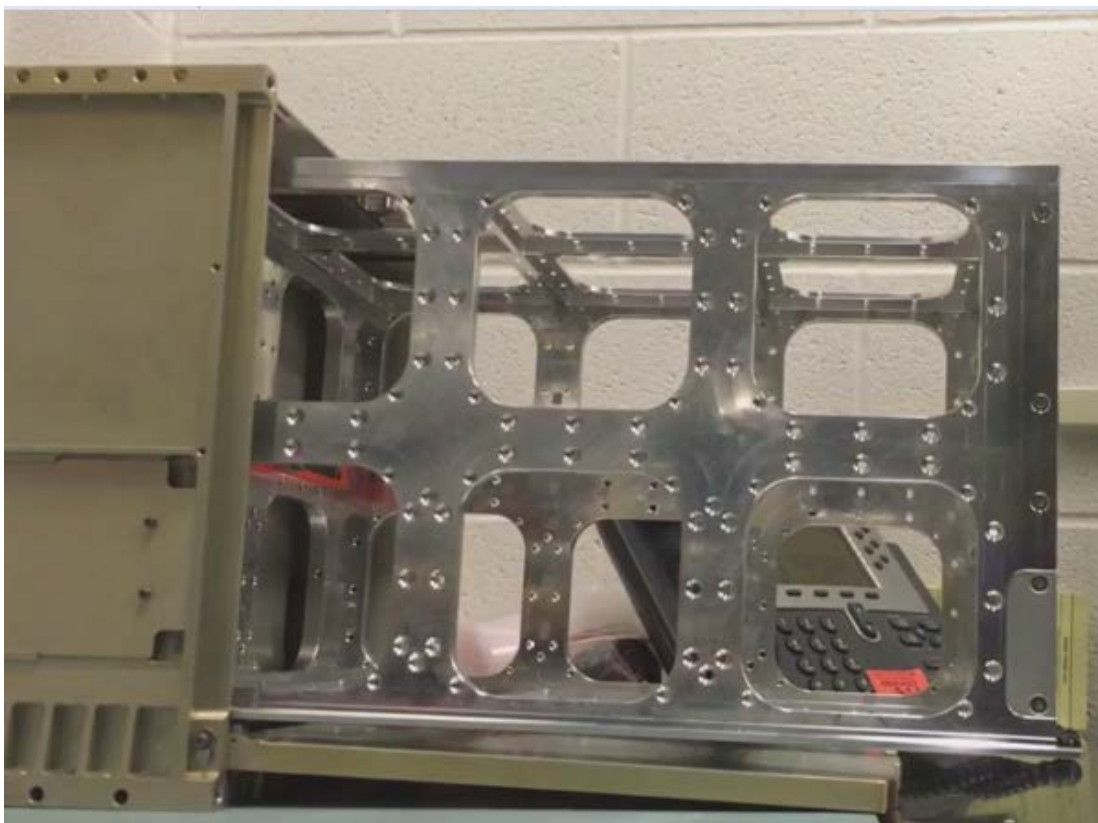


Figure 57. 12U Chassis Prevented from Full Deployment due to Friction Caused by a Gravitational Torque

An empty 6U chassis (~1.5 kg) can be deployed horizontally in gravity. However, it is good to recall that the CSD is not rated for in-gravity deployments, and PSC warned that CSD surface finishes would experience wear and ultimately skew results [3]. To reduce the effects of wear on the CSD rail system, deployment testing in a lab environment was only done using the chassis baseplate at 0.59 kg. The lighter weight of a baseplate is advantageous because it has a lower moment of inertia profile, which allowed any induced rotations to have higher rates, thus making it easier to analyze.

Accelerometer readings were not expected to be the most indicative of what actually happened during a mission deployment, as the ejected plate would likely hit the CSD door (due to gravity) and would be grabbed by hand. Further accelerometer data analysis showed an average acceleration of 13.3853 m/s^2 , with a standard deviation of 4.9503 m/s^2 . It is good to note that while reading the Slam Stick's values, one can see up to a 20% amplitude deviation in accelerometer data. As mentioned earlier in Section 3.2, the deviation for the slam stick is 20%. This subsequently yielded an average dynamic push plate force of 7.8963 N . As shown below in Fig. 58, the direction of translation motion is in the Y direction. (See Fig. 35 for axis.)

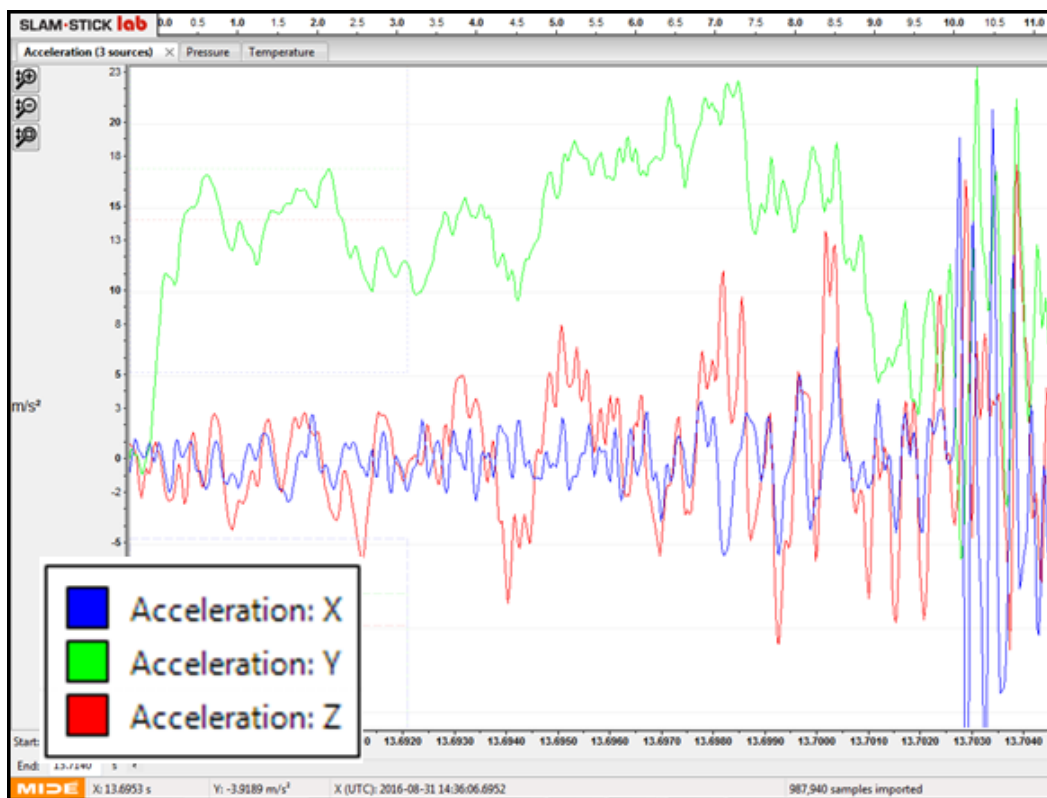


Figure 58. Slam Stick Lab Test Output (Base Plate Only)

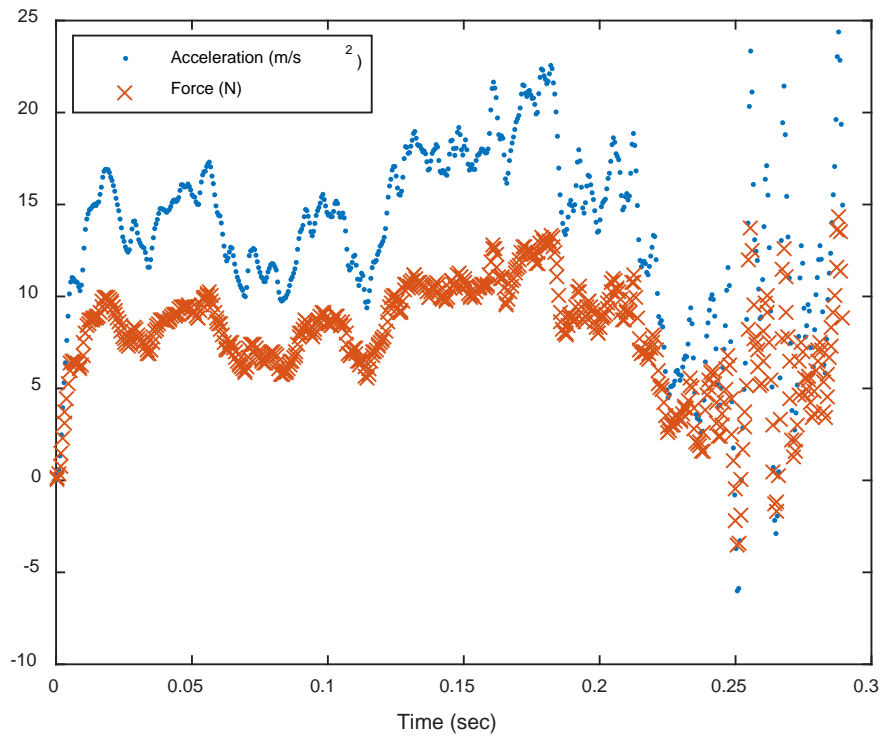


Figure 59. Slam Stick Linear Translation Acceleration (Y Axis Isolated)

Because the baseplate is allowed to freely accelerate, there is a much lower average dynamic push plate force versus what was observed in the static push-pull gauge experiment. In order to calculate velocity and subsequent distance over time from this measured acceleration, the *y-axis* linear acceleration data is integrated to compute velocity, and doubly integrated to compute displacement. In Fig. 60, the integrated accelerometer data is compared with the analytical model predictions. Likewise, the twice-integrated *y-axis* accelerometer data is compared with the analytical model predictions in Fig. 61.

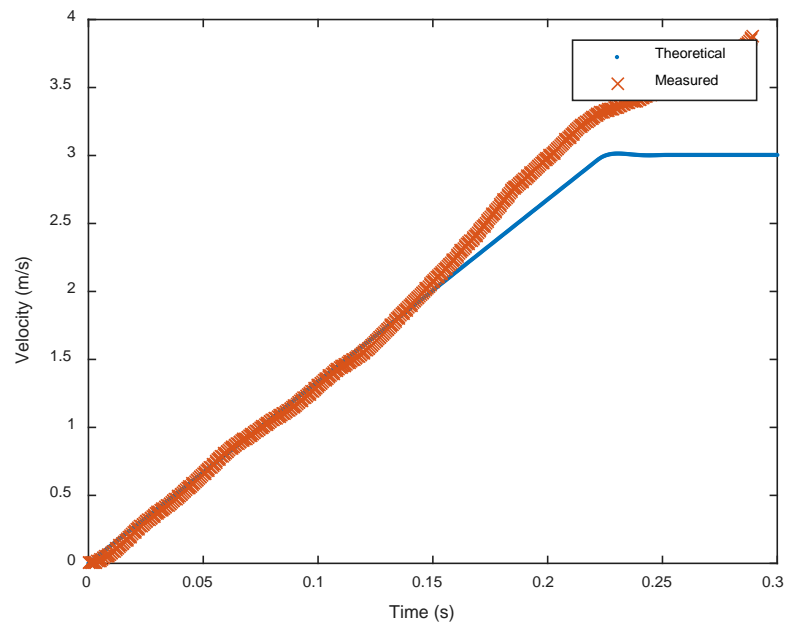


Figure 60. Slam Stick Y Axis Linear Velocity: Model Prediction vs. Measured Data

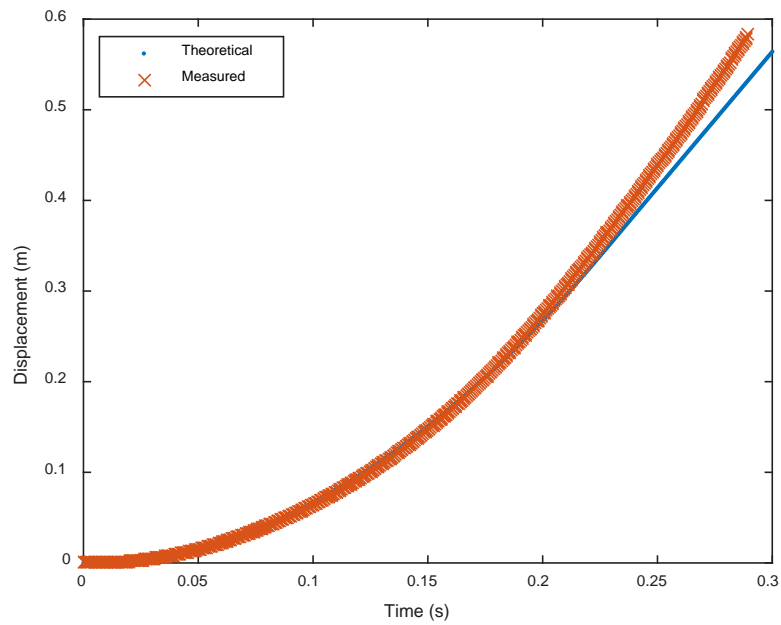


Figure 61. Slam Stick Y Axis Linear Displacement: Model Prediction vs. Measured Data

The RMS error between the predicted velocity and the measured was 0.2900 m/s, and the RMS error for displacement was even better at 0.0096 m. Overall, the measured and predicted values were in agreement with PSC's theoretical data seen in Fig. 62, as well with an ejection velocity of roughly 3 m/s [2]. During this test, interference with catching the plate, along with the effects of gravity corrupts data, as seen previously in Fig. 58. This corruption of data confirms the need for a way to simulate a micro-g environment in order to calculate these key profiles. Moreover, there will be a need to study the other two non-translational accelerations that have been seen.

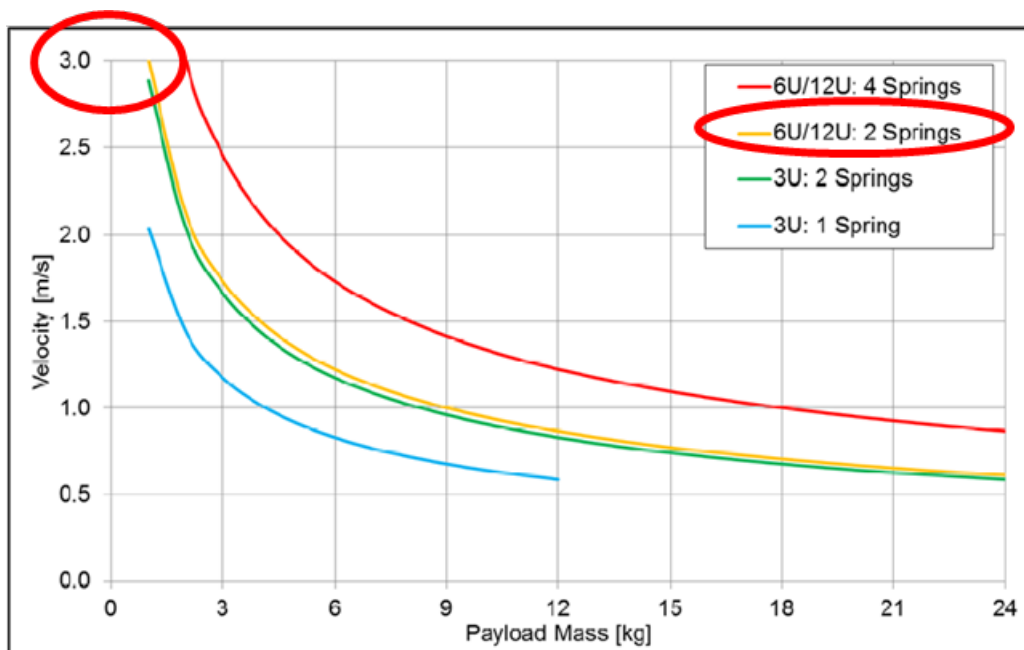


Figure 62. PSC Payload Ejection Velocity Profiles Based on C-9 Experiments (Configuration Agreement Circled) [2]

4.3 CSD Ejection Tests with IMU Results

The methodology of this experiment is described in Section 3.3 in Chapter III, and its corresponding test plan in Appendix A.2. To determine the accuracy of the NGIMU, each axis of the accelerometer underwent a calibration check with a handheld shaker stick, and the gyroscope was tested on a direct drive rotational platter set at consistent known angular velocities. The results of the accelerometer check are below in Table 4 (full test report Appendix B.2), and the gyroscope check are below in Table 5.

Table 4. NGIMU Accelerometer Check Results

	X Axis	Y Axis	Z Axis
Mean (m/s ²)	7.4007	6.9083	7.565
Standard Deviation (m/s ²)	2.7401	1.9441	3.6145
RMS Error (against 9.7 m/s ²)	3.5793	3.4082	4.194

Table 5. NGIMU Gyroscope Check Results

	X Axis (200°/s)	X Axis (270°/s)	X Axis (468°/s)	Y Axis (200°/s)	Y Axis (270°/s)	Y Axis (468°/s)	Z Axis (200°/s)	Z Axis (270°/s)	Z Axis (468°/s)
Mean (°/s)	199.7000	269.6837	467.5829	220.3646	270.2228	468.6228	200.0217	270.0224	468.0535
Standard Deviation (°/s)	0.3129	0.3364	0.3181	0.1381	0.1636	0.2370	0.1514	0.1844	0.2397
RMS Error (°/s)	0.4333	0.4617	0.5244	0.3899	0.4721	0.6663	0.1529	0.1857	0.2455

During this experiment, the previous tests conducted with the Slam Stick were repeated with the newly acquired IMU six times. This time, the test was done with the anodized base plate (to meet PSC specs) along with the IMU housing, giving a payload mass of 0.6963 kg. Moreover, a 6U CSD was used since this type would be used on EM-1, and for future capability can fit in the

NASA GRC drop towers. As done prior, the plate was ejected horizontally, and the accelerometer was integrated once to find velocity over time, and integrated again to find displacement over time. Upon review, the accelerometer data was not as clean as the Slam Stick's output, as shown below in Fig. 63. This is most likely due to bias and built-in error. Recalling the calibration reports, the Slam Stick yielded RMS error propagations ranging from $0.6583 - 1.5771 \text{ m/s}^2$, as it is specifically designed as an industrial/lab shock data collector, while the NGIMU accelerometer yielded RMS error propagations ranging from $3.5793 - 4.194 \text{ m/s}^2$, as this is designed more as a commercial human motion tracker. Moreover, it is good to note that as described in Section 3.3, there is an expected deviation of about 0.0025 g's (0.0245 m/s^2) when reading the NGIMU's accelerometer data.

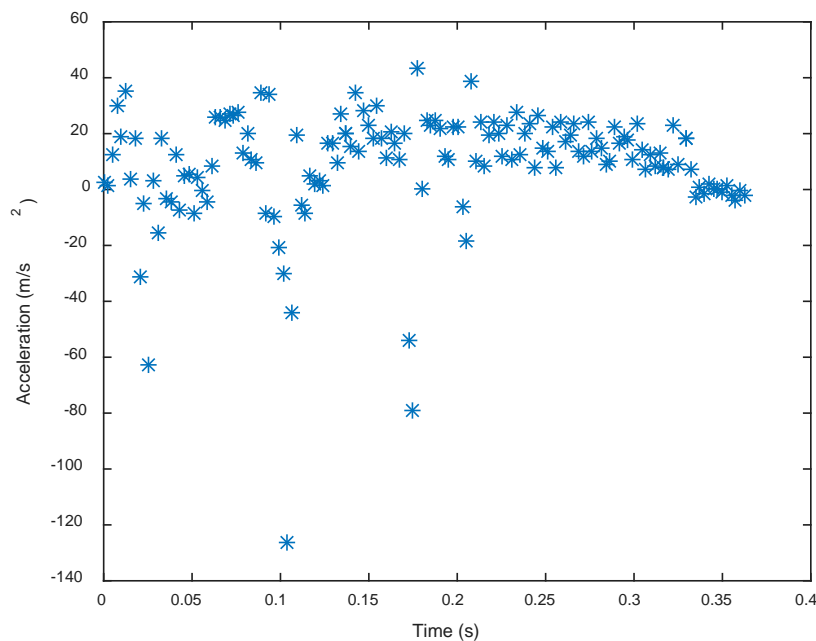


Figure 63. NGIMU Accelerometer Readout for Base Plate Deployment (Y Axis Isolated)

The six deployments yielded similar data, so for this chapter, the first deployment will be discussed here. The payload was considered to begin motion if three consecutive data points were $3\text{-}\sigma$ (0.1429 m/s^2) above the noise floor standard deviation. The first data point in the three consecutive data points was designated as the initial state of the payload. Data was truncated at the last acceleration data point before data readings returned below the noise floor. The average acceleration from this data is 9.1503 m/s^2 , with a standard deviation of 20.8535 m/s^2 , which subsequently yielded an average deployment force of 6.3713 N . The corresponding linear velocity profile via integration is shown below in Fig. 64. Comparing with the base MATLAB simulation, the RMS error is 0.4831 m/s , which was not as close as what was calculated for the Slam Stick. There are drops in velocity (which correlate with the negative/zero acceleration points in Fig. 63), and it is suspected that this is caused by the oscillation of the door, which both contacts the plate and re-engages the locking clamps. After a second integration, the displacement profile was developed (shown below in Fig. 65), and this yielded against the model an RMS error of 0.0428 .

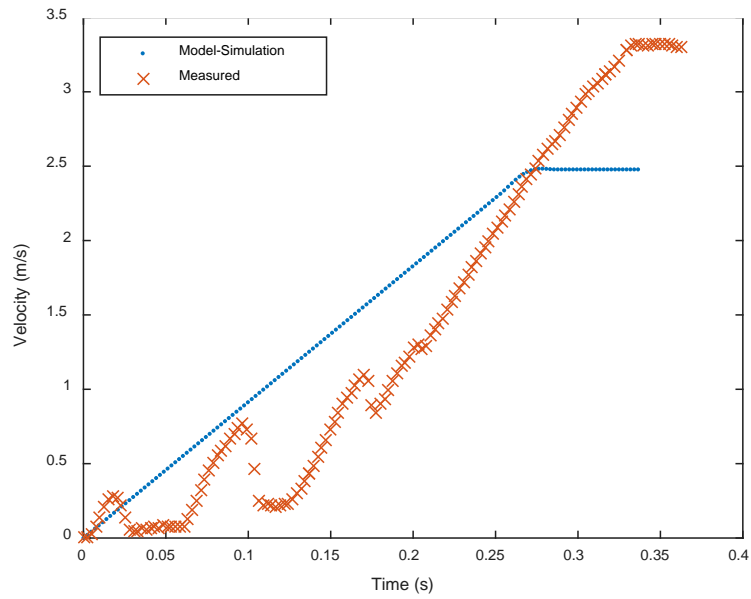


Figure 64. NGIMU Y Axis Linear Velocity: Model Prediction vs. Measured Data

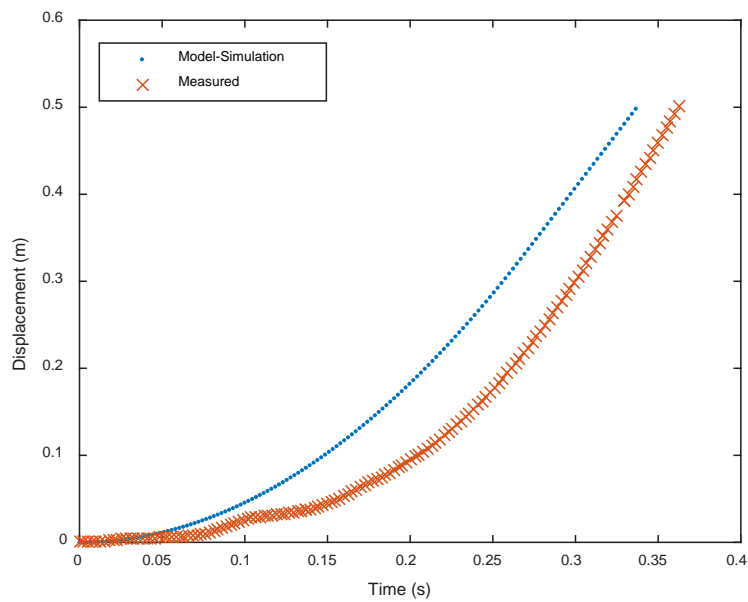


Figure 65. NGIMU Y Axis Linear Displacement: Model Prediction vs. Measured Data

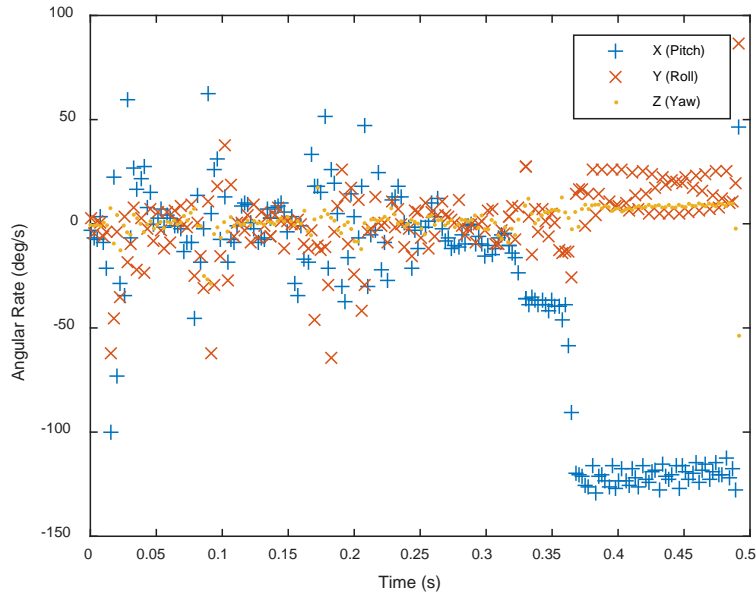


Figure 66. NGIMU Angular Rates

Looking at the gyroscope data as seen in Fig. 66, the plate pitches downwards as expected (-x-axis) when ejected from the CSD. The plate also slightly rolls to the right (y-axis) because of the minor offset caused by the IMU's placement due to mass imbalance. The IMU shifts the center of mass of the plate system slightly past the geometric center. To consider gyroscopic data points, they have to exceed $3\text{-}\sigma$ ($0.4286^\circ/\text{s}$) standard deviations above the noise floor for three consecutive data points. $3\text{-}\sigma$ was chosen because it went beyond the amplified noise of the gyroscope as the payload was being deployed. What was interesting to see was that there was a two-stage increase in angular velocity. As seen above in Fig. 66 the first increase (at an average slope of $4.338^\circ/\text{s}^2$) occurred 0.3143 s after triggering, and plateaus at 0.332 s an average rate of $38.927^\circ/\text{s}$ ($2.975^\circ/\text{s}$ standard deviation) about the $-x$ axis. The gyroscope data then jumps up again (at an average slope of $26.923^\circ/\text{s}^2$) to an average angular rate of $120.98^\circ/\text{s}$

(4.083 °/s standard deviation) about the $-x$ -axis from 0.3599 – 0.3675 s. When reading this data, it should be considered that there is an expected 0.0902°/s deviation, as described in Section 3.3. This was very interesting, because the angular rate jump was a likely indication of when the ejection moment was applied to the payload, and subsequently when the payload was released from the CSD (the sudden spike towards the second plateau).

Comparing the gyroscope data to the accelerometer data, these suspected instances of moment application and payload release were confirmed because when analyzing acceleration data in Fig. 63, acceleration rates begin dropping at 0.332 s. This was further confirmed when analyzing Fig. 64, because the ejection velocity of the payload stops increasing and plateaus at 0.332 s. Using 0.332 s as a reference, Fig. 65 would indicate that the push plate stops (and subsequently applies any moments) after the payload travels 0.4005 m. This conclusion does not make sense, because the CSD rails were measured to be 0.3378 m. Moreover, the Slam Stick experiments conducted prior did not experience these errors. The only difference in hardware was the accelerometer/IMU used, and that the Slam Stick experiment did not use an anodized base plate. One possible explanation to why this data reflects these numbers could be due to the oscillations of the door. As mentioned earlier, a high-speed camera was set up to provide a visual account for deployment events. Unexpectedly, it was noticed that the door oscillated substantially, and the video revealed that the door contacted the bottom of the payload at least five times. Moreover, the video showed that the payload was actually pushed back in to the CSD during the first few oscillations.



Figure 67. CSD Door Striking Base Plate

To try to isolate the payload ejection from perturbations, the base plate was ejected five times from the CSD with the door open. Even though this would result in reduced friction due to the clamps not being engaged, this allowed the isolation of the deploying mechanism, which allowed it to be better characterized. The data from each of the five runs were consistent with each other, so only one run will be discussed. Upon review, the accelerometer data was much cleaner, as seen below in Fig. 68. Moreover, the derived velocity and displacement profiles matched the model predictions much better, as seen below in Fig. 69 and Fig. 70. The RMS errors were 0.1535 m/s for velocity, and 0.0139 m for displacement. These are 68.2261% and

67.5234% reductions in error, respectively. Because of this, it can be concluded that the door was the source of the deployment interference as seen previously.

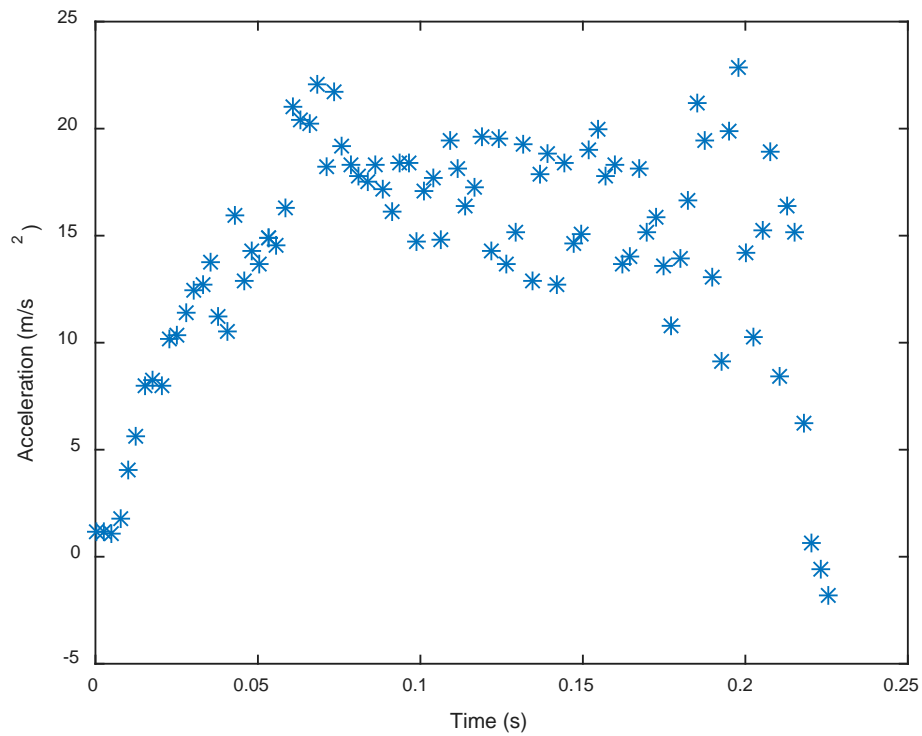


Figure 68. NGIMU Accelerometer Readout for Base Plate Deployment (No Door)

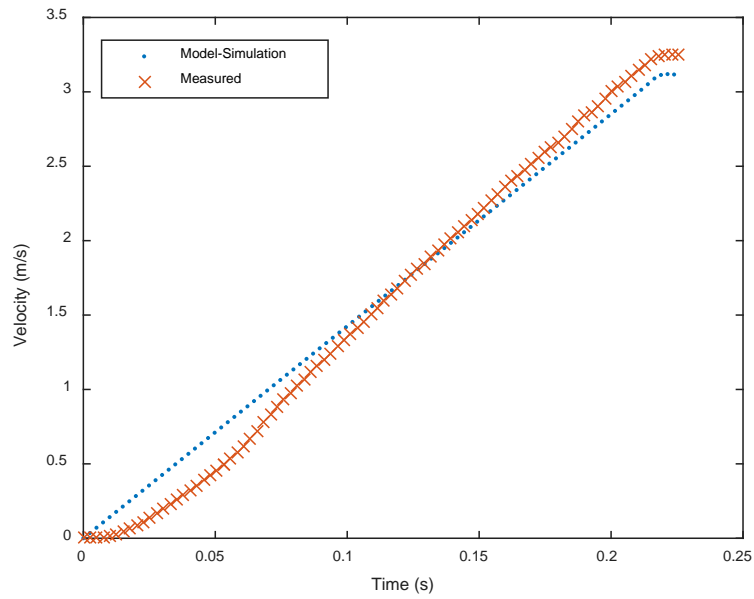


Figure 69. NGIMU Linear Velocity: Model Prediction vs. Measured Data (No Door)

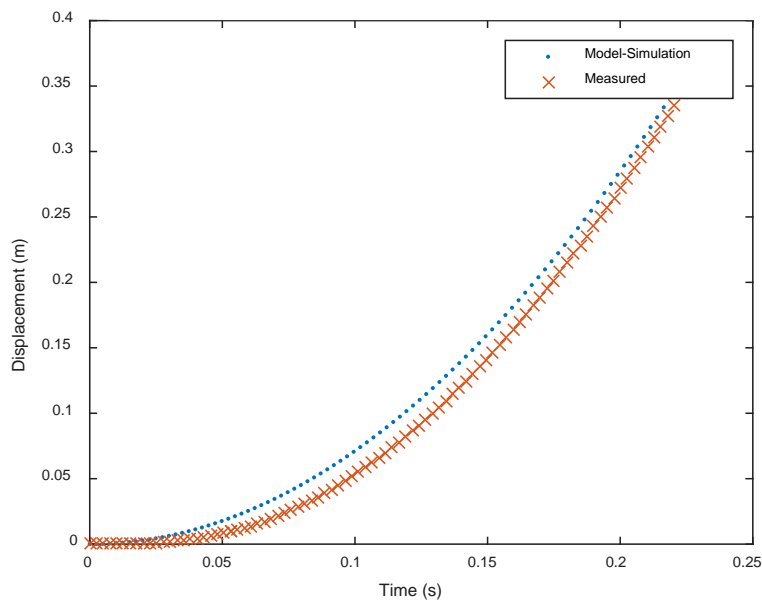


Figure 70. NGIMU Linear Displacement: Model Prediction vs. Measured Data (No Door)

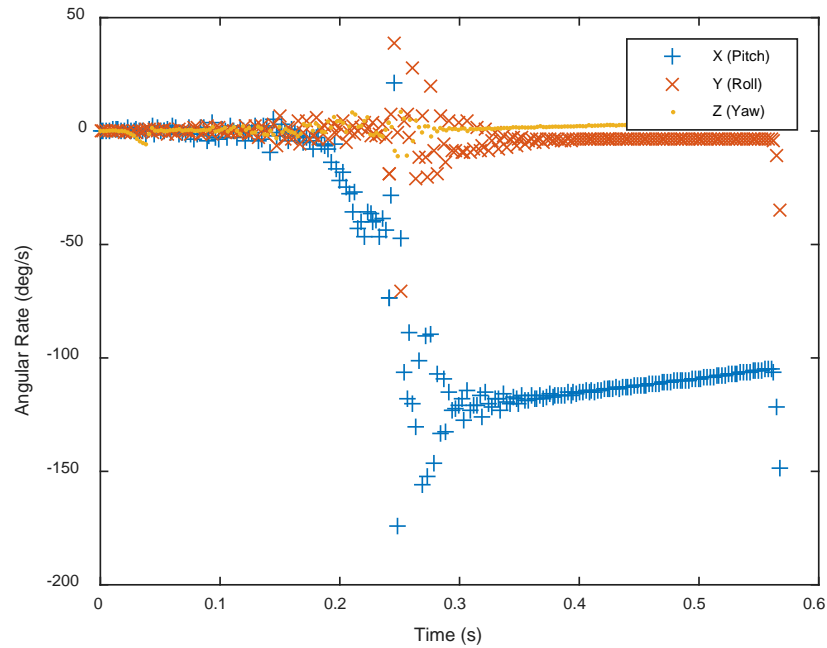


Figure 71. NGIMU Angular Rates (No Door)

As seen above in Fig. 71, the first increase (at an average slope of $3.128^{\circ}/s^2$) occurred 0.1850 s after triggering, and plateaus at 0.2154 s an average rate of $40.866^{\circ}/s$ ($3.944^{\circ}/s$ standard deviation) about the $-x$ axis. It then jumped up again (at an average slope of $4.075^{\circ}/s^2$) to an average angular rate of $114.357^{\circ}/s$ ($8.915^{\circ}/s$ standard deviation) about the $-x$ -axis at 0.2610 s. As done before, the comparison between the gyroscope data and the accelerometer data confirmed these suspected instances of moment application and payload release. In Figure 68, acceleration rates begin dropping at 0.2154 s. This was again confirmed when analyzing Fig. 69, because the ejection velocity of the payload stopped increasing and plateaus at 0.2154 s. Using 0.2154 s as a reference, Fig. 70 would indicate that the push plate stopped (and subsequently applies any moments) after the payload travels 0.3194 m. This conclusion fits the

0.3378 m rail length profile better, and gives an exact location when the initial push plate moment was applied.

4.4 Rail Friction Test Results

The methodology of this experiment is described in Section 3.4 in Chapter III, and its corresponding test plan in Appendix A.3. For these tests, there were four main configurations tested in order to vary payload masses: base plate only, one mass stack, two mass stacks, and two heavy mass stacks. These were repeated for both the bottom part of the rail (with the roller bearings), and the top (the flat surface).

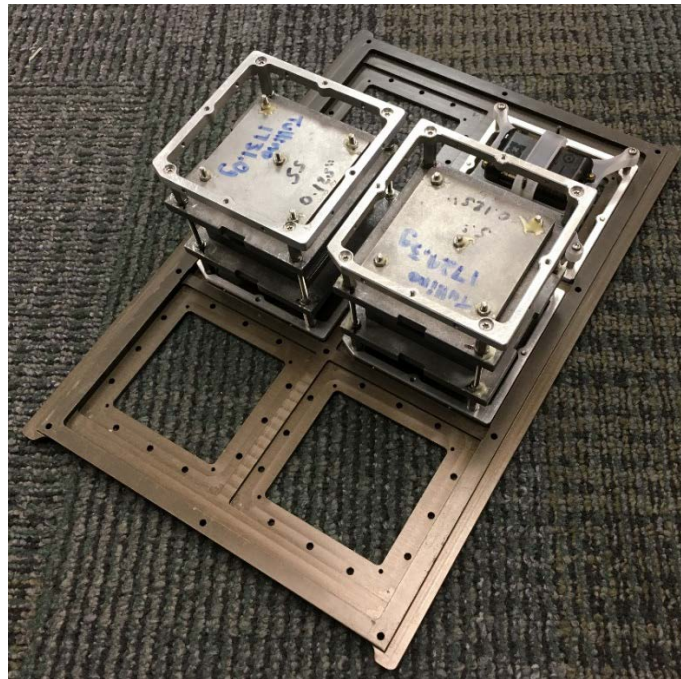


Figure 72. Friction Test Setup with Two Mass Stacks

4.4.1 Determine Friction via Inclination



Figure 73. CSD Attached to Tilting Apparatus with Inclinometer

This experiment was repeated three times for both the bottom of the CSD guide rail, and the top of the rail. This was done using the custom-built apparatus as shown below in Fig. 73, with an inclinometer to determine angle. Results are subsequently shown in for the top of the rail, and Table 7 for the bottom of the rail. The average coefficient of kinetic friction from this method for the top of the rail was 0.7313, with a standard deviation of 0.1310. Analyzing the normalcy of the top of the rail readings via the Shapiro-Wilks test using the same $\alpha=0.05$, $W = 0.8770$, with a P-value of 0.1459. From these results, it can be concluded from the test to assume the distribution is normal, and that the null hypothesis can be accepted. Further analysis of the data distribution (as seen in Fig. 74) confirms that the distribution of data can indeed be considered normal, even though there is a spread corresponding with the standard deviation. This will be discussed in greater extent later in this section. The average coefficient of kinetic

friction for the bottom of the rail was 0.0065, with a standard deviation of 0.0027. Normality analysis via the Shapiro-Wilks test yields $W=0.7575$, and a P-value of 0.0066, thus the null hypothesis is rejected. Moreover, analysis of the distribution in Fig. 75 confirms this. Despite this, one must consider the fact that the coefficient of kinetic friction values are in the thousandths, and thus are quite small overall.

Table 6. Top of Rail Coefficients of Kinetic Friction (Inclination Method)

	θ_1	μ_1	θ_2	μ_2	θ_3	μ_3
Plate Only (696.3g)	35°	0.7002	35°	0.7002	35°	0.7002
1 Mass stack (2427.1g)	39.7°	0.8302	42.7°	0.9228	42.7°	0.9228
2 Mass Stacks (4156.6 g)	39.7°	0.8302	42.7°	0.9228	42.7°	0.9228
2 Heavy Stacks (4470g)	30.1°	0.5797	31°	0.6009	32°	0.6249

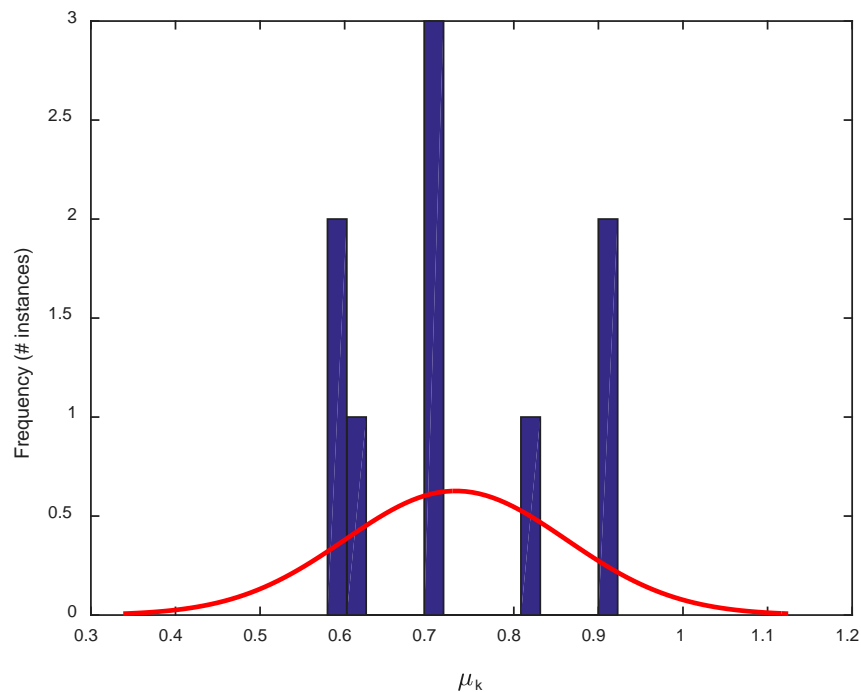
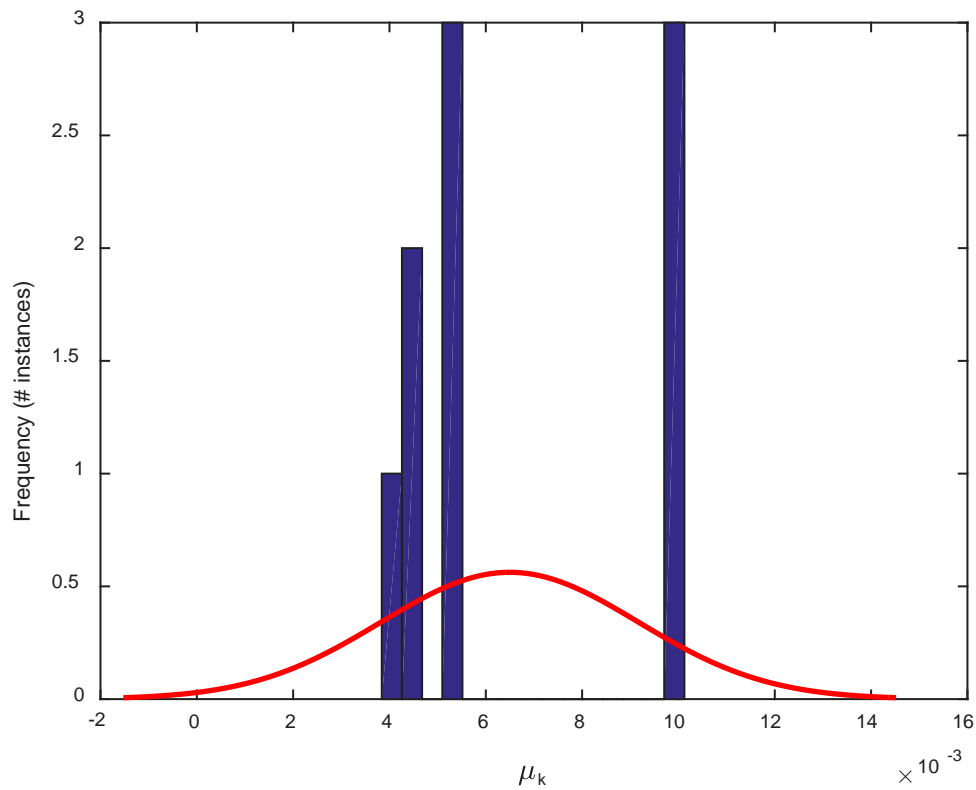


Figure 74. Top of Rail Coefficients of Kinetic Friction Distribution (Inclination Method)

Table 7. Bottom of Rail Coefficients of Kinetic Friction (Inclination Method)

	θ_1	μ_1	θ_2	μ_2	θ_3	μ_3
Plate Only (696.3g)	0.57°	0.009949	0.58°	0.010123	0.57°	0.009949
1 Mass stack (2427.1g)	0.30°	0.005236	0.30°	0.005236	0.30°	0.005236
2 Mass Stacks (4156.6 g)	0.28°	0.004887	0.27°	0.004712	0.27°	0.004712
2 Heavy Stacks (4470g)	0.25°	0.004538	0.26°	0.004538	0.22°	0.003840

**Figure 75. Bottom of Rail Coefficients of Kinetic Friction Distribution (Inclination Method)**

What was interesting was that the base plate had a lower coefficient of friction, as well as the heaviest weight. It makes sense why a lighter object would experience less friction: less weight means that the microscopic roughness of the two surfaces are not pressed as hard into

each other, thus resulting in less resistance to sliding. However, it was odd why the heaviest of the weights actually experienced less friction. One theory was that Coulomb Friction oversimplifies how two objects interact when they slide across a surface. It could also be that the force of gravity overcame the force of friction earlier due to more mass allowing it to supersede the force of friction sooner. An issue with this method was that this test had to be redone because the inclining plate shifted during test, and was not completely level. Moreover, this could also be a result of wear on the rails from running these tests several times.

Alternatively, shape of the plate could have changed by attaching the several stacks, and a resulting torque could change to the shape. This bending could result in changes to the friction due to changes in direct load. The angled configuration also results in a changing moment due to CG/support misalignment, which could be causing this difference also [55].

4.4.2 Determine Friction via Suspended Mass

For the suspended mass method, the brass masses (Fig. 76) were individually weighed to verify mass, especially since they were older and developed oxidation, which could affect mass. Verification results are displayed in Table 8. These tests were conducted three times on each side of the CSD rails to verify accuracy of kinetic friction coefficient readings, and results are shown in Table 9 and Fig. 78 for the top rail results, and Table 10 and Fig. 79 for the bottom rail results. The average kinetic coefficient of friction from this method for the top of the rail was 0.7028, with a standard deviation of 0.0089. The Shapiro-Wilks test concluded that the distribution yields a $W = 0.7672$, with a P-value of 0.005. From these results, the distribution is not normal, and the null hypothesis should be rejected. However, upon further analysis (as

seen in Fig. 78), shows that even though the data is indeed not normal, most of the readings (8 out of 12) are highly concentrated around ~ 0.72 . From this analysis, there is confidence in the null hypothesis, and thus can be accepted. *The* average kinetic coefficient of friction from this method for the bottom of the rail was 0.0076, with a standard deviation of 0.0042. The Shapiro-Wilks test concluded that the distribution yields a $W = 0.7575$, with a P-value of 0.0066. From these results, the distribution is not normal, and the null hypothesis should be rejected. Moreover, analysis of the distribution in Fig. 79 confirms this. Despite this, one must consider the fact that the coefficient of kinetic friction values are in the thousandths, and thus are quite small overall.



Figure 76. Brass Masses

Table 8. Brass Mass Calibration

Theoretical	1 g	2 g	2 g	5 g	10 g	10 g	20 g	50 g	100 g	100 g	200 g	500 g	1000 g
Actual	1 g	2 g	2 g	5 g	10 g	10 g	20 g	50.1 g	100.3 g	100.3 g	200.6 g	501.4 g	1002.8 g

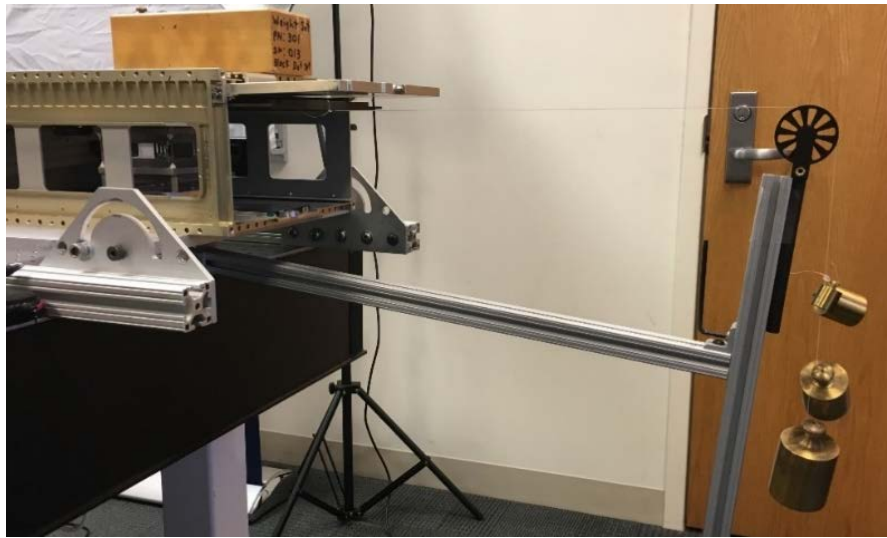


Figure 77. Suspended Mass Apparatus (In Rail Top Testing Configuration)

Table 9. Top of Rail Coefficients of Kinetic Friction (Suspended Mass Method)

	m_1	μ_1	m_2	μ_2	m_3	μ_3
Plate Only (696.3g)	501.4 g	0.7201	501.4 g	0.7201	501.4 g	0.7201
1 Mass stack (2427.1g)	1805.0 g	0.7437	1805.0 g	0.7437	1805.0 g	0.7437
2 Mass Stacks (4156.6 g)	3005.0 g	0.7229	3005.0 g	0.7229	3005.0 g	0.7229
2 Heavy Stacks (4470g)	3175.1 g	0.7103	3175.1 g	0.7103	3174.8 g	0.7102

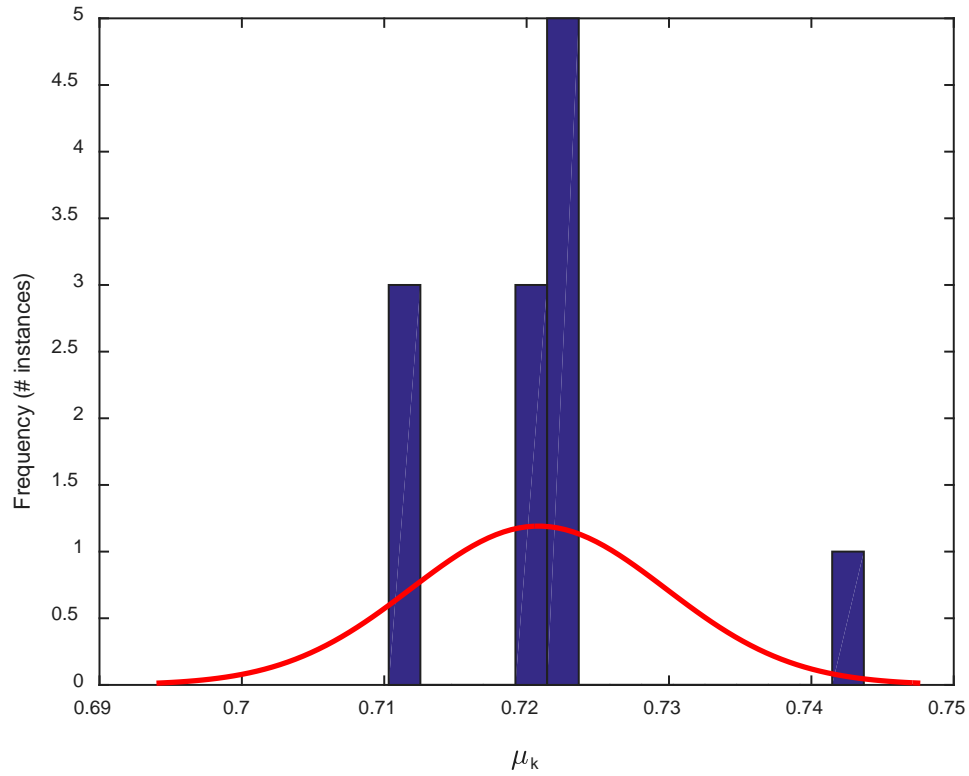


Figure 78. Top of Rail Coefficients of Kinetic Friction Distribution (Suspended Mass Method)

Table 10. Bottom of Rail Coefficients of Kinetic Friction (Suspended Mass Method)

	m ₁	μ ₁	m ₂	μ ₂	m ₃	μ ₃
Plate Only (696.3g)	10 g	0.01436	10 g	0.01436	10 g	0.014361626
1 Mass stack (2427.1g)	15 g	0.006180	15 g	0.006180	15 g	0.006180215
2 Mass Stacks (4156.6 g)	19 g	0.004571	19 g	0.004571	20 g	0.004811625
2 Heavy Stacks (4470g)	20 g	0.004474	20 g	0.004474	20 g	0.004474273

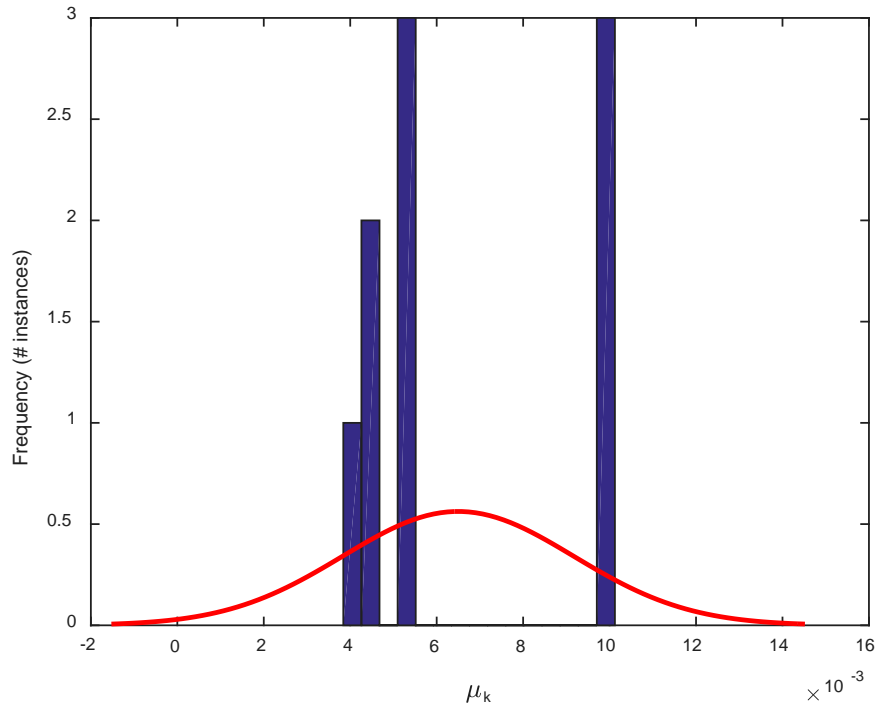


Figure 79. Bottom of Rail Coefficients of Kinetic Friction Distribution (Suspended Mass Method)

4.4.3 Determine Friction via Impulse-Deceleration

This method was repeated at least 12 times per scenario due to the possibility of encountering considerable noise during impulse runs. To determine when data was to be taken, a criteria of 3σ was used to determine when to consider sampling data for analysis after the initial impulse. Upon reading the raw data, it was observed that a quarter of the impulses were unusable due to the amount of noise created by the test. (Fig. 80 is an example.) The rest of the data was consistent in appearance, so to be concise, individual examples will be discussed. The first example was from the base plate only case sliding upon the top of the CSD rail, as shown in Fig. 81.

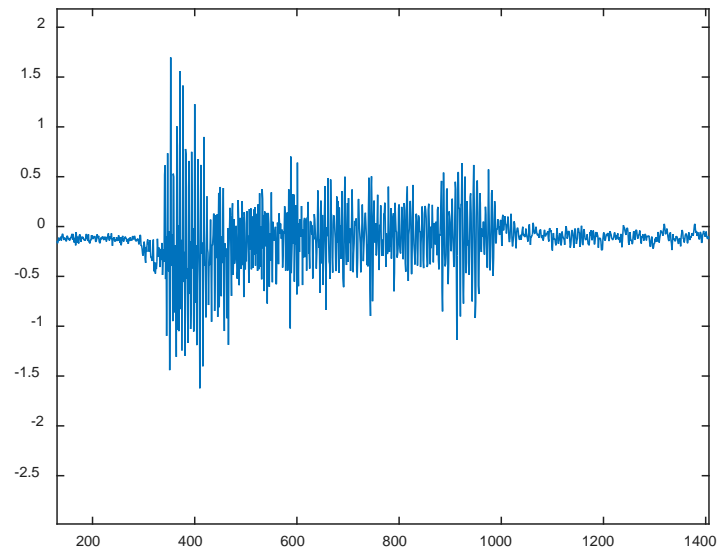


Figure 80. Noisy Raw Accelerometer Data from Impulse-Deceleration Test

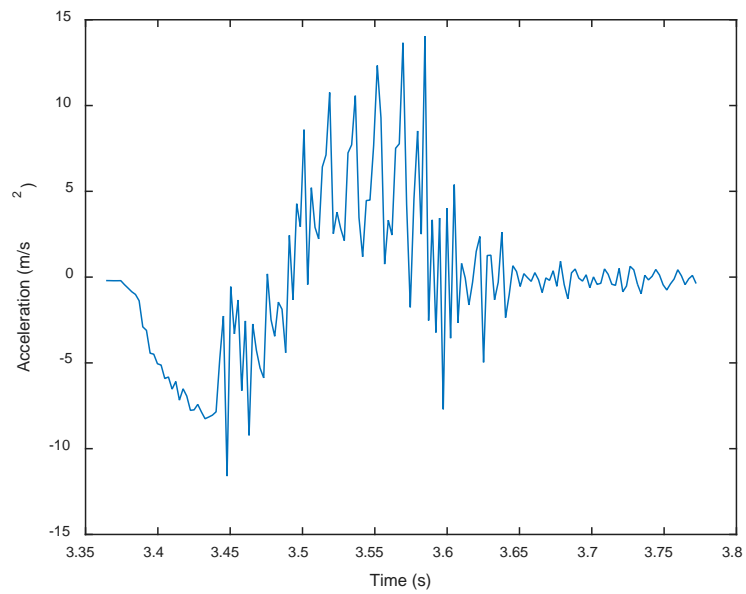


Figure 81. Friction Impulse Test: Top Rail with Base Plate Only

Fig. 81 describes the first scenario tested, where the CSD was placed upside down and the base plate was tapped into the rails. The acceleration was initially negative because recalling how the IMU was situated, tapping the base plate into the CSD in typical configuration means that the base plate was entering the CSD along the $-Y$ -axis. Once the initial impulse had run its course, the acceleration jumped to the opposite side of the axis, indicating an opposing acceleration. In this case, it was the deceleration due to friction. Using the 3σ guidelines, once the data consistently stayed above the 3σ mark for at least three data points, the average of the acceleration slope was taken from the designated starting point, until when acceleration in the opposite direction takes over and brings motion back across the demarcation towards rest. For this case, the average deceleration is 5.5975 m/s^2 , with a standard deviation of 3.8261 , yielding a kinetic friction coefficient of 0.5708 by dividing the deceleration by g (9.806 m/s^2). All results for the top side of the rail are summarized in Table 11.

Use of the two stacks and two heavy stacks were not possible, because the amount of force required to cause an impulse would overcome the accuracy of the deceleration because the effort of imparting an impulse to this configuration was met with an impulse in response. This was seen with the two mass stacks case, as the values determined were clearly a deviation from the other two cases, as seen in Table 11. In fact, looking at the big-picture, this was a significant deviation from the overall results gathered from the other friction tests as well (discussed later). The bottom side of the CSD rail proved to be less accurate in readings, because of the low amount of friction involved. This can be shown from the example of the base plate only case, where one can see the low slope at which the object decelerates. (See Fig. 82 below.)

The good news was that just like for the top of the rail series of cases, the bottom of the rail series exhibited consistent results as shown in Fig. 82. This is summarized below in Table 12. The average deceleration experienced in this series was 0.005475 m/s^2 with an overall standard deviation of the set of 0.0010904, yielding an average kinetic friction coefficient of 0.006871. Because there were only two possible data points for the rail top and three data points for the rail bottom, a histogram and analyzing the data via the Shapiro-Wilks test are not necessary.

Table 11. Data from Impulse-Deceleration Tests (Top of Rail)

	Average Deceleration	Standard Deviation	μ_k
Plate Only (696.3g)	5.5975 m/s^2	3.8261	0.5708
1 Mass stack (2427.1g)	6.4741 m/s^2	3.8261	0.6602

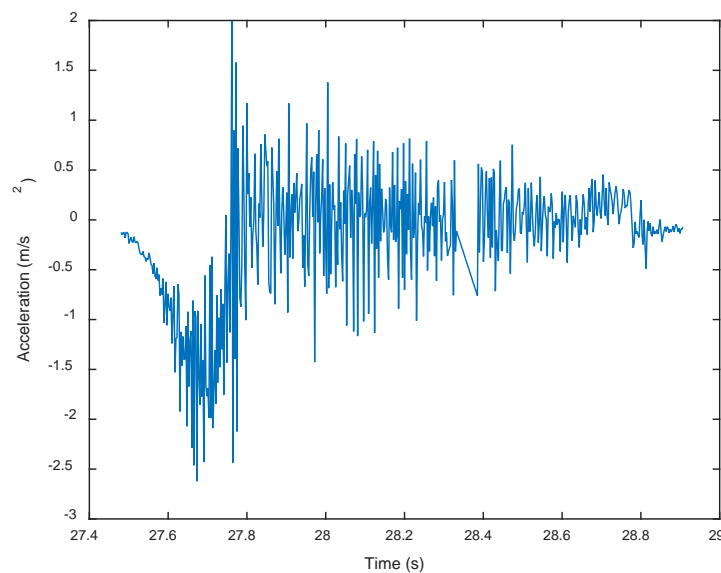


Figure 82. Friction Impulse Test: Bottom Rail with Base Plate Only

Table 12. Data from Impulse-Deceleration Tests (Bottom of Rail)

	Average Deceleration	Standard Deviation	μ_k
Plate Only (696.3g)	0.03845 m/s ²	0.4059 m/s ²	0.003922
1 Mass stack (2427.1g)	0.05572 m/s ²	0.4016 m/s ²	0.005682
2 Mass Stacks (4156.6 g)	0.06303 m/s ²	0.6168 m/s ²	0.006427
2 Heavy Stacks	0.05797 m/s ²	0.6522 m/s ²	0.005911

4.4.4 Friction Overall Characterization

When looking at the entire collection of friction coefficient values, a better idea of the nature of the friction profiles become known. Recalling Student's t-Test from earlier, since each method of friction measurement was repeated only three times (to avoid excessive wear,) the confidence interval of the data is large compared to a set of data that has more data points. Keeping this in mind, values collected from all three values are evaluated together as one whole set, as seen for the top of the guide rail in Fig. 83 and for the bottom in Fig. 84. For the top of the rail, the Shapiro-Wilks test yielded a $W = 0.8770$, and a P-value of 0.1459. From these results, the null hypothesis can be accepted, and the distribution can be assumed to be normal. With this, the average coefficient of kinetic friction of the entire set for the top of the rail is 0.7158, with a standard deviation of 0.0866.

For the bottom of the rail, the Shapiro-Wilks test yielded a $W = 0.7703$, and a P-value of 0.0002. From these results, the null hypothesis is rejected by the test, and the distribution cannot be assumed to be normal. Fig. 84 confirms this, however if one looks at the data closer, one will notice that the measured coefficients of kinetic friction for the bottom of the rail are

considerably small. In other words, even though there may be a large standard deviation, all the values are in the thousandths. However, if one were to neglect the numbers for the base plate only (which deviated significantly from the rest of measured values as seen previously), the distribution would have a $W=0.9297$, with a P-value of 0.1708. In this case, the null hypothesis would be accepted, and the distribution would be considered normal. With this consideration, the average coefficient of kinetic friction of the entire set for the top of the rail is 0.0047, with a standard deviation of 0.00005844.

Evaluating the three methods against each other, the suspended mass method was the most accurate because it was the most controlled method, yet the easiest of the three to control and evaluate. The incline method performed almost as well as the suspended mass, however there could be an error in reading the inclinometer, as such a device was very sensitive to disturbances in angles. If an angle is not held steady enough (the tilt plate can flex), the readings could be skewed. In fact, it was because of this phenomenon that this experiment had to be redone. Finally, the impulse method was the least accurate, as the mean acceleration profiles had relatively large (compared to the other methods) standard deviations that at times were larger than the mean acceleration itself. What this means was while there was obvious deceleration, the standard deviation implies that positive acceleration could also be happening. An example would be a deceleration of 0.05797 m/s^2 , with a standard deviation of 0.6522.

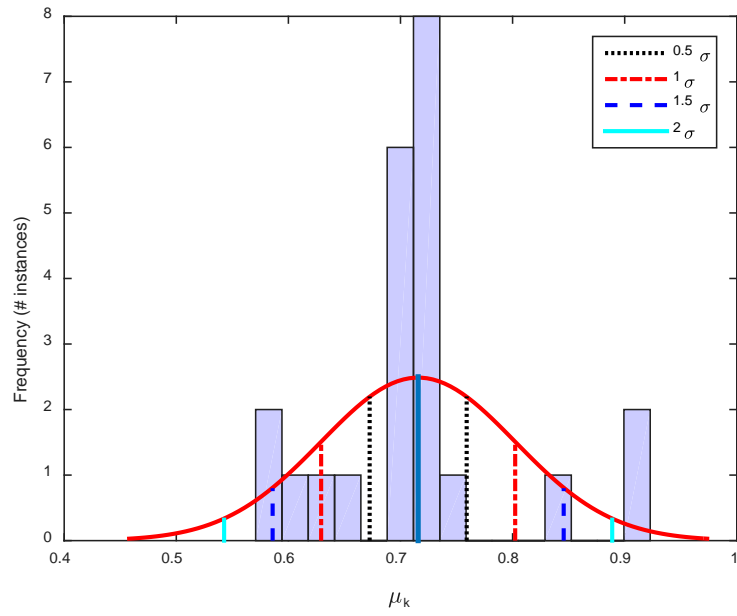


Figure 83. Kinetic Friction Distribution for Top Rail

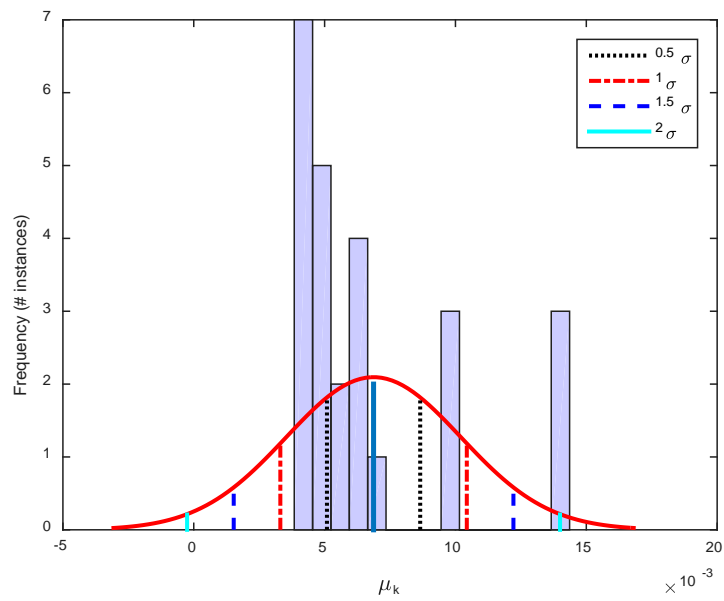


Figure 84. Kinetic Friction Distribution for Top Rail

4.5 Door Interference Experimental Results

The methodology of this experiment is described in Section 3.5 in Chapter III, and its corresponding test plan in Appendix A.4. As mentioned previously, analysis of the door was not planned until an informal use of a high-speed camera revealed that upon ejection, the door significantly oscillated, and made repeated contact with the underside of the ejecting payload base plate. To determine the accuracy of the PCB Piezotronics 352C22, each accelerometer underwent a calibration check.

Table 13. PCB Accelerometer Check Results

	#1	#2	#3	#4
Mean (m/s^2)	9.7284	9.5578	9.6808	9.7931
Standard Deviation (m/s^2)	0.1712	0.1838	0.3630	1.3210
RMS Error (against 9.7 m/s^2)	0.1722	0.2375	0.3666	1.3079

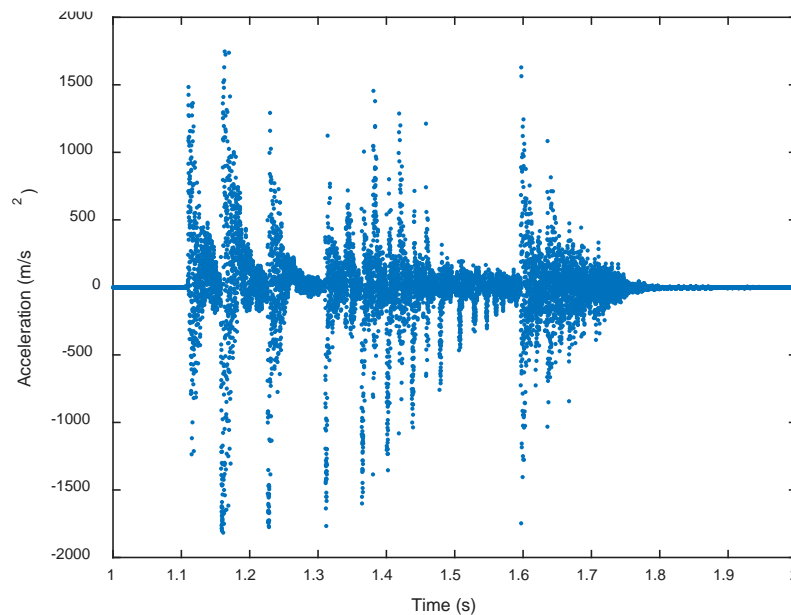


Figure 85. Door Accelerometer Readout Example (Top Right Quadrant Location)

Five of the door tests were conducted, and all had the same characteristic profiles of vibrations, as shown in Fig. 85. Of note about these readings was even though the high accelerations could be plausible, they did not match up well with the synchronized high-speed camera. For example, it took roughly 1 ms to reach the first peak in the accelerometer data, yet from the high-speed camera data, it took 50 ms for the door to open up. The video was analyzed further to see if the first transient was caused by the door release mechanism. Moreover, when integrating the data to find velocity and displacement, the data continued growing exponentially to impossible levels. It was coming across that phenomenon that perhaps the error was caused by the accelerometer's gravity cancellation feature. Given the barriers surrounding the accelerometer data, it was decided to analyze the motion of the door via the high-speed camera data alone for now. With that, 85 points of data were recorded based on the location of the black dot focal point that was being used while recording, as seen in Fig. 86. The change in pixel location was used to determine the angle of the door at that particular time step (since high-speed camera time steps were constant and determined by frame rate). The accuracy of this data is within +/- one pixel. The collected data yielded the following characterization of the door's angle versus time, as seen in Fig. 87.



Figure 86. Phantom Camera Control GUI (Focus Point Circled)

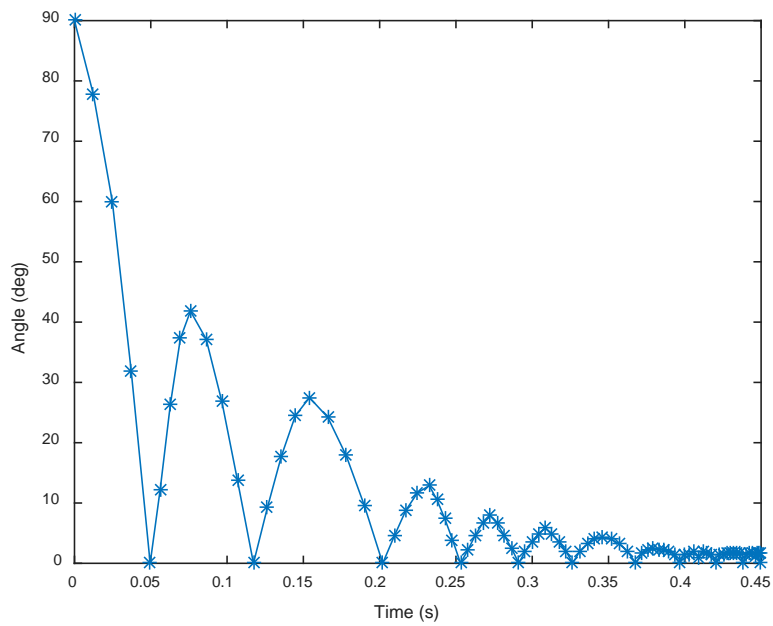


Figure 87. Door Orientation During Ejection

This profile takes the shape of an exponentially decaying sinusoid. Even though the door's oscillation profile is definitely not linear, it can be described using linear systems. The characteristic equation for this type of sinusoid can be described via Eq. (34).

$$\theta = |Ae^{-\zeta t} \cos(\omega t + \varphi)| \quad (34)$$

Using the least squares method, two of Eq. (34) were fit to the profile shown in Figure 87. This was done because the motion of the door was characterized by before it starts hitting the payload (before the fourth peak in Fig. 87) and when it started hitting the payload at the fourth peak and four times after that. With that:

$$\theta_{0-0.2s} = |93.5349e^{-10.0052t} \cos(36.5752t)| \quad (35)$$

Which has 21 residual values, and a mean squared error of 100.8871°.

This equation yielded the a function

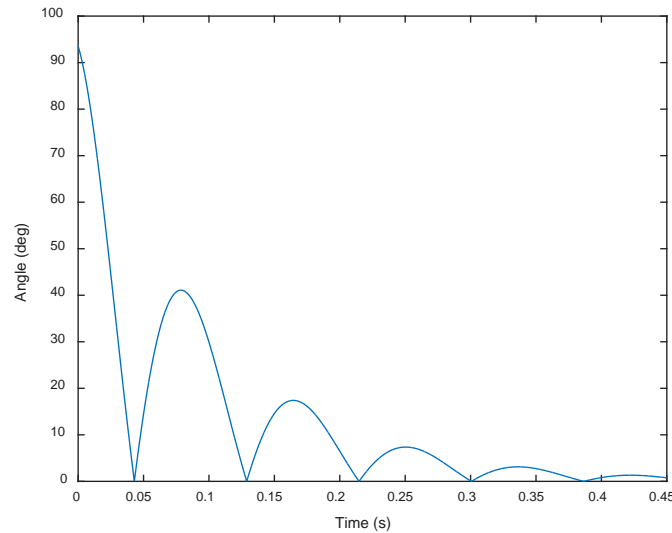


Figure 88. Modeling of CSD Door Orientation from 0-0.2 s

$$\theta_{0.2-0.45\text{ s}} = |60.9507e^{-7.8510t} \cos(81.4662t + \pi/4)| \quad (36)$$

Which had 65 residual values, and a mean squared error of 2.9529°. This equation yielded the following function:

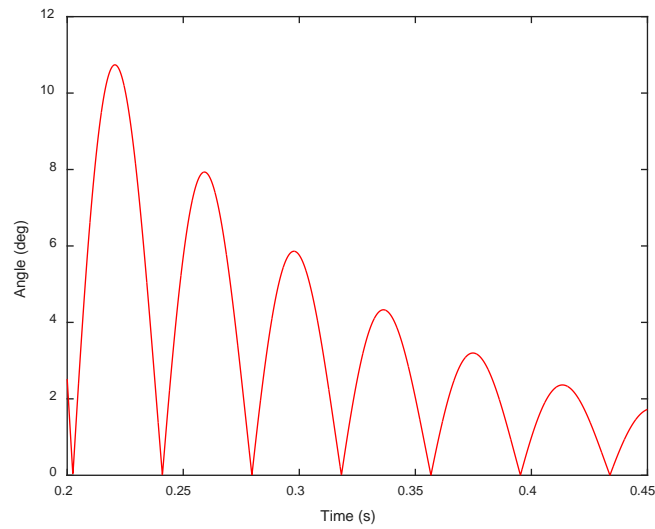


Figure 89. Modeling of CSD Door Orientation from 0.2-0.45 s

Combining the two functions and comparing with the original data yields Fig. 90.

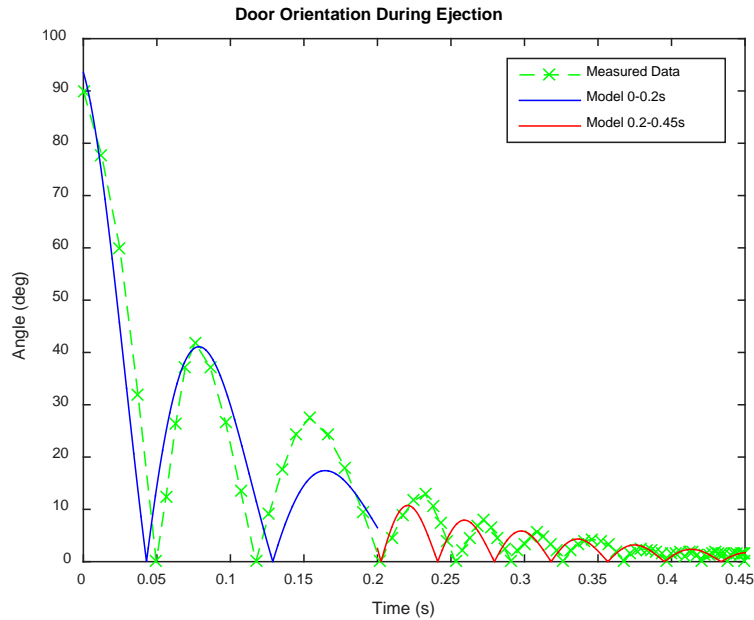


Figure 90. Full Modeling of CSD Door

4.6 Push Plate Feet Contact Experimental Results

The methodology of this experiment is described in Section 3.6 in Chapter III, and its corresponding test plan in Appendix A.5. Because there was a mass limit on how much mass a test payload should weigh, a 6U chassis was 3-D printed in an attempt to meet the 0.8 kg threshold. As mentioned previously, this was important because the 3-D printed chassis was ejected upwards vertically (as seen in Figure 91) in order to prevent gravity from influencing initial angular rates. Data was collected via the NGIMU. As seen in Fig. 92, the result was a 6U chassis without a top panel, and the bottom structure cut out, as both of these took up a significant fraction of the chassis' mass. The final mass of the test article was 0.502 kg, well within the requirement. By virtue of its geometry and using the coordinate system in Fig. 93, the

center of mass was centered on the Y-axis, and X-axis, and slightly offset on the Z-axis (19.4mm from the bottom of the base plate).



Figure 91. Vertical Ejection of 3-D Printed 6U Chassis

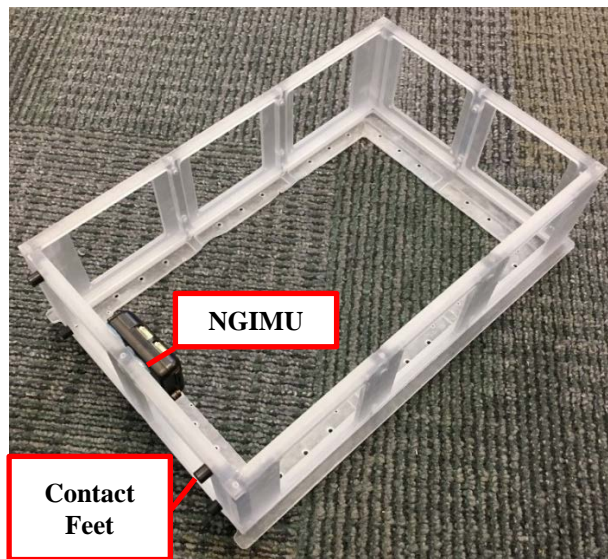


Figure 92. 3-D Printed 6U Chassis with Contact Feet and IMU

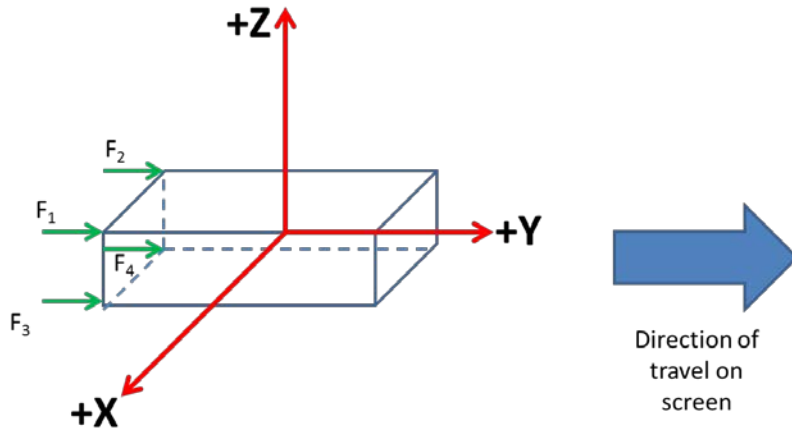


Figure 93. Diagram Demonstrating Force Distribution in Model [8]

The primary moments of inertia about the center of gravity were:

$$\begin{bmatrix} 4808.55 & 0 & 0 \\ 0 & 9624.29 & 0 \\ 0 & 0 & 13168.57 \end{bmatrix} \text{ kg} * \text{ mm}^2$$

The following test cases were run: all four feet, three of the feet, two of the feet, and one of the feet. The criterion for release was the sudden drop in acceleration towards 3σ noise threshold, and averages of initial angular rates were taken at these points. In these cases, initial rates only were compared because of the small amount of time that was allotted until gravity interfered with the deployment of the 3-D printed CubeSat. Knowledge of initial angular rates gave an indication on where to tune the model based on the equations of motion described earlier.

4.6.1 All Feet Contact

Given the physical parameters of the 3-D printed chassis, the full contact configuration will yield a predicted initial angular rate only around the X-axis at -11.05 °/s, as seen in Fig. 94. Sample data from one of the three runs conducted with the ejected printed chassis set to the 4-foot configuration is shown below in Fig. 95. Based on the three ejections, the following statistics were gathered in Table 14 for the four-foot configuration. However, upon comparing the three runs with the predicted model, a stark difference is noticed in the error figures.

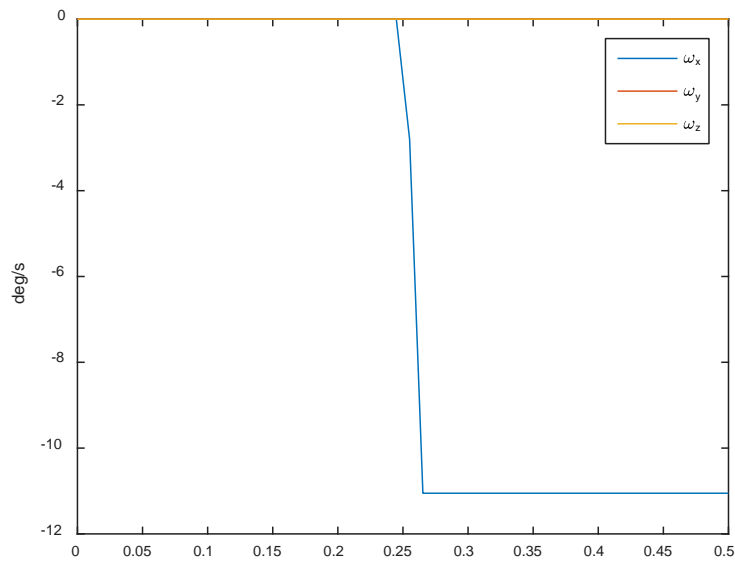


Figure 94. All Feet Contact Case Simulation Prediction

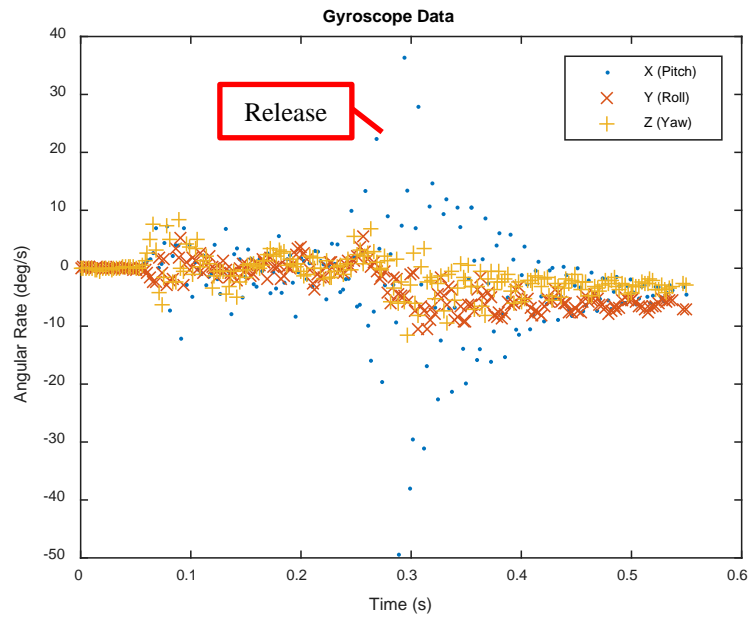


Figure 95. All Feet Contact Case IMU Readout

Table 14. Four Feet Contact Case Statistics

	X Axis	Y Axis	Z Axis
Average (°/s)	-4.5786	-3.8407	-2.3472
Standard Deviation (°/s)	1.2511	0.9467	3.3438

Table 15. All Feet Contact Case Measurements

	Run 1			Run 2			Run 3		
	X Axis	Y Axis	Z Axis	X Axis	Y Axis	Z Axis	X Axis	Y Axis	Z Axis
Actual (°/s)	-4.3112	-2.9731	-6.2052	-5.9417	-3.6986	-0.7095	-3.4828	-4.8504	-0.1268
Error with Model (°/s)	-6.7388	2.9731	6.2052	-5.1083	3.6986	0.7095	-7.5672	4.8504	0.1268

4.6.2 Three Feet Contact

In this case, foot #1 (per Fig. 93) was disengaged. Seen in Fig. 96, the model predicted initial rates of $-4.631^\circ/\text{s}$ on the X-axis, $0.07992^\circ/\text{s}$ on the Y-axis, and $-4.683^\circ/\text{s}$ on the Z-axis. Again, sample data is taken from one of three ejection runs set to the same three-foot configuration. The graph showing the initial angular rates recorded by the IMU is shown below in Fig. 97. To make things more clear, statistics were once again analyzed and presented below in Table 16 to describe the averages and standard deviations of the three three-foot chassis deployments. However, significant errors were found when data from all three IMU runs were compared with the original model prediction as presented in Table 17.

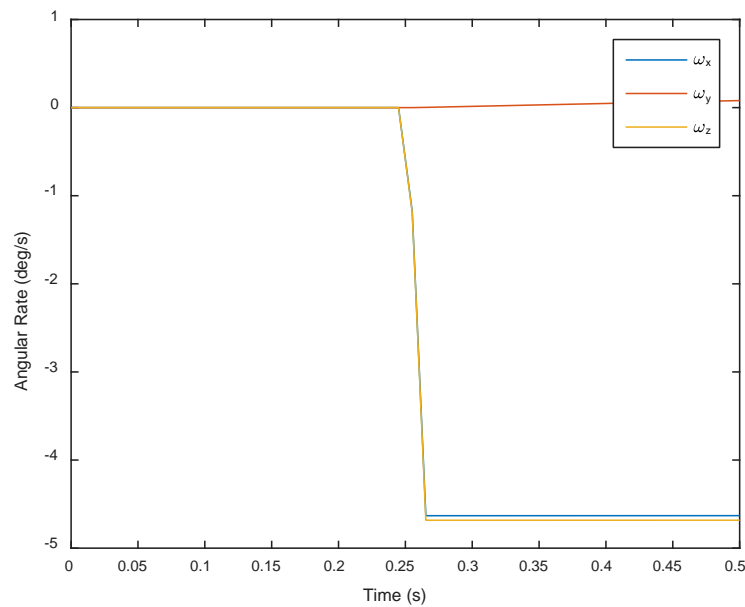


Figure 96. Three Feet Contact Case Simulation Prediction

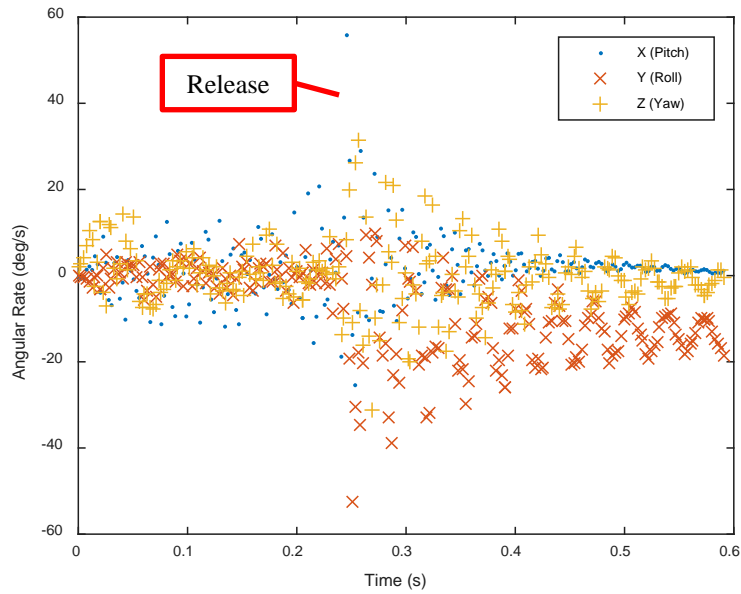


Figure 97. Three Feet Contact Case IMU Readout

Table 16. Three Feet Contact Case Statistics

	X Axis	Y Axis	Z Axis
Average (°/s)	6.5196	-11.6256	-2.9458
Standard Deviation (°/s)	4.1396	1.5148	2.6440

Table 17. Three Feet Contact Case

	Run 1			Run 2			Run 3		
	X Axis	Y Axis	Z Axis	X Axis	Y Axis	Z Axis	X Axis	Y Axis	Z Axis
Actual (°/s)	6.9214	-10.2094	-5.9874	10.4436	-11.4447	-1.6531	2.1937	-13.2228	-1.1969
Error with Model (°/s)	-11.5524	10.2893	1.3044	-15.0746	11.5246	-3.0299	-6.8247	13.3027	-3.4861

4.6.3 Two Feet Contact

In this case, foot #2 and #4 (per Fig. 93) were disengaged. As seen in Fig. 98, the model predicted initial rates of $-11.05^\circ/\text{s}$ on the X-axis, $-0.5721^\circ/\text{s}$ on the Y-axis, and $14.06^\circ/\text{s}$ on the Z-axis. As before, a printout from one of the two-foot configuration deployments is presented below in Fig. 99. Statistics were once again analyzed and presented below in Table 18 to describe the averages and standard deviations of the three three-foot chassis deployments. Unfortunately, when comparing the theoretical data with the collected data in Table 19, the trend of significant error seems to continue.

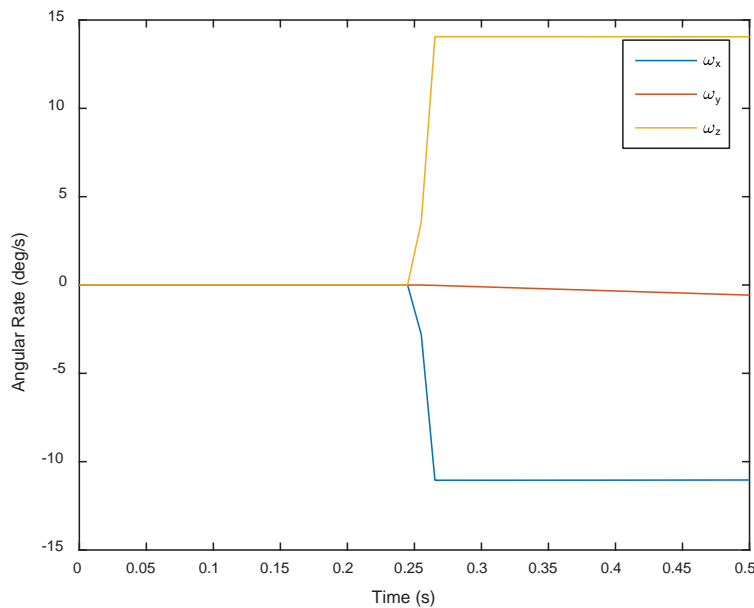


Figure 98. Tabs Only Contact Case Simulation Prediction

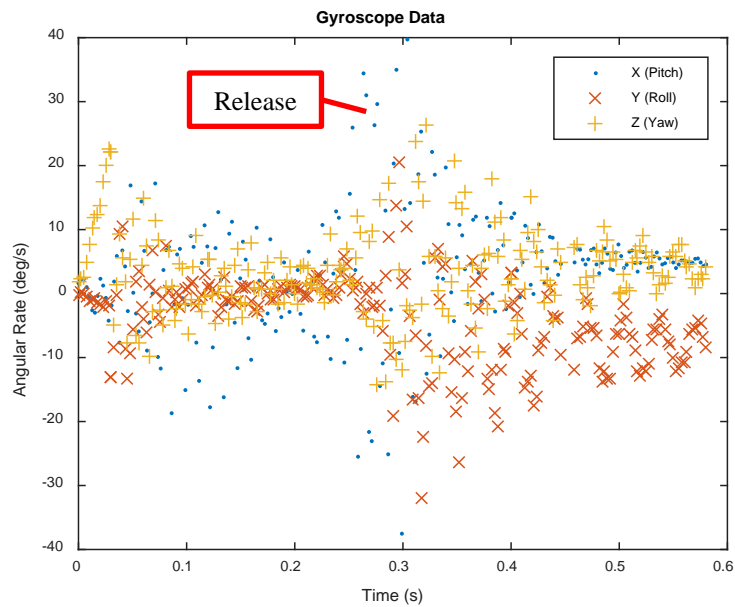


Figure 99. Two Feet Contact Case IMU Readout

Table 18. Two Feet Contact Case Statistics

	X Axis	Y Axis	Z Axis
Average (°/s)	3.6588	-5.5860	4.9272
Standard Deviation (°/s)	1.7333	1.9749	0.5327

Table 19. Two Feet Contact Case

	Run 1			Run 2			Run 3		
	X Axis	Y Axis	Z Axis	X Axis	Y Axis	Z Axis	X Axis	Y Axis	Z Axis
Actual (°/s)	2.7602	-5.0546	5.3883	5.6569	-7.7722	4.3441	2.5593	-3.9312	5.0492
Error with Model (°/s)	-13.8102	4.4825	-19.4483	-16.7069	7.2001	-18.4041	2.5593	-3.9312	5.0492

4.6.4 One Foot Contact

In this case, only foot #1 (per Fig. 93) engaged the push plate. As seen in Fig. 100, the model predicted initial rates of $-30.31^\circ/\text{s}$ on the X-axis, $-1.57^\circ/\text{s}$ on the Y-axis, and $14.07^\circ/\text{s}$ on the Z-axis. As with the previous cases, below in Fig. 101 is a sample initial angular rate profile gathered from the printed chassis with only one foot engaged. Furthermore, the following are statistics in Table 20 based on measured data in order to get a good idea of the level of consistency these deployments are turning out to yield. Moreover, comparing with collected and predicted data found in Table 21 yielded the worst deviation ($-51.141^\circ/\text{s}$).

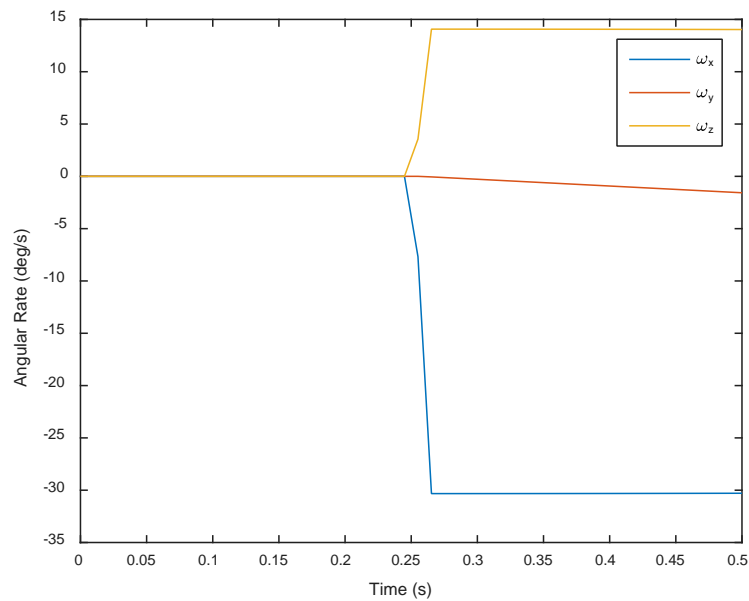


Figure 100. One Foot Contact Case Simulation Prediction

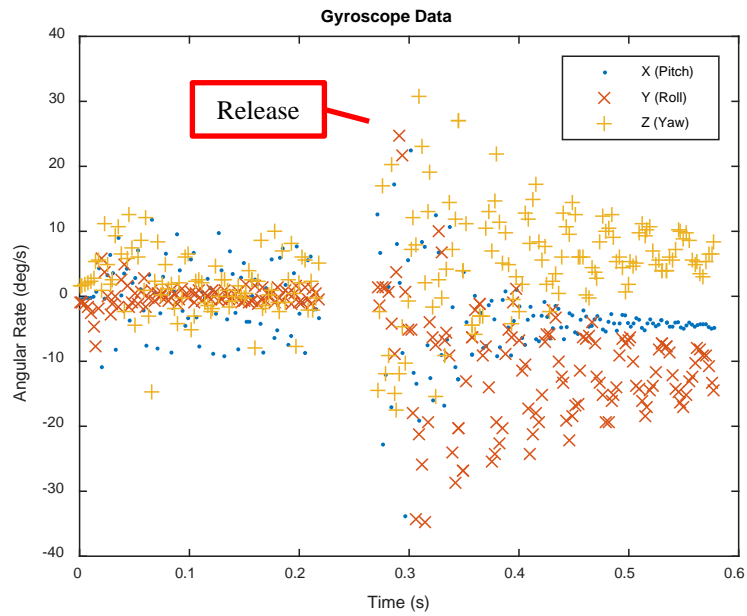


Figure 101. One Foot Contact Case IMU Readout

Table 20. One Foot Contact Case Statistics

	X Axis	Y Axis	Z Axis
Average (°/s)	-4.1579	-9.8192	5.9675
Standard Deviation (°/s)	1.3684	2.7142	2.0462

Table 21. One-Foot Contact Case

	Run 1			Run 2			Run 3		
	X Axis	Y Axis	Z Axis	X Axis	Y Axis	Z Axis	X Axis	Y Axis	Z Axis
Actual (°/s)	-5.4832	-6.6979	3.976	-2.7501	-11.6256	8.0643	-4.2403	-11.1340	5.8621
Error with Model (°/s)	-51.6775	3.5477	16.4779	-51.141	1.5295	15.7276	-50.2666	-4.3821	15.4939

4.6.5 Tabs Only Contact

In this case, only the tabs were engaging the push plate. NASA was suggesting this configuration for EM-1 CubeSats (see Fig. 102). As seen in Fig. 103, the model predicted initial rates of $11.05^\circ/\text{s}$ on the X-axis, $0^\circ/\text{s}$ on the Y-axis, and $0^\circ/\text{s}$ on the Z-axis. Fig. 104 shows how nicely the payload is being ejected during this phase, however it still seems that error continues to propagate. Even though Table 22 show is good statistics, Table 23 still shows that there is significant error that needs to be dealt with.

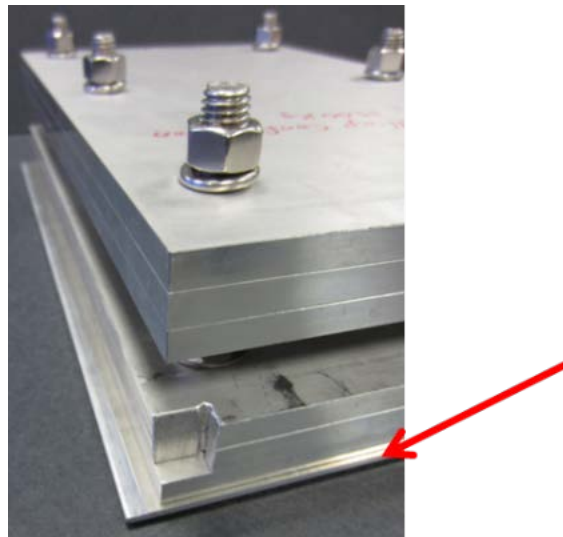


Figure 102. NASA Experimental CSD Test Mass with Tab Bar [19]

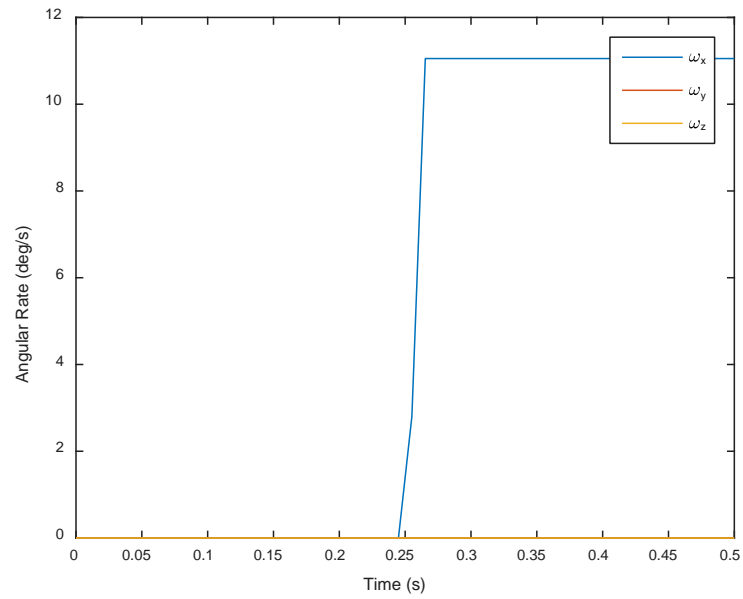


Figure 103. Tabs Only Contact Case Simulation Prediction

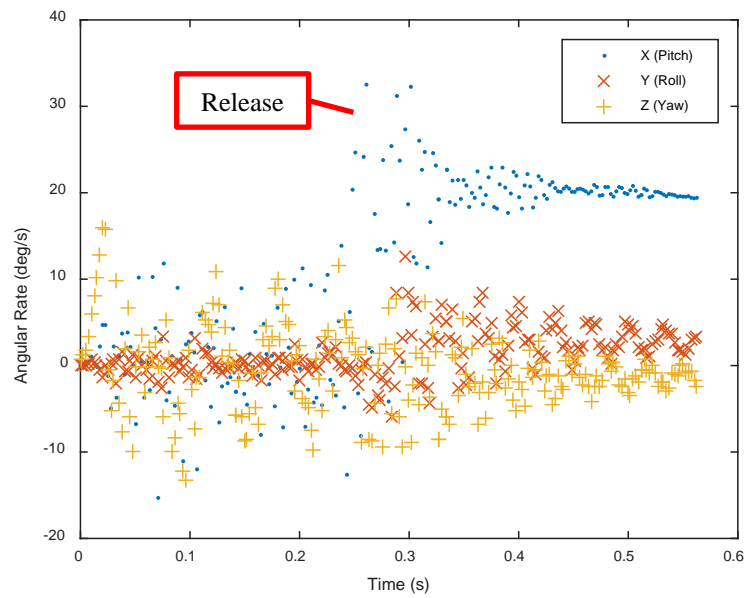


Figure 104. Tabs Only Contact Case IMU Readout

Table 22. Tabs Only Contact Case Statistics

	X Axis	Y Axis	Z Axis
Average (°/s)	20.3938	-1.8017	-1.8298
Standard Deviation (°/s)	0.618294169	4.121121891	0.514104688

Table 23. Tabs Only Contact Case

	Run 1			Run 2			Run 3		
	X Axis	Y Axis	Z Axis	X Axis	Y Axis	Z Axis	X Axis	Y Axis	Z Axis
Actual (°/s)	21.3675	-5.1177	-2.4079	20.8310	-3.0995	-1.6576	19.9566	2.8121	-1.4239
Error with Model (°/s)	-10.3175	5.1177	2.4079	-9.781	3.0995	1.6576	-8.9066	-2.8121	1.4239

4.6.6 Push Plate Feet Contact Overall

From the data collected, it was apparent that the model needed further tuning in order to accurately reflect what the IMU is presenting, especially since the IMU readings for each scenario were reasonably consistent, especially since most of them have small standard deviations amongst each other. It was suspected that the large differences between measured and theoretical, was that the model did not account for perturbations in the push plate. Another aspect was that the model might be using rough values in order to estimate dimensions and payload configuration.

4.7 MATLAB Simulation Model Tuning Results

Initially, the deployment model produced results consistent with Euler's Equation and was able to simulate instantaneous moments. Fig. 105 and Fig. 106 describe an arbitrary scenario in which (using Fig. 93 as a guide) F1 applies 10% of the push force, F2 applies 0%,

F3 applies 70%, and F4 applies 20% to a CubeSat with a defined mass (~ 8 kg) and Moments of Inertia (MOI). It was obvious that Euler's Formulas can be used to predict the relationship between the applied moments and the angular rates. An interesting prediction was that in this scenario, the angular rate on the 1-axis (pitch) would tumble a little under $15^\circ/\text{s}$. This was previously demonstrated in this chapter via IMU data. Overall, this surpassed PSC's range of expected angular rates. [2]

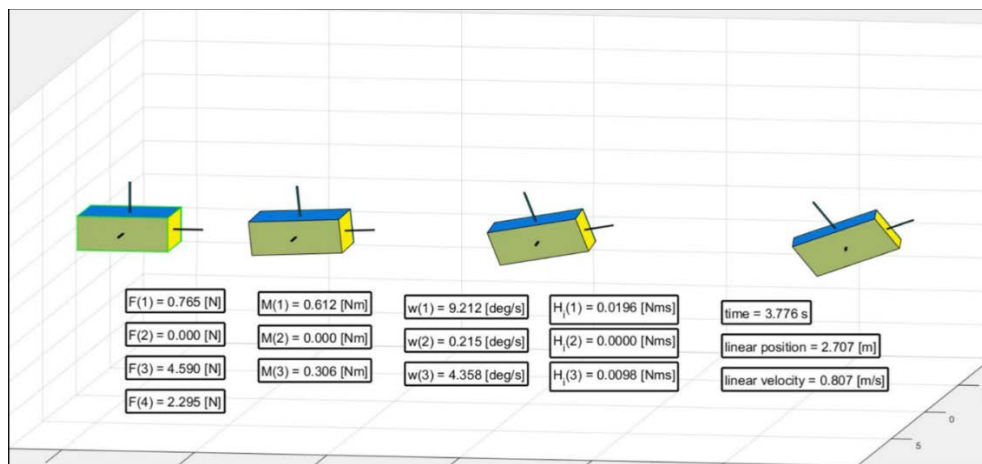


Figure 105. Deployment Model (Using Sample Force Distributions)

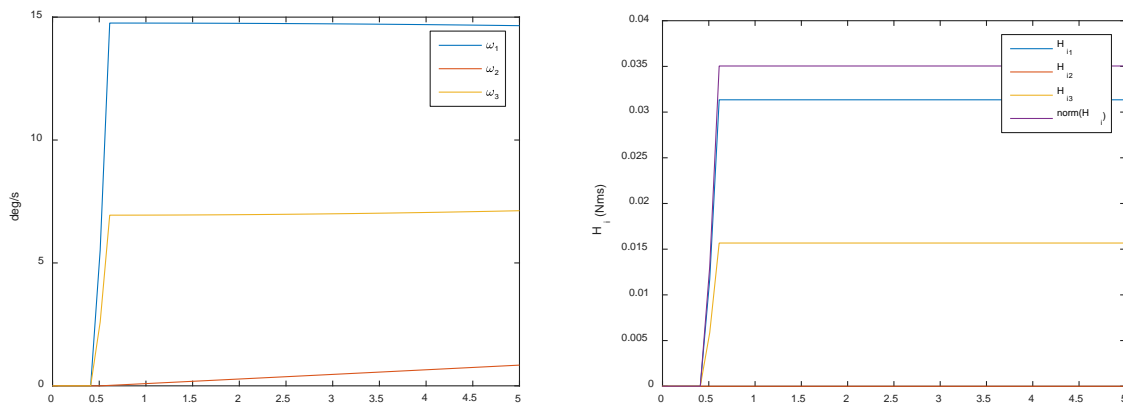


Figure 106. Spacecraft Angular Rates (left) & Inertial Frame Angular Momentum (right)

Originally, this model did not account for any perturbations (e.g. jostling, friction, etc.), and the moment during an ejection was applied at an ambiguous location on the guide rail (last 0.5 in). With the IMU deployment tests, the exact location where moments were applied were found and incorporated into the model. The friction coefficients and door forces found during this thesis were also found, and their incorporation into the model should be done in the future in order to further improve the model. The algorithm developed however states that in microgravity conditions, half of the payload normal force would apply to each of the top and bottom rails in order to account for initial surface contact when the CSD door opened and the clamping rail disengages from the payload. When simulating horizontal deployment in gravity conditions, the force of friction was dependent on the location of the payload's center of mass. If the center of mass were within the CSD rail, then the bottom of the rail's coefficient of kinetic friction would apply. Once the center of mass went beyond the envelope of the CSD rails in the y direction, the moment of the plate was calculated. The payload was then characterized as a lever. In this case, the force of gravity pulled down the payload end that is outside of the CSD. With the rail lip acting as a fulcrum, the top CSD rail to the backside of the payload applied a normal force. This normal force increased all the way until deployment.

Other means to improve the simulation-model was the incorporation of user-defined parameters, where the code prompts the user to define the boundary conditions he may be working under so that he may be able to accurately characterize an ejection scenario.

Summary

In this chapter, the results from the analysis conducted were examined as well as the investigative questions answered. In Chapter V, conclusions and significance from this research will be presented. In addition, recommendations for action and future research will be presented.

V. Conclusions and Recommendations

Chapter Overview

This thesis described the experimental methods undertaken in order to quantify the linear and angular rates a payload experienced while being deployed by the Canisterized Satellite Dispenser (CSD). Chapter I discussed how initial qualification tests on the CSD were enough to provide a rough estimate on how well it worked, but still left many unanswered questions that payload customers needed to either answer themselves, or accept the risk of the unknowns surrounding the deployment of the CSD.

The second chapter discusses how Planetary Systems Corp's (PSC's) initial tests created more questions to be answered, and as time went on, the need to answer these questions increased, especially since NASA and the Department of Defense (DoD) become more interested in employing the CSD for their missions. Also discussed were the equations of motion that govern flight dynamics of a spacecraft, and what would need to be used to map out the CSD's performance profile. Moreover, Chapter II discusses various ways that could be employed to evaluate the actual deployment properties of the CSD through various potential methods.

Chapter III covers the testing and validating that would need to be done in order to develop a better idea on how the CSD operated and what it does to its payloads. The validation process was discussed and the theory behind each experiment was explained in order to characterize friction, door transients, push plate contact, accelerometer and gyroscopic sensor

usage, as well as the employment of high-speed photography to capture discrete processes that undergo during a payload deployment.

Chapter IV discusses the data that was collected and analyzed in order to tune the MATLAB simulation to better represent what a payload experienced while being dispensed by the CSD. It also discussed some unexpected results that were encountered, and some of which need further study. The fourth chapter also described the results from the analysis as well as answered the investigative questions outlined in the first chapter.

Conclusions of Research

From the Push Plate Force Test, the average static force measured was at 4.42 lbs (19.661 N) with a 1- σ standard deviation of 0.17 lbs (0.776 N), which was within PSC's CSD specs between 15.6–46.7 N [2]. Using a CubeSat base plate of 0.59 kg, accelerometer data analysis showed an average linear deployment acceleration of 13.3853 m/s², with a standard deviation of 4.9503 m/s². This subsequently yields an average dynamic push plate force of 7.8963 N. After integrating accelerometer data once to find linear velocity, which had a root mean square (RMS) error between the predicted velocity from the analytical model of 0.2900 m/s. Integrating again to find linear displacement, the RMS error for displacement was even better at 0.0096 m when comparing the model prediction and the integrated displacement values.

The deployment experiment was repeated again with a new IMU, along with hard anodizing the base plate, as PSC specifications warrant at a minimum the tabs be anodized. The average acceleration from this data is 9.1503 m/s², with a standard deviation of 20.8535 m/s².

This subsequently yielded an average deployment force of 6.3713 N. Comparing the velocity profile of the integrated data and the predicted model, the RMS error is 0.4831 m/s. Regarding the twice integrated accelerometer data with the predicted displacement, the RMS error was calculated to be 0.0428 m. Intermittent oscillations in velocity and the gap growth between predicted and integrated data were noticed, which is indicative of deployment interference. The oscillation of the CSD door was suspected to be the culprit, so the test was repeated yielding much better results of RMS errors of 0.1535 m/s for velocity, and 0.0139 m for displacement. The corresponding gyroscopic data yielded the locations on when and where tipoff moments were applied to the payload (after 0.3194m of payload deployment travel), as well as when the payload left the confines of the CSD guide rail (after 0.3378 m of travel)

The average acceleration from this data is 9.1503 m/s^2 , with a standard deviation of 20.8535 m/s^2 , which subsequently yielded an average deployment force of 6.3713 N. Comparing the velocity profile of the integrated data and the predicted model, the RMS error is 0.4831 m/s. Comparing the twice integrated accelerometer data with the predicted displacement, the RMS error was calculated to be 0.0428 m. Intermittent oscillations in velocity and the gap growth between predicted and integrated data were noticed, which is indicative of deployment interference.

The average acceleration from this data is 9.1503 m/s^2 , with a standard deviation of 20.8535 m/s^2 , which subsequently yielded an average deployment force of 6.3713 N. Comparing the velocity profile of the integrated data and the predicted model, the RMS error is 0.4831 m/s. Comparing the twice integrated accelerometer data with the predicted displacement, the RMS error was calculated to be 0.0428 m. Intermittent oscillations in velocity and the gap

growth between predicted and integrated data were noticed, which is indicative of deployment interference.

From the Push Plate Feet Contact experiment, it was apparent that the model needs further tuning with respect to tip-off rates caused by the push plate feet, where there were instances when the model was off by $\sim 50^\circ/\text{s}$ on an axis. This conclusion was arrived at because the multiple runs of measured IMU data was consistent in performance, and had small standard deviations amongst each other. It was suspected that the deviations between theoretical and measured values were due to the analytical model not accounting for perturbations in the push plate. Moreover, the model most likely deviated from measured values because the parameters used may not have been precise enough.

Overall, deploying in a lab environment with gravity makes characterization very difficult. Encountered issues due to gravity included:

- Risk of wear on CSD surface finishes
- Induced gravitational moments as payloads leave the CSD
- Horizontal deployments require small-mass payloads in order to successfully eject (~ 3 kg payload could not deploy due to friction caused by a gravitational torque)
- Vertical deployments upwards limit payload mass to less than 0.8 kg
- Vertical downward deployments may induce moments within the CSD guide rails due to offset between tabs and center of mass
- IMU data implies that initial oscillations/chattering during deployment could be induced due to gravity moments within the guide rails.

Recommendations for Action

It is recommended that the door be modified with a catch mechanism (i.e. latch, locking clip, Velcro, etc.) or dampener in order to counteract the oscillations it experiences. The risk of the door striking the underside of a payload can yield mission crippling effects, such as damage to delicate solar panels and arrays.

Moreover, it is recommended that the push plate be stiffened because the feet variation tests and the high-speed camera tests seem to indicate that the push plate significantly flexed during deployment, which could lead to induced transient errors.

Finally, from initial data, it is not suggested to use NASA's recommendation of simplifying the push plate contact with a tab bar in lieu of the standard contact feet around the center of mass, because of running the risk of significant moments that were seen in Chapter IV. Adhering to original specifications yields the lowest risk because moments will be reduced, which subsequently reduces initial angular rates.

Recommendations for Future Research

The first suggestion is to conduct 2.2 s drop tower at NASA's Zero-G Facility at Glenn Research Center as described in Chapter II, where the model will be compared with a control variable: a deployment conducted micro-gravity. During these drop-tower experiments, CubeSat payload center of mass and push plate contact forces will be varied in order to characterize how the geometry of the payload affects its deployment. Data from these deployments will provide the necessary adjustments to further tune the model beyond what can

be done in an in-gravity lab environment in order to make it a more accurate representation of deployment.

During the Push Plate Force Test major deviation force spikes (20.91N) and drops (18.68N) at specific depths of 0.1m and 0.14 m, respectively, occurred. Either if desired, future studies could use a more precise measurement tool, by using load cells, or suspended masses could be used to get a more accurate reading, as well as differentiate whether these spikes were caused by human error, or a mechanical trait of the CSD.

During the deployment tests with the IMU, the improvement in RMS errors and much closer correlation between predicted and measured data curves prove that the door was a major source of interference. Now that the door's motion was characterized and force profile equation of motion was derived, further analyses in these equations and accelerometers would be beneficial to understand further the door accelerometer data. Once the door's dynamics is better understood, the next logical step is to use its characterization in the model to replicate the perturbations seen in the deployment tests. Moreover, the rail friction algorithm described in Chapter IV should be incorporated into the model in order to account for the effects of friction in micro-gravity and horizontal gravity conditions. Even though the preferred method of finding the coefficient of kinetic friction is the suspended mass method, if one wanted to retry the impulse-deceleration method, a low pass filter could be used to filter out the excess noise and isolate the actual signal associated with motion because during these tests the data was quite noisy. The filter could have a cutoff frequency based on a Fast Fourier Transform analysis, and the random components should have small total energy and show as a steady frequency data set. If data from the FFT converge asymptotically to a flat line at some value, one can either filter

where the FFT data approaches the asymptote, keeping the frequencies below the asymptote, or modify the data by subtracting that value from all the FFT values and reconstruct the data from the modified FFT. The former method has better theoretical basis, and should reduce noise levels in the data [55].

Another item that could be studied is the degree in which the tab clamps are reapplied due to door oscillations, and measure how much resistance the clamps apply to the tabs as the payload is being ejected. In addition, it was noted that after the base plate was anodized, the surface was smoother, but at the same time had a tendency to mildly stick when pinched. A future study in seeing how surface coatings could affect performance would also prove to be beneficial to improving deployment performance, primarily in reducing interference/friction during deployment, as these interferences add perturbations during deployment, thus reducing mission risk. With respect to the results of the Push Plate Feet Contact, the model should be looked at closer to see if there is an error in the code. Moreover, a direct model using the measured material and deployment data of the 3-D printed chassis should be created in order to identify the differences between the initial model. These differences would subsequently identify what in the model needs to be adjusted in order to match experimental data. These differences would allow better understanding on how moments are applied, which will subsequently make the model much more accurate.

Summary

Overall, it is obvious there are many areas of study as described earlier that still needs to be looked at in order to fully characterize the CSD. The result is to subsequently enable the

modeling of angular and linear rates during deployment. One can see how complex this research has become, not because of the nature of the experiments that have been conducted, but because of the integration that is required in order to piece the results of each individual experiment together, and use their collective results to improve the analytical model. The difficulty of this research has already led to the conclusion that micro-gravity experiments are needed in order to fully capture the data needed to assess accurately the performance of a payload as it is ejected from the CSD, and use it to tune the analytical model. Moreover, it would be invaluable to assess future onboard telemetry data, perhaps from the NASA SLS EM-1 CubeSat missions, and use this data to tune the analytical model even further. This is worth the effort, however, because once this is attained, CubeSat mission planners will have a means to predict how their missions will act during deployment operations, and will allow them to undertake the necessary planning and contingencies to better ensure mission success.

Appendix A.1 – Test Plan: CSD Push Plate Force Profile Testing

AFIT/ENY
12U CSD Push Plate
WRIGHT-PATTERSON AFB, OH

PROCEDURE:
REVISION:
DATE REVISED:
NUMBER OF PAGES:

CSD_PushPlate_TP
2
22 Aug 2016
14

**AFIT / ENY
OPERATIONS**

**6U/12U CSD Push Plate
Force Profile Testing**

SYSTEM UNDERGOING TESTING

6U/12U Canisterized Satellite Dispenser

ASSOCIATED FUNCTIONAL TEST PLAN VERSION

N/A

PREPARED BY:

Test Engineer _____
Test Conductor _____

DATE _____

REVIEWED / APPROVED BY:

AF Customer _____
Test Director _____

DATE _____

Revision	Notes	Prepared By
0	- Initial procedure	Capt Stephen Tullino 12 Aug 2016
1	- Procedure adjusted to focus on force profile WRT push-plate depression location	Capt Stephen Tullino 22 Aug 2016

TABLE OF CONTENTS

	Page
1.0 ABBREVIATIONS AND ACRYONMS.....	1
2.0 TEST DESCRIPTION AND OBJECTIVES	1
2.1 PURPOSE.....	1
2.2 SCOPE	1
2.3 OBJECTIVES/SUCCESS CRITERIA	1
3.0 DOCUMENTATION	2
3.1 REFERENCE DOCUMENTS.....	2
3.2 SPECIFICATIONS	2
3.3 DRAWINGS.....	2
4.0 TEST REQUIREMENTS AND RESTRICTIONS	2
4.1 TRAINING	2
4.2 MAXIMUM PERSONNEL:.....	2
4.3 LIST OF EQUIPMENT	2
5.0 SAFETY REQUIREMENTS	3
5.1 PERSONNEL PROTECTIVE EQUIPMENT REQUIREMENTS	3
5.2 EMERGENCY PROCEDURES.....	3
5.3 TEST AREA ACCESS DURING OPERATIONS	3
5.4 SPECIAL INSTRUCTIONS	3
6.0 PRE-TEST SETUP	3
7.0 TEST SERIES FLOW / PLAN	5
7.1 SETUP	5
7.2 TEST	7
7.3 TEARDOWN	8
8.0 EMERGENCY RESPONSE	9
APPENDIX 1.0 – Force Reading Recording.....	10
APPENDIX 2.0 – Test Log.....	11

PERSONNEL

LOCATION DETERMINED BY TC

DATE_____

The following personnel are designated as test team members, and are chartered to perform their assignment as follows:

Test Conductor (TC) – Responsible for the timely performance of the test as written. This includes coordinating and directing the activities of the Red Crew and other test support teams. TC is responsible for coordinating all pretest activities and outside support required, including (but not limited to) security, fire, medical, and safety. TC is responsible for initialing completion on each step of the master test procedure.

Name_____ Signature_____

Test Director (TD) – Responsible for overall facility and test safety. Responsible for ensuring all test goals are met and all critical data is acquired. Supervises test activities to ensure procedures are followed. Has authority to perform real-time redlines on test procedures as required to ensure test requirements and goals are met.

Name_____ Signature_____

Red Crew Leader (RCL) – Responsible for directing the activities of Red Crew members. Reports directly to the TC and ensures all Red Crew tasks are completed. Responsible for ensuring all RCM's have all required certifications and training. Responsible for ensuring all required equipment is available, accessible, and serviceable.

Name N/A Signature_____

Test Panel Operator (TPO) – Responsible for operating the facility control systems during test operations as directed by TC. TPO is responsible for notifying the TC of any anomalous conditions.

Name N/A Signature_____

Red Crew Member (RCM) – Reports to the RCL. RCM is responsible for performing test-related tasks as directed by RCL.

Name N/A Signature_____

Name_____ Signature_____

Functional Test Conductor – Responsible for performing functional test in support of test.

Name N/A Signature_____

Name_____ Signature_____

EXCEPTIONS – When filling all positions is not possible, the Test Conductor will assume the duties of any empty position until the completion of the test or a suitable replacement is designated.

ALL TEST TEAM MEMBERS – Responsible for the safe performance of the test. Have read and understood all portions of the test procedure. Any Test Team Member can declare an emergency or unsafe condition.

1.0

1.0 ABBREVIATIONS AND ACRYONMS

AFIT	Air Force Institute of Technology
FOD	Foreign Object Debris
IPA	Isopropyl Alcohol
PPE	Personal Protective Equipment
RCL	Red Crew Leader
RCM	Red Crew Member
STE	Special Test Equipment
TC	Test Conductor
TD	Test Director
TOP	Test Operating Procedure
TPO	Test Panel Operator

2.0

2.0 TEST DESCRIPTION AND OBJECTIVES

2.1

2.1 PURPOSE

This procedure provides the means to perform deployment testing for test articles supplied relating to the 6U/12U CUBESAT CHASSIS. The 6U/12U CUBESAT CHASSIS test campaign is a structure and model validation plan intended to mitigate technology concerns for a future flight in a Planetary Systems Corp Canisterized Satellite Dispenser (PSC-CSD). The test location will be configured with the proper special test equipment (STE) to direct and measure “maximum predicted environments” associated with launching the 6U/12U Chassis according to the PSC-CSD Payload Specification.

2.2

2.2 SCOPE

This procedure tests the CSD push plate forces in order to identify applied force variations along different depression positions of the CSD push plate. These variations will determine linear velocities and accelerations within the CSD, as well as the prediction of rudimentary deployment linear and angular rates when given center of mass data and chassis-pusher plate contact point locations for a given 6U/12U Chassis.

2.3

2.3 OBJECTIVES/SUCCESS CRITERIAComplete Success

1. Forces are within a maximum deviation of +/- 7% of mean force

Marginal Success

2. Forces are within a maximum deviation of +/- 10% of mean force

Unsuccessful

3. Forces exceed a deviation of +/- 10% of mean force

3.0	3.0 <u>DOCUMENTATION</u>
	The completion of each applicable event shall be verified by initialing to the left of the item number. Deviations from these procedures will be coordinated with the Test Conductor. (NOTE: TD has the local authority to approve red-line revisions to this procedure).
<u> </u> 3.1	3.1 REFERENCE DOCUMENTS Planetary Systems Corporation Canisterized Satellite Dispenser (CSD) Data Sheet (2002337C Rev – 3 Aug 2015)
<u> </u> 3.2	3.2 SPECIFICATIONS The following list of specifications shall be used as a guide: Planetary Systems Corporation CSD Operating and Integration Procedure (3000257B 18 Jan 2016) Planetary Systems Corporation Payload Specification for 3U, 6U, 12U AND 27U (2002367 Rev - 25 July 2012)
<u> </u> 3.3	3.3 DRAWINGS NONE
4.0	4.0 <u>TEST REQUIREMENTS AND RESTRICTIONS</u>
<u> </u> 4.1	4.1 TRAINING The following training is required for personnel using these procedures: All personnel: Job Site General Lab Safety Briefing AT LEAST ONE PERSON PRESENT MUST BE TRAINED BY PSC TO OPERATE CSD (OR SUPERVISE CSD OPERATION)
<u> </u> 4.2	4.2 MAXIMUM PERSONNEL: Control Room: 3
<u> </u> 4.3	4.3 LIST OF EQUIPMENT <ul style="list-style-type: none"> - 1 – ESD Mat - 1 - 12U CSD - 1 - Push-pull gauge kit - 1 - Non-marking tape (e.g. Kapton tape) - 4 (minimum) - 10-32 (#10) UNF SHC screws

- 4 (minimum) - Washers for #10 screws (McMaster-Carr PN 93574A438 or similar), max OD is 0.33 in
- 1 - 5/32 inch hex key (minimum 1.5 inch shank length)
- 1 - Hex key or screwdriver <0.10 inch wide
- 1 – Force measuring apparatus (AFIT made)

Ensure all tools associated with this experiment/test/operation are accounted for prior to initiating system/item test. Ensure all FOD is picked up from around the test facility.

5.0**5.0 SAFETY REQUIREMENTS****____ 5.1****5.1 PERSONNEL PROTECTIVE EQUIPMENT REQUIREMENTS**

Standard PPE: Gloves, boots – soles and heels made of semi-conductive rubber containing no nails.

All jewelry will be removed by test members while working on the test facility. No ties or other loose clothing permitted (at TD discretion).

____ 5.2**5.2 EMERGENCY PROCEDURES**

In the event of an emergency that jeopardizes the safety of the operators or other personnel perform Section 11.0 emergency procedures at the end of this document.

____ 5.3**5.3 TEST AREA ACCESS DURING OPERATIONS**

The test facility room will be limited to test personnel only. Personnel will not be allowed access to the test area unless cleared by the TD.

____ 5.4**5.4 SPECIAL INSTRUCTIONS**

A qualified technician should provide orientation for clean room awareness and the proper faculty member / instructor should be consulted on test-series set points prior to test operations commencing.

Test Crew members shall place all cellular telephones on “silent mode” or turn off prior to completing any portion of this procedure.

6.0**6.0 PRE-TEST SETUP****____ 6.1**

TC

VERIFY all pages in this procedure are intact and complete.

____ 6.2

TC



READ procedure and input any specific information required to perform operation.

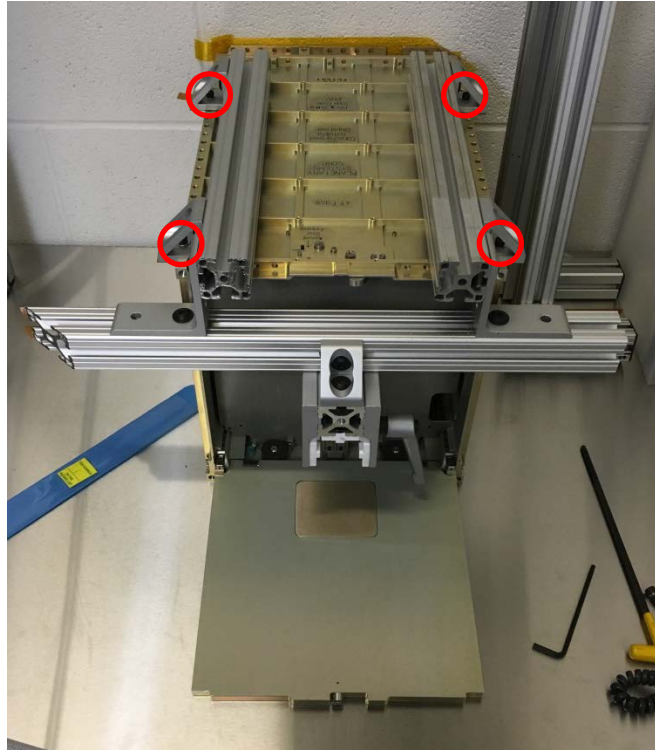
____ 6.3

TC

VERIFY with Facility Management that no open Work Orders / Issues are listed for the location's impeding operations.

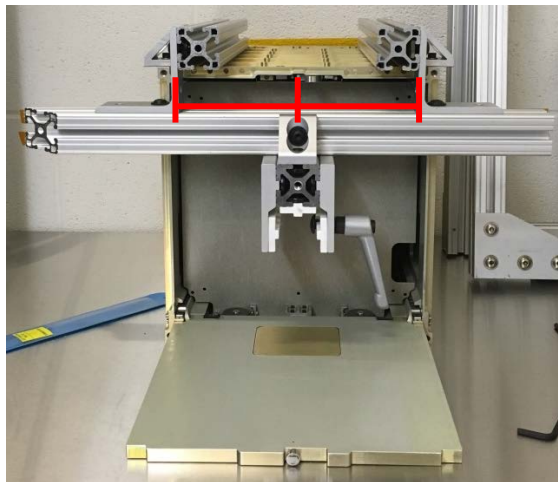
____ 6.4	TC	PERFORM Setup Brief with Test Crew Members and note any redline changes on Appendices.
____ 6.5	TC	VERIFY Test Team has donned standard PPE (and noted restrictions / special instructions).
____ 6.6	TC	PERFORM Pre-Operation Brief with Test Crew Members <ul style="list-style-type: none"> – Objective – Personnel and assigned roles/duties – Safety: materials, PPE, communication, etc. – Sequence of events – Emergency procedures
____ 6.6.1	TC	RECORD Pre-Test Brief Time _____
____ 6.6.2	TC	VERIFY all personnel involved with the operation have signed this procedure.
____ 6.7	TC	VERIFY push-pull gauge information <ul style="list-style-type: none"> - Identification Number: _____ - Calibration Date / Due Date: _____ / _____

7.0		7.0 <u>TEST SERIES FLOW / PLAN</u>
7.1		7.1 SETUP
____ 7.1.1	RCM	PLACE CSD on ESD non-slip mat
____ 7.1.2	RCM	OPEN CSD (if closed) by carefully inserting a hex key or screwdriver (<0.10in wide) in manual release slot and pull up on Latch Lock with approximately 5 lbf. The tool can be inserted about 0.35 inches before stopping against an internal cover
		
____ 7.1.3	RCL	TAPE all contact surfaces of AFIT force gauge housing unit with Kapton tape. See figure below.
		
____ 7.1.4	RCL	INSTALL AFIT force gauge housing unit using the 10-32 bolts and washers (4 each). Choose the threaded holes on top of the CSD closest to the door, and furthest away from the door along the housing brace. Torque using an Allen wrench to hand-tight.



____ 7.1.5

VERIFY gauge rod guide rail is centered with brackets



____ 7.1.6

RCL

ATTACH non-marking tape onto push-pull gauge flat push face head.



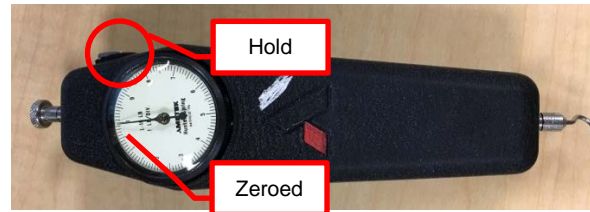
7.2

7.2 TEST

7.2.1

RCL

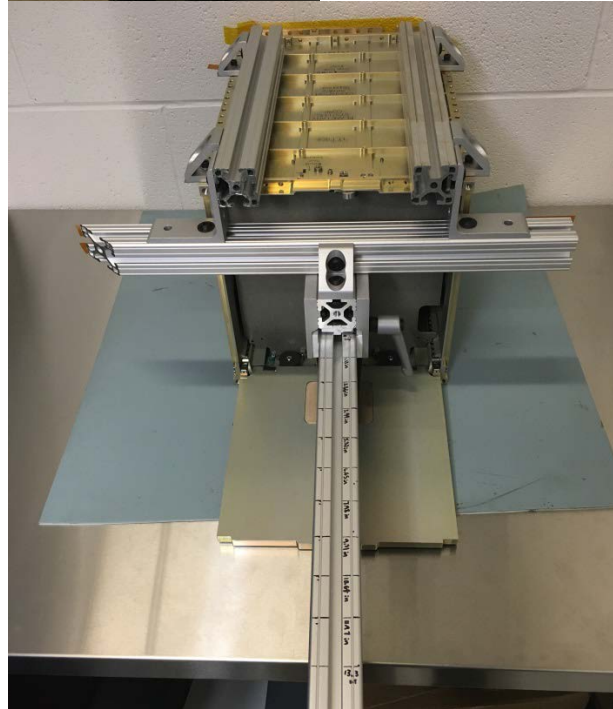
ENSURE force gauge is zeroed and is set to hold maximum reading (i.e. reading is locked on meter). There is usually a button to engage this feature. (see example)



7.2.2

RCL

INSERT Guide rod (with gauge attached) until hitting zero mark



7.2.3

RCL

PUSH push-plate back using hand to give enough clearance to set guide-rod at desired depth

7.2.4

RCL

PUSH guide rod to desired depth and lock using side lever on assembly.

7.2.5

RCL

GENTLY release push-plate and **RECORD** the pushing force (i.e. the plate exerts a force on an object) of CSD push-plate at each measurement point.

7.2.6

RCL

REPEAT for each depth according to table in Appendix 1

7.3**7.3 TEARDOWN****7.3.1**RCM **UNINSTALL** assembly and remove all Kapton tape**7.3.2**RCM **VERIFY** CSD is clean and clear of all debris and damage (especially marking tapes on pusher plate)**7.3.3**RCM **CLOSE** the CSD door. Using a thumb, push the Latch closed until a “click/ping” is heard.**7.3.4**RCM **VERIFY** door is properly closed. There shall be approximately 0.030 inches of movement even after the Latch is closed. A lack of movement signifies something is jammed against the Door. Contact PSC for troubleshooting**7.3.5**RCM **VERIFY** the Latch Lock is below the indicator line next to the manual door release cutout. If above the line, the Door Latch is not properly closed. Contact PSC for troubleshooting.

8.0		8.0 <u>EMERGENCY RESPONSE</u> NOTE: Perform the following steps in the event of a fire or other anomaly which cannot be safely managed by normal securing operations. TC shall have authority (On-Scene Command) over the situation until relieved from support organizations.
_____ 8.1	TC	If necessary, EVACUATE and/or Dial 9-911 to notify fire department of emergency
_____ 8.2	ANY	If necessary, Brief fire department and medics when they arrive.
_____ 8.3	TD	Continue to Monitor Facility until condition has been secured.
		END OF EMERGENCY RESPONSE

APPENDIX 1.0 – Force Reading Recording**Circle unit of measurement used: lbf / N**

Depth (in)	Force 1	Force 2	Force 3
1.33			
2.66			
3.99			
5.32			
6.65			
7.98			
9.31			
10.64			
11.97			
13.30			

APPENDIX 2.0 – Test Log

ITEM	TIME	EVENT / STATUS
(#)	(HHMM)	(Description)
1		
2		
3		
4		
5		
6		
7		
8		
9		
10		
11		
12		
13		
14		
15		
16		
17		
18		
19		
20		
21		
22		
23		
24		
25		
26		
27		

Appendix A.2 – Test Plan: Deployment Test

AFIT/ENY
6U/12U CSD Deployment
WRIGHT-PATTERSON AFB, OH

PROCEDURE:
REVISION:
DATE REVISED:
NUMBER OF PAGES:

CSD_Deploy_TP
2
1 Dec 2016
11

**AFIT / ENY
OPERATIONS**

**6U/12U
Deployment Testing**

SYSTEM UNDERGOING TESTING ASSOCIATED FUNCTIONAL TEST PLAN VERSION

6U/12U Canisterized Satellite Dispenser N/A

PREPARED BY:

Test Engineer _____
Test Conductor _____

DATE _____

REVIEWED / APPROVED BY:

AF Customer _____
Test Director _____

DATE _____

CSD_Deploy_TP

Revision	Notes	Prepared By
0	- Initial procedure	Capt Stephen Tullino 29 Aug 2016
1	- Inclusion in of new IMU	Capt Stephen Tullino 1 Dec 2016

TABLE OF CONTENTS

	Page
1.0 ABBREVIATIONS AND ACRYONMS.....	1
2.0 TEST DESCRIPTION AND OBJECTIVES	1
2.1 PURPOSE.....	1
2.2 SCOPE	1
2.3 OBJECTIVES/SUCCESS CRITERIA	1
3.0 DOCUMENTATION	2
3.1 REFERENCE DOCUMENTS.....	2
3.2 SPECIFICATIONS	2
3.3 DRAWINGS.....	2
4.0 TEST REQUIREMENTS AND RESTRICTIONS	2
4.1 TRAINING	2
4.2 MAXIMUM PERSONNEL:.....	2
4.3 LIST OF EQUIPMENT	2
5.0 SAFETY REQUIREMENTS	3
5.1 PERSONNEL PROTECTIVE EQUIPMENT REQUIREMENTS	3
5.2 EMERGENCY PROCEDURES.....	3
5.3 TEST AREA ACCESS DURING OPERATIONS	3
5.4 SPECIAL INSTRUCTIONS	3
6.0 PRE-TEST SETUP	3
7.0 CSD deployment test	5
7.1 ACCELEROMETER/IMU SETUP	5
7.2 EXPERIMENTAL SETUP	6
7.3 TEARDOWN	9
7.4 DATA ACQUISITION	9
8.0 EMERGENCY RESPONSE	10
APPENDIX 1.0 – Test Log.....	11

PERSONNEL

DATE_____

The following personnel are designated as test team members, and are chartered to perform their assignment as follows:

Test Conductor (TC) – Responsible for the timely performance of the test as written. This includes coordinating and directing the activities of the Red Crew and other test support teams. TC is responsible for coordinating all pretest activities and outside support required, including (but not limited to) security, fire, medical, and safety. TC is responsible for initialing completion on each step of the master test procedure.

Name_____ Signature_____

Test Director (TD) – Responsible for overall facility and test safety. Responsible for ensuring all test goals are met and all critical data is acquired. Supervises test activities to ensure procedures are followed. Has authority to perform real-time redlines on test procedures as required to ensure test requirements and goals are met.

Name_____ Signature_____

Red Crew Leader (RCL) – Responsible for directing the activities of Red Crew members. Reports directly to the TC and ensures all Red Crew tasks are completed. Responsible for ensuring all RCM's have all required certifications and training. Responsible for ensuring all required equipment is available, accessible, and serviceable.

Name_____ Signature_____

Test Panel Operator (TPO) – Responsible for operating the facility control systems during test operations as directed by TC. TPO is responsible for notifying the TC of any anomalous conditions.

Name_____ Signature_____

Red Crew Member (RCM) – Reports to the RCL. RCM is responsible for performing test-related tasks as directed by RCL.

Name_____ N/A _____ Signature_____

Name_____ Signature_____

Functional Test Conductor – Responsible for performing functional test in support of test.

Name_____ N/A _____ Signature_____

Name_____ Signature_____

EXCEPTIONS – When filling all positions is not possible, the Test Conductor will assume the duties of any empty position until the completion of the test or a suitable replacement is designated.

ALL TEST TEAM MEMBERS – Responsible for the safe performance of the test. Have read and understood all portions of the test procedure. Any Test Team Member can declare an emergency or unsafe condition.

1.0

1.0 ABBREVIATIONS AND ACRYONMS

AFIT	Air Force Institute of Technology
FOD	Foreign Object Debris
IPA	Isopropyl Alcohol
PPE	Personal Protective Equipment
RCL	Red Crew Leader
RCM	Red Crew Member
STE	Special Test Equipment
TC	Test Conductor
TD	Test Director
TOP	Test Operating Procedure
TPO	Test Panel Operator

2.0

2.0 TEST DESCRIPTION AND OBJECTIVES

2.1

2.1 PURPOSE

This procedure provides the means to perform deployment testing for test articles supplied relating to the 6U/12U CUBESAT CHASSIS. The 6U/12U CUBESAT CHASSIS test campaign is a structure and model validation plan intended to mitigate technology concerns for a future flight in a Planetary Systems Corp Canisterized Satellite Dispenser (PSC-CSD). The location of choice will be configured with the proper special test equipment (STE) to direct and measure “maximum predicted environments” associated with launching the 6U/12U Chassis according to the PSC-CSD Payload Specification.

2.2

2.2 SCOPE

This procedure records the CSD payload base plate acceleration in order to identify applied acceleration, velocity, and displacements versus time, along with kinetic force variations during ejection. This data will be used to verify CSD Deployment MATLAB model, as well as verify PSC theoretical performance parameters.

2.3

2.3 OBJECTIVES/SUCCESS CRITERIAComplete Success

1. Payload is ejected and data can be retrieved

Marginal Success

2. Payload is ejected and data is inconclusive, or external disturbance is induced

Unsuccessful

3. Payload cannot deploy or data cannot be extracted from accelerometer/IMU

3.0	3.0 <u>DOCUMENTATION</u>
	The completion of each applicable event shall be verified by initialing to the left of the item number. Deviations from these procedures will be coordinated with the Test Conductor. (NOTE: TD has the local authority to approve red-line revisions to this procedure).
<u>3.1</u>	3.1 REFERENCE DOCUMENTS Planetary Systems Corporation Canisterized Satellite Dispenser (CSD) Data Sheet (2002337C Rev – 3 Aug 2016)
<u>3.2</u>	3.2 SPECIFICATIONS The following list of specifications shall be used as a guide: Planetary Systems Corporation CSD Operating and Integration Procedure (3000257B 18 Jan 2016) Planetary Systems Corporation Payload Specification for 3U, 6U, 12U AND 27U (2002367 Rev - 25 July 2012) Midé Slam Stick X User's Manual X-Io Technologies NGIMU User's Manual
<u>3.3</u>	3.3 DRAWINGS NONE
4.0	4.0 <u>TEST REQUIREMENTS AND RESTRICTIONS</u>
<u>4.1</u>	4.1 TRAINING The following training is required for personnel using these procedures: All personnel: Job Site General Lab Safety Briefing AT LEAST ONE PERSON PRESENT MUST BE TRAINED BY PSC TO OPERATE CSD (OR SUPERVISE CSD OPERATION)
<u>4.2</u>	4.2 MAXIMUM PERSONNEL: Control Room: 3
<u>4.3</u>	4.3 LIST OF EQUIPMENT <ul style="list-style-type: none"> - 1 – ESD Mat or surface to bolt CSD onto - 4 – 10-32x3/4" bolts (if bolting CSD)

- 4 M9 Screws (if using NGIMU)
- 1 – 10mm Allen Wrench (if bolting CSD)
- 1 – 6U/12U CSD
- 1 – CubeSat base plate
- Accelerometer/IMU (i.e. Midé Slam Stick X (polymer) or X-io NGIMU)
- NGIMU interface (if using NGIMU)
- USB Cable
- Slam Stick/NGIMU Software Suite

Ensure all tools associated with this experiment/test/operation are accounted for prior to initiating system/item test. Ensure all FOD is picked up from around the test facility.

5.0**5.0 SAFETY REQUIREMENTS****5.1****5.1 PERSONNEL PROTECTIVE EQUIPMENT REQUIREMENTS**

Standard PPE: Boots – soles and heels made of semi-conductive rubber containing no nails.

All jewelry will be removed by test members while working on the test facility. No ties or other loose clothing permitted (at TD discretion).

5.2**5.2 EMERGENCY PROCEDURES**

In the event of an emergency that jeopardizes the safety of the operators or other personnel perform Section 11.0 emergency procedures at the end of this document.

5.3**5.3 TEST AREA ACCESS DURING OPERATIONS**

The test facility room will be limited to test personnel only. Personnel will not be allowed access to the test area unless cleared by the TD.

5.4**5.4 SPECIAL INSTRUCTIONS**

A qualified technician should provide orientation for clean room awareness and the proper faculty member / instructor should be consulted on test-series set points prior to test operations commencing.

Test Crew members shall place all cellular telephones on “silent mode” or turn off prior to completing any portion of this procedure.

6.0**6.0 PRE-TEST SETUP****6.1**

TC

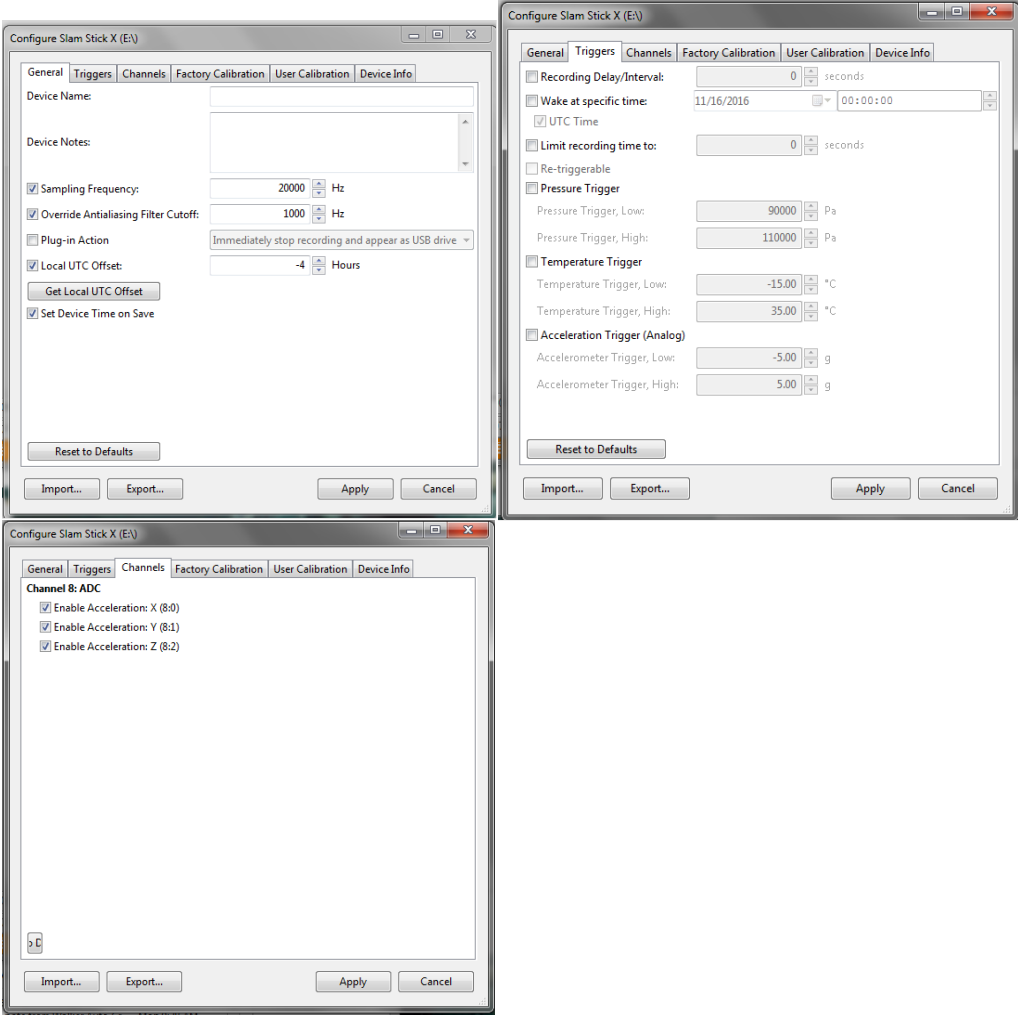
VERIFY all pages in this procedure are intact and complete.

6.2

TC

READ procedure and input any specific information required to perform operation.

____ 6.3	TC	VERIFY with Facility Management that no open Work Orders / Issues are listed for the noted location impeding operations.
____ 6.4	TC	PERFORM Setup Brief with Test Crew Members and note any redline changes on Appendices.
____ 6.5	TC	VERIFY Test Team has donned standard PPE (and noted restrictions / special instructions).
____ 6.6	TC	PERFORM Pre-Operation Brief with Test Crew Members <ul style="list-style-type: none"> – Objective – Personnel and assigned roles/duties – Safety: materials, PPE, communication, etc. – Sequence of events – Emergency procedures
____ 6.6.1	TC	RECORD Pre-Test Brief Time _____
____ 6.6.2	TC	VERIFY all personnel involved with the operation have signed this procedure.
____ 6.7	TC	VERIFY Midé Slam Stick information <ul style="list-style-type: none"> - Identification Number: _____ - Calibration Date / Due Date: _____ / _____ - N/A for X-lo NGIMU

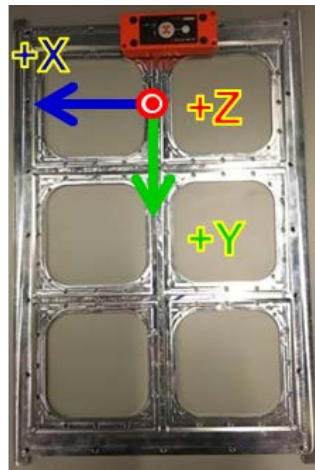
7.0		7.0 CSD DEPLOYMENT TEST
7.1		7.1 ACCELEROMETER/IMU SETUP
		WARNING: DO NOT USE USB ON US GOVERNMENT COMPUTERS
7.1.1		SLAM STICK SETUP (USE / NOT USE)
7.1.1.1	TC	CONNECT Slam Stick X to a computer via the USB cable provided to charge.
7.1.1.2	TPO	ENSURE computer has Slam Stick Lab software installed per Slam Stick X User's Manual. A copy of the User's Manual is located on the Slam Stick, and can be accessed via normal external data storage retrieval (e.g. like a USB flash drive).
7.1.1.3	TPO	OPEN Slam Stick Lab and set datalogger to the following settings per figures: (Please note to use "Get Local UTC Offset" button for most accurate time) For further details, please refer to Slam Stick X User's Manual.
		
7.1.1.4	TPO	APPLY settings. Close out of program and unplug USB when charged enough.

7.1.2	TD	(USE / NOT USE) NGIMU SETUP
____ 7.1.2.1	TC	CONNECT NGIMU via USB cable to computer (assuming the NGIMU needs charging)
____ 7.1.2.2	TC	PRESS power button. LED lights should light up.
____ 7.1.2.3	TPO	OPEN up NGIMU-Software folder in set directory and select NGIMU GUI application
____ 7.1.2.4	TPO	SELECT desired connection. Choose the serial option (typically there is a wireless option as well, but we will assume the battery isn't charged)
____ 7.1.2.5	TPO	SELECT Settings Tab (not top menu option) on GUI. Set settings as shown below.
____ 7.1.2.6	TPO	SELECT Settings top menu option. Select "write to device" to apply settings to NGIMU
____ 7.1.2.7	TC	PRESS power button. LED lights should turn off.
____ 7.1.2.8	TC	UNPLUG USB cable when NGIMU is charged enough.
7.2		7.2 EXPERIMENTAL SETUP
____ 7.2.1A	RCL	(USE / NOT USE) PLACE CSD –Y side on ESD non-slip mat and orient for deploying
____ 7.2.1B	RCL	(USE / NOT USE) Attach CSD –Y side to compatible surface (i.e. tilt plate or vibe table head) with 4 10-32x3/4" bolts. Torque bolts to hand-tightness.
____ 7.2.2	TC	OPEN CSD (if closed) by carefully inserting a hex key or screwdriver (<0.10in wide) in manual release slot and pull up on Latch Lock with approximately 5 lb _f . The tool can be inserted about 0.35in before stopping against an internal cover

**7.2.3A**

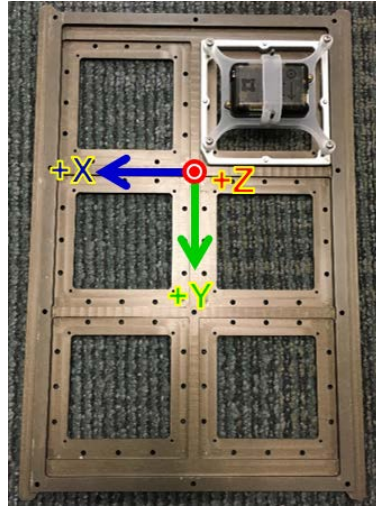
TC

(USE / NOT USE) INSTALL Slam Stick on internal base plate of 6U/12U Chassis (or standalone base plate) according to figure. Use accelerometer wax to affix to rear center of base plate IAW figure.

**7.2.3B**

TC

(USE / NOT USE) INSTALL NGIMU with housing on rear part of internal base plate of 6U/12U chassis (or standalone base plate) with 4 M9 screws per figure. Hand tighten screws.



- ____ **7.2.4** TD **VERIFY** CSD is clean and clear of all debris and damage
- ____ **7.2.5** TC **INSERT** entire chassis/base plate into CSD carefully.
- ____ **7.2.6** TC **PRESS** "X" button (on Slam Stick) or power button (on NGIMU) to activate. LED lights should light up.
- ____ **7.2.7** TC **CLOSE** the CSD door. Using a thumb, push the Latch closed until a "click/ping" is heard.



- ____ **7.2.8** TD **VERIFY** door is properly closed. There shall be approximately 0.030 inches of movement even after the Latch is closed. A lack of movement signifies something is jammed against the Door. Contact PSC for troubleshooting
- ____ **7.2.9** TD **VERIFY** the Latch Lock is below the indicator line next to the manual door release cutout. If above the line, the Door Latch is not properly closed. Contact PSC for troubleshooting.



7.2.10	TD	DESIGNATE one person to stop the payload once it's ejected
7.2.11	TPO	(USE / NOT USE) EXECUTE remote NGIMU data acquisition per step 7.4.3, if desired.
7.2.12	TC	OPEN CSD (if closed) by carefully inserting a hex key or screwdriver (<0.10in wide) in manual release slot and pull up on Latch Lock with approximately 5 lbf. The tool can be inserted about 0.35in before stopping against an internal cover. Upon opening, the payload will automatically be ejected.
7.2.13	RCL	CATCH payload and press the "X" button (on the Slam Stick) or power button (on the NGIMU) to turn off unit.
7.2.14	TD	REPEAT ejection steps two more times (or as many times needed).
7.3		7.3 TEARDOWN
7.3.1	TD	VERIFY CSD is clean and clear of all debris and damage
7.3.2	TC	CLOSE the CSD door per step 7.2.7
7.3.3	TD	VERIFY door is properly closed per step 7.2.8
7.3.4	TD	VERIFY the Latch Lock per step 7.2.9
7.3.5	TD	REMOVE the Slam Stick from the base plate/chassis
7.4		7.4 DATA ACQUISITION
7.4.1	TD	(USE / DO NOT USE) SLAM STICK
7.4.1.1	TC	CONNECT Slam Stick via micro USB cable
7.4.1.2	TPO	EXTRACT data
7.4.2	TD	(USE / DO NOT USE) NGIMU
7.4.2.1	TC	CONNECT NGIMU via micro USB cable.

____ 7.4.2.2	TC	PRESS power button. LED lights should light up.
____ 7.4.2.3	TPO	OPEN up NGIMU-Software folder in set directory and select NGIMU GUI application
____ 7.4.2.4	TPO	SELECT desired connection. Choose the serial option (typically there is a wireless option as well, but we will assume the battery isn't charged)
____ 7.4.2.5	TPO	SELECT "Tools" menu and select "SD Card File Converter" from drop-down menu.
____ 7.4.2.6	TPO	SELECT the desired SD card file and then select the directory to save the extracted data.
7.4.3	TD	(USE / DO NOT USE) NGIMU REMOTE DATA ACQUISITION (FOR USE DURING TESTS)
____ 7.4.3.1	TPO	OPEN up NGIMU-Software folder in set directory and select NGIMU GUI application while NGIMU IS ON
____ 7.4.3.2	TPO	SELECT desired connection. Choose the wireless option.
____ 7.4.3.3	TPO	SELECT "Tools" menu and select "Data Logger" from drop-down menu.
____ 7.4.3.4	TPO	SET the desired directory to save file, file name, and logging period.
____ 7.4.3.5	TPO	PRESS Start button to commence. Data will automatically save onto desired directory once logging period has finished.

8.0		8.0 <u>EMERGENCY RESPONSE</u> NOTE: Perform the following steps in the event of a fire or other anomaly which cannot be safely managed by normal securing operations. TC shall have authority (On-Scene Command) over the situation until relieved from support organizations.
____ 8.1	TC	If necessary, EVACUATE and/or Dial 9-911 to notify fire department of emergency
____ 8.2	ANY	If necessary, Brief fire department and medics when they arrive.
____ 8.3	TD	Continue to Monitor Facility until condition has been secured.
		END OF EMERGENCY RESPONSE

APPENDIX 1.0 – Test Log

ITEM	TIME	EVENT / STATUS
(#)	(HHMM)	(Description)
1		
2		
3		
4		
5		
6		
7		
8		
9		
10		
11		
12		
13		
14		
15		
16		
17		
18		
19		
20		
21		
22		
23		
24		
25		
26		
27		

Appendix A.3 – Test Plan: Friction Tests

AFIT/ENY
6U CSD Friction Determination
WRIGHT-PATTERSON AFB, OH

PROCEDURE:
REVISION:
DATE REVISED:
NUMBER OF PAGES:

CSD_Friction_TP
1
15 Jan 2017
13

**AFIT / ENY
OPERATIONS**

**6U CSD
Friction Determination**

SYSTEM UNDERGOING TESTING

ASSOCIATED FUNCTIONAL TEST PLAN VERSION

6U Canisterized Satellite Dispenser N/A

PREPARED BY:

Test Engineer _____
Test Conductor _____

DATE _____

REVIEWED / APPROVED BY:

AF Customer _____
Test Director _____

DATE _____

Revision	Notes	Prepared By
0	- Initial procedure	Capt Stephen Tullino 15 Jan 2017

TABLE OF CONTENTS

	Page
1.0 ABBREVIATIONS AND ACRYONMS.....	1
2.0 TEST DESCRIPTION AND OBJECTIVES	1
2.1 PURPOSE.....	1
2.2 SCOPE	1
2.3 OBJECTIVES/SUCCESS CRITERIA	1
3.0 DOCUMENTATION	2
3.1 REFERENCE DOCUMENTS.....	2
3.2 SPECIFICATIONS	2
3.3 DRAWINGS.....	2
4.0 TEST REQUIREMENTS AND RESTRICTIONS	2
4.1 TRAINING	2
4.2 MAXIMUM PERSONNEL:.....	2
4.3 LIST OF EQUIPMENT	2
5.0 SAFETY REQUIREMENTS	3
5.1 PERSONNEL PROTECTIVE EQUIPMENT REQUIREMENTS	3
5.2 EMERGENCY PROCEDURES.....	3
5.3 TEST AREA ACCESS DURING OPERATIONS	3
5.4 SPECIAL INSTRUCTIONS	3
6.0 PRE-TEST SETUP	4
7.0 CSD Push plate contact deployment test	5
7.1 IMU SETUP.....	5
7.2 INCLINE METHOD TEST	5
7.3 IMPULSE DECELERATION TEST	8
7.4 SUSPENDED MASS TEST	8
7.5 REPEAT 7.2 – 7.4 WITH CSD ATTACHED TO TILT PLATE ON +Y AXIS (UPSIDE DOWN) TO TEST FRICTION OF TOP SIDE OF GUIDE RAIL.....	9
7.6 TEARDOWN	9
7.7 DATA ACQUISITION	10
8.0 EMERGENCY RESPONSE	11
APPENDIX 1.0 – Friction Reading Log.....	12
APPENDIX 2.0 – Test Log.....	13

PERSONNEL

DATE _____

The following personnel are designated as test team members, and are chartered to perform their assignment as follows:

Test Conductor (TC) – Responsible for the timely performance of the test as written. This includes coordinating and directing the activities of the Red Crew and other test support teams. TC is responsible for coordinating all pretest activities and outside support required, including (but not limited to) security, fire, medical, and safety. TC is responsible for initialing completion on each step of the master test procedure.

Name _____ Signature _____

Test Director (TD) – Responsible for overall facility and test safety. Responsible for ensuring all test goals are met and all critical data is acquired. Supervises test activities to ensure procedures are followed. Has authority to perform real-time redlines on test procedures as required to ensure test requirements and goals are met.

Name _____ Signature _____

Red Crew Leader (RCL) – Responsible for directing the activities of Red Crew members. Reports directly to the TC and ensures all Red Crew tasks are completed. Responsible for ensuring all RCM's have all required certifications and training. Responsible for ensuring all required equipment is available, accessible, and serviceable.

Name _____ Signature _____

Test Panel Operator (TPO) – Responsible for operating the facility control systems during test operations as directed by TC. TPO is responsible for notifying the TC of any anomalous conditions.

Name _____ Signature _____

Red Crew Member (RCM) – Reports to the RCL. RCM is responsible for performing test-related tasks as directed by RCL.

Name N/A Signature _____

Name _____ Signature _____

Functional Test Conductor – Responsible for performing functional test in support of test.

Name N/A Signature _____

Name _____ Signature _____

EXCEPTIONS – When filling all positions is not possible, the Test Conductor will assume the duties of any empty position until the completion of the test or a suitable replacement is designated.

ALL TEST TEAM MEMBERS – Responsible for the safe performance of the test. Have read and understood all portions of the test procedure. Any Test Team Member can declare an emergency or unsafe condition.

1.0

1.0 ABBREVIATIONS AND ACRYONMS

AFIT	Air Force Institute of Technology
CSD	Canisterized Satellite Dispenser
FOD	Foreign Object Debris
PPE	Personal Protective Equipment
RCL	Red Crew Leader
RCM	Red Crew Member
STE	Special Test Equipment
TC	Test Conductor
TD	Test Director
TOP	Test Operating Procedure
TPO	Test Panel Operator

2.0

2.0 TEST DESCRIPTION AND OBJECTIVES

2.1

2.1 PURPOSE

This procedure provides the means to perform deployment testing for test articles supplied relating to the 6U CUBESAT CHASSIS. The 6U CUBESAT CHASSIS test campaign is a structure and model validation plan intended to mitigate technology concerns for a future flight in a Planetary Systems Corp Canisterized Satellite Dispenser (PSC-CSD). The location of choice will be configured with the proper special test equipment (STE) to direct and measure “maximum predicted environments” associated with launching the 6U Chassis according to the PSC-CSD Payload Specification.

2.2

2.2 SCOPE

This procedure tests to find the coefficients of kinetic friction of the top and bottom sides of the CSD guide rail. This data will be used to verify CSD Deployment MATLAB model, as well as verify PSC theoretical performance parameters.

2.3

2.3 OBJECTIVES/SUCCESS CRITERIAComplete Success

1. Payload is ejected and data can be retrieved

Marginal Success

2. Payload is ejected and data is inconclusive, or external disturbance is induced

Unsuccessful

3. Payload cannot deploy or data cannot be determined

3.0	3.0 <u>DOCUMENTATION</u>
	The completion of each applicable event shall be verified by initialing to the left of the item number. Deviations from these procedures will be coordinated with the Test Conductor. (NOTE: TD has the local authority to approve red-line revisions to this procedure).
____ 3.1	3.1 REFERENCE DOCUMENTS Planetary Systems Corporation Canisterized Satellite Dispenser (CSD) Data Sheet (2002337C Rev – 3 Aug 2016)
____ 3.2	3.2 SPECIFICATIONS The following list of specifications shall be used as a guide: Planetary Systems Corporation CSD Operating and Integration Procedure (3000257B 18 Jan 2016) Planetary Systems Corporation Payload Specification for 3U, 6U, 12U AND 27U (2002367 Rev - 25 July 2012) X-Io Technologies NGIMU User's Manual
____ 3.3	3.3 DRAWINGS NONE
4.0	4.0 <u>TEST REQUIREMENTS AND RESTRICTIONS</u>
____ 4.1	4.1 TRAINING The following training is required for personnel using these procedures: All personnel: Job Site General Lab Safety Briefing AT LEAST ONE PERSON PRESENT MUST BE TRAINED BY PSC TO OPERATE CSD (OR SUPERVISE CSD OPERATION)
____ 4.2	4.2 MAXIMUM PERSONNEL: Control Room: 3
____ 4.3	4.3 LIST OF EQUIPMENT <ul style="list-style-type: none"> - 4 – 10-32x3/4" bolts - 1 – 10mm Allen Wrench - 1 – Inclinator

- 1 – Tilt plate
- 1 – C Clamp
- 1 – Pulley system
- 1 – Spool of low mass string/line
- 1 – Set of brass weights
- 1 – 6U CSD
- 1 – 6U chassis base plate
- 2 – ~1.7 kg mass stacks
- 2 – ~1.9 kg mass stacks
- X-io NGIMU
- NGIMU interface
- USB Cable
- NGIMU Software Suite
- Shims (as needed) for c clamp application

Ensure all tools associated with this experiment/test/operation are accounted for prior to initiating system/item test. Ensure all FOD is picked up from around the test facility.

5.0

5.0 SAFETY REQUIREMENTS

____ 5.1

5.1 PERSONNEL PROTECTIVE EQUIPMENT REQUIREMENTS

Standard PPE: Boots – soles and heels made of semi-conductive rubber containing no nails.

All jewelry will be removed by test members while working on the test facility. No ties or other loose clothing permitted (at TD discretion).

____ 5.2

5.2 EMERGENCY PROCEDURES

In the event of an emergency that jeopardizes the safety of the operators or other personnel perform Section 8.0 emergency procedures at the end of this document.

____ 5.3

5.3 TEST AREA ACCESS DURING OPERATIONS

The test facility room will be limited to test personnel only. Personnel will not be allowed access to the test area unless cleared by the TD.


____ 5.4



5.4 SPECIAL INSTRUCTIONS

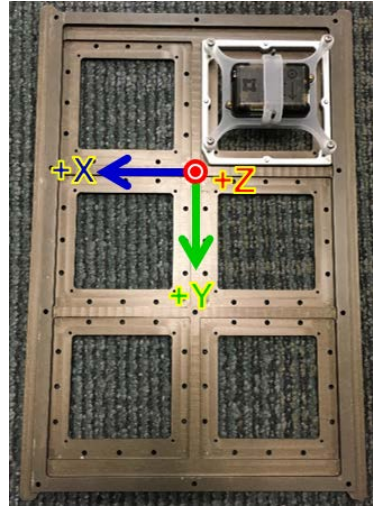
A qualified technician should provide orientation for clean room awareness and the proper faculty member / instructor should be consulted on test-series set points prior to test operations commencing.

Test Crew members shall place all cellular telephones on “silent mode” or turn off prior to completing any portion of this procedure.

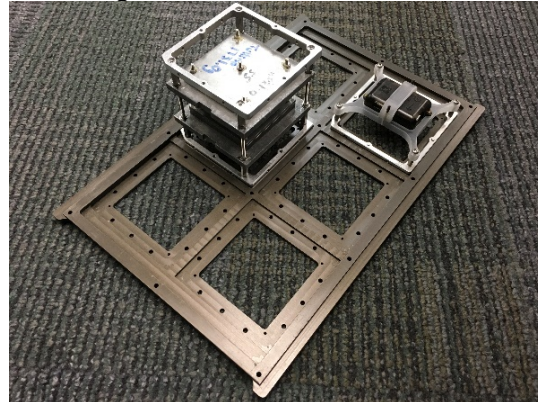
6.0		6.0 <u>PRE-TEST SETUP</u>
____ 6.1	TC	VERIFY all pages in this procedure are intact and complete.
____ 6.2	TC	READ procedure and input any specific information required to perform operation.
____ 6.3	TC	VERIFY with Facility Management that no open Work Orders / Issues are listed for the noted location impeding operations.
____ 6.4	TC	PERFORM Setup Brief with Test Crew Members and note any redline changes on Appendices.
____ 6.5	TC	VERIFY Test Team has donned standard PPE (and noted restrictions / special instructions).
____ 6.6	TC	PERFORM Pre-Operation Brief with Test Crew Members <ul style="list-style-type: none"> – Objective – Personnel and assigned roles/duties – Safety: materials, PPE, communication, etc. – Sequence of events – Emergency procedures
____ 6.6.1	TC	RECORD Pre-Test Brief Time _____
____ 6.6.2	TC	VERIFY all personnel involved with the operation have signed this procedure.

7.0		7.0 <u>CSD PUSH PLATE CONTACT DEPLOYMENT TEST</u>
7.1		7.1 IMU SETUP
		WARNING: DO NOT USE USB ON US GOVERNMENT COMPUTERS
____ 7.1.1	TC	CONNECT NGIMU via USB cable to computer (assuming the NGIMU needs charging)
____ 7.1.2	TC	PRESS power button. LED lights should light up.
____ 7.1.3	TPO	OPEN up NGIMU-Software folder in set directory and select NGIMU GUI application
____ 7.1.4	TPO	SELECT desired connection. Choose the serial option (typically there is a wireless option as well, but we will assume the battery isn't charged)
____ 7.1.5	TPO	SELECT Settings Tab (not top menu option) on GUI. Set settings as shown below.
____ 7.1.6	TPO	SELECT Settings top menu option. Select "write to device" to apply settings to NGIMU
____ 7.1.7	TC	PRESS power button. LED lights should turn off.
____ 7.1.8	TC	UNPLUG USB cable when NGIMU is charged enough.
7.2		7.2 INCLINE METHOD TEST
____ 7.2.1	RCL	ATTACH CSD –Y side to tilt plate with 4 10-32x3/4" bolts in order to test friction of bottom side of CSD guide rail. Hand tighten.
____ 7.2.2	TC	OPEN CSD (if closed) by carefully inserting a hex key or screwdriver (<0.10in wide) in manual release slot and pull up on Latch Lock with approximately 5 lb _f . The tool can be inserted about 0.35in before stopping against an internal cover
		

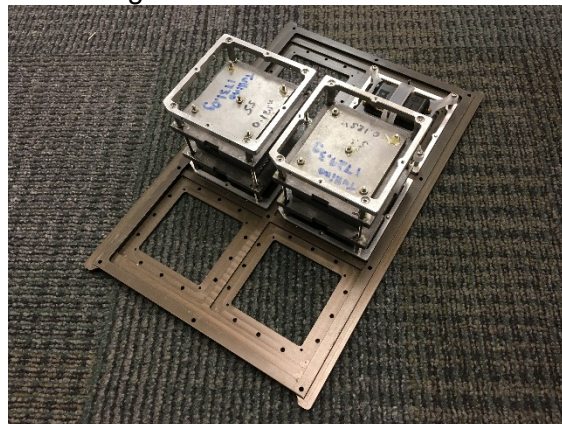
____ 7.2.3	TC	INSTALL inclinometer to tilt plate parallel along the side of CSD
____ 7.2.4	TC	PUSH push plate all the way back and secure with a C clamp. Use shims as needed to increase clearance and to protect CSD from scratches
		 
____ 7.2.5	TC	VERIFY initial angle state $0^{\circ} \pm 0.1^{\circ}$
____ 7.2.6	TC	INSTALL NGIMU with housing on rear part of internal base plate of 6U/12U chassis (or standalone base plate) with 4 M9 screws per figure. Hand tighten screws.



- ____ 7.2.7 TC **INSERT** chassis base plate into CSD.
- ____ 7.2.8 TC **SLIGHTLY** tilt CSD and lock tilt plate.
- ____ 7.2.9 TC **GENTLY** tap base plate to see if it slides out at a steady speed. If it stops, increase angle. If it slides out prior to tapping, reduce angle. Repeat until ideal angle is found. Verify 3x and record angles in Appendix 1.0.
- ____ 7.2.10 TC **REPEAT** test with 1 ~1.7 kg mass stack

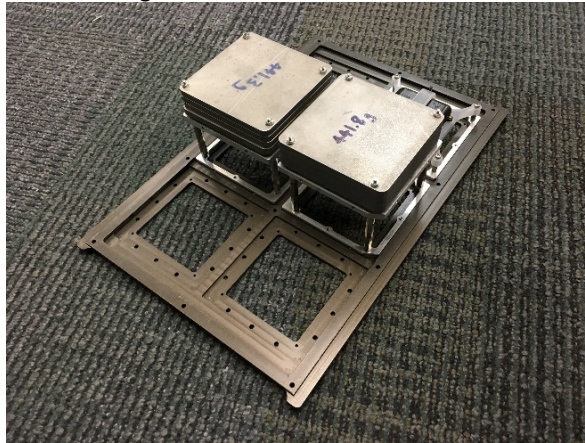


- ____ 7.2.11 TC **REPEAT** test with 2 ~1.7 kg mass stacks



____ 7.2.12

TC

REPEAT test with 2 ~1.9 kg mass stack**7.3****7.3 IMPULSE DECELERATION TEST**

____ 7.3.1

TC

AFTER completion of incline test, reset tilt plate to initial angle state of $0^\circ \pm 0.1^\circ$

____ 7.3.2

TC

INSERT chassis base plate into CSD.

____ 7.3.3

TC

PRESS the power button on the NGIMU to activate. LED lights should light up.

____ 7.3.4

TC

QUICKLY AND FIRMLY tap the plate enough to let it speed up and slow down naturally (not too strong causing it to fly out of the CSD, but not too weak where it barely moves). Verify 3x.

____ 7.3.5

TC

PRESS NGIMU power button to turn off unit.

____ 7.3.6

TC

REPEAT test with 1 ~1.7 kg mass stack

____ 7.3.7

TC

REPEAT test with 2 ~1.7 kg mass stacks

____ 7.3.8

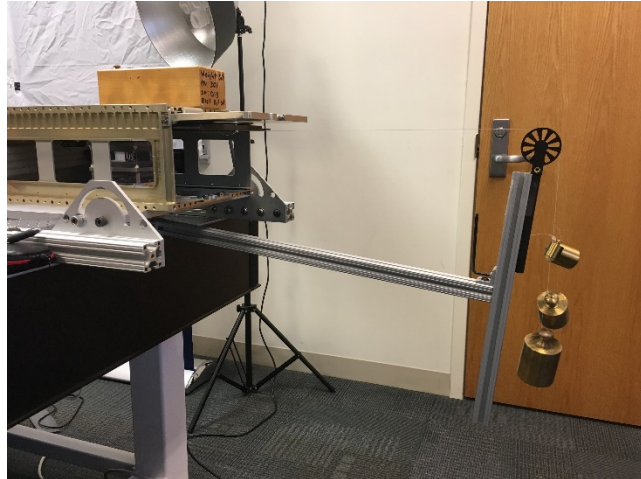
TC

REPEAT test with 2 ~1.9 kg mass stack**7.4****7.4 SUSPENDED MASS TEST**

____ 7.4.1



RCL

INSTALL pulley system under the tilt plate (tilt plate is still at $0^\circ \pm 0.1^\circ$)



- ____ 7.4.2 TC **ATTACH** string/line to end of base plate. Thread string/line along pulley.
- ____ 7.4.3 TC **ADJUST** pulley system to ensure string/line is parallel to the ground
- ____ 7.4.4 TC **SET** base plate into CSD
- ____ 7.4.5 TC **ADD** brass masses to string/line. Gently tap base plate to see if it slides out at a steady speed. If it stops, increase mass. If it slides out prior to tapping, reduce mass. Repeat until ideal angle is found. Verify 3x and record angles in Appendix 1.0.
- ____ 7.4.6 TC **REPEAT** test with 1 ~1.7 kg mass stack
- ____ 7.4.7 TC **REPEAT** test with 2 ~1.7 kg mass stacks
- ____ 7.4.8 TC **REPEAT** test with 2 ~1.9 kg mass stack
- 7.5 7.5 REPEAT 7.2 – 7.4 WITH CSD ATTACHED TO TILT PLATE ON +Y AXIS (UPSIDE DOWN) TO TEST FRICTION OF TOP SIDE OF GUIDE RAIL
- 7.6 7.6 TEARDOWN
- ____ 7.6.1 TC **VERIFY** CSD is clean and clear of all debris and damage



7.6.2	TC	CLOSE the CSD door. Using a thumb, push the Latch closed until a “click/ping” is heard.
		
7.6.3	TC	VERIFY door is properly closed. There shall be approximately 0.030 inches of movement even after the Latch is closed. A lack of movement signifies something is jammed against the Door. Contact PSC for troubleshooting
7.6.4	TC	VERIFY the Latch Lock is below the indicator line next to the manual door release cutout. If above the line, the Door Latch is not properly closed. Contact PSC for troubleshooting.
		
7.6.5	TC	REMOVE the NGIMU from the base chassis. Ensure no beeswax residue
7.7		7.7 DATA ACQUISITION
7.7.1	TC	CONNECT NGIMU via micro USB cable.
7.7.2	TC	PRESS power button. LED lights should light up.
7.7.3	TPO	OPEN up NGIMU-Software folder in set directory and select NGIMU GUI application
7.7.4	TPO	SELECT desired connection. Choose the serial option (typically there is a wireless option as well, but we will assume the battery isn't charged)
7.7.5	TPO	SELECT “Tools” menu and select “SD Card File Converter” from drop-down menu.

____ 7.7.6	TPO	SELECT the desired SD card file and then select the directory to save the extracted data.
____ 7.7.7	TD	(USE / DO NOT USE) NGIMU REMOTE DATA ACQUISITION (FOR USE DURING TESTS)
____ 7.7.8	TPO	OPEN up NGIMU-Software folder in set directory and select NGIMU GUI application
____ 7.7.9	TPO	SELECT desired connection. Choose the wireless option.
____ 7.7.10	TPO	SELECT “Tools” menu and select “Data Logger” from drop-down menu.
____ 7.7.11	TPO	SET the desired directory to save file, file name, and logging period.
____ 7.7.12	TPO	PRESS Start button to commence. Data will automatically save onto desired directory once logging period has finished.

8.0		8.0 <u>EMERGENCY RESPONSE</u>
		NOTE: Perform the following steps in the event of a fire or other anomaly which cannot be safely managed by normal securing operations. TC shall have authority (On-Scene Command) over the situation until relieved from support organizations.
____ 8.1	TC	If necessary, EVACUATE and/or Dial 9-911 to notify fire department of emergency
____ 8.2	ANY	If necessary, Brief fire department and medics when they arrive.
____ 8.3	TD	Continue to Monitor Facility until condition has been secured.
		END OF EMERGENCY RESPONSE

APPENDIX 1.0 – Friction Reading Log

BOTTOM OF CSD RAIL – INCLINE METHOD			
	Measurement 1 (deg)	Measurement 2 (deg)	Measurement 3 (deg)
Base Plate Only			
+1 ~1.7 kg Mass Stack			
+2 ~1.7 kg Mass Stacks			
+2 ~1.9 kg Mass Stacks			

BOTTOM OF CSD RAIL – SUSPENDED MASS METHOD			
	Measurement 1 (g)	Measurement 2 (g)	Measurement 3 (g)
Base Plate Only			
+1 ~1.7 kg Mass Stack			
+2 ~1.7 kg Mass Stacks			
+2 ~1.9 kg Mass Stacks			

TOP OF CSD RAIL – INCLINE METHOD			
	Measurement 1 (deg)	Measurement 2 (deg)	Measurement 3 (deg)
Base Plate Only			
+1 ~1.7 kg Mass Stack			
+2 ~1.7 kg Mass Stacks			
+2 ~1.9 kg Mass Stacks			

TOP OF CSD RAIL – SUSPENDED MASS METHOD			
	Measurement 1 (g)	Measurement 2 (g)	Measurement 3 (g)
Base Plate Only			
+1 ~1.7 kg Mass Stack			
+2 ~1.7 kg Mass Stacks			
+2 ~1.9 kg Mass Stacks			

* IMPULSE DECELERATION REQUIRES IMU ANALYSIS

APPENDIX 2.0 – Test Log

ITEM	TIME	EVENT / STATUS
(#)	(HHMM)	(Description)
1		
2		
3		
4		
5		
6		
7		
8		
9		
10		
11		
12		
13		
14		
15		
16		
17		
18		
19		
20		
21		
22		
23		
24		
25		
26		
27		

Appendix A.4 – Test Plan: Door Interference Test

AFIT/ENY
6U CSD Door Interference Test
WRIGHT-PATTERSON AFB, OH

PROCEDURE:
REVISION:
DATE REVISED:
NUMBER OF PAGES:

CSD_Door_TP
1
5 Jan 2017
19

AFIT / ENY
OPERATIONS

6U CSD
Door Interference Test

SYSTEM UNDERGOING TESTING

ASSOCIATED FUNCTIONAL TEST PLAN VERSION

6U Canisterized Satellite Dispenser

N/A

PREPARED BY:

Test Engineer _____
Test Conductor _____

DATE _____

REVIEWED / APPROVED BY:

AF Customer _____
Test Director _____

DATE _____

CSD_Door_TP

Revision	Notes	Prepared By
0	- Initial procedure	Capt Stephen Tullino 5 Jan 2017

TABLE OF CONTENTS

	Page
1.0 ABBREVIATIONS AND ACRYONMS.....	1
2.0 TEST DESCRIPTION AND OBJECTIVES	1
2.1 PURPOSE.....	1
2.2 SCOPE	1
2.3 OBJECTIVES/SUCCESS CRITERIA	1
3.0 DOCUMENTATION	2
3.1 REFERENCE DOCUMENTS.....	2
3.2 SPECIFICATIONS	2
3.3 DRAWINGS.....	2
4.0 TEST REQUIREMENTS AND RESTRICTIONS	2
4.1 TRAINING	2
4.2 MAXIMUM PERSONNEL:.....	2
4.3 LIST OF EQUIPMENT	2
5.0 SAFETY REQUIREMENTS	3
5.1 PERSONNEL PROTECTIVE EQUIPMENT REQUIREMENTS	3
5.2 EMERGENCY PROCEDURES.....	3
5.3 TEST AREA ACCESS DURING OPERATIONS	3
5.4 SPECIAL INSTRUCTIONS	3
6.0 PRE-TEST SETUP	4
7.0 CSD DOOR test	5
7.1 DATALOGGER SETUP	5
7.2 CAMERA SETUP.....	11
7.3 CSD SETUP.....	13
7.4 EXECUTION	15
7.5 TEARDOWN	16
7.6 OPTIONAL CAMERA DATA FILE SAVES	17
8.0 EMERGENCY RESPONSE	18
APPENDIX 1.0 – Test Log.....	19

PERSONNEL

DATE _____

The following personnel are designated as test team members, and are chartered to perform their assignment as follows:

Test Conductor (TC) – Responsible for the timely performance of the test as written. This includes coordinating and directing the activities of the Red Crew and other test support teams. TC is responsible for coordinating all pretest activities and outside support required, including (but not limited to) security, fire, medical, and safety. TC is responsible for initialing completion on each step of the master test procedure.

Name _____ Signature _____

Test Director (TD) – Responsible for overall facility and test safety. Responsible for ensuring all test goals are met and all critical data is acquired. Supervises test activities to ensure procedures are followed. Has authority to perform real-time redlines on test procedures as required to ensure test requirements and goals are met.

Name _____ Signature _____

Red Crew Leader (RCL) – Responsible for directing the activities of Red Crew members. Reports directly to the TC and ensures all Red Crew tasks are completed. Responsible for ensuring all RCM's have all required certifications and training. Responsible for ensuring all required equipment is available, accessible, and serviceable.

Name _____ Signature _____

Test Panel Operator (TPO) – Responsible for operating the facility control systems during test operations as directed by TC. TPO is responsible for notifying the TC of any anomalous conditions.

Name _____ Signature _____

Red Crew Member (RCM) – Reports to the RCL. RCM is responsible for performing test-related tasks as directed by RCL.

Name N/A Signature _____

Name _____ Signature _____

Functional Test Conductor – Responsible for performing functional test in support of test.

Name N/A Signature _____

Name _____ Signature _____

EXCEPTIONS – When filling all positions is not possible, the Test Conductor will assume the duties of any empty position until the completion of the test or a suitable replacement is designated.

ALL TEST TEAM MEMBERS – Responsible for the safe performance of the test. Have read and understood all portions of the test procedure. Any Test Team Member can declare an emergency or unsafe condition.

1.0

1.0 ABBREVIATIONS AND ACRYONMS

AFIT	Air Force Institute of Technology
CSD	Canisterized Satellite Dispenser
FOD	Foreign Object Debris
PPE	Personal Protective Equipment
RCL	Red Crew Leader
RCM	Red Crew Member
STE	Special Test Equipment
TC	Test Conductor
TD	Test Director
TOP	Test Operating Procedure
TPO	Test Panel Operator

2.0

2.0 TEST DESCRIPTION AND OBJECTIVES

2.1

2.1 PURPOSE

This procedure provides the means to perform deployment testing for test articles supplied relating to the 6U CUBESAT CHASSIS. The 6U CUBESAT CHASSIS test campaign is a structure and model validation plan intended to mitigate technology concerns for a future flight in a Planetary Systems Corp Canisterized Satellite Dispenser (PSC-CSD). The location of choice will be configured with the proper special test equipment (STE) to direct and measure “maximum predicted environments” associated with launching the 6U Chassis according to the PSC-CSD Payload Specification.

2.2

2.2 SCOPE

This procedure tests the motion of the 6U CSD door during payload ejection. This data will be used to identify if the door is interfering with the payload during ejection. This data will be used for future motion characterization, and determination of amount of force the door imparts on an ejecting payload if there is contact. Ultimately, this data will tune the CSD Deployment MATLAB model.

2.3

2.3 OBJECTIVES/SUCCESS CRITERIAComplete Success

1. Payload is ejected and data can be retrieved

Marginal Success

2. Payload is ejected and data is inconclusive, or external disturbance is induced

Unsuccessful

3. Payload cannot deploy or data cannot be extracted from recorded data

3.0**3.0 DOCUMENTATION**

The completion of each applicable event shall be verified by initialing to the left of the item number. Deviations from these procedures will be coordinated with the Test Conductor. (NOTE: TD has the local authority to approve red-line revisions to this procedure).

____ 3.1**3.1 REFERENCE DOCUMENTS**

Planetary Systems Corporation Canisterized Satellite Dispenser (CSD)
Data Sheet (2002337C Rev – 3 Aug 2016)

____ 3.2**3.2 SPECIFICATIONS**

The following list of specifications shall be used as a guide:

Planetary Systems Corporation CSD Operating and Integration
Procedure (3000257B 18 Jan 2016)

Planetary Systems Corporation Payload Specification for 3U, 6U, 12U
AND 27U (2002367 Rev - 25 July 2012)

____ 3.3**3.3 DRAWINGS**

NONE

4.0**4.0 TEST REQUIREMENTS AND RESTRICTIONS****____ 4.1****4.1 TRAINING**

The following training is required for personnel using these procedures:

All personnel:

Job Site General Lab Safety Briefing

**AT LEAST ONE PERSON PRESENT MUST BE TRAINED BY PSC TO
OPERATE CSD (OR SUPERVISE CSD OPERATION)**

____ 4.2**4.2 MAXIMUM PERSONNEL:**

Control Room: 4

____ 4.3**4.3 LIST OF EQUIPMENT**

- 1 – Secured vibe table head
- 8 – 10-32x3/4” bolts
- 1 – 10 mm Allen Wrench

- 1 – 10 mm 50 in-lb torque wrench
- 1 – 6U CSD
- 1 – CubeSat Chassis base plate
- 1 – Phantom v16 High Speed Camera
- 1 – Phantom camera Ethernet cable
- 1 – Phantom camera power cable
- 1 – Computer with Phantom Camera Control suite
- 1 – Computer with DataPhysics SingalCalcMobilyzer
- 1 – DataPhysics Abacus tower
- 2 – Signal conditioners
- 5 – Coaxial cables
- 4 – Single-axis accelerometers (PCB Piezotronics 352C22)
- 1 – Photography linen
- 4 – Photography lights
- USB Cable
- NGIMU Software Suite

Ensure all tools associated with this experiment/test/operation are accounted for prior to initiating system/item test. Ensure all FOD is picked up from around the test facility.

5.0

5.0 SAFETY REQUIREMENTS

____ 5.1

5.1 PERSONNEL PROTECTIVE EQUIPMENT REQUIREMENTS

Standard PPE: Boots – soles and heels made of semi-conductive rubber containing no nails.

All jewelry will be removed by test members while working on the test facility. No ties or other loose clothing permitted (at TD discretion).

____ 5.2

5.2 EMERGENCY PROCEDURES

In the event of an emergency that jeopardizes the safety of the operators or other personnel perform Section 8.0 emergency procedures at the end of this document.

____ 5.3

5.3 TEST AREA ACCESS DURING OPERATIONS

The test facility room will be limited to test personnel only. Personnel will not be allowed access to the test area unless cleared by the TD.

____ 5.4

5.4 SPECIAL INSTRUCTIONS

A qualified technician should provide orientation for clean room awareness and the proper faculty member / instructor should be consulted on test-series set points prior to test operations commencing.

Test Crew members shall place all cellular telephones on “silent mode” or turn off prior to completing any portion of this procedure.

6.0		6.0 <u>PRE-TEST SETUP</u>
____ 6.1	TC	VERIFY all pages in this procedure are intact and complete.
____ 6.2	TC	READ procedure and input any specific information required to perform operation.
____ 6.3	TC	VERIFY with Facility Management that no open Work Orders / Issues are listed for the noted location impeding operations.
____ 6.4	TC	PERFORM Setup Brief with Test Crew Members and note any redline changes on Appendices.
____ 6.5	TC	VERIFY Test Team has donned standard PPE (and noted restrictions / special instructions).
____ 6.6	TC	PERFORM Pre-Operation Brief with Test Crew Members <ul style="list-style-type: none"> – Objective – Personnel and assigned roles/duties – Safety: materials, PPE, communication, etc. – Sequence of events – Emergency procedures
____ 6.6.1	TC	RECORD Pre-Test Brief Time _____
____ 6.6.2	TC	VERIFY all personnel involved with the operation have signed this procedure.

7.0

7.0 CSD DOOR TEST

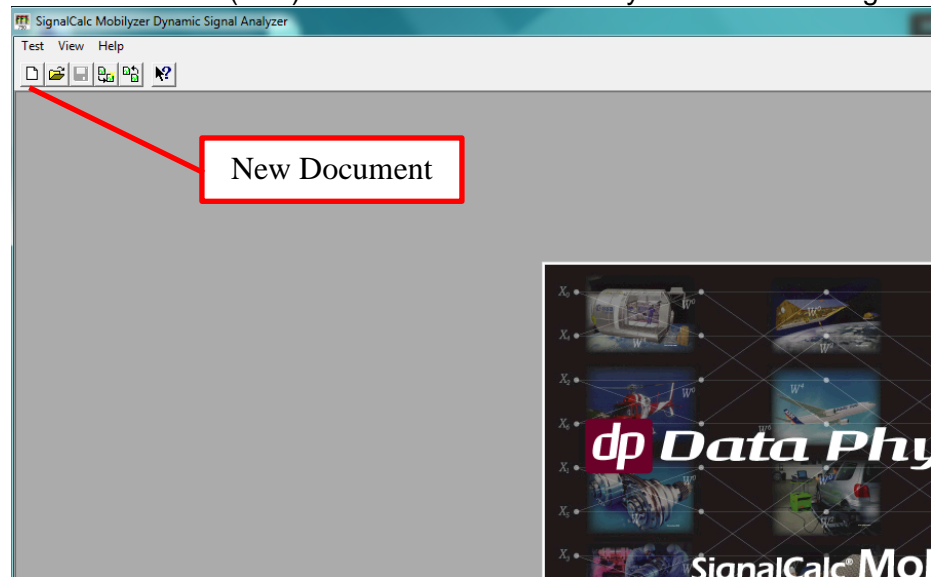
7.1

7.1 DATALOGGER SETUP

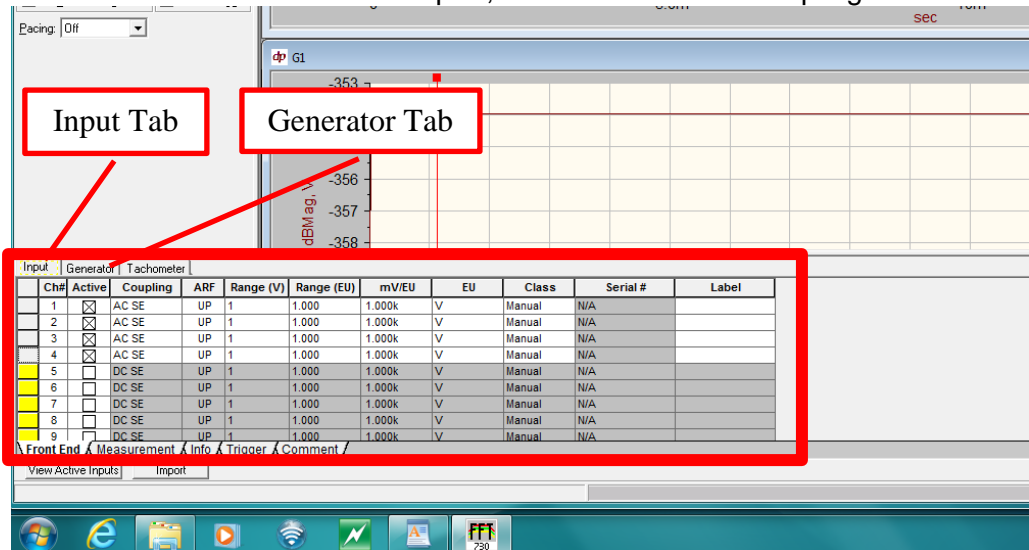
7.1.1

TPO **OPEN** Data Physics SingalCalcMobilyzer

7.1.2

TPO **CLICK** on blank (new) document icon to start Synchronous Average

7.1.3

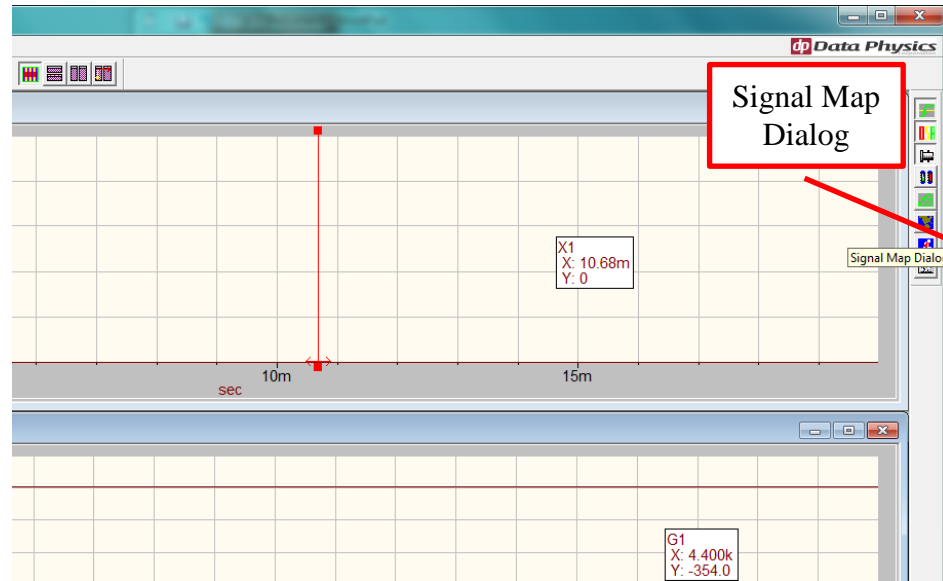
TPO **SELECT** Channels 1-4 under "Input", set to ACSE under coupling

7.1.4

TPO **CLICK** on Generator Tab. Select Ch 1 to be on. Set to Square Wave, Level at 5.2 (since camera reads 5V, 5.2 is a safety factor), and set Frequency to 0.125 Hz to ensure period is 8s long.

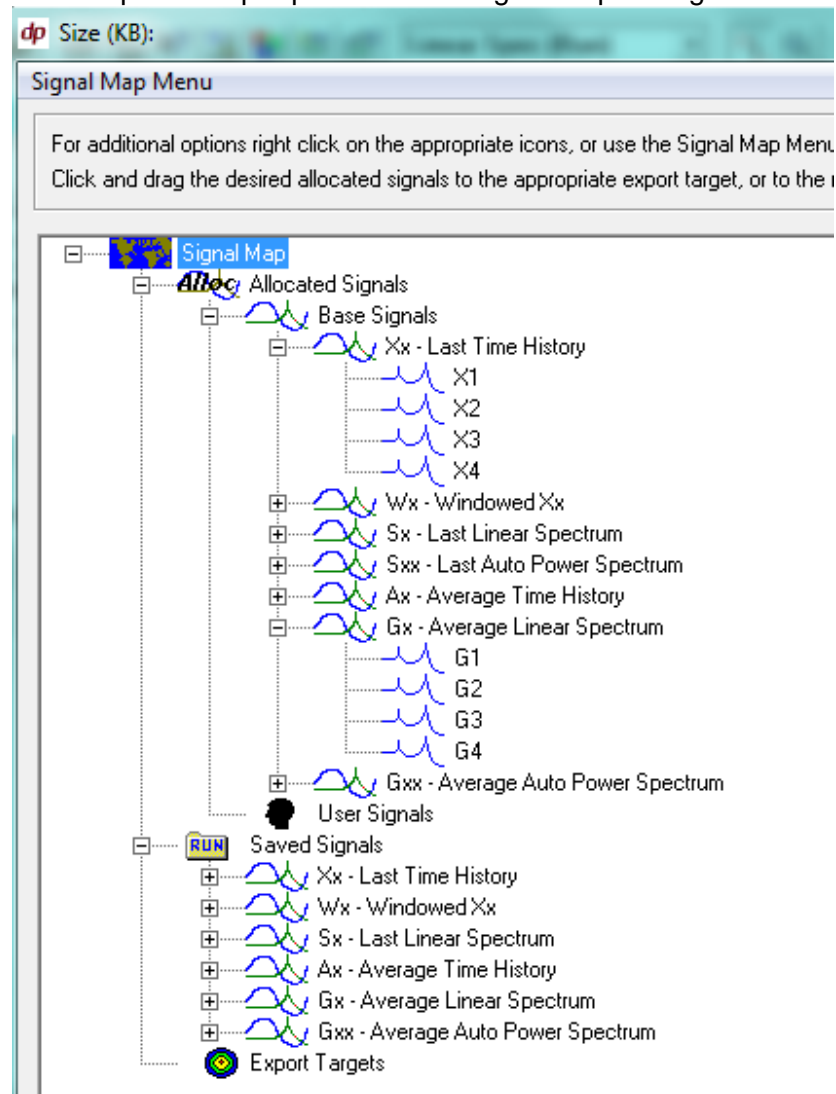
7.1.5

TPO **SELECT** Signal Map Dialog

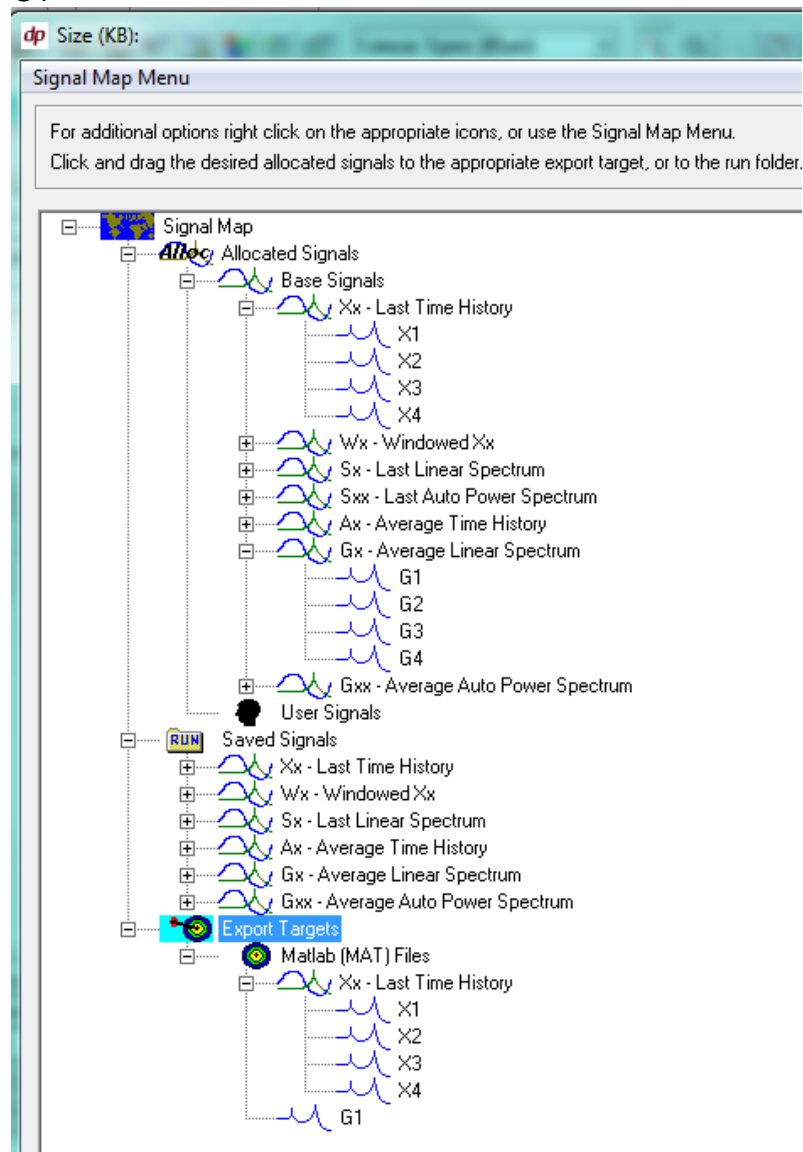


7.1.6

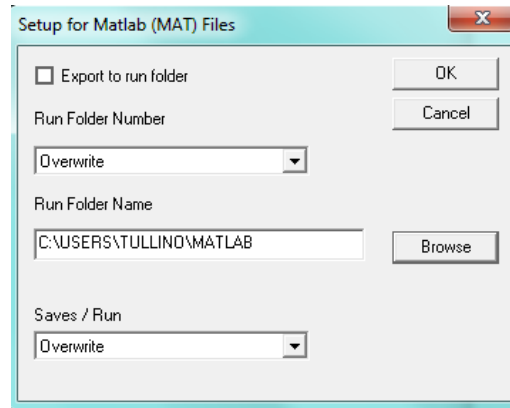
TPO

OPEN up menus per picture in the Signal Map Dialog

- ____ 7.1.7 TPO **LEFT** click Export Targets to see an arrow in the bullseye, then right click Export Targets
- ____ 7.1.8 TPO **SELECT** “Matlab” in Select Export Targets popup window. Click OK.
- ____ 7.1.9 TPO **EXPAND** Export Targets to view Matlab Files header
- ____ 7.1.10 TPO **RIGHT** click and drag desired allocated signals one at a time under the Matlab Files Header per figure below. The desired signals are: X1, X2, X3, X4, and G1

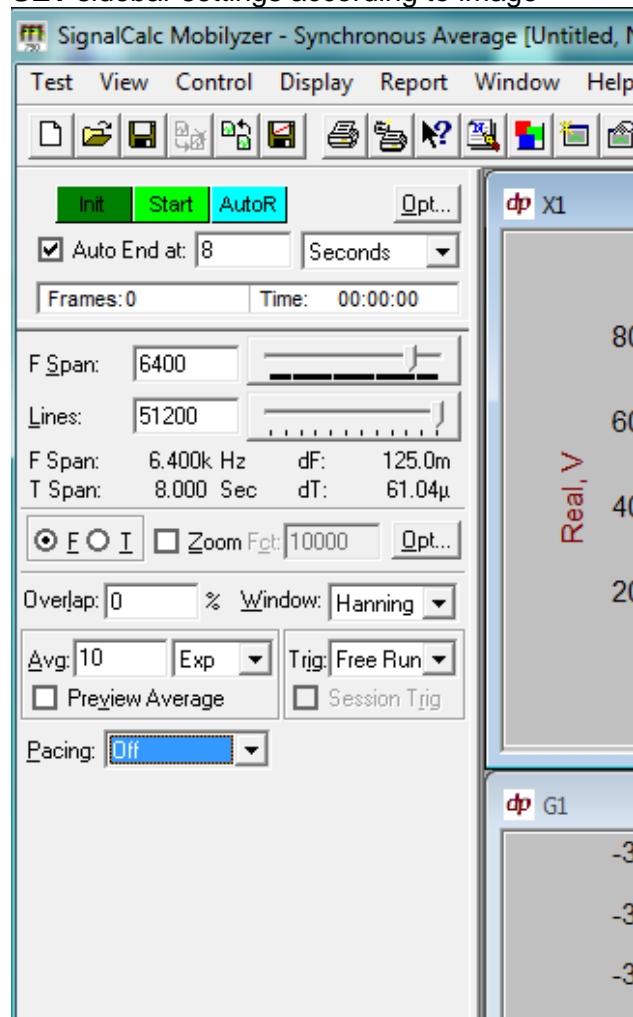


- ____ 7.1.11 TPO **RIGHT** click “Matlab (MAT) Files” to display “Setup for Matlab (MAT) Files”. Set desired directory. See example below



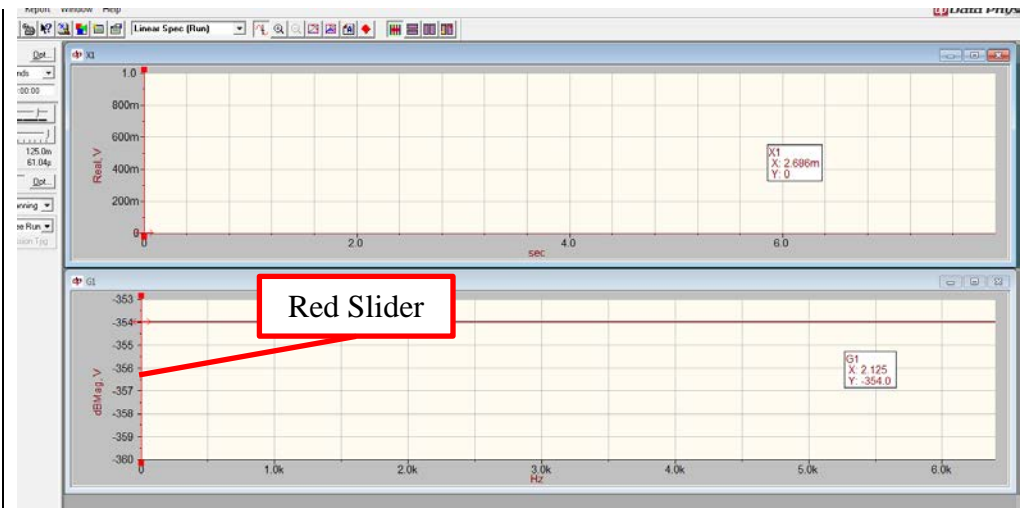
____ 7.1.12 TPO **CLICK** OK, and then click OK again to return to main menu

____ 7.1.13 TPO **SET** sidebar settings according to image



____ 7.1.14 TPO **CLICK** “Test” on top menu bar, select “Save as” to verify destination folder and to create a new test folder

____ 7.1.15 TPO **DRAW** red slider to 0 Hz initiation point for data logging/signal generating plot



____ 7.1.16

TC

CONNECT Data Physics Abacus Tower (Lan 1 socket) via Ethernet cable to computer with Data Physics



____ 7.1.17

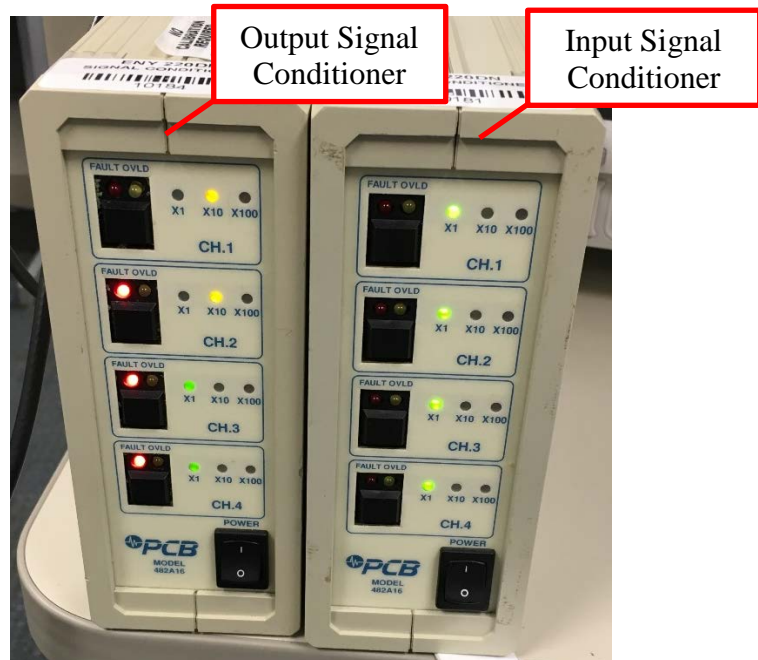
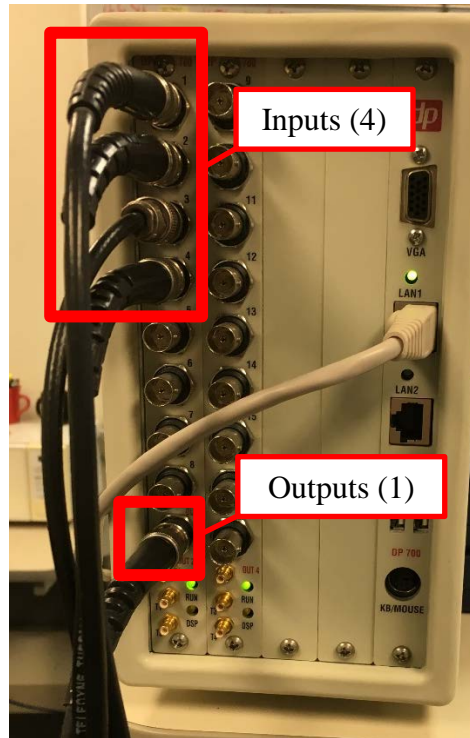
TPO

CONNECT Inputs 1-4 feeds on Data Physics tower to a signal conditioner output connections with coaxial cables. Set amplification to X1

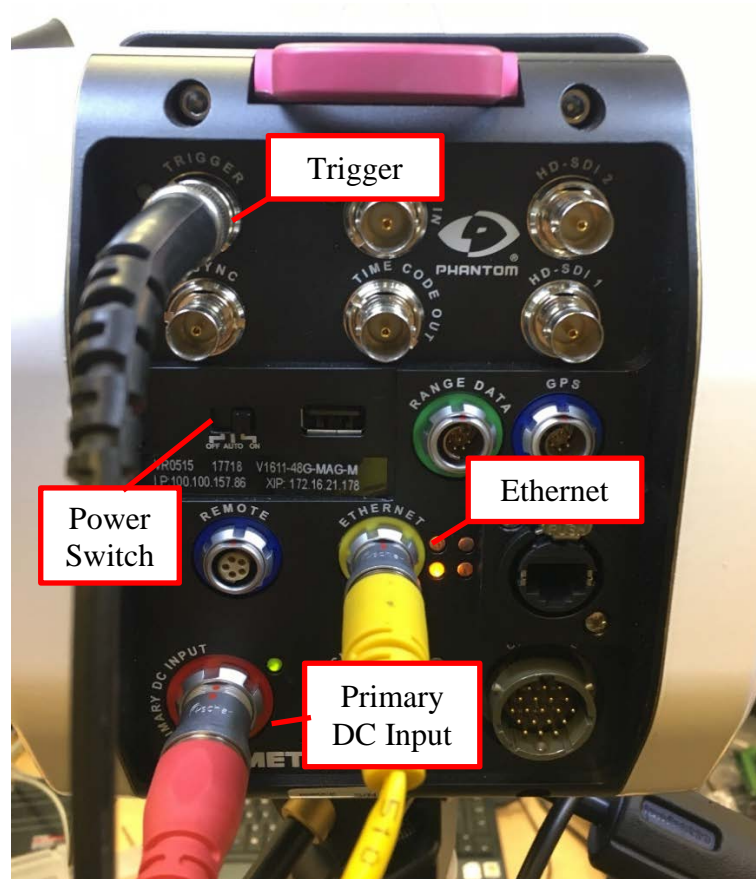
____ 7.1.18

TPO

CONNECT output 1 feed to another signal conditioner's input connection with a coaxial cable. Set amplification to X10



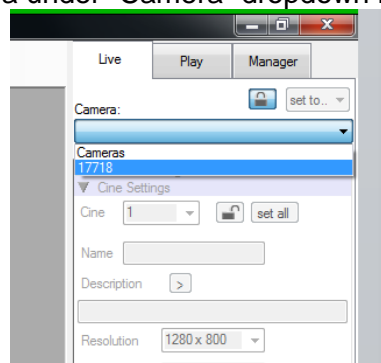
- | | | |
|--------------|-----|--|
| _____ 7.1.19 | TPO | CONNECT the 4 accelerometers to the input connections to the Input Signal Conditioner |
| _____ 7.1.20 | TPO | CONNECT the output connection of the Output Signal Conditioner to the camera's "Trigger" connection via coaxial cable |



7.2

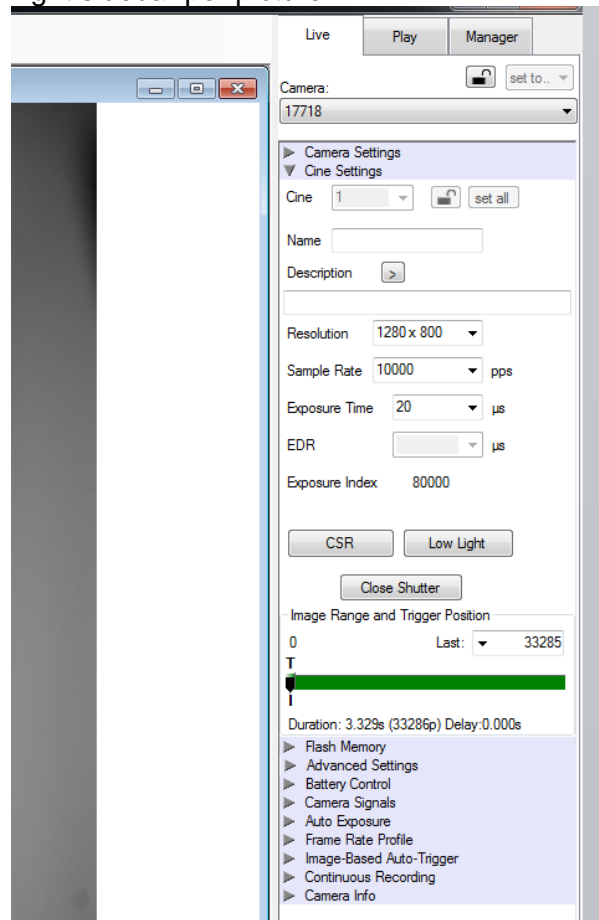
7.2 CAMERA SETUP

- | | | |
|---|--|--|
| <p>____ 7.2.1</p> <p>____ 7.2.2</p> <p>____ 7.2.3</p> <p>____ 7.2.4</p> <p>____ 7.2.5</p> | <p>TC</p> <p>TC</p> <p>TPO</p> <p>TPO</p> <p>TPO</p> | <p>CONNECT Ethernet cable from camera to computer, and connect primary DC power input to camera</p> <p>SWITCH Camera power switch to “On”</p> <p>OPEN Phantom Camera Control (PCC)</p> <p>SELECT “Live” Tab</p> <p>SELECT desired camera under “Camera” dropdown menu</p> |
|---|--|--|



7.2.6

TPO

SET settings on right sidebar per picture

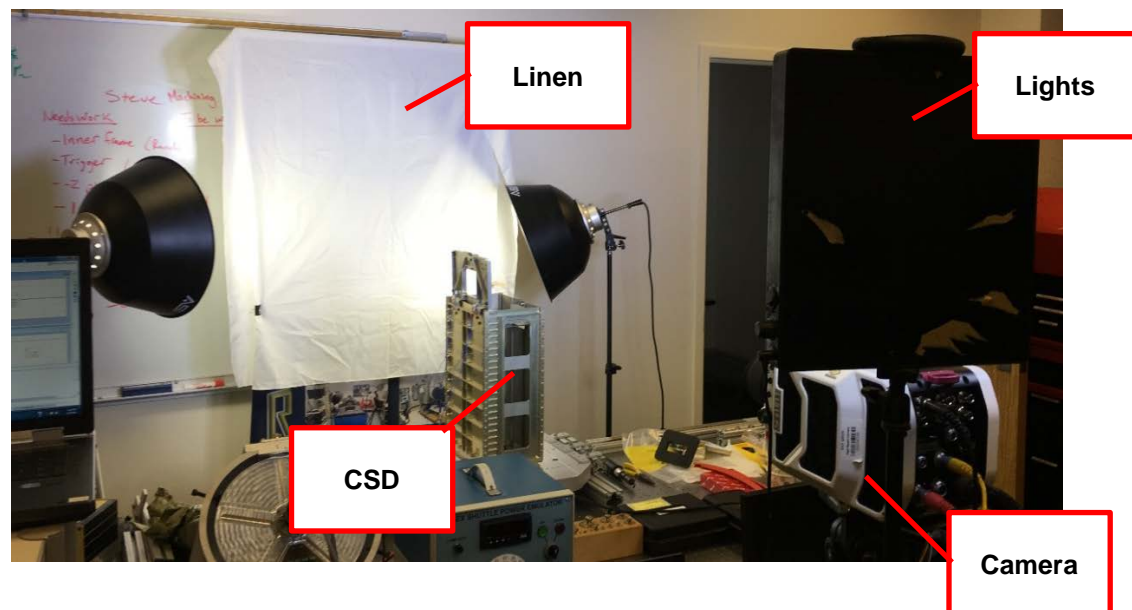
7.2.7


TC

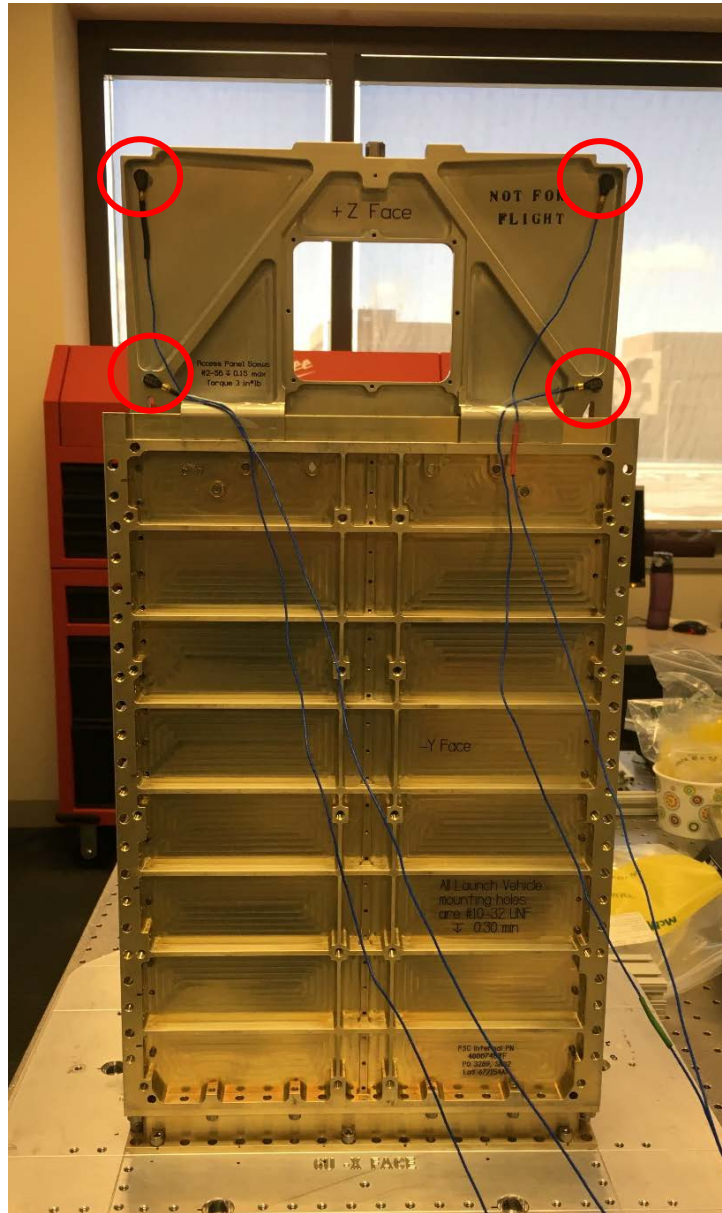
SET UP photography linen backdrop behind CSD

7.2.8

TC

SET UP lighting where lights are shining on the linen, as well as directly onto the CSD door

_____ 7.2.9		ADJUST camera aperture setting to its maximum to allow the most light into the lens. Adjust focus by hand until picture is clear
7.3		7.3 CSD SETUP
_____ 7.3.1	RCL	ATTACH CSD –Z side to secured vibe table head with 8 10-32x3/4” bolts. Torque bolts to standard 50 in-lbs.
_____ 7.3.2	TC	<p>OPEN CSD (if closed) by carefully inserting a hex key or screwdriver (<0.10in wide) in manual release slot and pull up on Latch Lock with approximately 5 lb_f. The tool can be inserted about 0.35in before stopping against an internal cover</p> 
_____ 7.3.3	TD	VERIFY CSD and base plate is clean and clear of all debris and damage
_____ 7.3.4	TC	VERIFY CSD side panels are removed. Remove if required per PSC spec.
_____ 7.3.5	TC	ATTACH accelerometers to each corner of CSD door using beeswax per figure below. Tape down cables to secure to door.



INSERT entire base plate into CSD carefully until fully seated against push plate.

____ 7.3.6 TC

CLOSE the CSD door. Using a thumb, push the Latch closed until a “click/ping” is heard.

____ 7.3.7 TC



7.3.8

TC

VERIFY door is properly closed. There shall be approximately 0.030 inches of movement even after the Latch is closed. A lack of movement signifies something is jammed against the Door. Contact PSC for troubleshooting

7.3.9

TC

VERIFY the Latch Lock is below the indicator line next to the manual door release cutout. If above the line, the Door Latch is not properly closed. Contact PSC for troubleshooting.



7.4 EXECUTION

7.4

VERIFY camera and data logger hardware is powered on. Verify connections

7.4.1

TPO

SELECT "Capture" in Phantom Camera Control under "Live" tab

7.4.2

TPO

SELECT "Int" and then "Start" to commence data logging and send out trigger command

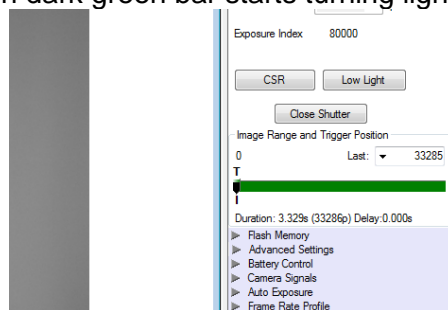
7.4.3

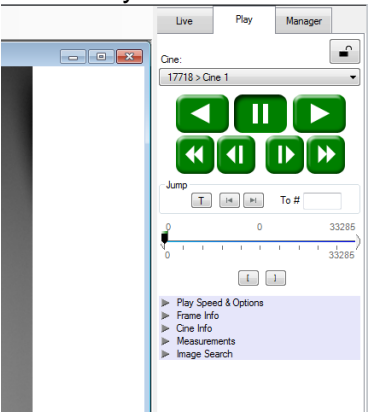
TPO

VERIFY on PCC when dark green bar starts turning light green

7.4.4

TPO



7.4.5	TC	<p>IMMEDIATELY OPEN CSD when PCC green bar starts turning light green by carefully inserting a hex key or screwdriver (<0.10in wide) in manual release slot and pull up on Latch Lock with approximately 5 lbf. The tool can be inserted about 0.35in before stopping against an internal cover. Upon opening, the payload will automatically be ejected. (N.B.: the camera only gives ~3.2 s of record time when triggered)</p>
7.4.6	TPO	<p>AFTER data is captured, click “Play” tab</p> 
7.4.7	TPO	<p>CROP start and finish of desired video portion via the slide bars</p>
7.4.8	TPO	<p>SELECT “Save Cine” to save in desired directory in .cine format</p>
7.4.9	TPO	<p>EXTRACT MAT file from Data Physics data logger in previously set directory. Look for a folder named MATLAB.</p>
		<p>CAUTION: DATA LOGGER AND CAMERA DATA WILL BE OVERWRITTEN EACH TIME A TEST IS REPEATED – SAVE FILES BEFORE STARTING A NEW TEST</p>
7.4.10	TD	<p>REPEAT ejection steps four more times (or as many times needed).</p>
7.5		<p>7.5 TEARDOWN</p>
7.5.1	TC	<p>VERIFY CSD is clean and clear of all debris and damage</p>
7.5.2	TC	<p>CLOSE the CSD door</p>
7.5.3	TC	<p>VERIFY door is properly closed</p>
7.5.4	TC	<p>VERIFY the Latch Lock is below the indicator line next to the manual door release cutout. If above the line, the Door Latch is not properly closed. Contact PSC for troubleshooting.</p>



REMOVE the accelerometers from the CSD door. Ensure no beeswax residue

____ 7.5.5

TC

POWER OFF data logger and camera hardware

____ 7.5.6

TC

DISCONNECT all cables from data logger and camera

____ 7.5.7

TC

7.6 OPTIONAL CAMERA DATA FILE SAVES

7.6

(USE / NOT USE) Create .avi file

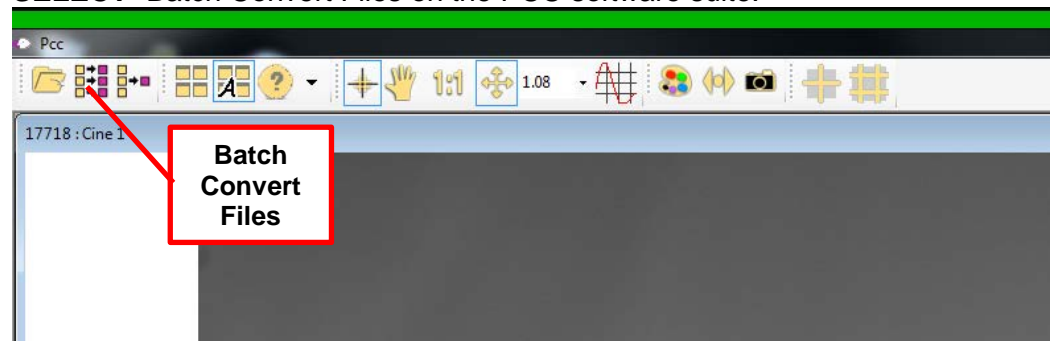
7.6.1

TD

SELECT "Batch Convert Files on the PCC software suite.

____ 7.6.1.1

TPO



OPEN desired directory to save in. A window called "Multifile Convert Destination" will pop up.

____ 7.6.1.2

TPO

SET desired directory/folder, give desired file name, and select .avi under "Save as type" dropdown menu.

____ 7.6.1.3

TPO

CLICK "Convert"

____ 7.6.1.4

TPO

(USE / NOT USE) Create .tiff files

7.6.2

TD

SELECT "Batch Convert Files on the PCC software suite.

____ 7.6.2.1

TPO

OPEN desired directory to save in. A window called "Multifile Convert Destination" will pop up.

____ 7.6.2.2

TPO

____ 7.6.2.3	TPO	SET desired directory/folder, give desired file name, and select "TIFF 8.24 Images *.tif" under "Save as type" dropdown menu.
____ 7.6.2.4	TPO	NAME file as "Name+4" or +5. The +4/5 determines how many digit counter places will be used for the image number. (i.e +4 ensures that 9999 frames are saved)
____ 7.6.2.5	TPO	CLICK "Convert"

8.0		8.0 <u>EMERGENCY RESPONSE</u>
		NOTE: Perform the following steps in the event of a fire or other anomaly which cannot be safely managed by normal securing operations. TC shall have authority (On-Scene Command) over the situation until relieved from support organizations.
____ 8.1	TC	If necessary, EVACUATE and/or Dial 9-911 to notify fire department of emergency
____ 8.2	ANY	If necessary, Brief fire department and medics when they arrive.
____ 8.3	TD	Continue to Monitor Facility until condition has been secured.
		END OF EMERGENCY RESPONSE

APPENDIX 1.0 – Test Log

ITEM	TIME	EVENT / STATUS
(#)	(HHMM)	(Description)
1		
2		
3		
4		
5		
6		
7		
8		
9		
10		
11		
12		
13		
14		
15		
16		
17		
18		
19		
20		
21		
22		
23		
24		
25		
26		
27		

Appendix A.5 – Test Plan: Push Plate Feet Contact Test

AFIT/ENY
6U CSD Push Plate Feet Contact
WRIGHT-PATTERSON AFB, OH

PROCEDURE:
REVISION:
DATE REVISED:
NUMBER OF PAGES:

CSD_Feet_TP
1
5 Jan 2017
10

**AFIT / ENY
OPERATIONS**

**6U CSD
Push Plate Feet Contact**

SYSTEM UNDERGOING TESTING

ASSOCIATED FUNCTIONAL TEST PLAN VERSION

6U Canisterized Satellite Dispenser N/A

PREPARED BY:

Test Engineer _____
Test Conductor _____

DATE _____

REVIEWED / APPROVED BY:

AF Customer _____
Test Director _____

DATE _____

Revision	Notes	Prepared By
0	- Initial procedure	Capt Stephen Tullino 5 Jan 2017

TABLE OF CONTENTS

	Page
1.0 ABBREVIATIONS AND ACRYONMS.....	1
2.0 TEST DESCRIPTION AND OBJECTIVES	1
2.1 PURPOSE.....	1
2.2 SCOPE	1
2.3 OBJECTIVES/SUCCESS CRITERIA	1
3.0 DOCUMENTATION	2
3.1 REFERENCE DOCUMENTS.....	2
3.2 SPECIFICATIONS	2
3.3 DRAWINGS.....	2
4.0 TEST REQUIREMENTS AND RESTRICTIONS	2
4.1 TRAINING	2
4.2 MAXIMUM PERSONNEL:.....	2
4.3 LIST OF EQUIPMENT	2
5.0 SAFETY REQUIREMENTS	3
5.1 PERSONNEL PROTECTIVE EQUIPMENT REQUIREMENTS	3
5.2 EMERGENCY PROCEDURES.....	3
5.3 TEST AREA ACCESS DURING OPERATIONS	3
5.4 SPECIAL INSTRUCTIONS	3
6.0 PRE-TEST SETUP	3
7.0 CSD Push plate contact deployment test	5
7.1 IMU SETUP.....	5
7.2 EXPERIMENTAL SETUP	5
7.3 TEARDOWN	7
7.4 DATA ACQUISITION	8
8.0 EMERGENCY RESPONSE	9
APPENDIX 1.0 – Test Log.....	10

PERSONNEL

DATE _____

The following personnel are designated as test team members, and are chartered to perform their assignment as follows:

Test Conductor (TC) – Responsible for the timely performance of the test as written. This includes coordinating and directing the activities of the Red Crew and other test support teams. TC is responsible for coordinating all pretest activities and outside support required, including (but not limited to) security, fire, medical, and safety. TC is responsible for initialing completion on each step of the master test procedure.

Name _____ Signature _____

Test Director (TD) – Responsible for overall facility and test safety. Responsible for ensuring all test goals are met and all critical data is acquired. Supervises test activities to ensure procedures are followed. Has authority to perform real-time redlines on test procedures as required to ensure test requirements and goals are met.

Name _____ Signature _____

Red Crew Leader (RCL) – Responsible for directing the activities of Red Crew members. Reports directly to the TC and ensures all Red Crew tasks are completed. Responsible for ensuring all RCM's have all required certifications and training. Responsible for ensuring all required equipment is available, accessible, and serviceable.

Name _____ Signature _____

Test Panel Operator (TPO) – Responsible for operating the facility control systems during test operations as directed by TC. TPO is responsible for notifying the TC of any anomalous conditions.

Name _____ Signature _____

Red Crew Member (RCM) – Reports to the RCL. RCM is responsible for performing test-related tasks as directed by RCL.

Name N/A Signature _____

Name _____ Signature _____

Functional Test Conductor – Responsible for performing functional test in support of test.

Name N/A Signature _____

Name _____ Signature _____

EXCEPTIONS – When filling all positions is not possible, the Test Conductor will assume the duties of any empty position until the completion of the test or a suitable replacement is designated.

ALL TEST TEAM MEMBERS – Responsible for the safe performance of the test. Have read and understood all portions of the test procedure. Any Test Team Member can declare an emergency or unsafe condition.

1.0

1.0 ABBREVIATIONS AND ACRYONMS

AFIT	Air Force Institute of Technology
CSD	Canisterized Satellite Dispenser
FOD	Foreign Object Debris
PPE	Personal Protective Equipment
RCL	Red Crew Leader
RCM	Red Crew Member
STE	Special Test Equipment
TC	Test Conductor
TD	Test Director
TOP	Test Operating Procedure
TPO	Test Panel Operator

2.0

2.0 TEST DESCRIPTION AND OBJECTIVES

2.1

2.1 PURPOSE

This procedure provides the means to perform deployment testing for test articles supplied relating to the 6U CUBESAT CHASSIS. The 6U CUBESAT CHASSIS test campaign is a structure and model validation plan intended to mitigate technology concerns for a future flight in a Planetary Systems Corp Canisterized Satellite Dispenser (PSC-CSD). The location of choice will be configured with the proper special test equipment (STE) to direct and measure “maximum predicted environments” associated with launching the 6U Chassis according to the PSC-CSD Payload Specification.

2.2

2.2 SCOPE

This procedure tests the tip-off rate concept due to distribution/imbalance of the push plate contact feet. This data will be used to verify CSD Deployment MATLAB model, as well as verify PSC theoretical performance parameters.

2.3

2.3 OBJECTIVES/SUCCESS CRITERIAComplete Success

1. Payload is ejected and data can be retrieved

Marginal Success

2. Payload is ejected and data is inconclusive, or external disturbance is induced

Unsuccessful

3. Payload cannot deploy or data cannot be extracted from accelerometer/IMU

3.0	3.0 <u>DOCUMENTATION</u>
	The completion of each applicable event shall be verified by initialing to the left of the item number. Deviations from these procedures will be coordinated with the Test Conductor. (NOTE: TD has the local authority to approve red-line revisions to this procedure).
____ 3.1	3.1 REFERENCE DOCUMENTS Planetary Systems Corporation Canisterized Satellite Dispenser (CSD) Data Sheet (2002337C Rev – 3 Aug 2016)
____ 3.2	3.2 SPECIFICATIONS The following list of specifications shall be used as a guide: Planetary Systems Corporation CSD Operating and Integration Procedure (3000257B 18 Jan 2016) Planetary Systems Corporation Payload Specification for 3U, 6U, 12U AND 27U (2002367 Rev - 25 July 2012) X-Io Technologies NGIMU User's Manual
____ 3.3	3.3 DRAWINGS NONE
4.0	4.0 <u>TEST REQUIREMENTS AND RESTRICTIONS</u>
____ 4.1	4.1 TRAINING The following training is required for personnel using these procedures: All personnel: Job Site General Lab Safety Briefing AT LEAST ONE PERSON PRESENT MUST BE TRAINED BY PSC TO OPERATE CSD (OR SUPERVISE CSD OPERATION)
____ 4.2	4.2 MAXIMUM PERSONNEL: Control Room: 3
____ 4.3	4.3 LIST OF EQUIPMENT <ul style="list-style-type: none"> - 1 – Secured vibe table head - 8 – 10-32x3/4" bolts - 1 – 10mm Allen Wrench

- 1 – 10 mm 50 in-lb torque wrench
- 1 – 6U
- 1 – 3-D Printed CubeSat Chassis
- 4 – Door contact feet
- X-io NGIMU
- NGIMU interface
- USB Cable
- NGIMU Software Suite

Ensure all tools associated with this experiment/test/operation are accounted for prior to initiating system/item test. Ensure all FOD is picked up from around the test facility.

5.0**5.0 SAFETY REQUIREMENTS****5.1****5.1 PERSONNEL PROTECTIVE EQUIPMENT REQUIREMENTS**

Standard PPE: Boots – soles and heels made of semi-conductive rubber containing no nails.

All jewelry will be removed by test members while working on the test facility. No ties or other loose clothing permitted (at TD discretion).

5.2**5.2 EMERGENCY PROCEDURES**

In the event of an emergency that jeopardizes the safety of the operators or other personnel perform Section 8.0 emergency procedures at the end of this document.

5.3**5.3 TEST AREA ACCESS DURING OPERATIONS**

The test facility room will be limited to test personnel only. Personnel will not be allowed access to the test area unless cleared by the TD.

5.4**5.4 SPECIAL INSTRUCTIONS**

A qualified technician should provide orientation for clean room awareness and the proper faculty member / instructor should be consulted on test-series set points prior to test operations commencing.

Test Crew members shall place all cellular telephones on “silent mode” or turn off prior to completing any portion of this procedure.

6.0**6.0 PRE-TEST SETUP****6.1**

TC

VERIFY all pages in this procedure are intact and complete.

6.2


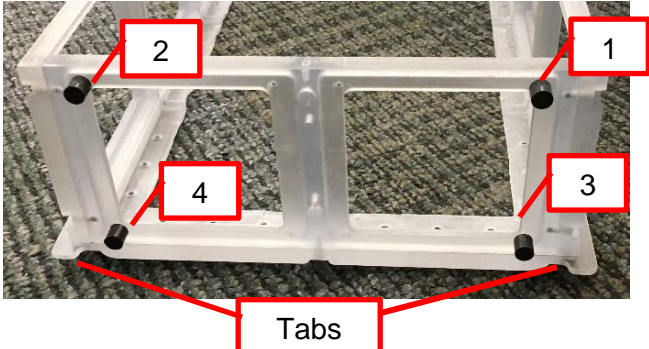
TC

READ procedure and input any specific information required to perform operation.

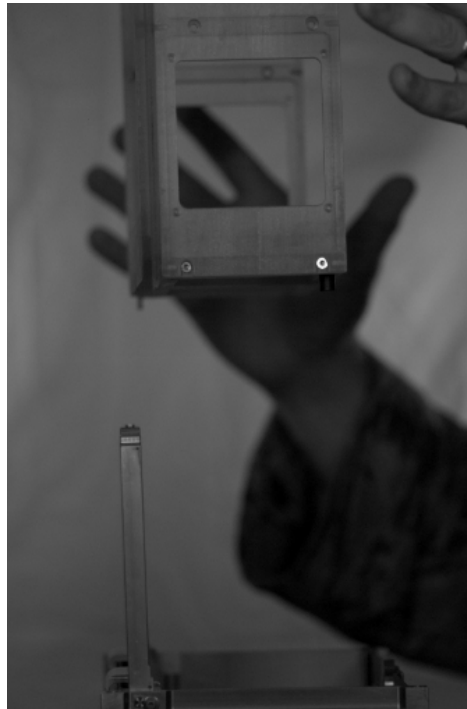
_____ 6.3	TC	VERIFY with Facility Management that no open Work Orders / Issues are listed for the noted location impeding operations.
_____ 6.4	TC	PERFORM Setup Brief with Test Crew Members and note any redline changes on Appendices.
_____ 6.5	TC	VERIFY Test Team has donned standard PPE (and noted restrictions / special instructions).
_____ 6.6	TC	PERFORM Pre-Operation Brief with Test Crew Members <ul style="list-style-type: none"> – Objective – Personnel and assigned roles/duties – Safety: materials, PPE, communication, etc. – Sequence of events – Emergency procedures
_____ 6.6.1	TC	RECORD Pre-Test Brief Time _____
_____ 6.6.2	TC	VERIFY all personnel involved with the operation have signed this procedure.

7.0		7.0 <u>CSD PUSH PLATE CONTACT DEPLOYMENT TEST</u>
7.1		7.1 IMU SETUP
		WARNING: DO NOT USE USB ON US GOVERNMENT COMPUTERS
____ 7.1.1	TC	CONNECT NGIMU via USB cable to computer (assuming the NGIMU needs charging)
____ 7.1.2	TC	PRESS power button. LED lights should light up.
____ 7.1.3	TPO	OPEN up NGIMU-Software folder in set directory and select NGIMU GUI application
____ 7.1.4	TPO	SELECT desired connection. Choose the serial option (typically there is a wireless option as well, but we will assume the battery isn't charged)
____ 7.1.5	TPO	SELECT Settings Tab (not top menu option) on GUI. Set settings as shown below.
____ 7.1.6	TPO	SELECT Settings top menu option. Select "write to device" to apply settings to NGIMU
____ 7.1.7	TC	PRESS power button. LED lights should turn off.
____ 7.1.8	TC	UNPLUG USB cable when NGIMU is charged enough.
7.2		7.2 EXPERIMENTAL SETUP
____ 7.2.1	RCL	ATTACH CSD –Z side to secured vibe table head with 8 10-32x3/4" bolts. Torque bolts to standard 50 in-lbs.
____ 7.2.2	TC	OPEN CSD (if closed) by carefully inserting a hex key or screwdriver (<0.10in wide) in manual release slot and pull up on Latch Lock with approximately 5 lb _f . The tool can be inserted about 0.35in before stopping against an internal cover



7.2.3	TC	INSTALL NGIMU on rear part of internal base plate of 3-D printed 6U chassis with beeswax according to figure.
		
7.2.4	TC	VERIFY CSD and chassis is clean and clear of all debris and damage
7.2.5	TC	VERIFY CSD side panels are removed. Remove if required per PSC spec.
7.2.5	TD	DESIGNATE one person to stop the payload once it's ejected
7.2.6	TC	SET chassis feet to the following configurations using figure below as a guide. Each configuration is to be tested 5 times.
		<ul style="list-style-type: none"> • All 4 feet • Only Feet 2, 3, 4 • Only Feet 3, 4 • Only Foot 1 • No feet – tabs only
		
7.2.7	TC	PRESS the power button on the NGIMU to activate. LED lights should light up.
7.2.8	TC	INSERT entire chassis/base plate into CSD carefully until fully seated against push plate.

		DO NOT CLOSE CSD DOOR AND CONTINUE TO HOLD DOWN THE PAYLOAD IN THE CSD
____ 7.2.9	TD	(USE / NOT USE) EXECUTE remote NGIMU data acquisition per step %%%, if desired.
____ 7.2.10	TC	QUICKLY release hold of the payload, allowing it to eject upwards into the air
____ 7.2.11	RCL	CATCH the payload when it stops midair.



____ 7.2.12	TC	PRESS NGIMU power button to turn off unit.
____ 7.2.13	TD	REPEAT ejection steps four more times (or as many times needed).
7.3		7.3 TEARDOWN
____ 7.3.1	TD	VERIFY CSD is clean and clear of all debris and damage
____ 7.3.2	TC	CLOSE the CSD door. Using a thumb, push the Latch closed until a “click/ping” is heard.



____ 7.3.3	TC	VERIFY door is properly closed. There shall be approximately 0.030 inches of movement even after the Latch is closed. A lack of movement signifies something is jammed against the Door. Contact PSC for troubleshooting
____ 7.3.4	TC	VERIFY the Latch Lock is below the indicator line next to the manual door release cutout. If above the line, the Door Latch is not properly closed. Contact PSC for troubleshooting.
____ 7.3.5	TC	REMOVE the NGIMU from the base chassis. Ensure no beeswax residue
7.4		7.4 DATA ACQUISITION
____ 7.4.1	TC	CONNECT NGIMU via micro USB cable.
____ 7.4.2	TC	PRESS power button. LED lights should light up.
____ 7.4.3	TPO	OPEN up NGIMU-Software folder in set directory and select NGIMU GUI application
____ 7.4.4	TPO	SELECT desired connection. Choose the serial option (typically there is a wireless option as well, but we will assume the battery isn't charged)
____ 7.4.5	TPO	SELECT "Tools" menu and select "SD Card File Converter" from drop-down menu.
____ 7.4.6	TPO	SELECT the desired SD card file and then select the directory to save the extracted data.

7.4.7	TD	(USE / DO NOT USE) NGIMU REMOTE DATA ACQUISITION (FOR USE DURING TESTS)
____ 7.4.7.1	TPO	OPEN up NGIMU-Software folder in set directory and select NGIMU GUI application
____ 7.4.7.2	TPO	SELECT desired connection. Choose the wireless option.
____ 7.4.7.3	TPO	SELECT “Tools” menu and select “Data Logger” from drop-down menu.
____ 7.4.7.4	TPO	SET the desired directory to save file, file name, and logging period.
____ 7.4.7.5	TPO	PRESS Start button to commence. Data will automatically save onto desired directory once logging period has finished.

8.0		8.0 <u>EMERGENCY RESPONSE</u> NOTE: Perform the following steps in the event of a fire or other anomaly which cannot be safely managed by normal securing operations. TC shall have authority (On-Scene Command) over the situation until relieved from support organizations.
____ 8.1	TC	If necessary, EVACUATE and/or Dial 9-911 to notify fire department of emergency
____ 8.2	ANY	If necessary, Brief fire department and medics when they arrive.
____ 8.3	TD	Continue to Monitor Facility until condition has been secured.
		END OF EMERGENCY RESPONSE

APPENDIX 1.0 – Test Log

ITEM	TIME	EVENT / STATUS
(#)	(HHMM)	(Description)
1		
2		
3		
4		
5		
6		
7		
8		
9		
10		
11		
12		
13		
14		
15		
16		
17		
18		
19		
20		
21		
22		
23		
24		
25		
26		
27		

Bibliography

- [1] F. Azure, R. Hevner and W. Holemans, "Lessons Learned Measuring 3U and 6U Payload Rotation and Velocity when Dispensed in Reduced Gravity Environment," 21 April 2015.
- [2] R. Henver, "Canisterized Satellite Dispenser (CSD) Data Sheet (2002337D)," Planetary Systems Corporation, 4 August 2016. [Online]. Available: <http://www.planetarysystemscorp.com/web/wp-content/uploads/2016/08/2002337D-CSD-Data-Sheet.pdf>.
- [3] W. Holemans and C. Flood, Interviewees, *Interview with PSC on CSD Deployment Profiles*. [Interview]. 28 July 2016.
- [4] W. Holemans and R. Henver, "Canisterized Satellite Dispenser". United States of America Patent US 2014/0319283 A1, 30 October 2014.
- [5] D. Miller, "Vibrational Analysis of a 12U Chassis," Air Force Institute of Technology, Wright-Patterson AFB, 2016.
- [6] W. Lan, *CubeSat Design Specification*, San Luis Obispo, California: California Polytechnic State University, 2006.
- [7] Innovative Solutions in Space, "QuadPack CubeSat Deployer," [Online]. Available: <https://www.isispace.nl/wp-content/uploads/2016/02/quadpack-1.png>. [Accessed 14 October 2016].
- [8] E. Swenson, Interviewee, *MECH 632 Intermediate Spaceflight Dynamics & Thesis Advisor*. [Interview]. April - September 2016.
- [9] R. Henver, "Payload Specification for 3U, 6U, 12U and 27U," Planetary Systems Corporation, 4 August 2016. [Online]. Available: <http://www.planetarysystemscorp.com/web/wp-content/uploads/2016/08/2002367D-Payload-Spec-for-3U-6U-12U-27U.pdf>.

- [10] Pumpkin Inc., *Picture of SUPERNOVA CubeSat CSD Contact Feet*, Wright-Patterson AFB: AFIT, 2016.
- [11] Pumpkin Inc., *Picture of CSD Push Plate after SUPERNOVA Vibe Test*, Wright-Patterson AFB, 2016.
- [12] Pumpkin Space Systems, "6U SUPERNOVA Structure Kit Owner's Manual," 2014. [Online]. Available: http://www.cubesatkit.com/docs/SUPERNOVA_User_Manual-RevA0.pdf.
- [13] F. Azure, R. Hevner, W. Holemans, G. Moore and R. Williams, "Lessons Learned Testing and Flying Canisterized Satellite Dispensers (CSD) for Space Science Missions," Palo Alto, CA, 13-15 November 2013.
- [14] F. Karmali and M. Shelhamer, "The dynamics of parabolic flight: flight characteristics and," vol. 63, no. 5-6, pp. 594-602, 2008.
- [15] European Space Agency, "Space for Educators," [Online]. Available: http://www.esa.int/Education/Microgravity_and_drop_towers. [Accessed 1 November 2016].
- [16] G. Röthlisberger, B. Jutzeler and D. Arce, "Phase A Structure and Configuration," SwissCube, 2006 15 June. [Online]. Available: http://www.goldstem.org/Swiss%20Cube/09%20-%20Structures%20and%20configuration/S3-A-STRU-1-4-Structure_Configuration.pdf. [Accessed 22 January 2017].
- [17] S. Rossi, A. Ivanov, M. Richard, V. Gass and A. Roesch, "Four Years (almost) of SwissCube Operations," in *SmallSat pre-Conference Workshop*, Logan, UT, 2013.
- [18] S. Clark, "NASA adding to list of CubeSats flying on first SLS mission," *Spaceflight Now*, 8 April 2015. [Online]. Available: <http://spaceflightnow.com/2015/04/08/nasa-adding-to-list-of-cubesats-flying-on-first-sls-mission/>. [Accessed 1 November 2016].
- [19] S. Spearing, Interviewee, *NASA Marshall SLS Secondary Payload Program Consultation*. [Interview]. 14 November 2016.

- [20] NASA TV, "NASA Space Launch System's First Flight to Send Small Sci-Tech Satellites Into Space," NASA Press Office, 2 February 2016. [Online]. Available: <https://www.nasa.gov/press-release/nasa-space-launch-system-s-first-flight-to-send-small-sci-tech-satellites-into-space>. [Accessed 1 November 2016].
- [21] E. Swenson, Interviewee, *MECH-632 Intermediate Spacecraft Dynamics Lecture - Part 6*. [Interview]. 2016.
- [22] E. Swenson, Interviewee, *MECH-632 Intermediate Spaceflight Dynamics Lecture - Part 4*. [Interview]. 2016.
- [23] E. Swenson, Interviewee, *MECH-632 Intermediate Spaceflight Dynamics Lecture - Part 8*. [Interview]. 2016.
- [24] Dimension Engineering LLC, "A Beginner's Guide to Accelerometers," [Online]. [Accessed 1 December 2016].
- [25] S. K. Tullino, Artist, *Author Created Graphics*. [Art]. Air Force Institute of Technology, 2017.
- [26] SparkFun Electronics, "Tutorials," SparkFun Electronics, [Online]. Available: <https://learn.sparkfun.com/tutorials/gyroscope/all.pdf>. [Accessed 1 December 2016].
- [27] G. A. Wood, "Data Smoothing and Differentiation Procedures in Biomechanics," *Nedlands*, 1982, pp. 310-314.
- [28] A. K. Prasad, "Particle Image Velocimetry," *Current Science*, vol. 79, no. 1, pp. 51-60, 10 July 2000.
- [29] A. J. Lingenfelter, Interviewee, *High Speed Camera Consultation*. [Interview]. 19 December 2016.
- [30] L. C. Elonen-Wright, "NASA GRC Zero Gravity Research Facility," 24 January 2008. [Online]. Available: <http://facilities.grc.nasa.gov/zerog/>. [Accessed 19 September 2016].

- [31] E. Neumann, Interviewee, *NASA GRC Zero-G Facility Consultation*. [Interview]. October 2016.
- [32] L. C. Elonen-Wright, "NASA GRC 2.2 Second Drop Tower," National Aeronautics and Space Administration, 1 February 2008. [Online]. Available: <http://facilities.grc.nasa.gov/drop/>. [Accessed 19 September 2016].
- [33] D. J. Gotti, *A Collection of 2.2 Second Drop Tower Information*, Cleveland, Ohio: NASA Glenn Research Center - National Center for Space Exploration Research, 2005.
- [34] D. Del Rosso, "Reduced Gravity Research," 30 September 2016. [Online]. Available: https://jsc-aircraft-ops.jsc.nasa.gov/Reduced_Gravity/index.html.
- [35] J. Dewitt, Interviewee, *Assistance with Manufacturing CSD Force Profile Testing Apparatus*. [Interview]. August 2016.
- [36] Mide, *Slam Stick X User's Manual*, 2015.
- [37] Mide, "Slam Stick Vibration Data Loggers Data Sheet," Mide, 9 January 2017. [Online]. Available: http://info.mide.com/hubfs/slam-stick/datasheet/slam-stick-vibration-data-loggers-datasheet.pdf?hsCtaTracking=c32024f3-178f-4f3b-bbf1-6ec4d131432f%7Cbba56a47-81d6-4103-a678-76dc75b24772&__hstc=190384372.443bd682f44b37216227fc4700f8989b.1471022337078.14845. [Accessed 30 January 2017].
- [38] Analog Devices, "SparkFun Datasheets," SparkFun Electronics, 2009. [Online]. Available: <https://www.sparkfun.com/datasheets/Sensors/Accelerometer/ADXL345.pdf>. [Accessed 13 October 2016].
- [39] InvenSense Inc., "SparkFun Datasheets," 30 March 2010. [Online]. [Accessed 13 October 2016].
- [40] Analog Devices, "Technical Documentation," Analog Devices, 2009. [Online]. Available: http://www.analog.com/media/en/technical-documentation/datasheets/ADIS16400_16405.pdf. [Accessed 13 October 2016].

- [41] X. Gang, Interviewee, *Bosch Product Consultation*. [Interview]. 25 October 2016.
- [42] "BMI160 Datasheet," Bosch, 10 February 2015. [Online]. Available: https://ae-bst.resource.bosch.com/media/_tech/media/datasheets/BST-BMI160-DS000-07.pdf. [Accessed 23 October 2016].
- [43] R. Nave, "Friction Plot," Georgia State University, [Online]. Available: hyperphysics.phy-astr.gsu.edu/hbase/frict2.html#kin. [Accessed 1 November 2016].
- [44] "The Coefficient of Kinetic Friction," Pellissippi State Community College, [Online]. Available: http://www.pstcc.edu/departments/natural_behavioral_sciences/Web%20Physics/Experiment%2005web.htm. [Accessed 1 November 2016].
- [45] D. L. Kunz, *Intermediate Dynamics for Aeronautics & Astronautics*, Wright-Patterson AFB, Ohio: Ar Force Insitute of Technology, 2015, pp. 155-168.
- [46] A. M. Wahl, *Mechanical Springs*, 1st ed., Cleveland, OH: Penton Publishing Company, 1944, pp. 329-347.
- [47] National Instruments, "FFT Fundamentals (Sound and Vibration Measurement Suite)," National Instruments, 2009. [Online]. Available: http://zone.ni.com/reference/en-XX/help/372416A-01/svtconcepts/fft_funda/. [Accessed 10 February 2017].
- [48] Vision Research, "Ultrahigh-Speed Cameras Manual," Vision Research, 22 July 2016. [Online]. Available: http://www.phantomhighspeed.com/Portals/0/Docs/ZDOC-64110-MA-0001%20Rev3_MANUAL_WEB-UHSvXX12.pdf?ver=2016-10-12-134529-530. [Accessed 20 December 2016].
- [49] R. Masters, "How I Shot & Edited – The White Infinity Setup," [Online]. Available: <http://digital-photography-school.com/how-i-shot-edited-the-white-infinity-setup/>. [Accessed 31 January 2017].
- [50] E. Swenson, Interviewee, *MECH-632 Intermediate Spacecraft Dynamics Lecture - Part 3*. [Interview]. 2016.

- [51] A. J. Wheeler and A. R. Ganji, Introduction to Engineering Experimentation, 1st ed., Upper Saddle River, New Jersey: Prentice Hall, 1996, pp. 136-140.
- [52] J. C. Lansey, "Box and whiskers plot (without statistics toolbox)," 16 September 2015. [Online]. Available: <http://www.mathworks.com/matlabcentral/fileexchange/42470-box-and-whiskers-plot--without-statistics-toolbox-?requestedDomain=www.mathworks.com>. [Accessed 29 August 2016].
- [53] S. Wolverton, "Normality Tests in SPSS (Lecture Notes)," [Online]. Available: <http://geography.unt.edu/~wolverton/Normality%20Tests%20in%20SPSS.pdf>. [Accessed 26 February 2017].
- [54] D. C. Montgomery, G. C. Runger and N. F. Hubele, Engineering Statistics, 4th ed., John Wiley & Sons, Inc., 2007, pp. 152-154.
- [55] C. Hartsfield, Interviewee, *Thesis Data Consultation*. [Interview]. January 2017.
- [56] R. Henver, *3000257B CSD Operating and Integration Procedure*, Planetary Systems Corp, 2016.
- [57] X-io Technologies, *Next Generation IMU User's Manual*, 2016.

REPORT DOCUMENTATION PAGE				Form Approved OMB No. 074-0188	
<p>The public reporting burden for this collection of information is estimated to average 1 hour per response, including the time for reviewing instructions, searching existing data sources, gathering and maintaining the data needed, and completing and reviewing the collection of information. Send comments regarding this burden estimate or any other aspect of the collection of information, including suggestions for reducing this burden to Department of Defense, Washington Headquarters Services, Directorate for Information Operations and Reports (0704-0188), 1215 Jefferson Davis Highway, Suite 1204, Arlington, VA 22202-4302. Respondents should be aware that notwithstanding any other provision of law, no person shall be subject to any penalty for failing to comply with a collection of information if it does not display a currently valid OMB control number.</p> <p>PLEASE DO NOT RETURN YOUR FORM TO THE ABOVE ADDRESS.</p>					
1. REPORT DATE (DD-MM-YYYY) 23 Mar 2017		2. REPORT TYPE Master's Thesis		3. DATES COVERED (From – To) Oct 2015 – Mar 2017	
4. TITLE AND SUBTITLE Testing and Evaluating Deployment Profiles of the Canisterized Satellite Dispenser (CSD)				5a. CONTRACT NUMBER	
				5b. GRANT NUMBER	
				5c. PROGRAM ELEMENT NUMBER	
6. AUTHOR(S) Tullino, Stephen K., Captain, USAF				5d. PROJECT NUMBER NA	
				5e. TASK NUMBER	
				5f. WORK UNIT NUMBER	
7. PERFORMING ORGANIZATION NAMES(S) AND ADDRESS(S) Air Force Institute of Technology Graduate School of Engineering and Management (AFIT/EN) 2950 Hobson Way, Building 640 WPAFB OH 45433-8865				8. PERFORMING ORGANIZATION REPORT NUMBER AFIT-ENY-MS-17-M-296	
9. SPONSORING/MONITORING AGENCY NAME(S) AND ADDRESS(ES) Air Force Research Labs / Space Vehicles 3550 Aberdeen Ave Kirtland AFB, NM 87108				10. SPONSOR/MONITOR'S ACRONYM(S) AFRL/RV	
				11. SPONSOR/MONITOR'S REPORT NUMBER(S)	
12. DISTRIBUTION/AVAILABILITY STATEMENT DISTRIBUTION STATEMENT A: APPROVED FOR PUBLIC RELEASE; DISTRIBUTION UNLIMITED					
13. SUPPLEMENTARY NOTES This material is declared a work of the U.S. Government and is not subject to copyright protection in the United States.					
14. ABSTRACT Planetary Systems Corporation (PSC) developed the Canisterized Satellite Dispenser (CSD) to provide a more secure and predictable deployment system for CubeSats of different sizes. The CSD is designed to provide predictable and consistent payload deployment performance. Though the CSD has proven its safety and reliability, there is still not enough data required to predict accurately CSD linear and angular deployment rates. In this research, various analytical models were developed, and their predictions were compared with respect to experimental deployments. Any errors were analyzed to tune the models to better understand the deployment dynamics and the variables that affect performance.					
15. SUBJECT TERMS CubeSat, Canisterized Satellite Dispenser, Planetary Systems Corp, simulation, model, characterization, linear velocity, angular rates, micro gravity, deployment					
16. SECURITY CLASSIFICATION OF:			17. LIMITATION OF ABSTRACT UU	18. NUMBER OF PAGES XX	19a. NAME OF RESPONSIBLE PERSON Eric D. Swenson, PhD
a. REPORT U	b. ABSTRACT U	c. THIS PAGE U			19b. TELEPHONE NUMBER (Include area code) (937) 255-3636, x 3329 (eric.swenson@afit.edu)